Investigating the structure and function of the FtsH protease family in *Synechocystis* sp. PCC 6803

Jianfeng Yu

Thesis submitted for the Degree of

Doctor of Philosophy

2013

Department of Life Science, Imperial College London

I hereby declare that this thesis, submitted in fulfilment of the requirement for the degree of Doctor of Philosophy of Imperial College London, represents my own work and that all else is appropriately referenced.

Abstract

FtsH proteases are found throughout nature and contain a conserved ATPase domain, flanked by an N-terminal transmembrane domain and a Zn^{2+}-binding protease domain. They play diverse roles in maintaining cellular activity. In the case of oxygenic photosynthetic organisms, FtsH-mediated degradation of damaged D1 protein is crucial for the operation of the photosystem II repair cycle needed to prevent photoinhibition. Four FtsH homologues are present in the model cyanobacterium *Synechocystis* sp. PCC 6803. One of these, FtsH2 (Slr0228), is known to be important for D1 degradation. However the structure of the FtsH2 complex is unknown and little is known about the structure and function of the other FtsH homologues. In this work, all four FtsH homologues were isolated via C-terminal GST tagging in tandem with affinity chromatography. Analysis of the purified FtsH complexes revealed the presence of FtsH1(Slr1390)/FtsH3(Slr1604) and FtsH2/FtsH3 heterocomplexes, whereas FtsH4 (Sll1463) appeared to form homocomplexes. Single particle analysis using electron microscopy revealed that the FtsH2-GST/FtsH3 complex was a hexameric particle of diameter ~120 Å with the two types of protomer alternately arranged around the central pore. Inactivation of the protease activity of FtsH2 did not abolish the function of the FtsH2/FtsH3 complex. FtsH2 and FtsH4 are mainly localised in the thylakoid membranes, whereas FtsH3 is dual targeted to both thylakoid and cytoplasmic membranes. FtsH1 is likely to be present in the cytoplasmic membrane. *In vitro* studies of *E. coli* over-expressed cytosolic domains of FtsH from *Thermosynechococcus elongatus* confirmed that the FtsH2, FtsH3 and FtsH4 homologues exhibited both ATPase and CTPase activity but that only FtsH4 could degrade casein. Homologues of *E.coli* YccA (Sll1150) and *Arabidopsis* EGY2 (Sll0862) were co-purified with the FtsH2-GST/FtsH3 complex. However, preliminary studies suggest neither is critical for FtsH-mediated D1 degradation. Strikingly, Psb29 (Sll1414) was found to be important for accumulation of FtsH2/FtsH3 complex, but further work is required to determine the mechanism.

Acknowledgements

Firstly, I would like to thank our collaborators, in particular Dr Jon Nield at Queen Mary University of London for solving the protein structure works, and Prof. Michael Hippler at University of Munster for processing the mass spectrometry samples. Their support and contribution are invaluable.

Secondly, I would like to thank Prof. Conrad Mullineaux and his team at Queen Mary University of London for helping us with fluorescence microscopy. I especially thank Dr Samantha Bryan and Miss Joanna Sarchaz for their kind support.

It was a pleasure to have worked along with Dr Marko Boehm at the beginning of this project, his guidance and support, both as friend and colleague has been inspirational. I would also like to thank Dr Myles Barker for his contribution in the preliminary work, of which paved way to the smooth progress of this project. I would like to offer special thanks to Dr Franck Michoux, who has been mentoring me when I first came to this lab as a master student, and equipped me with the essential skills I use daily in the lab. I am also grateful to the rest members in the photosynthesis groups, the friendly and active atmosphere is enjoyable, keep it up!

Finally, I sincerely thank my supervisor Prof. Peter Nixon for offering me such a great and unusual opportunity to become a PhD student. The past four years have been a life changing experience; I have learnt so much knowledge and improved logical thinking, though still not quite there yet. I really appreciate all the help and guidance from him.

Also, I acknowledge the funding body BBSRC and Imperial College London for supporting my study.

Contents

List of figures

List of tables

Abbreviations

ADP	adenosine diphosphate
APS	ammonium persulphate
APX	ascorbate peroxidase
ATP	adenosine-5'-triphosphate
β-DM	n-dodecyl-β-D-maltoside
bp	base pairs
BSA	bovine serum albumin
cab	chlorophyll a/b binding
CET	cyclic electron transport chain
Chl	chlorophyll
CtpA	C-terminal processing protease
CTP	cytosine-5'-triphosphate
Cx	X-fold symmetry
Cyt *b*559	cytochrome *b*559
Cyt *b6f*	cytochrome *b6f* complex
DCMU	3-(3,4-dichlorophenyl)-1,1-dimethylurea
dNTP	2'deoxyribonucleoside triphosphate
ΔpH	proton gradient
EDTA	ethylenediaminetetraacetic acid
EF-G	elongation factor G
EM	electron microscopy
FNR	ferredoxin-$NADP^+$ reductase
FRP	fluorescence recovery protein
FtsH	filament temperature sensitive H
GFP	green fluorescent protein
GST	glutathione *S*-transferase
GTP	guanosine-5'-triphosphate
GWP	global warming potential
HEPES	4-(2-hydroxyethyl)-1-piperazineethanesulfonic acid
Hv	light
i-AAA	inter-membrane space facing mitochondrial FtsH family protease
iD1	intermediate D1
IPTG	isopropyl-ß-D-thiogalactopyranoside
kb	kilo base pairs
kDa	kilo Dalton
LB	Luria-Bertani medium
LET	linear electron transport chain
LHCI/II	light-harvesting complex on photosystem I or photosystem II

LPS	lipopolysaccharide
m-AAA	matrix facing mitochondrial FtsH family protease
MOPS	3-(N-morpholino)propanesulfonic acid
NADP+	oxidised β-nicotinamide adenine dinucleotide phosphate
NADPH	reduced β-nicotinamide adenine dinucleotide phosphate
NPQ	non-photochemical chlorophyll fluorescence quenching
NrtA	nitrate/nitrite transport system substrate-binding protein
OCP	orange carotenoid binding protein
$ODX_{(nm)}$	optical density at X (nm) wavelength
OEC	oxygen-evolving complex
P680	primary electron donor of photosystem II
P700	primary electron donor of photosystem I
PAA	polyacrylamide
PAGE	polyacrylamide gel electrophoresis
PBS	phosphate buffered saline
PC	plastocyanin
PCR	polymerase chain reaction
PD	protease domain
pD1	precursor D1 protein
PDM	PratA-defined membrane
Phe	pheophytin
PQ	plastoquinone
PSI	photosystem I
PSII	photosystem II
QA	plastoquinone molecule bound to D2
QB	plastoquinone molecule bound to D1
qE	energy-dependent non-photochemical chlorophyll fluorescence quenching
qI	photoinhibitory non-photochemical chlorophyll fluorescence quenching
qT	state-transition non-photochemical chlorophyll fluorescence quenching
RC	reaction-centre complex
RNA	ribonucleic acid
RO	reverse osmosis
ROS	reactive oxygen species
rpm	rounds per minute
Rubisco	ribulose 1,5-biphosphate carboxylase/oxygenase
S0-4	manganese cluster water oxidation centre S-states 0-4
SbtA	sodium bicarbonate transporter A
SDS	sodium dodecyl sulphate
SRH	second region of homology
TAE	tris-acetate-EDTA buffer
TE	tris-EDTA buffer
TEM	transmission electron microscopy
TEMED	N-N-N’-N’-tetramethylethylenediamine

TES	N-tris[hydroxymethyl]methyl-2-aminoethanesulfonic acid
Tg	teragram
TM	transmembrane domain
TPR	tetratricopeptide repeat protein
Tris	2-amino-2-hydroxy-methylpropane-1,3-diol
TW	terra (10^{12}) Watts
Tween-20	polyoxyethylene sorbitan monolaurate
UTP	uridine-5'-triphosphate
UTR	untranslated region
UV-B	ultraviolet light
v/v	volume per volume
w/v	weight per volume
WT	wild-type
WT-G	glucose-tolerant wild-type
X-Gal	5-bromo-4-chloro-3-indolyl-β-D-galactopyranoside
Y_D	redox active tyrosine on D2
Y_Z	redox active tyrosine on D1

Chapter 1: General introduction

1.1 The evolutionary and global impact of photosynthesis

Photosynthesis is the process that converts light energy into chemical energy; it captures light energy and stores it in chemical bonds by converting carbon dioxide from the atmosphere into organic compounds such as sugar (Arnon 1971). This process provides food, fuel and materials that are essential to daily life (Barber and Tran 2013). The release of dioxygen through oxygenic photosynthesis has had a great evolutionary impact on directing the evolution of life forms on earth (Kerr 2005). Free oxygen did not exist in the earth atmosphere until ~2 billion years ago, at which point oxygen produced by photosynthesis gradually accumulated and shifted the reducing atmosphere of earth to an oxidizing form; oxygen-breathing life forms did not appear until the oxygen level stabilized at ~20 % of atmospheric composition (Brimblecombe and Davies, 1981).

Nowadays, mankind is facing great challenges from food shortages, over-consumption of fossil fuels and climate change caused by excessive emission of CO_2 (Harries et al. 2001). Understanding photosynthesis could potentially help to tackle these problems by improving crop yields, producing renewable energy and more efficiently capturing CO_2 from the atmosphere.

According to figures released in the "Global Environment Outlook environment for development (GEO-4)", released by the end of 2007 by United Nations, the world population in 2007 was 6.7 billion, three times larger since the beginning of the 20th century. Moreover, the increase between 1987 and 2007 was 1.7 billion, a 34 % rise of population within the past 20 years; in other words, the growth of population has accelerated. The UN predicted the world population will hit 8 billion in the year 2025, which is another 20 % increase; the consequent demand for food and energy has been

listed as one of the top priorities by officials. Meanwhile, the land suitable for agriculture is limited and so to prevent environmental degradation and loss of biodiversity, therefore, it is crucial to increase yields on existing cropland (Cassman 1999; Tilman et al. 2002).

How to power 8 billion people through the 21st century is another problem. Certainly the reliance on fossil fuel is unsustainable and catastrophic, not only because the fossil fuel sources are depleting rapidly, but also the release of CO_2 into the atmosphere directly promotes global warming (Harries et al. 2001). The global surface temperature has increased 0.74 ± 0.18 ^{o}C between the start and the end of the 20th century (IPCC); further climate warming may reduce the stability of marine dissolved methane hydrate, and hence increase the methane seepage rate from 30 Tg to 90 Tg per year (Hill et al. 2006). Methane is a greenhouse gas which has a global warming potential (GWP) value of 25, whereas for carbon dioxide it is 1. The large emission of methane is likely to worsen the current climate change issues. Therefore, exploring alternative, carbon-neutral energy sources is essential and urgent for mankind before ecosystems get irreversibly damaged.

To generate the 20 TW of power that mankind requires per year, solar energy with a theoretical annual availability of 100,000 TW (Barber 2007) out competes others like water hydroelectric (~ 4.6 TW) and wind (50 TW) (de Winter and Swenson, 2006). On the other hand, the conversion of solar energy into biomass by photosynthesis is rather inefficient, currently between 0.1 and 1 % (Barber 2007). Storing 20 TW of power into biomass would mean that 30 % of the entire land area on Earth needs to be cultivated (Barber 2007). Therefore, there is a necessity and a huge potential to increase the efficiency of solar energy conversion. One possible route is to reduce the impact of photoinhibition on photoautotrophs when exposed to excessive light illumination, so as to help keep the photosynthetic system operating under stressful

conditions. As part of this goal, this thesis aims to characterise the FtsH family of proteases which play a major role in protecting photosynthetic organisms against light damage.

1.2 The molecular mechanisms of photosynthesis

Photosynthesis has been investigated over centuries so that the major chemical reactions and many of the molecular machineries participating in photosynthesis are now known in detail. To review the progress towards understanding photosynthesis, important milestones achieved in the history of photosynthesis research are described in the following paragraphs.

The foundation of photosynthesis research was established by Jan Ingenhousz in 1779, when he discovered that light plays an important physiological role in plants. Since then, it took almost a century to formulate the first minimal balanced chemical equation of photosynthesis (See Equation 1.1).

$$CO_2 + H_2O \rightarrow (CH_2O) + O_2 \qquad \textbf{(Equation 1.1)}$$

However, the equation was formulated based on oxygenic photosynthesis, which is performed by cyanobacteria, algae and plants, and cannot apply to anoxygenic photosynthetic organisms, e.g. green sulphur and purple bacteria. With a deeper understanding of both oxygenic and anoxygenic pathways, in 1931, Cornelis van Niel formulated a refined photosynthesis equation that is adaptable to both pathways (See Equation 1.2).

$$2H_2A + CO_2 \rightarrow (CH_2O) + 2A + H_2O \qquad \textbf{(Equation 1.2)}$$

van Niel's equation was proposed based on the hypothesis that both oxygenic and anoxygenic photosynthesis share similar metabolic pathways in which a hydrogen donor (H_2A) was photodissociated and the released proton is used in the light-independent reaction to catalyse the reduction of CO_2 to form carbohydrates.

In general, photosynthesis is a two-step process that begins with the light-dependent

reaction, where light energy is used to initiate electron flow across photosynthetic complexes, which subsequently drives the light-independent reactions, also known as Calvin-Benson cycle, by supplying ATP to aid the fixation of CO_2 into carbohydrates (Arnon 1971). The key feature that differentiates oxygenic photosynthesis from the anoxygenic pathway lies in the light-dependent reaction, where H_2O is split inside photosystem II to produce electrons, protons and O_2 molecules. Notably, unlike electrons and protons, which immediately participate in subsequent reactions, the molecular oxygen released from water splitting is a by-product of oxygenic photosynthesis which does not contribute to downstream reactions (Figure 1.1). In contrast, organisms performing anoxygenic photosynthesis are lacking photosystem II, hence unable to catalyse H_2O as the electron donor.

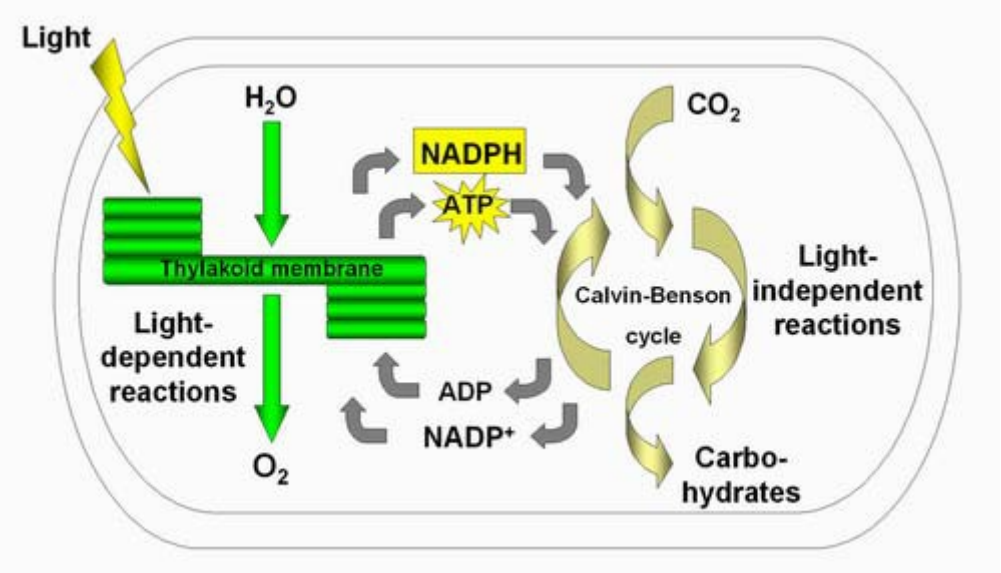

Figure 1.1: Schematic representation of oxygenic photosynthesis.
The key reactants involved in the light-dependent and light-independent reactions of oxygenic photosynthesis are represented in this cartoon. For further details refer to text.

Over the past centuries, photosynthesis has always been considered an important topic and has been studied extensively. Benefiting from recent technologies, a number of breakthroughs, especially in the field of structural biology, have been made in the last

decade. The major events in photosynthesis are now mostly understood, including the structures of many photosynthetic complexes (see section 1.2.2 and 1.2.3), the nature of the linear electron transport chain (LET) and the CO_2 fixation pathway (see section 1.2.1). On the other hand, there are still important gaps in knowledge that need to be filled, including the regulatory mechanisms underpinning the assembly and turnover of photosynthetic protein complexes, and the control and mechanisms of cyclic electron flow (CET).

1.2.1 Linear electron transport chain of oxygenic photosynthesis

Unlike the anoxygenic pathway that is only adopted by a limited number of photosynthetic bacteria, oxygenic photosynthesis is a highly conserved process performed by the majority of photosynthetic organisms, including cyanobacteria, algae and plants. Four protein complexes, photosystem II (PSII), cytochrome b_6f (Cyt b_6f), photosystem I (PSI) and ATP synthase, participate in the light-dependent reaction of oxygenic photosynthesis (Figure 1.2). Notably, PSII is unique to oxygenic photosynthesis, and also it is where the linear electron transport chain (LET) begins. When light energy is captured by the light-harvesting antenna of PSII, excitation energy is passed to the primary electron donor P680 (P for pigment, 680 for maximum absorption at 680nm) which triggers electron flow. The oxidising potential of $P680^+$/P680 is sufficient to drive the splitting of water at the oxygen-evolving complex (OEC), a Mn_4Ca cluster located on the lumenal side of PSII. The generated electrons are transferred to Cyt b_6f, a plastoquinol:plastocyanin oxidoreductase, via the plastoquinone pool, and then passed to PSI via plastocyanin. Notably, the passage of electrons within Cyt b_6f further increases the proton concentration in the lumen. The pH gradient (ΔpH) across the thylakoid membrane drives the ATP synthase and ATP is produced when protons in the lumen pass through the transmembrane channel of the ATP synthase. Similar to PSII, PSI uses photons to elevate the energy of electrons on the electron donor P700, with the released electron ultimately passed to

ferredoxin, which subsequently produces NADPH via the ferredoxin-$NADP^+$ reductase (FNR). NADPH is the main reducing molecule used in the Calvin-Benson cycle to produce carbohydrates. Oxidised $P700^+$ is subsequently reduced by an electron donated by reduced plastocyanin. Therefore, electrons from the oxidation of water are passed between PSII, Cyt b_6f and PSI in series, where the product of one becomes the substrate of the other (Hill and Bendall, 1960; Hill and Rich, 1983). The electron energy is elevated in PSII and PSI to enable electron flow through the LET, which is plotted as the Z-scheme of oxygenic photosynthesis (Figure 1.2 A).

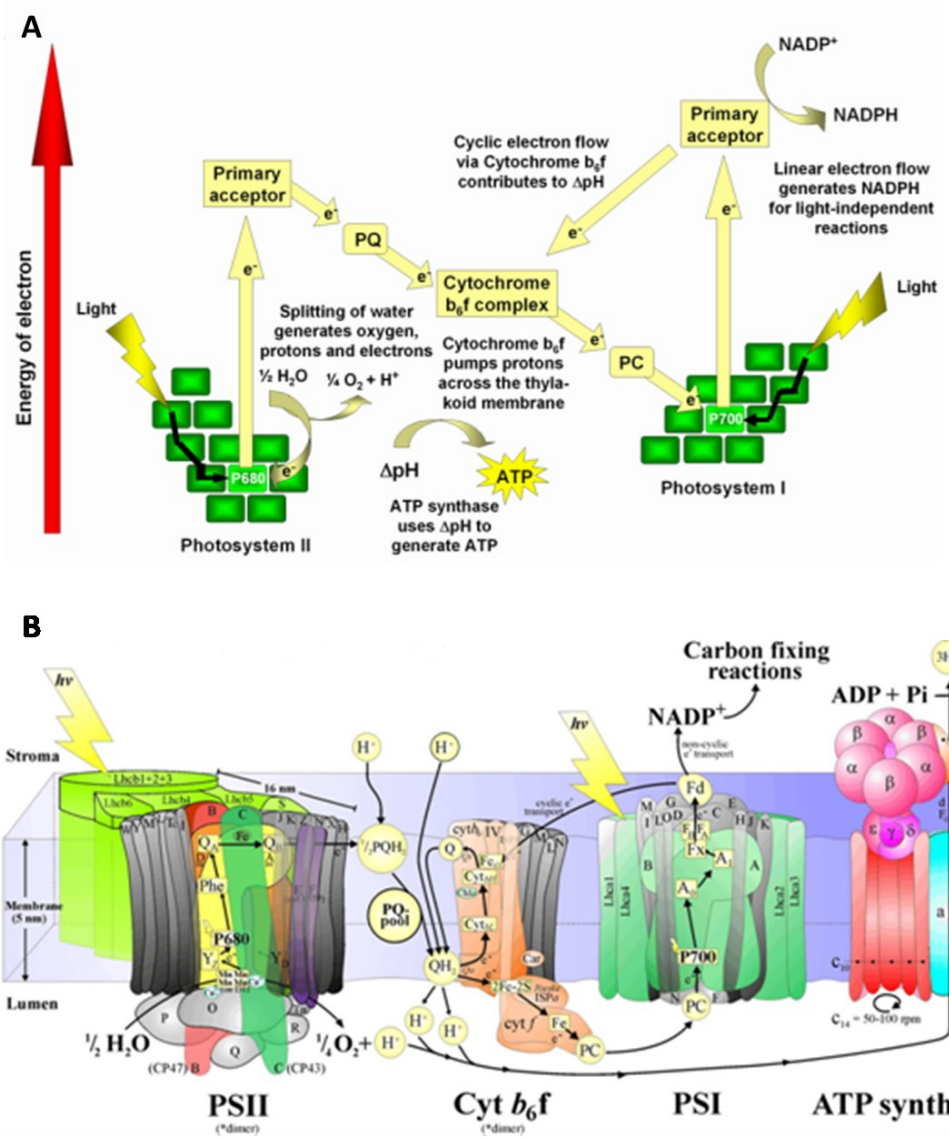

Figure 1.2: Higher plant photosynthetic electron transport.

(A) Schematic representation of the electron transport chain of oxygenic photosynthesis (Z-scheme). P680 and P700, primary electron donors of photosystem II and photosystem I respectively; e-, electron; PQ, plastoquinone; PC, plastocyanin. (B) The thylakoid membrane in chloroplasts. PSII, Cyt b_6f, PSI and ATP synthase protein complexes are depicted and labelled with subunit name (for example, Q is PsbQ in PSII and B is PsaB in PSI). Annotation: photons (*hv*) are absorbed by the PSII and PSI antenna (Lhcb and Lhca, respectively) which feed the PSII and PSI reaction centre chlorophylls (P680 and P700, respectively). PSII: P680, primary electron donor; Phe, pheophytin; Y_Z and Y_D, tyrosine Z and D; Q_A and Q_B, quinone electron acceptors; PQ, plastoquinone. Cyt b_6f: Fe_{ci}, iron-sulphur centre; Cyt_{bH}/Cyt_{bL}, cytochrome *b* high/low potential, Q, quinone molecule. PSI: PC, plastocyanin; P700, primary electron donor; A_0, chlorophyll 0; A_1, phyloquinone molecule; F_X/F_A/F_B iron-sulphur centres, Fd; ferredoxin, ATP synthase: CF_1, chloroplast coupling factor 1; CF_O, chloroplast coupling factor O. Figure adapted and updated from Nield (1997) by Dr. J. Nield (Imperial College, London).

1.2.2 Major differences between cyanobacterial and chloroplastic systems

Both cyanobacteria and chloroplasts perform oxygenic photosynthesis. Although there are many features exclusively adapted to each system, the major photosynthetic machineries inside cyanobacteria and chloroplasts share significant similarities that have been retained through evolution. The light-dependent reactions in both systems occur within the thylakoid membrane via LET through PSII, Cyt b_6f, and PSI with ATP made at the ATP synthase. Overall the structure and function of the four protein complexes are highly conserved. The major differences that distinguish the two systems are the dynamic arrangement of the thylakoid membrane (Andersson and Anderson 1980; Mullineaux 1999) in chloroplasts and the different light-harvesting antenna complexes attached to the photosystems (Grossman et al. 1995; Grossman et al. 1993).

In chloroplasts, the shape of thylakoid membranes can switch between stacked disk-shape cylinders (grana or appressed lamellae) and interconnecting membranes sheets (stroma or non-appressed lamellae), depending on the light intensity (Andersson and Anderson 1980). The dynamic membrane system is believed to be a regulatory mechanism that controls the reception of light-energy into the system. PSII and the respective light-harvesting antenna complexes are mainly located in the grana lamellae, whereas PSI and its antenna, along with ATP synthase are only located in the stroma lamellae (Dekker and Boekema 2005). Moreover, the Cyt b_6f protein complex is evenly distributed across thylakoid membranes (Allred and Staehelin 1986). On the other hand, thylakoid membranes in the cyanobacterium *Synechocystis* sp. PCC 6803 (hereafter *Synechocystis*) are present as three to ten concentric circular sheets near the cytoplasmic membrane (Figure 1.5), and the protein distribution is rather homogeneous, although more PSI complexes have been found in the outermost layers (Sherman et al. 1994).

Light-harvesting antennae are membrane protein complexes that interact with the photosystems. Their role is to capture additional light-energy and feed it to the photosynthetic electron transport chain (Grossman et al. 1995). The antennae in chloroplasts are termed light-harvesting complexes (LHCI for PSI and LHCII for PSII), containing both chlorophyll *a* and *b*. The antennae in cyanobacteria on the other hand, are phycobilisomes, in which biliprotein-rods are arranged in a fanlike-fashion around a biliprotein-core. Unlike light-harvesting complexes in chloroplasts, phycobilisomes are peripheral membrane proteins (Grossman et al. 1993; Hankamer et al. 2001).

It is also worth noting that the composition of PSII in chloroplasts is very similar, but not identical, to that in cyanobacteria. The major difference occurs in the identity of the peripheral subunits: PSII in chloroplasts contains PsbP and PsbQ, instead of PsbU and PsbV in cyanobacterial PSII, bound to the lumenal side of the complex. However, distant homologues of PsbP and PsbQ are found in cyanobacteria but their role remains unresolved (Nixon et al. 2010). In addition, PsbR and PsbTn, which have no cyanobacterial counterpart, also appear to be extrinsically attached to the OEC of chloroplast PSII (Barber et al. 1997). Nevertheless, the core structure of PSII from both eukaryotic and prokaryotic organisms, which includes D1, D2, CP43, CP47 and the oxygen-evolving complex, is highly conserved (Fig 1.3).

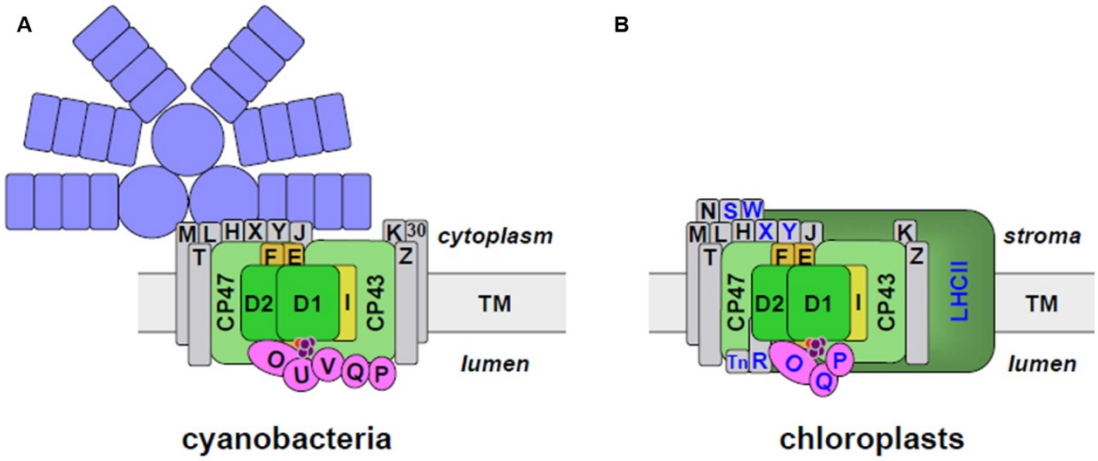

Figure 1.3: Schematic representation of subunit composition of PSII..
Homologous proteins from cyanobacteria (A) and chloroplasts (B) are labelled in identical colours. PSII subunits represented in gray boxes are proteins designated as Psb*, where * is the letter labelled in the box (e.g. "I" for PsbI). The dark yellow boxes labelled E and F represent cytochrome b_{559} (Cyt b_{559}), and the extrinsic subunits are plotted as pink circles. The large, fan-shape structure in blue represents the light-harvesting antenna complex on top of the cyanobacterial PSII, whereas, its counterpart in chloroplast is labelled LHCII and presented as a dark-green box flanking the subunits. This figure is adapted from (Nickelsen and Rengstl 2013).

1.2.3 Insight into the structure and function of cyanobacterial PS II

PSII is a light-driven water:plastoquinone oxidoreductase, which catalyses oxygen evolution at the OEC (Nixon et al. 2010b). In the past 10 years there has been dramatic progress in understanding the structure of PSII from cyanobacteria (Ferreira et al. 2004; Liu et al. 2004; Umena et al. 2011; Zouni et al. 2001).

Overall, PSII is a large protein-pigment complex that resides in the thylakoid membrane. The latest crystal structure revealed that each monomer in dimeric cyanobacterial PSII consists of 17 transmembrane subunits and 3 peripheral subunits, 35 chlorophylls, two pheophytins, 11 β-carotenes, more than 20 lipids, two plastoquinones, two haem irons, one non-haem iron, four manganese atoms, three or four calcium atoms, three Cl^- ions and one bicarbonate ion, with a total molecular mass of 350 kDa (Umena et al. 2011).

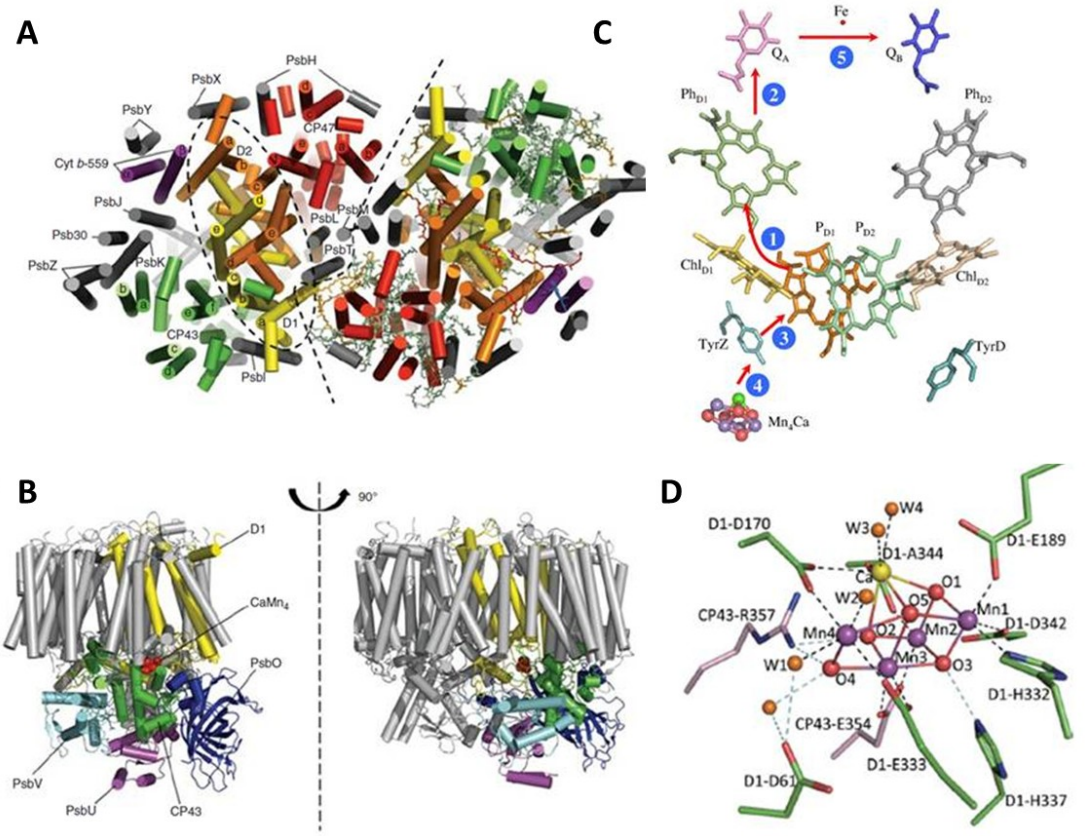

Figure 1.4: Structural details of cyanobacterial PSII.
(A) View from the cytoplasmic side of the membrane. The two monomers are separated by a black dashed line and the α-helical elements of each subunit are represented as cylinders. D1 (yellow), D2 (orange), CP43 (green), CP47 (red), cytochrome *b*-559 (purple) and the remaining 11 small sub-units (grey) are indicated in the monomer on the left side as well as the D1–D2–Cyt b-559 subcomplex (elliptical black dashed circle). The same colour coding system applies to the monomer on the right side where are also represented the co-factors of PSII: chlorophylls (green), carotenoids (orange), pheophytins (yellow), plastoquinones (red) and haem (blue). The co-factors are shown in stick form. (B) Two side views, differing by a rotation of 90˚, showing the lumenal subunits PsbO (dark blue), PsbV (light blue), PsbU (purple) and the large lumenal loop of CP43 interconnecting transmembrane helices e and f (green) that lies close to the Mn_4Ca cluster. Panel A and B are adapted from (Nixon et al. 2010a). (C) Schematic representation of charge separation within PSII reaction centre (Cardona et al. 2012). (D) The Mn_4Ca cluster and surrounding protein environment, purple; calcium, yellow; oxygen, red; D1, green; CP43, pink (Umena et al. 2011).

D1, D2, CP43 and CP47 are intrinsic transmembrane subunits of PSII located in the centre of the complex (Figure 1.4 A), which play essential roles in coordinating the OEC, positioning pigments and docking the plastoquinones that participate in

light-induced electron transport within the complex (Figure 1.4 B). The initial light-induced charge-separation is driven by P680, which is a cluster of pigments composed of four chlorophyll *a* (P_{D1}/P_{D2} and Chl_{D1}/Chl_{D2}) and two pheophytin a molecules (Ph_{D1}/Ph_{D2}) that absorb around 680 nm (Figure 1.4 C). Shortly after excitation, the excited state of P680 is stabilised by initiating electron transfer among the co-factors. Firstly, P680 donates an electron to pheophytin, Ph_{D1}, thence to the first quinone, Q_A, which acts as a one electron redox couple linking Ph_{D1} to the second quinone, Q_B. After electron donation, $P680^+$ is subsequently reduced by electron transfer from OEC via a tyrosine residue on D1, called Tyr_z or Y_z.

The detailed structure of OEC, the catalytic centre where water is split to produce electrons and molecular oxygen, from *T. vulcanus* was solved via X-ray crystallography (Umena et al. 2011). It is a cubic Mn_4CaO_5 cluster that is progressively oxidised by Yz to enable substrate water molecules to be oxidised (Figure1.4 D). The detailed water oxidation process is still not fully understood, however, the model proposed by Kok *et al.* in 1970 (Kok et al. 1970), also known as the Kok cycle, is largely consistent with the available experimental evidence. According to the Kok cycle model, the OEC exists in 5 different S-states or oxidation states. Stepwise oxidation of the S-states occurs upon each turnover of the PSII reaction centre with oxidation of water triggered by formation of the S_4 state. Even though the structure of the OEC has been solved, and artificial oxygen-evolving catalysts inspired by and sharing structural similarities with the OEC have been successfully developed (Rivalta et al. 2012; Symes et al. 2013), the mechanism of water splitting is unknown. The X-ray crystal structure of PSII identified 4 water molecules within hydrogen bonding distance of the Mn_4CaO_5 cluster, of which two (W2 and W3) (Figure 1.4 D) may be possible substrates of the reaction. However, it still cannot be excluded that one of the oxo-bridges in the OEC, at O5, is involved in forming molecular oxygen (Umena et al. 2011). Furthermore, protons released from

water oxidation are likely to be channelled out of the complex via a hydrogen-bond network (Umena et al. 2011).

1.3 Cyanobacteria as model organisms in photosynthesis research

Cyanobacteria are related to the most ancient prokaryotes that able to perform oxygenic photosynthesis, and are closely related to the organisms that gave rise to chloroplasts in plants and eukaryotic algae via endosymbiosis (Gould et al. 2008). Like chloroplasts, cyanobacteria perform photosynthesis via protein complexes embedded in a thylakoid membrane system (Figure 1.3). Because of the strong structural and genetic similarities between photosynthetic systems in cyanobacteria and chloroplasts, cyanobacteria are often used as model organisms to study photosynthesis.

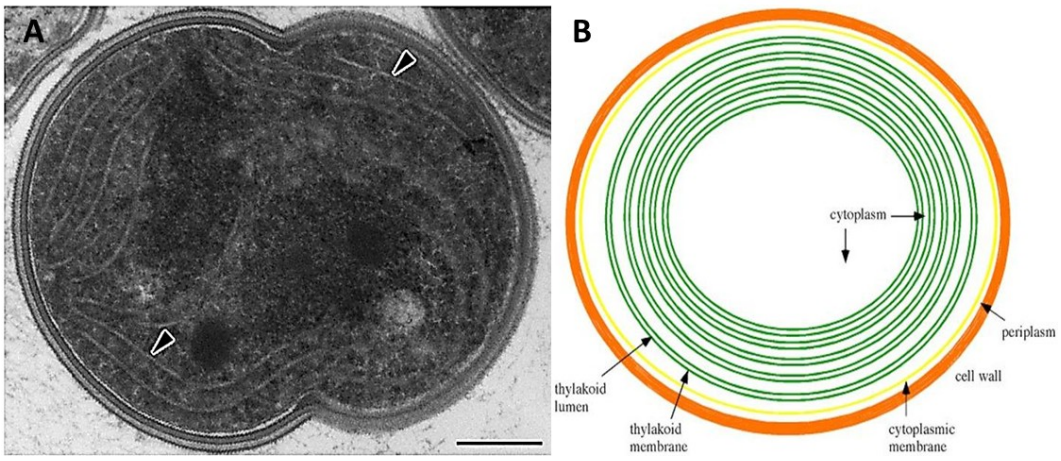

Figure 1.5: Membrane systems in a *Synechocystis* cell.
(A) Transmission electron micrograph of a dividing *Synechocystis* cell illustrating thylakoid membranes (arrowheads) that occur along the periphery of the cytoplasm. Scale bar = 400 nm. (B) Schematic overview of a cyanobacterial cell. Indicated are: thylakoid membranes (green) that contain photosynthetic and respiratory complexes and that separate the cytoplasm from the lumen; the cytoplasmic membrane (yellow) that separates the cytoplasm from the periplasm; and the outer membrane and cell wall. (Adapted from Vermaas 2001).

The cyanobacterium *Synechocystis* sp. PCC 6803 (hereafter *Synechocystis*) is one of the model strains used in photosynthetic research. It can grow both

photoautotrophically and photoheterophically (Okamoto et al. 1999; Williams 1988a); it is naturally transformable (Adami et al. 2005; Williams 1988a) and its genome has been fully sequenced.

Synechocystis is a great tool to study the function of genes *in vivo*, as it is very easy to transform and fast growing, which means obtaining a mutant is usually possible within a time-frame of 1-2 months. More importantly, a natural mutant of *Synechocystis*, namely the glucose-tolerant wild-type strain (hereafter WT-G), is capable of using glucose as an alternative carbon source in the absence of PSII activity, hence inactivation of photosynthesis in this strain does not result in lethality in the presence of low concentrations of glucose (Williams 1988b). Furthermore, *Synechocystis* cells can be easily stored under cryo-conditions to reduce the chance of incurring spontaneous mutations during long periods of maintenance.

On the other hand, for protein structural studies, another cyanobacterium, namely *Thermosynechococcus elongatus*, has proven more advantageous. *T. elongatus* is a thermophilic strain, originally found in a hot spring, which has an optimal growth rate at 55^{o}C, hence the proteins in this strain are more thermo-stable which offers a better chance to yield structural data. Structures of many cyanobacterial proteins, including PSII (Ferreira et al. 2004), were solved using native or *E. coli* over-expressed recombinant protein of *T. elongatus*, e.g. Psb27 (Michoux et al. 2012). Although many mutants have been made in this organism in the past decade, transformation of *T. elongatus* is still a great challenge. Although *T. elongatus* has been shown to be naturally transformable in some labs (Onai et al. 2004), most transformation protocols require a combination of electroporation and a delicate recovery growth period (Iwai et al. 2004), which is difficult to reproduce under different laboratory environments. Also, unlike strain WT-G of *Synechocystis*, none of the *T. elongatus* strains has been found capable of using an alternative carbon source, therefore, it is difficult to study

genes encoding essential photosynthetic proteins via mutagenesis. Overall, *Synechocystis* is a preferred strain to study the physiological functions of proteins *in vivo*, whereas proteins of *T. elongatus* are more desirable for *in vitro* applications.

1.4 The current model of PSII *de novo* assembly

PSII is a large protein-pigment complex consisting of at least 20 subunits and localised in the thylakoid membrane (see section 1.2.2 and 1.2.3). The assembly of PSII is a highly organised event involving auxiliary proteins (see section 1.4.1). In both cyanobacteria and chloroplasts, the *de novo* assembly of PSII is spatially organised (see section 1.4.2).

1.4.1 The assembly of PSII

Currently, the assembly of PSII is considered to occur by two distinctive pathways (reviewed by (Nickelsen and Rengstl 2013)): (1) the *de novo* assembly of PSII and (2) the PSII repair cycle (see section 1.5.4). The investigation of PSII assembly has been mostly based on analysing the subunit composition of intermediate complexes that are blocked at different stages of assembly either in mutants lacking essential PSII subunits or lacking auxiliary proteins assisting the assembly process (Nickelsen and Rengstl 2013). PSII is a massive complex consisting of at least 20 subunits and there are still many gaps in the model to be filled. Nevertheless, a few key stages of PSII assembly have now been elucidated. It is thought that assembly of PSII requires coordination of protein synthesis, translocation, post-translational modification and the biosynthesis of co-factors and the lipid bilayer membrane. In the case of eukaryotic cells, in which many photosynthesis-related proteins are encoded by the nuclear genome, gene expression is also regulated between the nuclear and chloroplast genomes (Zhang et al. 2009). As would be expected from their close evolutionary relationship, many aspects of PSII assembly are rather conserved in cyanobacteria, green algae and higher plants.

The assembly of PSII begins with the formation of reaction-centre complex (RC), where the D1 and D2 subunits form a hetero-dimeric complex. The integration of D1 requires assistance from several auxiliary protein assembly factors. The precursor D1 subunit (pD1) requires Alb3/Oxa1/YidC family insertases (Slr1471, Alb3) to aid folding and integration into the thylakoid membrane (Ossenbuhl et al. 2004; Ossenbuhl et al. 2006), CtpA (C-terminal processing protease) is also required to cleave the C-terminal extension of pD1 leaving space to dock the OEC and extrinsic proteins (Roose and Pakrasi 2004). Interestingly, unlike in plants, where the 9 residues at the C-terminal extension is removed by CtpA in a single step, the 16 residues at the C-terminus of cyanobacterial D1 is cleaved in two steps, giving rise to an intermediate form of D1 (iD1) which is mainly detected in the RC (Komenda et al. 2007a). Although the C-terminal extension is not essential for the assembly of PSII, mutants lacking the extension region exhibit decreased fitness (Ivleva et al. 2000; Kuvikova et al. 2005), indicating the D1 processing step contributes towards correct assembly. PratA, a periplasmic, tetratricopeptide repeat (TPR) protein, is another assembly factor found associated with formation of the RC complex in cyanobacteria. PratA is thought to act as a molecular scaffold for the assembly process and is potentially involved in the C-terminal processing of pD1. More importantly, it has been shown to deliver Mn^{2+} to D1, providing hints that the formation of OEC begins at very early stage of PSII *de novo* assembly (Klinkert et al. 2004; Schottkowski et al. 2009a; Stengel et al. 2012). D2 plays a dominant role in accumulation of chlorophyll *a* (Komenda et al. 2004), which raises the possibility that the D2 sub-complex might act as an anchor for enzymes involved in chlorophyll biosynthesis and subsequent loading of the pigments into the RC (Komenda et al. 2012b). An early integration of co-factors is generally believed to be beneficial as the co-factors would no longer require carriers to translocate through membrane interfaces and also potential toxicity is minimised. From the protein point of view, efficient integration of co-factors can also stabilise the apoproteins and avoid unnecessary degradation (Eichacker et al.

1996; Komenda et al. 2012b).

Formation of the RCII complex is thought to be aided by the Ycf48 assembly factor (HCF136 in *Arabidopsis thaliana*). Ycf48 is a seven-bladed beta-propeller that is believed to play a scaffolding role to stabilise the complex (Nixon et al. 2010b). Notably, although evidence of direct interaction between Ycf48 and D1 is still lacking, data from yeast two-hybrid analysis showed that Ycf48 interacts with pD1 but not with mature D1 (Komenda et al. 2008). The RC complex is then attached to one of the two inner antenna-proteins CP47 to form the RC47 complex (Boehm et al. 2011). The PAM68 auxiliary protein appears to play an important role in assembly of larger PSII complexes derived from the RC, and is currently thought to play a bridging role between PSII core proteins in the assembly process. Psb28 is another assembly protein identified at this stage (Kashino et al. 2002; Shi et al. 2012). Although the structure of Psb28 has been solved, little is known about its function (Yang et al. 2011). Physiological analysis showed that Psb28 might play a role in chlorophyll biosynthesis and/or be associated with the biosynthesis of the inner-antenna protein CP47, and the PSI subunits PsaA and PsaB (Dobakova et al. 2009).

Some PSII assembly factors display more diverse cellular functions, in particular, exhibiting interactions with multiple proteins and even PSI subunits, e.g. Psb28. Assembly factor Psb27 is a lumenal lipoprotein that binds transiently to CP43, monomeric PSII and even dimeric PSII and PSI (Komenda et al. 2012a; Nowaczyk et al. 2006; Roose and Pakrasi 2008). The major function of Psb27 might be to prevent premature binding of extrinsic subunits to enable post-translational processing at the lumenal side of the complexes (Roose and Pakrasi 2008). Strikingly, deletion of LPA19, the homologue of Psb27 in *A. thaliana*, results in impaired C-terminal processing of pD1, and disruption of the second homologue Psb27-H1 leads to decreased PSII repair efficiency (Chen et al. 2006). Therefore, in plants, the functions

of the two homologues of Psb27 seem to have diverged (Nickelsen and Rengstl 2013). Available data suggest Sll0606 (in *Synechocystis*), LPA2 and LPA3 (in *A. thaliana*) are auxiliary proteins involved in assembly of CP43, the second inner-antenna. Surprisingly, the three proteins share no homology, suggesting that PSII assembly at this stage diverged between prokaryotes and eukaryotes.

Upon attachment of the CP43 sub-complex, the extrinsic subunits dock onto the lumenal side of PSII. Two assembly factors from *A. thaliana* have been implicated to assist the process, CYP38 and LTO1. CYP38 is a member of the immunophilin family that mediates immune suppression (Nickelsen and Rengstl 2013), and is believed to bind to the E-loop of CP47 and assist D1 folding (Vasudevan et al. 2012), whereas, LTO1 is a lumenal thiol oxidoreductase that catalyzes the formation of disulphide bonds in PsbO (Karamoko et al. 2011). Several proteins have been suggested to involve in the dimerization of PSII, including Alb3 insertase and FKBP20-2 in *A. thaliana*.

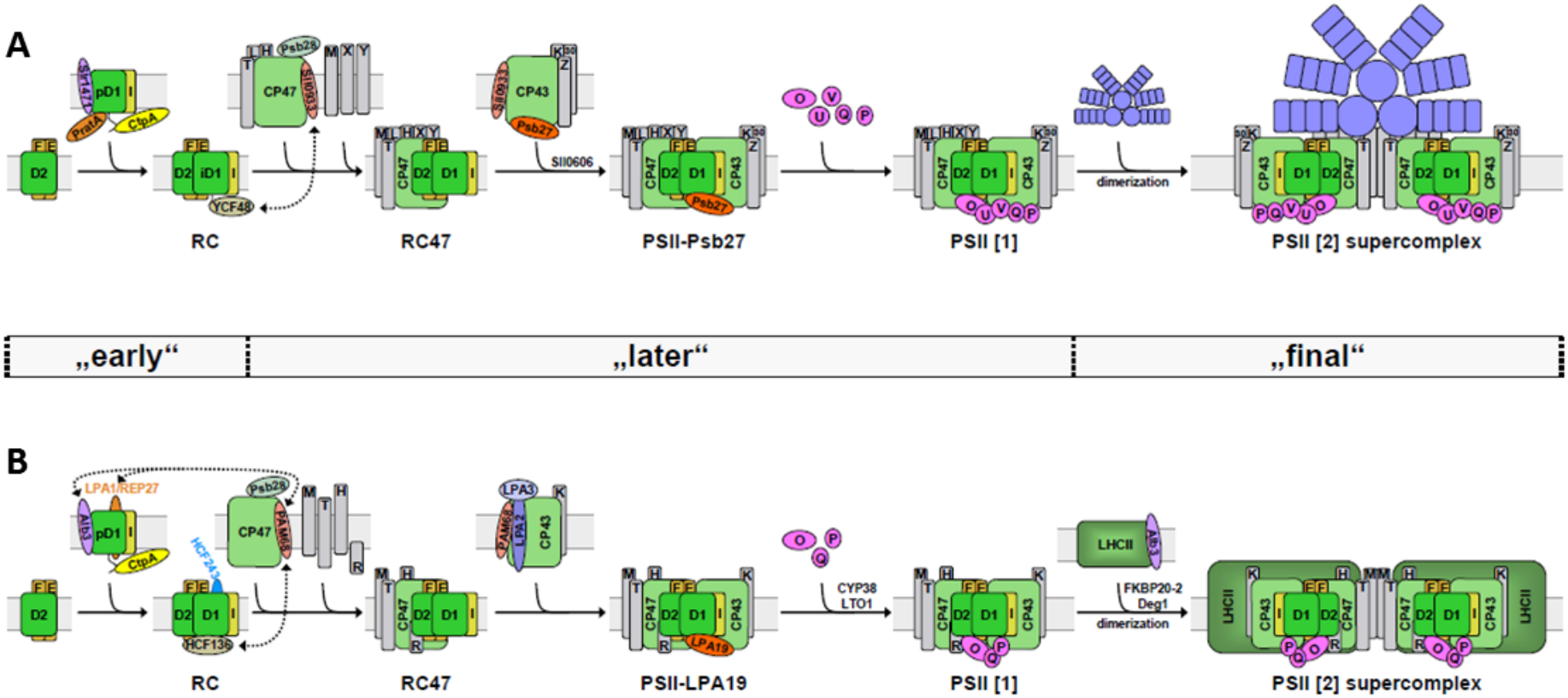

Figure 1.6: De novo assembly of PSII in (a) cyanobacteria and (b) chloroplasts.

The PSII assembly process between cyanobacterial and chloroplast are comparatively similar and defined into three stages: early, late and final. Homologous proteins are labelled in identical colours. The auxiliary proteins assisting the assembly process at each stage are shaped in ovals. PSII subunits represented in gray boxes are proteins designated as Psb*, where * is the letter labelled in the box (e.g. “I” for PsbI). The dark yellow boxes labelled E and F represent Cyt b_{559}. This figure is adapted from (Nickelsen and Rengstl 2013).

1.4.2 The localisation of PSII assembly

Assembly of PSII appears to be a highly organised event occurring at distinctive regions of the membrane (Stengel et al. 2012). In the case of the cyanobacterium *Synechocystis*, the *de novo* assembly of the D1/D2 reaction centre is located in specific membrane regions termed the PratA-defined membrane (PDM) due to the enriched accumulation of membrane-associated PratA (Schottkowski et al. 2009a). PratA is an auxiliary protein of PSII assembly involved in the maturation of pD1 (see section 1.4.1). Localisation studies showed PratA is also required for correct localisation of some PSII assembly factors such as Ycf48 and Slr1471, indicating PratA is not only a resident, but also involved in the development of the PDM region (Rengstl et al. 2011). Interestingly, PratA is a periplasmic protein, which does not have direct contact with the internal thylakoid membrane system. Therefore, PDM is believed to be localised at the junctions where thylakoid and cytoplasmic membranes make contact (Figure 1.5), so that assembled RC can be transported to thylakoid membranes for the subsequent assembly steps. It is worth noting that the composition of PDM has been experimentally confirmed to have both cytoplasmic and thylakoid membranes (Schottkowski et al. 2009a), and a recent structural study suggested PDMs are attached to the thylakoid centre, a rod-like structure connecting both membranes (Nickelsen and Rengstl 2013). Moreover, enzymes and precursor products associated with chlorophyll biosynthesis have also been identified in PDMs (Rengstl et al. 2011; Schottkowski et al. 2009b), indicating that a pipeline of biosynthesis and integration of co-factors might spatially be organised in the same region to coordinate the assembly process.

Chloroplasts in plants are considered to have originated from cyanobacteria via endosymbiosis, and have outer and inner chloroplast envelope membranes instead of outer and cytoplasmic membranes. The thylakoid system in higher plant chloroplasts is more complex than that of cyanobacteria, the localisation of photosynthetic

complexes is stringently partitioned in grana and stroma lamellae (see section 1.2.2). The highly organised and dynamic membrane system enables efficient energy harvesting and stress protection. However, the compact granal stacks restrict the access of ribosomes, hence it has been proposed that protein synthesis in chloroplasts occurs exclusively on the stroma lamellae (Yamamoto et al. 1981). This model is further backed by protein analysis, which showed the distribution of PSII subcomplexes is directly correlated to the height of the grana stacks (Danielsson et al. 2006).

1.5 Photoinhibition and PSII repair

The chemistry involved in light-driven water oxidation process eventually leads to damage to the PSII protein complex (Mattoo et al. 1984). In both chloroplasts and cyanobacteria, an effective mechanism is available to repair inactivated PSII (see section 1.5.4). Under illumination at moderate and low light intensities, the repair rate of PSII is able to match the rate of photodamage to maintain photosynthetic activity. However, when the repair rate fails to keep up with that of the damage, the overall photosynthesis rate will decline in a phenomenon termed chronic photoinhibition (Ohad et al. 1984). Although the molecular mechanism of photoinhibition is still under intense debate (see section 1.5.1), the consequent result of photoinhibition is the irreversible damage to PSII proteins and mainly the reaction centre protein D1.

1.5.1 Molecular mechanisms for photoinhibition of PSII

Beyond the phenomenon of photoinhibition, it is widely agreed that photoinhibition occurs at the reaction centre of PSII, especially the D1 subunit, which undergo rapid turnover under strong light illumination (Aro et al. 1993b; Ohad et al. 1994; Prasil et al. 1992). However, the details regarding the mechanisms of photodamage are still under intense debate (Murata et al. 2012). Two distinctive routes of photoinhibition have been proposed on the basis of the available data from both *in vitro* and *in vivo* studies.

The classic acceptor-side model (Aro et al. 1993a; Barber and Andersson 1992; Long et al. 1994; Vass et al. 1992), established on the basis that reactive oxygen species (ROS) are responsible for photoinhibition, suggests that under continuous strong illumination, the constant electron flow from PSII can lead to an over-reduced plastoquinone-pool, which might lead to a double reduction of Q_A and consequently causing its dissociation from D2 (Styring et al. 1990; Vass et al. 1992). As an essential element for electron transfer, dissociation of Q_A blocks electron flow within PSII, leading to enhanced accumulation of P680 triplet states (^{3}P680) which will then react with triplet oxygen ($^3O_2$), eventually resulting in the production of reactive oxygen species (ROS) (Vass et al. 1992). Other than dissociation of Q_A under strong illumination, ROS might also be produced via charge-recombination between Q_B^- and the S-states under low-light conditions (Keren et al. 2005a; Mattoo et al. 1984).

In contrast to the acceptor-side model which requires the presence of ROS, the donor-side model for photoinhibition is oxygen independent. It has been shown that the action spectrum of photodamage to PSII resembled the absorption spectra of manganese compounds (Hakala et al. 2005; Ohnishi et al. 2005; Sarvikas et al. 2006). Indeed various manganese compounds are also susceptible to light-induced damage (Antal et al. 2009; Hakala et al. 2006; Wei et al. 2011). Hence it is possible that the inactivation of PSII begins with damage and dissociation of the OEC. Consequently, without the supply of electrons from OEC, the cofactors at the reaction centre of PSII might form highly oxidizing radicals that are capable of extracting electrons from the surrounding protein moiety or PSII as a whole (Chen et al. 1992; Klimov et al. 1990).

The key evidence supporting the donor-side inhibition theory is based on *in vivo* studies showing manganese ions from OEC are the primary target of photodamage (Hakala et al. 2005; Ohnishi et al. 2005), hence electrons from donor-side are the limiting factors in photoinhibition. Although recent evidence suggests that ROS are

not directly causing damage to PSII, but rather inhibiting the repairing process (see section 1.5.3.1), it does not rule out the possibility that Q_A dissociation and charge recombination might contribute to photoinhibition.

1.5.2 Photodamage and repair

The phenomenon of photoinhibition as a whole is the result of imbalance in the rates of damage and repair. Hence studies on photoinhibition require consideration of both photodamage and PSII repair. With well-established experimental procedures in both plants (Moon et al. 1995) and cyanobacteria (Gombos et al. 1994; Murata et al. 2012; Wada et al. 1994), photodamage can be analysed separately from PSII repair by blocking the biosynthesis of D1 using antibiotics that inhibit protein synthesis, e.g. lincomycin. The separate analysis of photodamage and repair has shown that the rate of photodamage to PSII has a clear linear correlation with light intensity, whereas the repair rate reaches its maximum at a light intensity of 200 to 400 $\mu E.m^{-2}.s^{-1}$ white light (Allakhverdiev and Murata 2004). Hence repair of PSII is indeed the rate limiting step that leads to photoinhibition. Several mechanisms have been found to participate in the protection of PSII against photoinhibition, including the expression of various genes associated with ROS scavenging enzymes (Asada 1999; Di Mascio et al. 1990; Neely et al. 1988), non-photochemical quenching (NPQ) (Bugos and Yamamoto 1996; Lindahl et al. 2000) and dissipation of energy into other electron transport pathways (Murata et al. 2012).

1.5.3 Putative protective mechanisms against photoinhibition

Photosynthetic organisms have evolved a range of protective mechanisms to prevent photoinhibition. In this section, a few putative protective mechanisms used by cyanobacteria and higher plants are described, including the mediation of reactive oxygen species (see section 1.5.3.1), non-photochemical quenching (see section 1.5.3.2) and energy dissipation though alternative pathways (see section 1.5.3.3).

1.5.3.1 Protection against reactive oxygen species (ROS)

In general, ROS present in cells are the by-product of aberrant energy transfer from the photosystems to molecular oxygen ($^3O_2$). It could be singlet oxygen ($^1O_2$), which might be the result of energy transfer from chlorophyll molecules to $^3O_2$ (Knox and Dodge 1985; Zolla and Rinalducci 2002), or superoxide radicals ($O_2^{\cdot -}$) formed when electrons at the acceptor-side of PSI are transferred to $^3O_2$, which could further be converted to hydrogen peroxide (H_2O_2) and into hydroxyl radicals ($\cdot OH$) (Asada 1999). In the initial acceptor-side model of photoinhibition, ROS was proposed to have a direct role in photodamage to PSII reaction centre, however, by separately assessing photodamage when PSII repair process is blocked, it seems that the rate of photodamage to PSII is not accelerated drastically by the presence of ROS (Allakhverdiev and Murata 2004; Nishiyama et al. 2004; Nishiyama et al. 2001). Rather the main effect of ROS is to reduce global protein translation by primarily targeting the redox-controlled elongation factor G (EF-G), which leads to insufficient D1 synthesis (Ejima et al. 2012; Nishiyama et al. 2004; Nishiyama et al. 2001).

Several genes involved in the production of ROS-scavenging enzymes and antioxidants protect cells from oxidative stress. Bacterial catalase which is a scavenger of H_2O_2 has been shown to improve tolerance to photoinhibition (Miyagawa et al. 2000; Nishiyama et al. 2001; Shikanai et al. 1998). Interestingly, ascorbate peroxidase (APX) is the predominant scavenger of H_2O_2 in the chloroplasts of higher plants, however, it is rather unstable comparing to catalase (Asada 1999), which might contribute to the fact that higher plants have lower tolerance to H_2O_2 comparing to cyanobacteria and algae (Badger et al. 2000; Takeda et al. 1995; Tamoi et al. 1998). Antioxidants such as α-tocopherol, which is an effective scavenger of intracellular $^1O_2$ (Di Mascio et al. 1990; Neely et al. 1988), also aids to reduce the oxidative suppression on PSII repair (Hakala-Yatkin et al. 2011; Havaux et al. 2005).

1.5.3.2 Non-photochemical quenching

Non-photochemical quenching (NPQ) refers to the preventative mechanisms that restrict excessive light energy from passing through to the photochemical reactions. This process has been assessed by monitoring the reduction of chlorophyll fluorescence yields, and categorised into three groups according to the relaxation kinetics, namely energy-dependent quenching (qE), state-transition quenching (qT) and photoinhibitory quenching (qI) (Muller et al. 2001).

Among the three types of NPQ, qE is the major contributor as it respond to light stress on a timescale of seconds (Demmig-Adams and Adams III 1996; Horton and Ruban 1992; Kanervo et al. 2005; Long et al. 1994; Muller et al. 2001), and results in the relatively harmless thermal dissipation of absorbed light energy (Niyogi and Truong 2013). The molecular details of qE quenching are still largely unclear, and the quenching mechanisms vary among cyanobacteria, algae and plants, however, a few proteins and cofactors involved in qE-mediated heat dissipation have been identified. In principle, qE quenching occurs in the light-harvesting antenna protein complexes, which is believed to redirect energy transfer from chlorophyll to carotenoid, and consequently, carotenoid will dissipate energy in the form of heat (Demmig-Adams and Adams III 1996). The basis of qE quenching among cyanobacteria, algae and plants are similar, however, the quenching mechanisms between them are quite different. As cyanobacteria harvest light via phycobilisome antenna (see section 1.2.2), qE quenching is reliant on the orange carotenoid protein (OCP), which binds a single xanthophyll molecule (Kerfeld et al. 2003). Upon absorption of blue-green light via a xanthophyll pigment, OCP is switched from an inactive orange form (OCP^o) into an active red form (OCP^r), which is able to bind to the phycobilisome (Gwizdala et al. 2011). The structural details of binding and energy transfer are still unclear. The current hypothesis is that energy from excited bilin pigment at the core of phycobilisome is passed to the xanthophyll in OCP^r (Niyogi and Truong 2013). Moreover, qE quenching can be switched off via up-regulation of the Fluorescence

Recovery Protein (FRP), which promotes both dissociation of OCP^r from phycobilisome and reversion of OCP^r to OCP^o (Gwizdala et al. 2011).

Unlike cyanobacteria, qE quenching in green algae is performed via production of a specific type of LHC complex, namely LHCSR (or LI818 or LHCX1) (Bailleul et al. 2010; Niyogi and Truong 2013; Peers et al. 2009). Unlike regular LHC, chlorophylls inside LHCSR have an unusually short fluorescence lifetime that is even shorter at low pH conditions *in vitro* (Bonente et al. 2011). Beside up-regulation of LHCSR genes, LHC genes are typically down-regulated under high light, which shifts the equilibrium between the two types of light harvesting complexes towards enhanced qE quenching. Furthermore, LHCSR might also induce quenching in other LHC proteins in PSII (Elrad et al. 2002; Ferrante et al. 2012), and it is also implied to play a protective role for detached LHC proteins migrating between photosystems (Amarnath et al. 2012). It is worth mentioning that qE quenching in both green algae and plants is triggered via increased ΔpH across the thylakoid membrane, which initiates the xanthophyll cycle by activation of violaxanthin de-epoxidase which converts violaxanthin to zeaxanthin (Demmig-Adams and Adams III 1996).

Although both algae and plants harvest light energy via LHC complexes and qE quenching in both organisms is ΔpH-dependent and xanthophyll-dependent, the quenching mechanisms in plants seem to have evolved separately (Niyogi and Truong 2013). It has been shown that LHC complexes in plants have an intrinsic ability to switch between an efficient light-harvesting state to a photoprotective state in which excitation energy is dissipated (Kruger et al. 2012). The precise regulation mechanism is still to be unveiled, however, mutagenesis analysis have shown that the PsbS protein plays an essential role in this process (Lindahl et al. 2000). Protonation of PsbS promotes a rearrangement of the PSII complexes in the grana lamellae (Betterle et al. 2009; Goral et al. 2012) and has been implied to cause conformational changes

in the LHC complexes (Li et al. 2000; Ruban et al. 1993). PsbS is an integral membrane protein that belongs to the chlorophyll *a*/*b* binding (cab) protein superfamily, however, PsbS does not appear to bind pigments (Bonente et al. 2008). Surprisingly, although conserved genes encoding PsbS are also found in the green alga *Chlamydomonas reinhardtii*, the expression of which is also induced by light stress, there is presently no evidence that PsbS is translated or involved in NPQ in *C. reinhardtii* (Niyogi and Truong 2013). However, it remains a possibility that green algae might have both LHCSR and PsbS quenching mechanisms. Moreover, despite being essential to qE quenching in plants, thylakoid membranes isolated from the *psbS* mutant was able to perform qE quenching in the presence of high ΔpH (Johnson and Ruban 2011), which provides a hint that there might be other sensors to drive the conformational change of LHC.

When oxygenic photoautotrophs are under continuous strong illumination over a period of minutes, state transition quenching (qT) is initiated (Anderson 1986; Kanervo et al. 2005; Melis 1999; Reuter and Muller 1993). Unlike qE quenching, which mediates the energy flow from the light-harvesting antenna to photosystems, qT quenching adjusts the size and positioning of the antennae to acclimate the environment by fine-tuning the energy reception and the electron flow between photosystems (Escoubas et al. 1995; Lindahl et al. 1995; Reuter and Muller 1993). The size of the light-harvesting antennae is modified to cope with long-term illumination via regulation of both biosynthesis (Escoubas et al. 1995) and degradation (Lindahl et al. 1995) of the antenna proteins. Antenna proteins also migrate between photosystem I and photosystem II, during so-called state transitions, to regulate electron flow chain on thylakoid membrane as a short-term acclimation response (Murata and Sugahara 1969). In plant and green algae, the state transition response is regulated by the redox state of the plastoquinone pool, coupled with phosphorylation of the antenna. Under reducing conditions, this leads to the migration

of antenna complexes from PSII to PSI (Allen 2003; Bellafiore et al. 2005; Bonardi et al. 2005; Rochaix 2007; Tikkanen et al. 2006). The transfer of antenna from PSII to PSI is termed state 2, whereas the reverse process, regulated by phosphatase (Pribil et al. 2010; Shapiguzov et al. 2010), is termed state 1 (Allen and Forsberg 2001; Gal et al. 1997; Kanervo et al. 2005; Mullineaux and Emlyn-Jones 2005). Interestingly, the movement of phycobilisomes in cyanobacteria does not seem to involve phosphorylation, and the control mechanism is yet to be unveiled (Mullineaux and Emlyn-Jones 2005). qT quenching is associated with photoprotection, however, its impact is still debatable. In plants, only 15 to 20 % of the LHC complexes are involved in state transitions, whereas, up to 80 % of the LHC antenna in *C. reinhardtti* participate in state transitions (Kanervo et al. 2005). In the case of cyanobacteria, NPQ is closely correlated with state 2 transition (Campbell and Öquist 1996), however, there is no direct evidence that qT mediates photoprotection (Mullineaux and Emlyn-Jones 2005).

Photoinhibitory quenching (qI) is the slowest forming and relaxing NPQ among the three, with sustained quenching able to persist for several hours in the dark following illumination (Ruban et al. 2012). PSII undergoes rapid turnover under strong light illumination and it is suggested that qI quenching might be achieved by using inactive PSII complexes as energy sinks to reduce energy flux towards their functional neighbours (Aro et al. 1993a; Kanervo et al. 2005; Kettunen et al. 1997; Lee et al. 2001; Matsubara and Chow 2004). Typically, the repair rate of damaged PSII complexes is restricted by the *de novo* synthesis rate of D1 protein subunit encoded by the *psbA* gene (Figure 1.4). Interestingly, unlike most plants and algae which only have one copy of *psbA* (Zurawski et al. 1982), most cyanobacteria contain three copies of *psbA* (Golden et al. 1986). The expression level of each *psbA* gene is associated with both the quantity and quality of light (Campbell et al. 1998; Clarke et al. 1995; Clarke et al. 1993; Golden et al. 1986). Further studies on D1 homologues

suggest that the turnover rate of each homologue varies under strong illumination, hence qI quenching could be enhanced in cyanobacteria via altering the proportion of each D1 homologue (Campbell et al. 1998; Komenda et al. 2000; Sippola and Aro 2000).

The physiological role of NPQ in photoprotection was originally thought to be mainly at the level of reducing the rate of photodamage to PSII. However, using methods to monitor photodamage and repair separately has since revealed that defects in NPQ largely lead to impaired repair of PSII, rather than enhanced rates of photodamage (Murata et al. 2012; Sarvikas et al. 2006; Sarvikas et al. 2010; Takahashi et al. 2009). As described before (see section 1.5.3.1), the *de novo* synthesis of D1 in the PSII repair cycle is strongly inhibited by the level of ROS, which provides a hint that NPQ might aid the repair process by preventing generation of ROS.

1.5.3.3 Dissipation of energy via alternative electron transport pathways

Beside the primary electron transfer route within PSII (see section 1.2.3), secondary electron transfer pathways are proposed to protect PSII from oxidative damage in situations where electron transfer to $P680^+$ from the OEC is either absent or impaired (Stewart and Brudvig 1998). Under such circumstances, oxidation of the redox-active tyrosine in D2 (Y_D), β-carotene, Chlorophyll and Cyt b_{559} has been observed (Shinopoulos and Brudvig 2012). Further analysis on the secondary electron flow in PSII suggests that the β-carotene (Car_{D2}), coordinated by the D2 subunit, is likely to be the initial electron donor to P680 when electron transfer from OEC is restricted (Shinopoulos et al. 2013). Subsequently, the oxidised Car_{D2} is reduced by electron transfer from the terminal electron donor Cyt b_{559}, via a network of cofactors (Shinopoulos and Brudvig 2012). Moreover, Cyt b_{559} may be reduced by the plastoquinone pool which is ultimately reduced by the acceptor-side of PSII, thereby forming a cyclic electron pathway connecting the donor and acceptor side of PSII (Shinopoulos and Brudvig 2012).

In plants, cyclic electron transport around PSI (CET) is accelerated under various stress conditions, including strong illumination (Clarke and Johnson 2001; DalCorso et al. 2008; Miyake et al. 2004). It has been shown that CET plays an important role in counteracting photoinhibition in plants (Munekage et al. 2004; Takahashi et al. 2009). CET enables PSI to pass electrons back to the plastoquinone pool via reduced ferredoxin or NADPH, which consequently contributes to formation of ΔpH across thylakoid membrane (Figure 1.2 lower panel) and down-regulation of PSII activity by the qE mechanism (Kanervo et al. 2005; Munekage et al. 2004; Shikanai et al. 2002). Further studies on *A. thaliana* mutants with impaired CET suggest that CET contribute largely to the generation of ΔpH, which seems not only to enhance repair via protonation of PsbS and consequent NPQ, but also reduce the sensitivity of PSII to photodamage (Takahashi et al. 2009).

Photorespiration is another metabolic pathway that can be used to dissipate excess energy from LET (Badger et al. 2000; Niyogi 1999; Wingler et al. 2000). In general, photorespiration is a process which fixes O_2, instead of CO_2, at the level of ribulose-bisphosphate carboxylase/oxygenase (rubisco), to then form 2-phosphoglycolate and 3-phosphoglyceric acid (Wingler et al. 2000). This process is generally considered wasteful, however, blocking it leads to greater sensitivity to photoinhibition and oxidative damage (Niyogi 1999; Wingler et al. 2000). Interestingly, photorespiration in plants is partly due to the fact that rubisco is relatively unspecific for CO_2 and there might be a limitation of CO_2 supply to the cell. Hence it is probably less relevant to photoprotection in cyanobacteria due to the different kinetic properties of rubisco and the efficient carbon concentrating systems that most cyanobacteria possess (Badger et al. 2000).

The water-water cycle (also known as the Mehler-ascorbate peroxidase reaction or pseudocyclic electron transport) is another alternative electron pathway that is used in

plants under high light stress (Asada 1999; 2000; Badger et al. 2000; Kanervo et al. 2005). In this pathway, excess electrons from PSI are directly transferred to dioxygen, and the resulting superoxide radicals are ultimately converted into water and ascorbic acid by superoxide dismutase and ascorbate peroxidase. This process maintains LET between photosynthetic complexes, and is also thought to contribute to qE quenching.

1.5.4 PSII repair cycle

Photodamage to PSII is an inevitable process that occurs under all light intensities (see section 1.5). In both chloroplasts and cyanobacteria, photosynthetic activities are maintained by both *de novo* protein synthesis and efficient PSII repair mechanisms. Among the subunits in PSII, D1 is the main target of photodamage and is rapidly turned over with a half-life as short as 30 min (Tyysjärvi et al. 1994) Therefore a key aspect of PSII repair is the replacement of the inactive D1 from the reaction centre via partial disassembly and reassembly of the PSII complex. Due to the complexity of the repair process, and also the fact that the PSII *de novo* assembly and repair might spatially overlap and generate identical intermediate sub-complexes, there are still a few knowledge gaps to be filled.

A current model of the PSII repair cycle in cyanobacteria is shown in Figure 1.7. Following photoinactivation, there is partial disassembly of the damaged PSII complex to form the RC47 complex, which enables damaged D1 to be exposed for degradation. The replacement of D1 consists of two synchronised steps: the degradation of the inactive D1 and the *de novo* synthesis of D1. Once a new copy of D1 is integrated into the RC47 complex, possibly with the assistance of auxiliary proteins, PSII is re-assembled (see section 1.4.1).

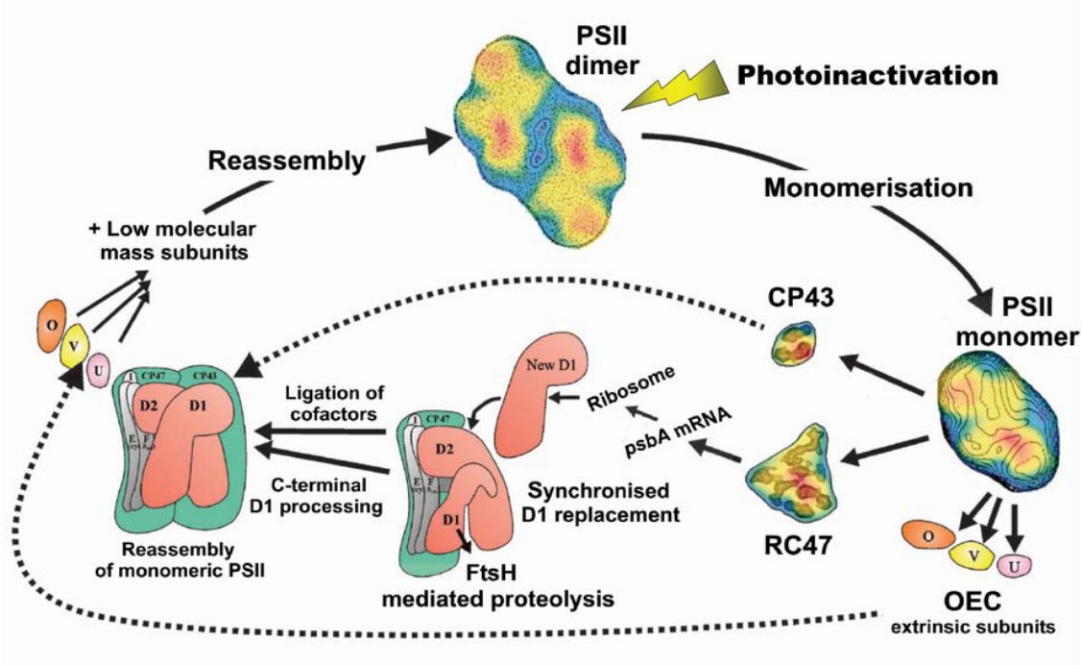

Figure 1.7: Model for the PSII repair cycle of cyanobacteria.
The various steps of the cyanobacterial PSII repair cycle are depicted in this hypothetical model for which the description can be found in the text. O, V and U symbolise the extrinsic subunits of the oxygen -evolving complex (OEC) PsbO, PsbV and PsbU respectively. RC47 signifies a PSII core complex lacking CP43. In this model, only the FtsH protease is suggested to mediate D1 protein removal and degradation. The figure was kindly donated by Dr. J. Nield and Dr. P. Silva; adapted from (Nixon et al. 2005).

Whilst the repair processes of PSII in plants and cyanobacteria have been proposed to be similar, there are clear signalling and spatial differences between the two systems. The signalling system in eukaryotes is largely dependent on phosphorylation, hence in contrast to the cyanobacterial system, the detachment of antenna and disassembly of PSII complexes in chloroplasts are under the regulation of kinases (Tikkanen et al. 2008). Also, the repair process of PSII in chloroplasts is restricted to the stroma lamellae as photosynthetic proteins localised in grana lamellae are not accessible to repair (Goral et al. 2010). The formation of thylakoid membranes in cyanobacteria is not as structured as their chloroplastic counterpart; therefore, the location where repair process takes place is still unclear. One of the models proposed according to the heterogeneous distribution of FtsH, the major protease responsible for D1 degradation,

suggests that D1 replacement might take place in defined “repair zones” where FtsH is available (Komenda et al. 2006a; Komenda et al. 2012b). Moreover, pD1 is found not only in PDM but also in thylakoid membranes, which raises the speculation that the sub-fraction of pD1 in the thylakoid membrane might be associated with PSII repair rather than *de-novo* assembly (Schottkowski et al. 2009a).

1.5.5 FtsH-mediated D1 degradation

Early studies based on *in vitro* experiments suggested that degradation of D1 in higher plant thylakoids required the involvement of members of both the DegP and FtsH family of proteases (Spetea et al. 1999). A two-protease model was proposed in which damaged D1 was initially cleaved by Deg2 in a GTP-dependent manner, and then the remaining 23-kDa N-terminal D1 fragment was degraded by FtsH, an ATP-dependent, Zn^{2+}-binding metalloprotease (Adam and Clarke 2002; Haussuhl et al. 2001; Lindahl et al. 2000). However, later studies using Deg2 protease-deficient mutants showed that D1 turnover was not affected *in vivo*. In contrast inactivation of FtsH resulted in impaired D1 degradation. Furthermore, the accumulation of the 23-kDa D1 cleavage product observed previously *in vitro* was not detected in the *in vivo* experiments (Bailey et al. 2002). Instead, full-length D1 was found stably accumulated in the FtsH null mutant, suggesting that the previously described degradation of D1 by Deg2 is not a physiologically relevant event, or only contributes under stress conditions (Barker et al. 2006; Huesgen et al. 2006).

Studies in *Synechocystis* provided the first evidence that FtsH played a major role in the initial steps of D1 degradation (Silva et al. 2003). FtsH is an important class of protease involved in diverse cellular activities, with interestingly, multiple FtsH homologues present in chloroplasts and cyanobacteria. In the plant *A. thaliana*, 4 FtsH homologues present in the thylakoid membranes can be divided into two groups based on functional and structural similarities: Type A (FtsH1 and FtsH5) and Type B

(FtsH2 and FtsH8) (Wagner et al. 2012). Both Type A and Type B proteases are involved in PSII repair, and interestingly, the two types of proteases were always co-purified in the immunoprecipitation experiments, which raised the speculation that the proteases might function as complexes (Garcia-Lorenzo et al. 2006; Zaltsman et al. 2005). Four FtsH homologues are present in the cyanobacterium *Synechocystis*. Among the 4 members, FtsH2 is associated with D1 degradation (Silva et al. 2003). Further work on understanding the molecular interaction between FtsH2 and D1 demonstrated that the N-terminal tail of D1 is essential for the degradation process (Komenda et al. 2007b). Therefore, upon photoinactivation, conformation changes in this N-terminal tail of D1 might contribute to the disassembly of PSII and allow docking with the FtsH protease to initiate degradation. Given that the *Synechocystis* mutant lacking FtsH2 is still able to grow photoautotrophically under low-light conditions, it is plausible that an alternative D1 degradation pathway exists which is capable of low level PSII repair.

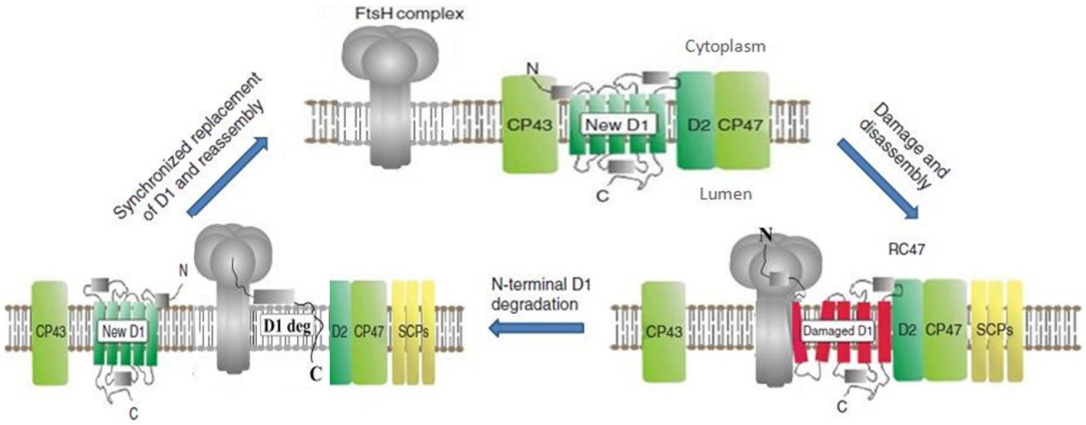

Figure 1.8: Schematic maps of the FtsH complex-mediated photosystem II repair cycle model.
The figure represents the three states during the repair cycle, details are described in text. D1, D2, CP43 and CP47 are four subunits of PS II (Umena et al. 2011). RCCII means dimeric PS II complex. SCPs means small CAB-like proteins. For clarity, assembly factors are not included. This figure is adapted from (Nixon et al. 2010b).

1.6 General introduction to the FtsH family of proteases

FtsH is a member of the AAA+ protease superfamily and plays an important role in

the PSII repair cycle (see section 1.5.4), and also it is to be the main focus of this thesis. FtsH is universally conserved in eubacteria, chloroplasts and mitochondria, with bacterial FtsH the one studied to greatest depth. In this section, a brief introduction to bacterial FtsH will be described, covering the basic features of the AAA+ superfamily (see section 1.6.1) and the proposed structure (see section 1.6.2) and mechanism (see section 1.6.3) of bacterial FtsH complexes. Moreover, some of the cellular functions involving bacterial FtsH are also described (see section 1.6.4).

1.6.1 The AAA+ superfamily of proteases

All members of the AAA+ superfamily of proteases contain at least one subunit that belongs to ATPase associated with diverse cellular activities (Neuwald et al. 1999), which utilises the energy released from ATP hydrolysis to drive degradation of substrate proteins. Five distinctive families of AAA+ proteases have been defined based upon the topology of the ATPase and auxiliary domains, namely FtsH, Lon, ClpXP, ClpAP/ClpCP and PAN (Neuwald et al. 1999; Schirmer et al. 1996). The common feature of the AAA+ family is the presence of the AAA+ domain, which interacts with, unfolds and translocates the substrates towards the peptidase domain. The translocation process requires either ATP binding or hydrolysis to initiate the conformational change of the AAA+ domain. The crystal structure of several AAA+ rings have been resolved to atomic resolution, a conserved large and a small domain are observed in all structures, where ATP or ADP is coordinated between the large domain of one protomer and the small domain of the neighbouring protomer (Erzberger and Berger 2006). On the other hand, information on the native FtsH protease complex is sparse, the relationship between subunits can also vary between families or even between homologous proteins in different species. For example, HslU and FtsH have been crystallised with C_6, C_3 and C_2 symmetry, therefore, it is still not clear how the AAA+ domain functions *in vivo* (Sauer and Baker 2011). Other than FtsH and Lon, which have both AAA+ and protease domain on the same

polypeptide chain, HslU, ClpX/ClpA/ClpC and PAN form complexes with a separate auxiliary peptidase HslV, ClpP and 20S. Despite the differences in the proteolytic sites, a common architectural feature of the protease domain in AAA+ proteases is the barrel-shape chamber that only allows entry of unfolded peptides (Sauer and Baker 2011).

1.6.2 Structure of FtsH proteases

FtsH proteases are universally conserved in eubacteria and endosymbiosis-derived organelles of eukaryotes, namely chloroplasts and mitochondria (Arnold and Langer 2002; Wagner et al. 2012). Among all five classes of AAA+ proteases in *Escherichia coli*, FtsH is the only one that is anchored on the cytoplasmic membrane and is essential for cell viability (Gottesman 2003). Most FtsH proteases identified to date carry two N-terminal transmembrane (TM) helices, yet, variants carrying only one or lacking TM also appear to exist (Langklotz et al. 2012). The highly conserved AAA+ domain, which defines FtsH as a member of AAA+ family, is located behind the TM region. The AAA+ domain is composed of three motifs, Walker A, Walker B and second region of homology (SRH), where Walker A and B motifs form a structural pocket docking ATP and the SRH is proposed to catalyse the hydrolysis of the nucleotide (Suno et al. 2006). The protease domain (PD), which features a Zn^{2+} binding motif HEXXH (X represents mostly uncharged residues), is located towards the C-terminus of the peptide chain, and is connected to the AAA+ module via a short linker region (see section 4.1). Besides the common "zincin" motif, the protease domains between FtsH proteases are less conserved and vary in length, which might reflect differences in substrate recognition (Graef et al. 2007). Interestingly, FtsH in *E. coli* exhibits self-cleavage property, which leads to the removal of seven residues from the C-terminus (Akiyama 1999). The self-cleavage process is reproducible *in vitro* in an ATP-hydrolysis dependent manner, however, its physiological influence is obscure as both full-length and cleaved proteases are active (Ito and Akiyama 2005).

A few crystal structures of the soluble domains of bacterial FtsH have been solved, with subsequent modelling suggesting the protease forms hexameric oligomers. Although structural information of native FtsH complexes is still sparse, *in vitro* data and comparative bioinformatics studies on other AAA+ proteases support the proposed hexameric-oligomer model, and it is widely accepted that the membrane-anchored protease degrades substrate proteins via translocation of the substrate through the central pore of the proteolytic chamber (Figure 1.9).

Further to the oligomerisation of FtsH, early studies on *m*-AAA protease, a yeast mitochondrial FtsH, discovered a possible regulatory interaction with prohibitins (Steglich et al. 1999). This discovery suggesting the proteolytic activity of FtsH proteases could be regulated via auxiliary proteins, which raised speculations that FtsH might form super-complex with adaptor modules *in vivo*. In support of this, *E. coli* FtsH extracted via non-ionic detergent forms a supercomplex with HflKC, which are homologues of prohibitin (Saikawa et al. 2004).

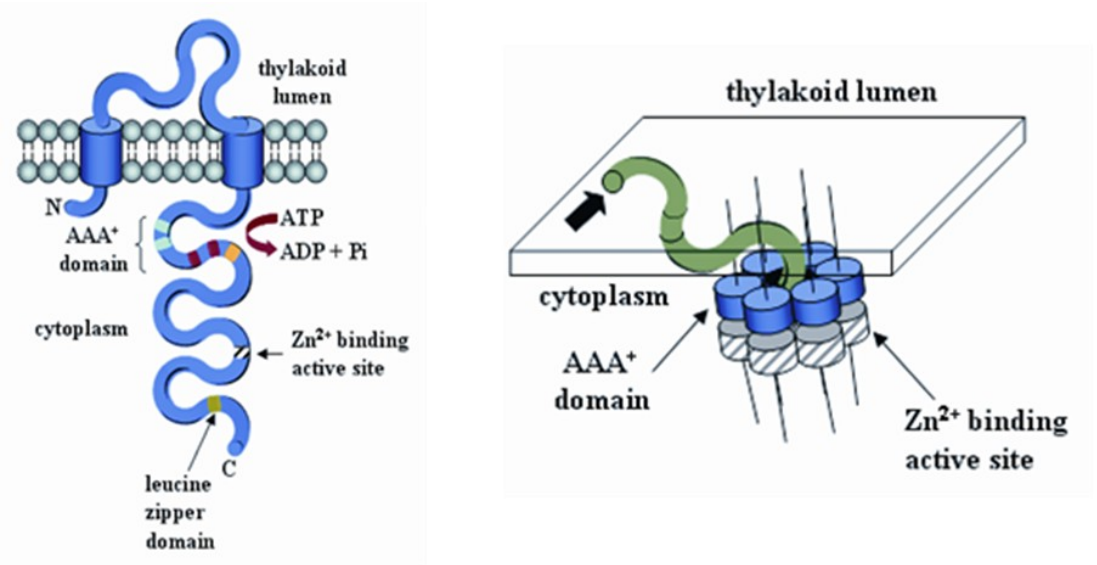

Figure 1.9: Schematic representation of bacterial FtsH proteases.
The topology of individual FtsH is consist of two transmembrane helices, a AAA+ domain and a Zn^{2+} binding protease domain (left panel). FtsH proteases are proposed to form hexameric complexes degrading substrates via the central pore (right panel). Figure adapted from Nixon et al. (2005) and Akiyama et al. (1996).

1.6.3 Structure of the cytosolic domains of FtsH and proposed mechanism of action

The high-resolution structure of an intact FtsH complex isolated from its native environment has still not been achieved. However, several X-ray crystal structures of bacterial FtsH proteases lacking the trans-membrane region have been determined (Bieniossek et al. 2009; Suno et al. 2006). Overall, the structures indicate a hexameric assembly of FtsH complexes in all cases. The dimensions of the FtsH complex from *Thermus thermophilus* are ~120 Å in diameter and 65 Å in height. The structures of the protease domains between species are highly similar, and all exhibit 6-fold symmetry. However, the arrangement of AAA+ module between structures is largely different between species. Although both structures of *T. thermophilus* and *Thermotoga maritima* support a conformational change of the AAA+ domain during ATP hydrolysis, with the "knick" motion driving substrates through the central pore to the proteolytic site. However, the structure of the AAA+ domain from *T. maritima* displays two-fold symmetry, whereas *T. thermophilus* FtsH shows three-fold symmetry. It is unclear whether the variation is naturally present, or due to an intentionally designed mutation in the flexible linker region of the *T. thermophilus* sequence that was aimed to improve crystal quality (Bieniossek et al. 2009; Langklotz et al. 2012). Other than FtsH, structures of other AAA+ proteases display 6-fold, 3-fold and 2-fold symmetries in the nucleotide-bound state. Consequently, it is still puzzling how the protomers within the hexameric complex coordinate during ATP hydrolysis.

One model proposed by (Suno et al. 2006), based on 3-fold symmetric structure of *T. thermophilus*, is that ATP hydrolysis is a synchronised process between neighbouring protomers. After three ATP molecules are docked in the pocket of "open" protomers, the three ATP-bound AAA+ domains close, enabling the "arginine finger" from the neighboring protomers to interact with the γ-phosphate of ATP molecules. Then the hydrolysis of ATP drives the adjacent protomer "open", and sequentially, ATP

molecules dock into the open pocket and drive the subsequent reactions.

1.6.4 General functions of FtsH proteases in bacteria

FtsH family proteases play diverse house-keeping roles in bacteria, including quality control of membrane proteins by removing damaged/unassembled proteins and degradation of short-lived soluble proteins that often associate with the stress response (Ito and Akiyama 2005). As the only AAA+ protease essential to cell viability in *E. coli*, the vital role that FtsH plays is maintaining the balance between lipopolysaccharide (LPS) and phospholipids. R-3-hydroxymyristoyl-ACP is a common precursor to the biosynthesis of LPS and phospholipids, supply of which is the rate limiting factor to the two competing pathways (Ogura et al. 1999). FtsH is responsible for the efficient degradation of LpxC deacetylase, a short-lived (half-life, ~ 4 min) enzyme involved in the synthesis of lipid A in the LPS pathway. Disruption of FtsH leads to the lethal over-accumulation of LPS, which can be rescued by up-regulating the fatty acid biosynthetic pathway (Ogura et al. 1999).

E. coli FtsH was also found to interact with YccA, a distant homologue of Bax Inhibitor-1 (BI-1) in the organelles of eukaryotes (Huckelhoven 2004), however, little is known about its function in prokaryotes (Ito and Akiyama 2005). YccA is subject to FtsH-mediated degradation (Kihara et al. 1998), however, its abundance and stability also negatively inhibit the activity of FtsH (van Stelten et al. 2009). As a membrane protein containing 7 transmembrane helices, the N-terminal cytosolic region of YccA is crucial to FtsH mediated degradation (Ito and Akiyama 2005), however, the N-terminal truncated protein can still bind to the FtsH complex and inhibit its function (Kihara et al. 1998). In summary, YccA displays both substrate and inhibitor roles for the FtsH complex.

Another important cellular function of FtsH in *E. coli* is the removal of the inactive

SecY translocon (van Stelten et al. 2009). SecY and secDF form a stable membrane complex which regulates the translocation of proteins cross the cytoplasmic membranes in an ATP-dependent manner (Nouwen et al. 2005; Tsukazaki et al. 2011). Aberrant Sec translocons disturb the permeability of the cytoplasmic membranes and hence compromise cellular activities. FtsH is the only protease known to degrade SecY, as unassembled SecY stably accumulates in the *ftsH* null mutant. In contrast, unassembled SecY is efficiently removed from the membrane, with a half-life of ~2 min in normal cells.

Another well characterised function of FtsH in *E. coli* is its role in stress responses, including rapid degradation of the heat shock sigma factor in the absence of heat shock (Herman et al. 1995; Tomoyasu et al. 1995) and bacteriophage encoded CII, CIII and Xis (Herman et al. 1997; Leffers and Gottesman 1998; Shotland et al. 2000). Noteworthy, other members of AAA+ family may also be involved in the degradation process (Kanemori et al. 1997; Leffers and Gottesman 1998), suggesting functional overlap between AAA+ proteases. In summary, FtsH is a universal protease involved in various cellular activities, which balances the lipid ratio, maintains the activity of membrane proteins, regulates gene expressions to cope the changing environment and prohibits pathogenic invasions.

1.7 Evolutionary conservation and diversity of FtsH proteases in plastids and mitochondria

In eukaryotic cells, FtsH are exclusively localised to chloroplasts and mitochondria. In contrast to most bacteria which only contain one *ftsH* gene, multiple genes encoding FtsH homologues are found in eukaryotes and cyanobacteria. In yeast and human, 3 FtsH homologues were identified in the mitochondria (Arlt et al. 1996), 4 FtsH homologues were found in most cyanobacteria, and 12 genes encoding FtsH and another 5 encoding iFtsH, a sub-family of variant FtsH homologues lacking the Zn^{2+} binding motif, were identified in plant *A. thaliana* (Wagner et al. 2012). Noteworthy,

all FtsH proteases in eukaryotic cells are localised in organelles and are encoded by nuclear genes. The translocation of the proteins to a particular membrane is directed by a signal peptide sequence at the N-terminus (Atorino et al. 2003; Rodrigues et al. 2011).

FtsH proteases play important and diverse roles in eukaryotic cells. One of the best characterised functions of mitochondrial FtsH is its involvement in maintaining the respiratory pathway. MrpL32 is a small protein subunit that activates the ribosomal large subunit to enable the consequent docking of the 37S small subunit (Nolden et al. 2005). A sub-group of mitochondrial FtsH, namely *m*-AAA, is responsible for the maturation of MrpL32 by removing the N-terminal tail from the precursor protein. Unprocessed MrpL32 is unable to bind with the 54S large subunit which consequently compromises protein biosynthesis in mitochondria, eventually leading to respiratory defects.

Chloroplastic FtsH proteases are located either in the thylakoid membrane or in the chloroplast envelope. In *A. thaliana*, several FtsH homologues localised in the thylakoid membranes are involved in D1 degradation in the PSII repair cycle (see section 1.5.4), whereas, the FtsH proteases residing in the chloroplast envelope are essential for embryogenesis (Wagner et al. 2012).

Interestingly, some FtsH homologues are found to interact with each other and possibly form complexes (Garcia-Lorenzo et al. 2006; Zaltsman et al. 2005), which leads to the speculation that apart from possible auxiliary proteins, the diverse functions of FtsH proteases in eukaryotes might also be related to the composition of FtsH isomers in the FtsH protease complex.

1.8 FtsH homologues in cyanobacteria *Synechocystis* sp. PCC6803

Cyanobacteria are photosynthetic bacteria that perform photosynthesis using a similar,

but more primitive system than that of chloroplasts (see section 1.2.2). With all the benefits described (see section 1.3), they have been used extensively as model organisms to study photosynthesis, photoinhibition and PSII repair process (see section 1.5). Early bioinformatic studies identified four putative FtsH homologues in the cyanobacterium *Synechocystis* sp. PCC 6803: FtsH1 (Cyanobase designation Slr1390), FtsH2 (Slr0228), FtsH3 (Slr1604) and FtsH4 (Sll1463) (Mann et al. 2000) (Sokolenko et al. 2002). FtsH1 and 3 are essential for cell viability whereas cells lacking FtsH4 display a wild-type like phenotype (Mann et al. 2000). Similar to the *var2* mutant of *A. thaliana*, FtsH2 in *Synechocystis* is involved in the degradation of damaged D1 protein, as well as the removal of unassembled and misassembled PSII sub-units *in vivo* (Komenda et al. 2006a; Silva et al. 2003). More extended studies also showed that FtsH2 is involved in the resistance to various abiotic stresses, including low level of inorganic carbon (Zhang et al. 2007), heat stress (Kamata et al. 2005) ultraviolet light (UV-B) stress (Cheregi et al. 2007) and osmotic stress (Stirnberg et al. 2007). Therefore, like the FtsH protease in *E. coli*, FtsH2 in *Synechocystis* appears to play diverse physiological roles in degrading both soluble and membrane-anchored substrates. The functions of the other 3 homologues remain unclear as mutagenesis on these proteases either resulted in lethality or lack of a distinguishable phenotype under the tested conditions.

1.9 Project aims

The background theme of this study was to investigate the molecular mechanisms of FtsH-mediated D1 degradation, hence the key focus of this work was to elucidate the structure, localisation and physiological functions of the FtsH proteases. Given that none of the four members of FtsH protease family in *Synechocystis* had been subjected to in-depth analysis, and more importantly, that the cyanobacterial FtsH isomers might be structurally and/or functionally related, the aim of this work was to characterise all four FtsH homologues in *Synechocystis*. The work presented in this thesis focused on three areas: (1) the structural characterisation of FtsH complexes in

Synechocystis (see Chapter 3), (2) the functional characterisation of FtsH proteases both *in vivo* and *in vitro* (see Chapter 4) and (3) the physiological characterisation of the substrates and the potential regulatory mechanisms of FtsH proteases in *Synechocystis* (see Chapter 5).

In order to achieve these aims, the following objectives were defined:

- C-terminal glutathione-S-transferase (GST) tagging to each FtsH homologue in *Synechocystis* to enable isolation of FtsH proteases for:
  - composition analysis via antibodies specific to each FtsH homologue.
  - structural analysis via transmission electron microscopy (TEM).
  - identification of substrate/auxiliary proteins via mass spectrometry.
- C-terminal green fluorescent protein (GFP) tagging to each FtsH homologue in *Synechocystis* to determine the localisation of each FtsH isomer via fluorescence microscopy.
- Generation of FtsH null and domain-inactive mutants to:
  - examine functional overlaps among FtsH complexes .
  - examine dispensability of domains within FtsH hetero-complexes.
  - enable further mutagenesis to analyse the functional interference of the C-terminal GST/GFP tag under reduced overall FtsH activity *in vivo*.
- Expression of the cytosolic region of FtsH isomers in *E. coli* to elucidate the NTPase and protease activities *in vitro*.
- Generation of *Synechocystis* mutants deficient of potential auxiliary proteins of FtsH complexes to explore the regulation mechanisms of FtsH proteases *in vivo*.

Chapter 2: Materials and Methods

2.1 Bioinformatic tools

The programs, internet-based servers and databases that were used for the bioinformatics analyses of the FtsH homologues in this study are listed below.

Protein and gene databases:

BLAST (Release 2.2.14; Altschul et al. 1990) (http://www.ncbi.nlm.nih.gov/BLAST/)

CyanoBase (Version 2006.9.12; Nakamura et al. 1998) (http://www.kazusa.or.jp/cyanobase/)

NCBI database (http://www.ncbi.nlm.nih.gov/)

Protein properties prediction servers:

EXPASY (Wilkins et al. 1999) (http://us.expasy.org/tools/)

SOSUI engine (http://bp.nuap.nagoya-u.ac.jp/sosui/sosui_submit.html)

Multiple sequence alignment and phylogenetic tree generation:

CLUSTALW (WorkBench 3.2 environment) (Thompson et al. 1994; Gonnet et al. 1992)

Montpellier (Guindon et al. 2010) (http://www.atgc-montpellier.fr/phyml/)

DNA sequence restriction mapping:

NEB cutter V2.0 (http://tools.neb.com/NEBcutter2/index.php)

ApE V2.0.45 (http://biologylabs.utah.edu/jorgensen/wayned/ape/)

2.2 Standard solutions and buffers

Buffers and standard solutions were prepared according to Sambrook et al. (1989) unless otherwise stated. Reverse Osmosis (RO) filtered water (Neptune model L993162, Purite Limited, UK) was used to prepare all buffers and solutions. Chemicals and organic solvents were analytical grade reagents and purchased from Bioline UK Limited; Fisher Scientific Limited, UK; Melford UK Limited; Merck Chemicals Limited, UK; Sigma-Aldrich Limited, UK and VWR International Limited, UK. Necessary solutions, media and other materials were sterilised by autoclaving at 121 ^{o}C (130 kPa) for ≥ 25 min. Thermo labile reagents were sterilized by filtration through 0.2-µm syringe tip or bottle top filters (Schleicher & Schuell MicroScience GmbH, Germany).

2.3 *E. coli* strains and growth conditions

2.3.1 *E. coli* strains

The *E. coli* 10-beta strain was used for cloning and plasmid DNA propagation, the DCM- strain was used to produce un-methylated plasmid vectors and The KRX strain was used to over-express recombinant protein (see table 2.1).

Table 2.1: List of *E. coli* strains

Strain	Description	Reference/Supplier
10-beta	High efficiency cloning strain	NEB
DCM-	Dam/Dcm methyltransferase free	NEB
KRX	Expression strain	Promega

2.3.2 *E. coli* growth conditions

E. coli cells were grown in liquid Luria-Bertani (LB) medium (1 % (w/v) bacto-tryptone, 0.5 % (w/v) yeast extract and 0.5 % (w/v) NaCl) (Sambrook et al. 1989) on an orbital shaker (Innova 4400 incubator-shaker, New Brunswick Scientific, UK) at 37 ^{o}C, 225 rpm. Cells grown on solid LB 1.5 % (w/v) agar plates were

incubated on the static shelf of the incubator at 37 ^{o}C overnight. For selective growth of the transformants, antibiotics were used at the following concentration: ampicillin (100 μg ml^{-1}), chloramphenicol (30 μg ml^{-1}), erythromycin (200 μg ml^{-1}) and kanamycin (50 μg ml^{-1}).

2.4 Cyanobacterial strains and growth conditions

2.4.1 Cyanobacterial strains

All cyanobacterial mutants created in this work were derived from the wild-type glucose-tolerant *Synechocystis* sp. PCC 6803 (WT-G and hereafter) strain, which was a gift from Dr. J. K. Williams (Dupont, Delaware, USA). The genomic DNA template of *Thermosynechococcus elongatus*, used to construct FtsH over-expression vectors in *E. coli*, were extracted from a cell culture provided by Prof. James Barber's group (Imperial College London, London, UK).

2.4.2 Cyanobacterial growth conditions

2.4.2.1 Routine growth conditions

WT-G strain was cultivated on BG-11 plates (BG-11 basic mineral medium (Stanier et al. 1971), with 0.3 % (w/v) sodium thiosulphate, 10 mM N-tris [hydroxymenthyl]methyl-2-aminoethanesulfonic acid (TES-KOH) pH = 8.2 (Hihara and Ikeuchi 1997) and 1.5 % (w/v) bacto agar (Becton Dickinson Biosciences Limited, UK), added separately after autoclaving; 5 mM of glucose and 10 μM 3-(3,4-dichlorophenyl)-1,1-dimethylurea (DCMU) were added where applicable (Williams 1988a). Plates were restreaked every one to two weeks. Liquid BG-11 cultures (5 mM N-tris[hydroxymenthyl]methyl-2-aminoethanesulfonic acid (TES-KOH) pH = 8.2; 5 mM of glucose was added where applicable) were grown in sterile, air-filter capped tissue culture flasks on an orbital shaker incubator (Innova 2100 shaker, New Brunswick Scientific, UK) at 100 rpm. Large volume cultures were

grown in glass vessels on a magnetic stirrer constantly bubbled with sterile air filtered through 0.2-μm pore filter (Midisart 2000, Sartorius Limitied, UK). The strains were incubated in the growth room set at 30 ^{o}C and illuminated with an incident fluorescent white light intensity of ~10 μE m^{-2} S^{-1} (on plates) and 20 to 70 μE m^{-2} S^{-1} (in liquid). Antibiotics were used for selective growth at the following concentration: chloramphenicol (30 μg ml^{-1}), erythromycin (15 μg ml^{-1}) and kanamycin (25 μg ml^{-1}). For long term storage, cells harvested from 30 to 50 ml cultures were resuspended in 1 ml BG-11, supplemented with 5 mM glucose and 15 % (v/v) glycerol, flash frozen in liquid nitrogen and kept at -80 ^{o}C.

2.4.2.2 Growth experiment under light stress

Synechocystis cells on plates were incubated in a temperature-controlled room set at 29 ^{o}C and illuminated with an incident fluorescent white light. The illumination intensities used in this work are listed in Table 2.2.

Table 2.2: Illumination intensities in growth experiments

Conditions	Intensity
High light	~132 μmol m^{-2} s^{-1}
Medium light	~24 μmol m^{-2} s^{-1}
Low light	~5 μmol m^{-2} s^{-1}

The experiments were performed with freshly restreaked cells on BG-11 plates and BG-11 plus 5mM glucose plates. After a 7-10 day growing period, plates were photographed (Canon Power Shot Pro 1, Canon, UK).

2.5 Estimation of cell concentration of liquid *E. coli* and cyanobacterial cultures

The optical density of *E. coli* cultures was determined by measuring the absorbance at

600 nm ($OD600_{nm}$), whereas the optical density of cyanobacterial cultures was measured at 730 nm ($OD730_{nm}$). In both cases, cell cultures were transferred into a 1 ml disposable cuvette and read under a Shimadzu spectrophotometer (UV-1601, Shimadzu, Japan).

2.6 DNA associated techniques

2.6.1Vectors and recombinant plasmids

Parental plasmid vector systems that formed the basis of this work were listed in Table 2.3. The origins of the antibiotic-resistance markers that were used to enable selective growth of the transformants were listed in Table 2.4.

Table 2.3: Commercial plasmid vectors used in this study.

Vector	Purpose	Supplier	Reference
pGEM-T Easy	Cloning	Promega Corporation	Marcus et al. (1996)
pRSET A	Expression	Gift from Dr E. Cota	Douse et al. (2012)

Table 2.4: Antibiotic resistance cassettes used to construct mutants.

Vector	Antibiotic-resistance cassette	Accession #	Reference
pDC039	Chloramphenicol (catI) from pACYC184	X06403	Rose (1988)
pRL425	Erythromycin (ermC) from pE194	NC_005908	Elhai and Wolk (1988)
pDC057	Kanamycin (aphI) from pUC4K	X06404	Taylor and Rose (1988)

2.6.2 Agarose gel electrophoresis

Agarose gel electrophoresis is a method to separate DNA fragments according to their length. The method was applied to identify the molecular weight of linear DNA and purify certain DNA fragments from a mixture. An agarose gel was prepared with molecular grade agarose (Bioline, UK; final [0.5-1 % (w/v)]) dissolved in Tris-acetate-EDTA buffer (TAE; 40 mM Tris-acetate, 1 mM EDTA pH = 8.0) and SYBR® safe stain (Life technologies, USA; final [1µg ml^{-1}]). A DNA sample was mixed with 6x DNA loading buffer (40 % (w/v) sucrose, 0.25 % (w/v) Orange G),

and then loaded in a well. The molecular marker that used to determine the DNA fragments size is 2-log DNA marker ladder (New England BioLabs Limited, UK) which contained fragments of the following sizes (in Kb) : 10.0, 8.0, 6.0, 5.0, 4.0, 3.0, 2.0, 1.5, 1.2, 1.0, 0.9, 0.8, 0.7, 0.6, 0.5, 0.4, 0.3, 0.2 and 0.1. The DNA marker was diluted 25 times in RO water and mixed with 6x DNA loading buffer before use. Approximately 0.2 μg DNA marker was used to label the gel. The gel electrophoresis was carried out in TAE buffer at 100-130 V in a horizontal mini gel system (PerfectBlue^{TM} Mini Gel system; Peqlab Limited, Germany). DNA was visualised by using a UV illuminator and photos were taken (BioDoc-IT^{TM} System, UVP; CA, USA).

2.6.3 DNA purification from agarose gels

Purification of DNA fragments from agarose gels was performed using the Qiagen gel extraction kit (Qiagen Limited, UK) according to the manufacturer's protocol hand book. In the final DNA elution step, DNA bound to the column was eluted with 30 μl EB buffer and stored at -20 ^{o}C.

2.6.4 DNA amplification by polymerase chain reaction (PCR)

2.6.4.1 DNA polymerase enzymes

There were two types of DNA polymerase enzymes used in this project: Taq polymerase (New England BioLabs Limited, UK) and Phusion polymerase (New England BioLabs Limited, UK). The Taq polymerase was very economical and robust to amplify DNA samples prepared from phenol-chloroform extraction procedure, which makes it a good tool for detection of mutant segregation in cyanobacteria. Beside, Taq polymerase was also used to add an A-overhang to the 3' end of blunt-end DNA fragments to enable T-A cloning with pGEM-T Easy vector system. The Phusion polymerase is fast and accurate, with the error rate 50-fold lower than

that of Taq, which makes it ideal to produce DNA fragments for cloning or production of samples for sequencing. However, due to the 3'-5' proofreading function, DNA products amplified by Phusion polymerase were blunt ended. Therefore, Taq polymerase was required to aid T-A cloning after Phusion PCR.

2.6.4.2 Phusion polymerase reaction conditions

A standard 20 µl Phusion PCR reaction mix contained 0.4 units of polymerase, 4 µl of 5x Phusion HF buffer (as supplied by New England BioLabs Limited, UK; no information about its composition available), 0.8 µl of 20 mM dNTP mixture (ABgene, UK; final [0.2 mM] for each nucleotide: dATP, dCTP, dGTP, dTTP), 1 µl of 10 µM (Sigma-Aldrich Limited, UK; final [0.5 µM]) of each forward and reverse primer and ~100 ng template DNA. The reaction mixture was made up to 20 µl with sterile RO water and well mixed. A 50 µl reaction mix contained the same concentration of each component was used to produce large quantity of PCR fragments for downstream cloning purpose. The PCR reaction mix can also be prepared with Failsafe^{TM} PCR buffer (Cam-bio Limited, UK) to enhance amplification with difficult-to-amplify DNA templates. The reaction mix contained 50 % (v/v) 2x Failsafe buffer, 1 unit polymerase, 5 µM of each primer and ~250 ng DNA template. The PCR reaction was performed in a thermocycler (PeqSTAR, Peqlab Limited, Germany). The PCR program consisted of an initial denaturation step at 98 ^{o}C for 30 s and 25-30 subsequent cycles of 98 ^{o}C for 7 s (denaturation), 55-60 ^{o}C for 15 s (primer annealing) and 72 ^{o}C for 30 s to 2 min (primer extension; 15-30 s per 1 kb). The final extension step was performed at 72 ^{o}C for 7 min.

2.6.4.3 Taq polymerase reaction conditions

Taq DNA polymerase produced sticky-ended PCR fragments and relatively economical to use when high fidelity is not required. By using Failsafe^{TM} PCR buffer

(Cam-bio Limited, UK), the reaction mix contained the same concentration of each component as the Phusion PCR mix, except the difference in polymerase type. The PCR program consisted of an initial denaturation step at 94 ^{o}C for 2 min and 30-35 cycles of 94 ^{o}C for 10 s (denaturation), 55-60 ^{o}C for 30 s (primer annealing) and 68 ^{o}C for 1.5 min s to 3.5 min (primer extension; 60 s per 1kb). The final extension step was performed at 68 ^{o}C for 10 min.

Table 2.5: List of PCR primers used in this project.

#	Name	Primers
1	TGS-F	GATATCGATATCCTCGTTCCCCGCGGGTCCCCTAGGATGTCCCCTATACTAGGTTA TTGGAAAATTAAGGGCCT
2	TGS-R	TCTAGATCTAGAGTTAACGGCGCCTTATTTTTCAAATTGGGGATGGGACCAATTGG ATCCATCCGATTTTGGAGGATGGTCGCCACCA
3	GFP-F	GGGTCCCCTAGGATGGCTAGCAAAGGAGAAGAACTTTTCACTGGAGT
4	GFP-R	AGATCTAGATCTTTTGTAGAGCTCATCCATGCCATGTGTAATCCCAGCAGCAGTT
5	FtsH1-F	TTGGGGATGGGTTTACTGGTAGCTGGCA
6	FtsH1-OE-R	TCGGACATTGCACAGATAGGGGGCTATCTAGAGATATCCTTACCGGCTAGAGCAG GCTGTT
7	FtsH1-OE-F	AACAGCCTGCTCTAGCCGGTAAGGATATCTCTAGATAGCCCCCTATCTGTGCAATG TCCGA
8	FtsH1-R	TCACTTACCATTGATTAAATTCCATGCAACCTATGGAAAAGTCCT
9	FtsH1-Seq 1	AAATCCAAGGCCCGGTTCCAAATGGAAGCAA
10	FtsH1-Seq 2	TTGCACGAAGAGGTGCAGTTAGCGGCGA
11	FtsH1-Seq 3	GTCTAGTGGCCTTGGAAGAGGAAGGCGA
12	FtsH2-F	TAACATATGAAATTTTCCTGGAGAACTGCCCTACTTTGGT
13	FtsH2-OE-R	TGACCATACTAAATTGGTTGGAGAAGGGAATTTTTATCTAGAGATATCTAGTTGGG GAATTAACTGTTCCTTGACGGGA
14	FtsH2-OE-F	TCCCGTCAAGGAACAGTTAATTCCCCAACTAGATATCTCTAGATAAAAATTCCCTTC TCCAACCAATTTAGTATGGTCA
15	FtsH2-R	TGGGCGACCCCTGCCCTTGCACATTTTCGAGT
16	FtsH2-Seq 1	GATGTGGCCGGTATTGACGAAGCCAAGGA
17	FtsH2-Seq 2	ACCGGAAGTTTCCATCGACTCCATTGCCCGCCGT
18	FtsH2-Seq 3	AACCGTTCTGAATACTCCGAAGAAGTAGCCA
19	FtsH3-F	TCTAGCGTGAGCAAAAATAATAAAAAATGGCGTAACGCGGGCCT
20	FtsH3-OE-R	ACTCTAGGAATTCCAATGCTTGGATTCTTATCTAGAGATATCAACTAGAAGTGCCA ATTTGGCATTGTTGTTAGCCA
21	FtsH3-OE-F	TGGCTAACAACAATGCCAAATTGGCACTTCTAGTTGATATCTCTAGATAAGAATCC AAGCATTGGAATTCCTAGAGT

22	**FtsH3-R**	**GAGCAAACCAAGTACCGAGTAGAGTAAGACCT**
23	**FtsH3-Seq 1**	**CTCACCGAAGTGGTGGACTTCCTGAAAAA**
24	**FtsH3-Seq 2**	**CCCCTGGATTTACCGGTGCTGACCTGTCCA**
25	**FtsH3-Seq 3**	**GATGAAACCGCTGCGGCGATCGATGAGGA**
26	**FtsH4-F**	**CAACCCATGGCCATCAAACCCCAACCCCAA**
27	**FtsH4-OE-R**	**TTTTTAAAGGGAGCAAAAAAGCAAGTTCCTTATCTAGAGATATCTACCACTAGGGT GCCAGGAGCTTGA**
28	**FtsH4-OE-F**	**TCAAGCTCCTGGCACCCTAGTGGTAGATATCTCTAGATAAGGAACTTGCTTTTTTG CTCCCTTTAAAAA**
29	**FtsH4-R**	**TTTTACCCCCAAACGATGCAACGCCTCAGCGGCCA**
30	**FtsH4-Seq 1**	**AGTGGTGGATTTTCTCAAATTTCCCCAACGTTACA**
31	**FtsH4-Seq 2**	**CCCTGGTTTTGCCGGGGCTGACTTGGCTAACT**
32	**FtsH4-Seq 3**	**CTGCCAAAGAAATTGACCTAGAGGTCAAAGAAATCGT**
33	**FtsH2-F1**	**GGGGGATCCGATGAAATTTTCCTGGAG**
34	**FtsH2-R1**	**GGGCTCGAGTAGTTGGGGAATTAACTG**
35	**FtsH4-F1**	**ATGGCCATCAAACCCCAACCCCAATGGC**
36	**FtsH4-R1**	**TTATACCACTAGGGTGCCAGGAGCTTG**
37	**FtsH2-K218A-F**	**AGTGGGCCCTCCCGGTACCGGTGCAACTCTCCTCGCCAAGGCGATCGCCGGGGA**
38	**FtsH2-K218A-R**	**TCCCCGGCGATCGCCTTGGCGAGGAGAGTTGCACCGGTACCGGGAGGGCCCACT**
39	**FtsH2-E272Q-F**	**AGCCAAAGAGAATGCCCCCTGTTTGATCTTCATTGATCAGATTGATGCCGTGGGTC GTCAACGG**
40	**FtsH2-E272Q-R**	**CCGTTGACGACCCACGGCATCAATCTGATCAATGAAGATCAAACAGGGGGCATTCT CTTTGGCT**
41	**FtsH2-R329A-F**	**ACCGCCCTGACGTGCTAGATTCTGCCTTGATGGCTCCCGGTCGTTTCGATCGCCAA GTGA**
42	**FtsH2-R329A-R**	**TCACTTGGCGATCGAAACGACCGGGAGCCATCAAGGCAGAATCTAGCACGTCAGG GCGGT**
43	**FtsH2-H433L-F**	**TGGTGGACAGCAAAAGTAAGCGGCTAATTGCTTATCTCGAAGTAGGCCACGCCATT GTGGGCACAT**
44	**FtsH2-H433L-R**	**ATGTGCCCACAATGGCGTGGCCTACTTCGAGATAAGCAATTAGCCGCTTACTTTTG CTGTCCACCA**
45	**FtsH2-E434Q-F**	**TGGTGGACAGCAAAAGTAAGCGGCTAATTGCTTATCACCAAGTAGGCCACGCCATT GTGGGCACAT**
46	**FtsH2-E434Q-R**	**ATGTGCCCACAATGGCGTGGCCTACTTGGTGATAAGCAATTAGCCGCTTACTTTTG CTGTCCACCA**
47	**FtsH2-D511N-F**	**TGACGAAGTAACCACTGGGGCTGGTGGTAACCTACAACAGGTAACTGAGATGGCT CGCCAGA**
48	**FtsH2-D511N-R**	**TCTGGCGAGCCATCTCAGTTACCTGTTGTAGGTTACCACCAGCCCCAGTGGTTACT TCGTCA**
49	**FtsH2-C266S-F**	**TGTTTAAAAAAGCCAAAGAGAATGCCCCCTCTTTGATCTTCATTGATGAGATTGAT GCCGTGGGTCGTCA**

50	**FtsH2-C266S-R**	**TGACGACCCACGGCATCAATCTCATCAATGAAGATCAAAGAGGGGGCATTCTCTTTGGCTTTTTTAAACA**
51	**FtsH3-K207A-F**	**AGGCCCCCCCGGAACCGGTGCAACCCTGTTGGCCAAAGCCGTGGC**
52	**FtsH3-K207A-R**	**GCCACGGCTTTGGCCAACAGGGTTGCACCGGTTCCGGGGGGGCCT**
53	**FtsH3-E261Q-F**	**AGCCAATGCTCCCTGTATCGTCTTCATCGATCAAATTGATGCCGTTGGTCGTCAACGGGGCGC**
54	**FtsH3-E261Q-R**	**GCGCCCCGTTGACGACCAACGGCATCAATTTGATCGATGAAGACGATACAGGGAGCATTGGCT**
55	**FtsH3-R318A-F**	**ACCGTCCCGATGTATTGGATTCTGCCTTGATGGCTCCCGGTCGTTTCGATCGCCAAGTGGT**
56	**FtsH3-R318A-R**	**ACCACTTGGCGATCGAAACGACCGGGAGCCATCAAGGCAGAATCCAATACATCGGGACGGT**
57	**FtsH3-H423L-F**	**TGAGCGAAAAACGCAAAACCCTAGTGGCTTACCTTGAAGCTGGCCACGCCTTGGTGGGTGCT**
58	**FtsH3-H423L-R**	**AGCACCCACCAAGGCGTGGCCAGCTTCAAGGTAAGCCACTAGGGTTTTGCGTTTTTCGCTCA**
59	**FtsH3-E424Q-F**	**TGAGCGAAAAACGCAAAACCCTAGTGGCTTACCATCAAGCTGGCCACGCCTTGGTGGGTGCT**
60	**FtsH3-E424Q-R**	**AGCACCCACCAAGGCGTGGCCAGCTTGATGGTAAGCCACTAGGGTTTTGCGTTTTTCGCTCA**
61	**FtsH3-D504N-F**	**AGAGGAAGTCACCACCGGTGCTTCCAACAACCTCCAACAGGTAGCCCGGGTCGCCCGCCA**
62	**FtsH3-D504N-R**	**TGGCGGGCGACCCGGGCTACCTGTTGGAGGTTGTTGGAAGCACCGGTGGTGACTTCCTCT**
63	**FtsH3-C255S-F**	**TGAGCAGGCTAAAGCCAATGCTCCCTCTATCGTCTTCATCGATGAAATTGATGCCGTTGGTCGTCA**
64	**FtsH3-C255S-R**	**TGACGACCAACGGCATCAATTTCATCGATGAAGACGATAGAGGGAGCATTGGCTTTAGCCTGCTCA**
65	**FtsH4-K220A-F**	**AGTCGGGCCTCCCGGCACAGGCGCAACCCTACTGGCTAAAGCGGCGGC**
66	**FtsH4-K220A-R**	**GCCGCCGCTTTAGCCAGTAGGGTTGCGCCTGTGCCGGGAGGCCCGACT**
67	**FtsH4-E274Q-F**	**AACAAGCCCCTTGCATTGTCTTCATTGACCAATTGGATGCCATTGGTAAATCCCGGGCC**
68	**FtsH4-E274Q-R**	**GGCCCGGGATTTACCAATGGCATCCAATTGGTCAATGAAGACAATGCAAGGGGCTTGTT**
69	**FtsH4-R333A-F**	**ACCGCCCGGAAACCTTGGATCCAGCTTTACTGGCTCCTGGCCGTTTCGATCGCCAGGTA**
70	**FtsH4-R333A-R**	**TACCTGGCGATCGAAACGGCCAGGAGCCAGTAAAGCTGGATCCAAGGTTTCCGGGCGGT**
71	**FtsH4-H438L-F**	**GTCGGATAAGGAGAAAAAAATTGTTGCCTACCTTGAAGTGGGCCACGCACTAGTGGGAGCAGTGA**
72	**FtsH4-H438L-R**	**TCACTGCTCCCACTAGTGCGTGGCCCACTTCAAGGTAGGCAACAATTTTTTTCTCCTTATCCGAC**

73	**FtsH4-E439Q-F**	**GTCGGATAAGGAGAAAAAAATTGTTGCCTACCATCAAGTGGGCCACGCACTAGTG GGAGCAGTGA**
74	**FtsH4-E439Q-R**	**TCACTGCTCCCACTAGTGCGTGGCCCACTTGATGGTAGGCAACAATTTTTTTCTCC TTATCCGAC**
75	**FtsH4-D515N-F**	**TTGACAGCATCACCACTGGCGCGGCCAATAATTTACAACGGGCCACGGACTTAGCA GA**
76	**FtsH4-D515N-R**	**TCTGCTAAGTCCGTGGCCCGTTGTAAATTATTGGCCGCGCCAGTGGTGATGCTGTC AA**
77	**FtsH4-C268S-F**	**TTATTTGAGCAAGCCAAAAAACAAGCCCCTTCCATTGTCTTCATTGACGAATTGGA TGCCATTGGTA**
78	**FtsH4-C268S-R**	**TACCAATGGCATCCAATTCGTCAATGAAGACAATGGAAGGGGCTTGTTTTTTGGCT TGCTCAAATAA**
79	**TheFtsH2-F**	**GGATCCCGCTCCAGCAATGTACCAGGGGGACCGGGCCAA**
80	**TheFtsH2-R**	**CTCGAGCTATTTTTCAAATTGGGGATGGGACCACAGTTGGGGCACAAATCGCTCTT TATCGGGAA**
81	**TheFtsH3-F**	**GGATCCCGTGCCCAAGCGGGTCCTGGCAA**
82	**TheFtsH3-R**	**CTCGAGCTAGGGAATCGTTGCCATCTTGACGTCGTT**
83	**TheFtsH4-F**	**GGATCCGGATCCGCGAAGGTCTATGTGGAGGGAGCAA**
84	**TheFtsH4-R**	**CTCGAGCTCGAGTTAGGCAGCGGCGGGAGTTTTCACCTGAGCCAGT**
85	**Sll0862-1F**	**GCCAAGCTCCTTGCCAAGCAGACGTGAA**
86	**Sll0862-2R**	**AACGATGGGGCATGGATGTTGAAATTTTCACTATTGGAAGTCCAGATATCGGGTAA AACAAGTGTGGAAATTAGAATTATTTCTCAGCTGGGGTT**
87	**Sll0862-3F**	**AACCCCAGCTGAGAAATAATTCTAATTTCCACACTTGTTTTACCCGATATCTGGACT TCCAATAGTGAAAATTTCAACATCCATGCCCCATCGTT**
88	**Sll0862-4R**	**GATTCCGCCCCTAAATTACTCCGGTAATACTGA**
89	**Sll1150-1F**	**CTTCTTCAGTTTCCGCTTTCTCCATGGCT**
90	**Sll1150-2R**	**TACAGCTAAAATTCTGAGCAACGAGATCTTACTAAAAATGATATCAGGGGGGAAAT TATTTTTCCCTTACCTTTAATATACTATCGACA**
91	**Sll1150-3F**	**TGTCGATAGTATATTAAAGGTAAGGGAAAAATAATTTCCCCCCTGATATCATTTTTA GTAAGATCTCGTTGCTCAGAATTTTAGCTGTA**
92	**Sll1150-4R**	**AGGGGGGGATGGGATTAATCGTCTCCAT**
93	**Sll1414-1F**	**AGTTTCTCGTTCTGCCGCCTCAGCTCTT**
94	**Sll1414-2R**	**AATGGGGCCTCATAGTGGGGCATGGATTGAAGATATCAGGGCCGATTACAAAGGG GGGGATAGT**
95	**Sll1414-3F**	**ACTATCCCCCCCTTTGTAATCGGCCCTGATATCTTCAATCCATGCCCCACTATGAG GCCCCATT**
96	**Sll1414-4R**	**ATTAACTCCCCATCCACTTCCACTTCGATGAT**

2.6.4.4 Overlap extension PCR

Overlap extension PCR (Lan et al. 2005) is an effective tool to manipulate DNA

sequences. In this project, it was used to insert/remove DNA sequences to/from the original templates, to enable addition of affinity-tag coding sequences, insertion of an antibiotic resistance marker or deletion of an entire ORF to create knockout mutants. The initial reactions (PCR 1 and PCR 2) were performed using the wild-type DNA templates, 50 µl Phusion PCR reactions were performed according to the standard settings. PCR 1 contained a forward primer that carrying identical sequence as the 5' end of the target sequence. The reverse primer in PCR 1 was designed to anneal to the 3' end of the target region but with the EcoRV and XbaI restriction sites inserted right at the upstream position of the STOP codon, and ~ 30 bp downstream sequences was also contained in the reverse primer. PCR 2 contained the forward primer that was complimentary to the reverse primer in PCR1. The reverse primer was complementary to the sequence 650 bp downstream the FtsH gene. PCR program setting is described in previous paragraphs. The resulting PCR fragments were separated by agarose gel electrophoresis and gel extracted to be used as DNA templates in a final PCR (PCR 3). PCR 3 was prepared as for a 50 µl standard reaction, but with a few alterations as listed below. The forward primer in PCR 3 is the forward primer used in PCR 1 and the other one is the reverse primer used in PCR 2. Approximately 2 µl of each PCR fragment from PCR 1and 2 were used as the template DNA, the amount of each template in the reaction mix is estimated equal.

2.6.5 Restriction endonuclease digestion

Restriction endonuclease digestions were performed under suitable conditions as recommended by the enzyme manufacturer's instructions (New England BioLabs Limited, UK). Approximately 1 µg of DNA was digested in 10 µl reaction mix, with 10 to 20 units of restriction endonuclease in the recommended buffer. Acetylated bovine serum albumin (BSA; supplied with enzymes by New England BioLabs Limited, UK; final [100 µg ml^{-1}]) was applied when necessary. Digestion took 40 min to 1 h to complete.

2.6.6 DNA ligation

DNA fragments were inserted into various recipient vectors using T4 DNA ligase according to the manufacturer's instruction (New England BioLabs Limited, UK). The molar ratio between the insert and vector was 3:1. The reaction mixtures were incubated at room temperature for 30 min.

2.6.7 DNA transformation of cells

2.6.7.1 Preparation of chemically competent *E. coli* cells

A single *E. coli* colony or 50 µl of the stock culture was inoculated into 10 ml LB medium and incubated at 37 ^{o}C under consistent sharking. After overnight incubation, the optical cell density was determined at 600 nm (OD_{600nm}), and then the culture was used to inoculate 500 ml LB medium supplemented with 20 mM [final] $MgSO_4$ to a starting concentration of OD_{600nm} = 0.1. The culture was incubated on an orbital shaker at 225 rpm, 37 ^{o}C until the optical density reach OD_{600nm} of 0.4-0.6. The cells were then harvested via centrifugation in a rotor (JA-14) pre-chilled to 4 ^{o}C, for 10 min at 4,500 g. The cell pellets were then gently resuspended by shaking in 200 ml ice-cold TFB1 buffer (100 mM RbCl, 50 ml $MnCl_2$, 10 mM $CaCl_2$, 15 % (v/v) glycerol, 30 mM potassium acetate, pH = 5.8, filter sterile). The cell suspension was kept on ice for 5 min and pelleted again via centrifugation (JA-14; 4,500 g, 10 min, 4 ^{o}C). The cell pellets were then carefully resuspended in ice-cold TFB2 buffer (10 mM RbCl, 75 mM $CaCl_2$, 15 % (v/v) glycerol, 10 mM MOPS pH = 6.5, filter sterile) and incubated on ice for 60 min. The cells were then aliquotted at 4 ^{o}C and flash frozen in liquid nitrogen and stored at -80 ^{o}C.

2.6.7.2 Transformation of chemically competent *E. coli* cells

In each transformation reaction, 50 µl of chemically competent *E. coli* cells was thawed on ice for ~10 min and then, approximately 0.2 µg of plasmid DNA or ligation

mixture was mixed with cells by gently pipetting up and down with an ice-cold pipette tip. After 30 min incubation on ice, cells were heat shocked at 37 ^{o}C for 2 min and incubated for 10 min on ice. 450 µl of liquid LB medium were added and cells incubated for 1 hour under vigorous shaking at 37 ^{o}C. Then 250 µl of the mix were directly plated onto LB 1.5 % (w/v) agar plates contains a suitable antibiotic selection and if applicable 0.5 mM isopropyl-β-D-thiogalactopyranoside (IPTG) and 80 µg ml^{-1} 5-bromo-4-chloro-3-indolyl-β-D-galactoside (X-Gal). The plates were incubated at 37 ^{o}C overnight.

2.6.7.3 Transformation of *Synechocystis* sp. PCC 6803

Synechocystis cells were transformed with recombinant plasmid DNA according to the protocol described by Williams (1988) and Nixon et al. (1992). Recipient cells that were grown in liquid BG-11 medium with 5 mM glucose were harvested in exponential growth phase (OD_{730nm} < 1) by centrifugation (centrifuge model Allegra 6R, Beckman Coulter Limited, UK; GH-3.8 rotor; 2,000 g, 15 min, 29 °C) and resuspended in fresh BG-11 medium yielding a cell suspension with a final OD_{730nm} of ~5.0. For each transformation reaction, 100 µl of the concentrated cell suspension were mixed with 1 to 10 µg of recombinant plasmid DNA. The mixture was incubated at 30 °C, supplied with continuous white light illumination at ~ 5 µmol m^{-2} s^{-1} for 4 to 6 h and occasional agitation. The transformation mixture was plated onto 4-µm cellulose nitrate membrane filters (Schleicher & Schuell MicroScience GmbH, Germany) placed on a BG-11 1.5 % (w/v) agar plate (5 mM glucose where applicable). After 24 h under continuous white light illumination at ~10 µmol m^{-2} s^{-1} the filter was transferred to a new plate containing suitable antibiotic(s). Resistant colonies appeared after seven to ten days. Transformants were restreaked at least three times, until PCR analyses were performed to test for segregation.

2.6.8 DNA extraction and purification

2.6.8.1 Mini plasmid DNA preparation from *E. coli*

The mini plasmid DNA preparation procedure is described in Birnoim and Doly (1979). A single colony was picked up from a plate and inoculated 3 ml LB liquid medium containing the appropriate antibiotic(s). The *E. coli* culture was incubated overnight on the shaker at 37 ^{o}C, 225 rpm. Cells were harvested from 1.5 ml culture by centrifugation in a microfuge (model 5410, Eppendorf AG, Germany) at 1,300 rpm for 1min. The cell pellet was resuspended in 50 µl P1 buffer (Plasmid-Midi-Kit, Qiagen Limited, UK). After 50 µl P2 buffer (Plasmid-Midi-Kit, Qiagen Limited, UK) was added, the sample was gently inverted 6 times immediately to lyse the cells efficiently without disturbing the genomic DNA. The mixture was then left at room temperature for 5 min and 50 µl ice-cold P3 buffer (Plasmid-Midi-Kit, Qiagen Limited, UK) was added. After 6 time gentle inversion, it was left on ice for 5 min. Then the precipitate was spun down in the microfuge at 1,300 rpm for 5 min. Supernatant was transferred to a new tube and 1 ml 100 % ethanol was added to precipitate plasmid DNA. The sample was incubated at room temperature for 5 min and then, DNA was pelleted in the microfuge at 1,300 rpm for 10 min. The supernatant was removed and 200 µl of 70 % ethanol was added to wash the DNA. 1min later, the ethanol was removed and the DNA sample was air dried until all the ethanol had evaporated. Finally, 50 µl autoclaved RO water was added to dissolve the plasmid DNA. The sample was stored at -20 ^{o}C.

2.6.8.2 Midi plasmid DNA preparation from *E. coli*

Midi plasmid DNA preparations were performed using Plasmid–Midi-Kit (Qiagen Limited, UK) according to the manufacturer's protocol (see Qiagen Plasmid purification Handbook. 11/1998, p. 13ff). The air-dried plasmid DNA pellet was resuspended in 400 µl elution buffer (EB) which is from Qiagen gel extraction kit (Qiagen Limited, UK).

2.6.8.3 Total cellular DNA extraction from *Synechocystis* sp. PCC6803

Total cellular DNA extractions from *Synechocystis* were performed according to the phenol-chloroform extraction method devised by Dr. Josef Komenda (Institute of Microbiology, Trebon, Czech Republic). A loopful *Synechocystis* cells from a BG-11 agar plate were resuspended in 200 µl of TE buffer (10 mM Tris/HCl pH = 8.0, 1 mM EDTA) and 200 µl of phenol (saturated with 10 mM Tris/HCl pH = 8.0, 1 mM EDTA) were added. The suspension was hand-extracted twice for 20 s and centrifuged in a microfuge (Denville 2600, Denville Scientific Inc. USA) at maximum speed for 5 min at 4 ^{o}C. The aqueous phase was transferred to a new tube and one volume of chloroform was added. The mix was hand extracted for 30 s and centrifuged in a microfuge at maximum speed for 5 min. The aqueous phase was transferred to a new tube and a tenth sample volume of 3 M sodium acetate (pH = 4.8) together with two volumes of 100 % (v/v) ethanol were added and mixed by gentle inversions. To allow DNA precipitation the sample was incubated at RT for 10 min, and then the DNA was pelleted in a microfuge at maximum speed for 30 min and the obtained pellet was washed with 70 % (v/v) ethanol, resuspended in 100 µl nuclease-free RO water and stored at –20 °C.

To extract high quality genomic DNA free of phenol contamination and suitable to be used as template DNA in Phusion PCR reactions, ZR Fungal/Bacterial DNA MiniPrep (Zymo Research Co. USA) Kit was used according to the manufacturer's protocol.

2.6.9 Estimation of DNA concentration and quality

The DNA concentrations were measured with a Shimadzu spectrophotometer (UV-1601, Shimadzu, Japan) at a wavelength of 260 nm. An absorbance value of 1 at 260 nm wavelength is equivalent to a concentration of ~50 µg ml^{-1} of double strand DNA (Sambrook et al. 1989). The quality of plasmid DNA was estimated visually

after agrose gel electrophoresis and UV illumination (BioDoc-IT™ System, UVP; CA, USA) (Video Graphic Printer UP-890CE; Sony, Japan)

2.6.10 DNA sequencing

The sequencing of plasmid and PCR fragment DNA was performed by Beckman Coulter Genomics Limited, UK. Samples were prepared according to the instruction from the service provider.

2.6.11 Construction of the C-terminal tagging cassettes

Isolation and *in situ* localisation of FtsH complexes was based on C-terminal tagging approach, which has either a GST tag that enable affinity purification, or a GFP tag that is fluorescent in confocal microscopy, fused to the C-terminus of each *Synechocystis* FtsH protease. In this section, the construction of the FtsH *gst/gfp* tagging system was described.

2.6.11.1 Outline of the C-terminal *gst/gfp* tagging strategy

As multiple proteins were to be fused with a GST tag, we decided to create a universal tagging cassette (Figure 2.1) that starts with a thrombin cleavage site (to enable tag removal after purification), following by the cDNA sequence of glutathione-S-transferase (GST) from *Schistosoma japonicum*, and then a *strep* II tag before the STOP codon. Three endonuclease restriction sites, KasI, HpaI and XbaI were designed 3' to the STOP codon; the HpaI site will be used as the insertion site for selectable markers. The whole tagging cassette was designed to be released by EcoRV and XbaI digestion; the AvrII, BamHI and KasI sites enable further modifications such as addition, removal or replacement of each module in the cassette, e.g. replacing the *gst* with the coding sequence of green fluorescent protein (GFP). Once the desirable selectable marker was integrated into the cassette (erythromycin in

this case), the GST tagging vector was completed. Though the whole cassette was designed to be released by digesting with enzyme EcoRV + XbaI; it can also be released via EcoRV + any downstream restriction site, that locates in the multiple cloning sites (MCS) region of the vector backbone and doesn't appear in the cassette sequence.

Working in parallel, each *ftsH* gene and 655 bp of downstream sequence was amplified by PCR using the genomic DNA template from WT *Synechocystis* and cloned into the pGEM-T Easy vector. EcoRV and XbaI sites were inserted immediately before the STOP codon of *ftsH* to enable the insertion of the GST tagging cassette. The *ftsH* gene and the downstream sequence act as flanking sequences for homologous recombination, via double crossover, when the plasmid vector is transformed into *Synechocystis* sp. PCC 6803.

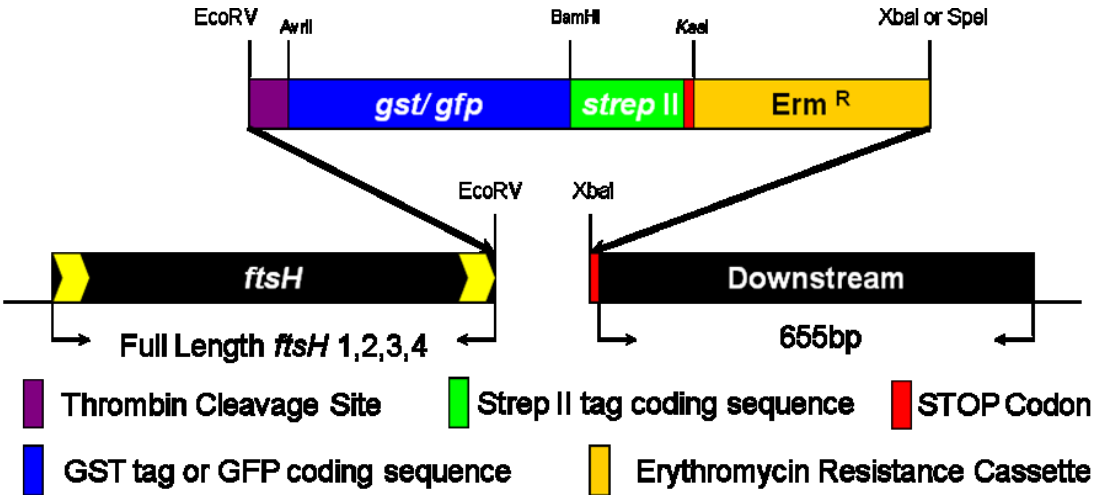

Figure 2.1: Cloning strategy and construct scheme.
A DNA tagging cassette which contains a thrombin cleavage site, GST/GFP and Strep II tag coding sequences as well as the erythromycin resistance cassette was ligated at the 3' end of each FtsH coding sequence.

2.6.11.2 Construction of backbone vectors carrying *ftsH* flanking sequences

Plasmid vectors carrying *ftsH* flanking sequences were constructed via overlap

extension PCR (Figure 2.2 A). Primer pairs FtsH(x)-F and FtsH(x)-OE-R, FtsH(x)-OE-F and FtsH(x)-R, where (x) represents the respective number 1-4, were used to setup the initial reactions, then the resulting PCR fragments were gel extracted and used as the DNA templates in the final PCR reaction (PCR3) along with primer pair FtsH(x)-F and FtsH(x)-R. The final PCR fragment carrying restriction sites EcoRV and XbaI in front of the STOP codon was then added with a 3' Adenine-tail and cloned into pGEM-T Easy vector. The resulting plasmid, namely pGEMFtsHx, where x represents the respective homologue (Figure 2.2 B), was checked via diagnostic digestion with NdeI and XbaI to examine the orientation of the insertion (Figure 2.2 C), and according to the digestion pattern on the gel, all FtsH inserts were successfully inserted into the plasmids and placed against the transcription direction of the *lacZ* operon. The sequence of each insert was then confirmed via sequencing.

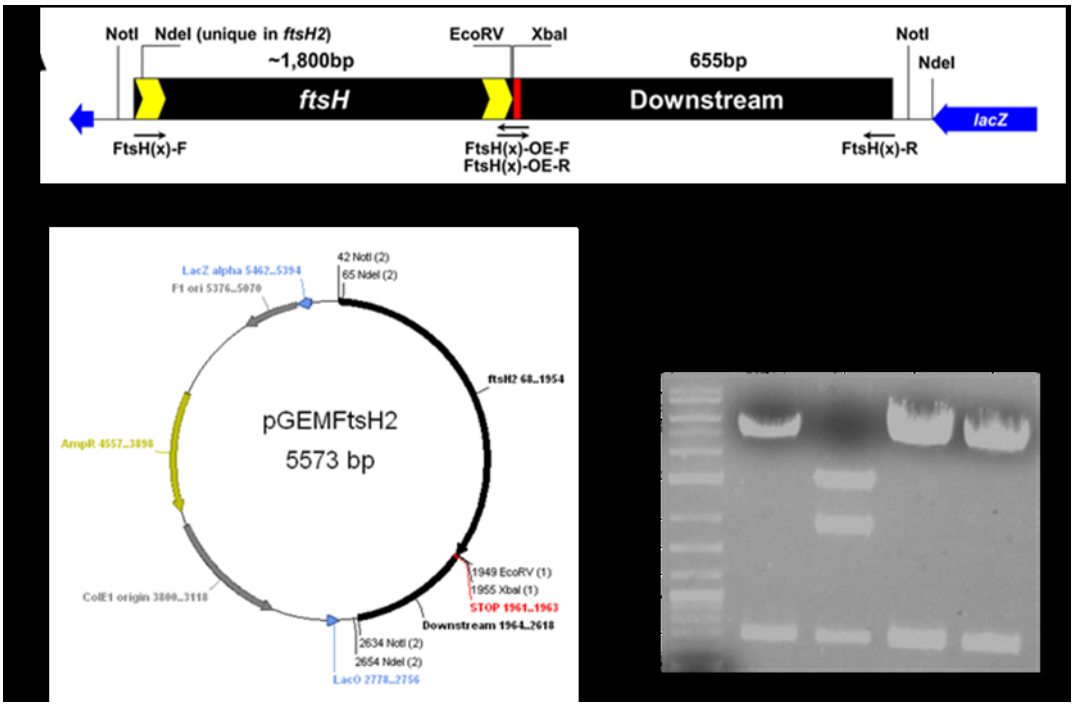

Figure 2.2: **Construction of the backbone vector carrying *ftsH* flanking sequences.**

(A) Schematic representation of the flanking sequence and how the restriction sites were introduced via overlap extension PCR. (B) Plasmid map of pGEMFtsH2 vector, which carries an additional NdeI site at the 5' end of the *ftsH2* ORF. (C) Restriction digests of each of the pGEMFtsHx vectors using NdeI and XbaI, where FtsHx represent the particular homologue.

2.6.11.3 Construction of the GST tagging vectors

PCR was used to amplify the *gst* gene from pGEX-6P-3 vector (Amersham, USA) using Phusion polymerase. The forward primer (Table 2.5) contained an EcoRV restriction site at the beginning of the 5' end followed by thrombin cleavage site sequences, then an AvrII site at just before the *gst* sequence. The reverse primer carried an XbaI site at the 5' end, followed by HpaI and KasI sites, then the complementary sequences for the STOP codon, *strep*II tag sequence and the *gst* sequence without its own STOP codon.

The *gst::strep*II fragment was then ligated into the pGEM-T Easy vector backbone to obtain the first parental vector pGST (Figure 2.3 A). An antibiotic resistance cassette, in this case, a cassette conferring erythromycin resistance, was inserted into the pGST plasmid via HpaI site to create the GST-Erm tagging cassette (Figure 2.3 B).

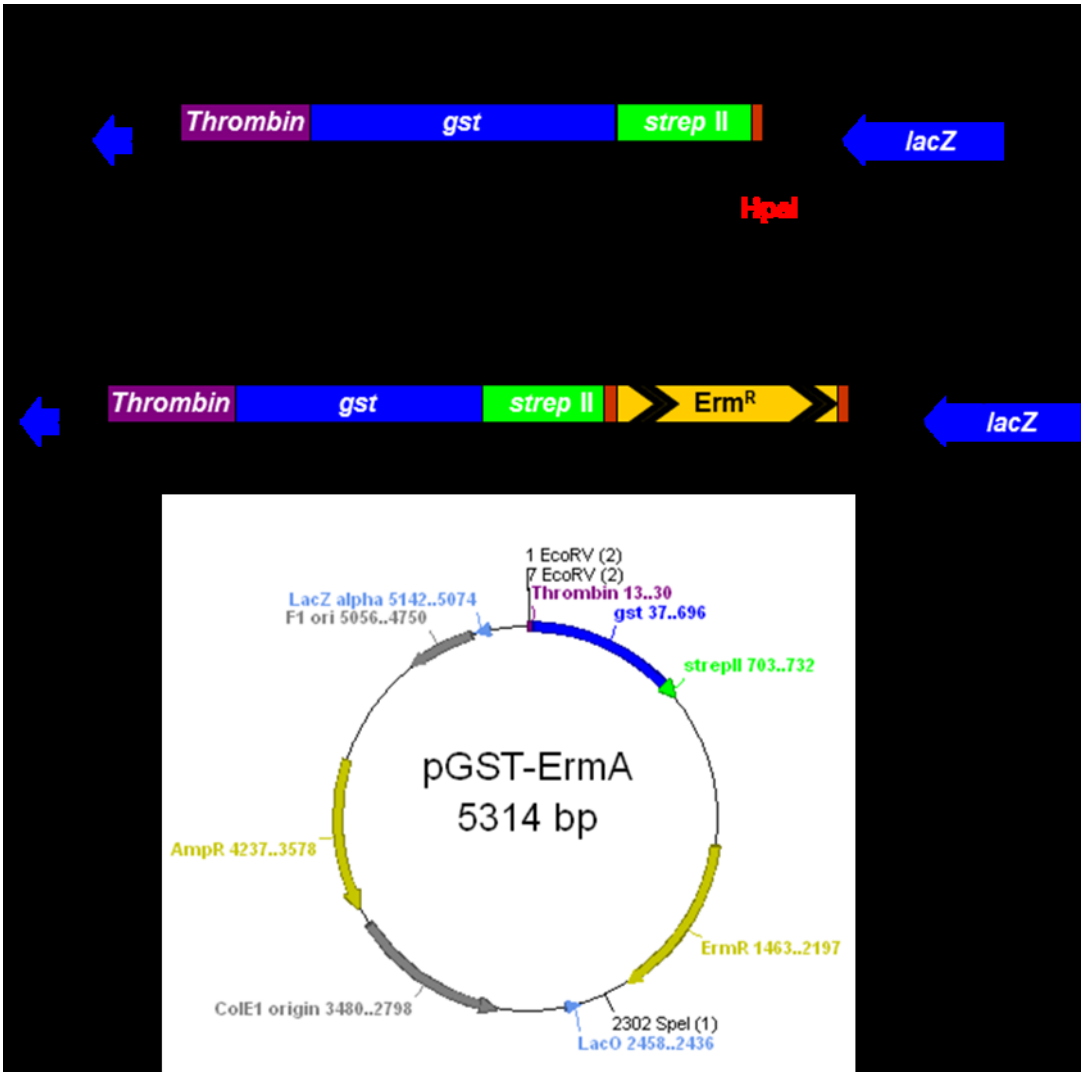

Figure 2.3: Construction of GST tagging vectors.
Schematic representations of the inserts found in (A) pGST, (B) pGST-ErmA and (C) the plasmid map of pGST-ErmA. A detailed description of the cloning strategy can be found in Materials and Methods. In panels (A) and (B), blue arrows represent *lacZ'* on the pGEM-T Easy vector backbone. Purple boxes represent the coding sequence of the thrombin cleavage site. Blue and green boxes indicate the *gst:strep II* tagging sequence. The yellow box indicates the erythromycin-resistance cassette; the black arrows show the direction of transcription.

Tagging cassettes that provide resistance to various antibiotics could be beneficial to tag mutants that already confer resistance to antibiotics. Therefore, to increase the availability of the tagging cassettes conferring different antibiotic resistance, three types of resistance markers that enable resistance to chloramphenicol, erythromycin and kanamycin were introduced into pGST vectors, and each resistance cassette was

inserted in two orientations (Figure 2.4 A1, B1 and C1). The orientation of the resistance cassettes were confirmed via endonuclease digestion (Figure 2.4 A2, B2, C2).

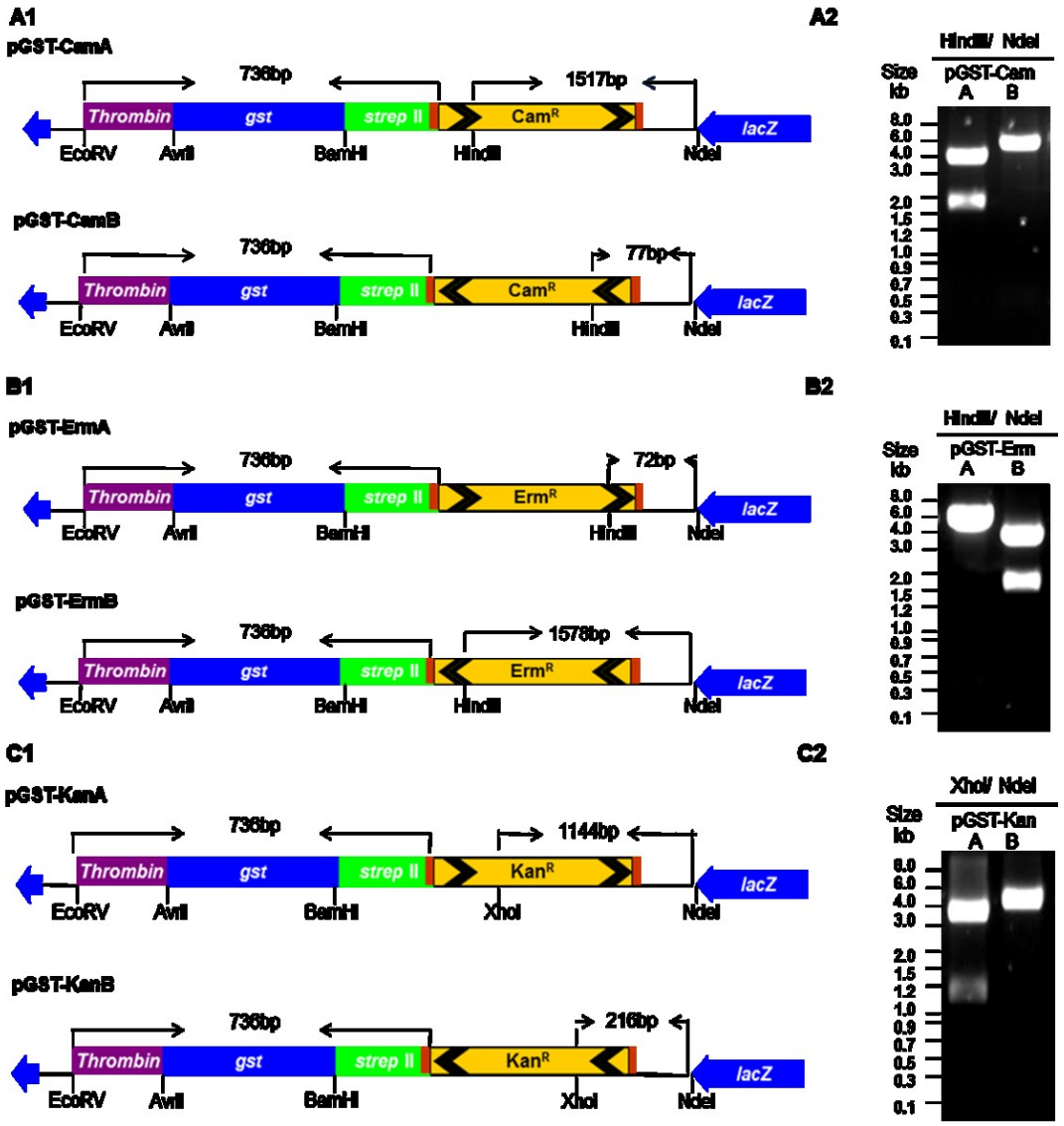

Figure 2.4: Schematic representation of GST tagging cassettes.
(A1, B1 and C1) show the schematic layout of each GST cassette, including the orientation of each antibiotic resistance cassette. The undrawn pGEM-T Easy vector backbone is ~3 kbp. (A2, B2 and C2) show the digestion pattern of each cassette on agarose gel. Cam^R: chloramphenicol resistance cassette; Erm^R: erythromycin resistance cassette; Kan^R: kanamycin resistance cassette.

2.6.11.4 Construction of the GFP tagging vectors

One of the objectives is to localise the FtsH homologues via fluorescence microscopy.

A GFP tag was to be fused to the C-terminus of each FtsH homologue to enable *in situ* localisation. The coding sequence of GFP+ was amplified from plasmid vector pMutin (Scholz et al. 2000), using primer pair GFP-F and GFP-R (Table 2.5) and then digested with AvrII and BglII to create compatible ends for ligation. pGST vector was digested with AvrII and BamHI to excise the *gst* insert, the vector backbone was gel purified and ligated with the *gfp* sequence. The resulting plasmid pGFP contains the same layout to pGST, except that the *gst* region was replaced with *gfp* and the BamHI site between *gst* and *strep*II is gone after BglII-BamHI ligation (Figure 2.5 A). The vector pGFP was then sequenced to confirm no mutation was generated during the cloning process, however, an additional BglII site was found between the *gfp* and *strepII* sequences due to incomplete digestion before ligation. The redundant BglII sequence introduced an additional Arg-Ser sequence to the GFP-StrepII linker region. An antibiotic resistance cassette was consequently inserted into the pGFP to yield the final GFP tagging vector (Figure 2.5 B and C).

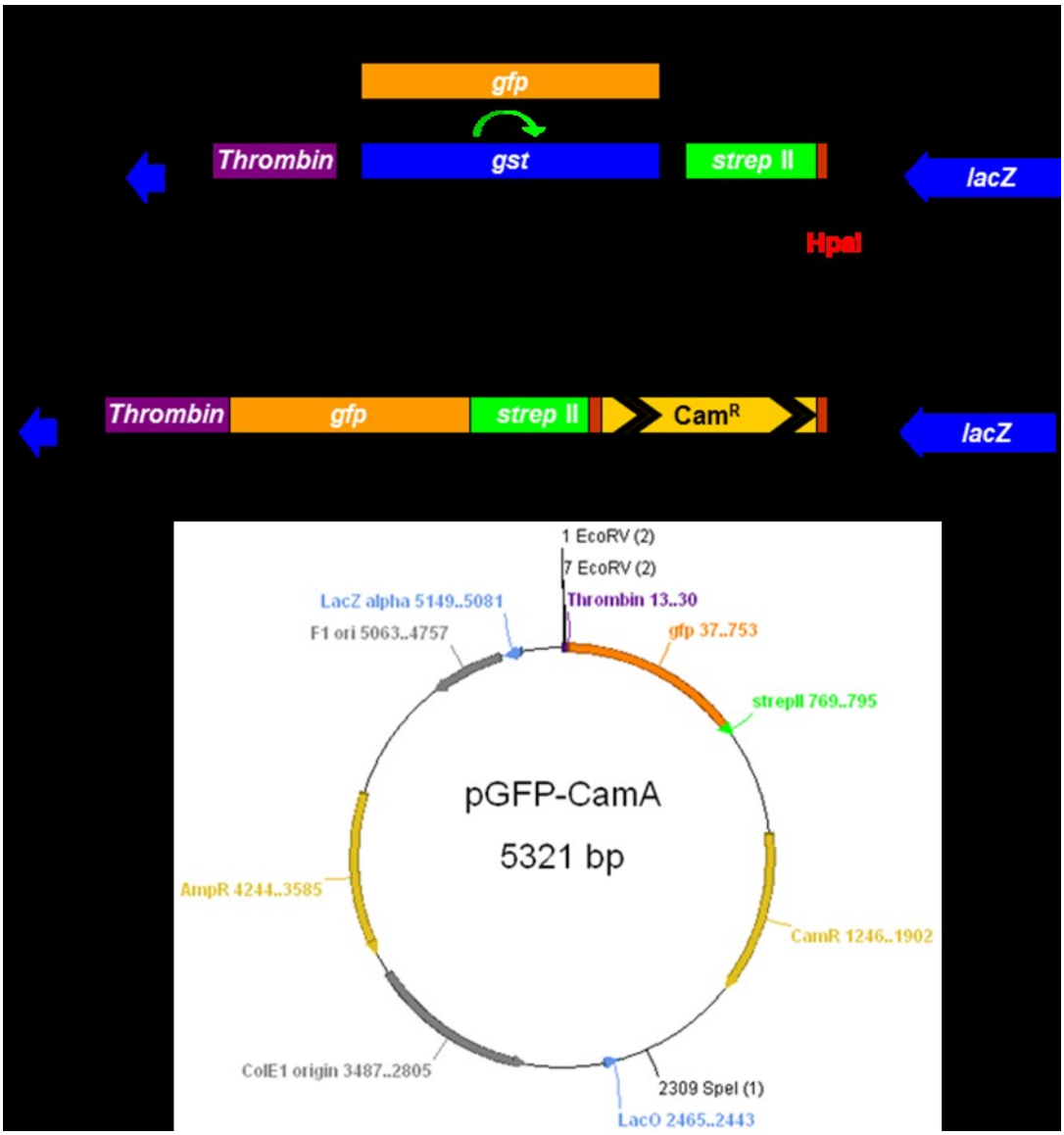

Figure 2.5: Construction of GFP tagging vectors.
Schematic representations of the inserts found in (A) pGFP, (B) pGFP-CamA and (C) the plasmid map of pGFP-CamA. A detailed description of the cloning strategy can be found in Materials and Methods. In panels (A) and (B), blue arrows represent *lacZ'* on the pGEM-T Easy vector backbone. Purple boxes represent the coding sequence of the thrombin cleavage site. Orange and green boxes indicate the *gst:strep II* tagging sequence. The yellow box indicates the chloramphenicol-resistance cassette; the black arrows show the direction of transcription.

Similar to the construction of GST tagging cassette, multiple antibiotic resistance cassettes which confer resistance to chloramphenicol, erythromycin and kanamycin were used to create a range of selections for the GFP tagging cassette (Figure 2.6).

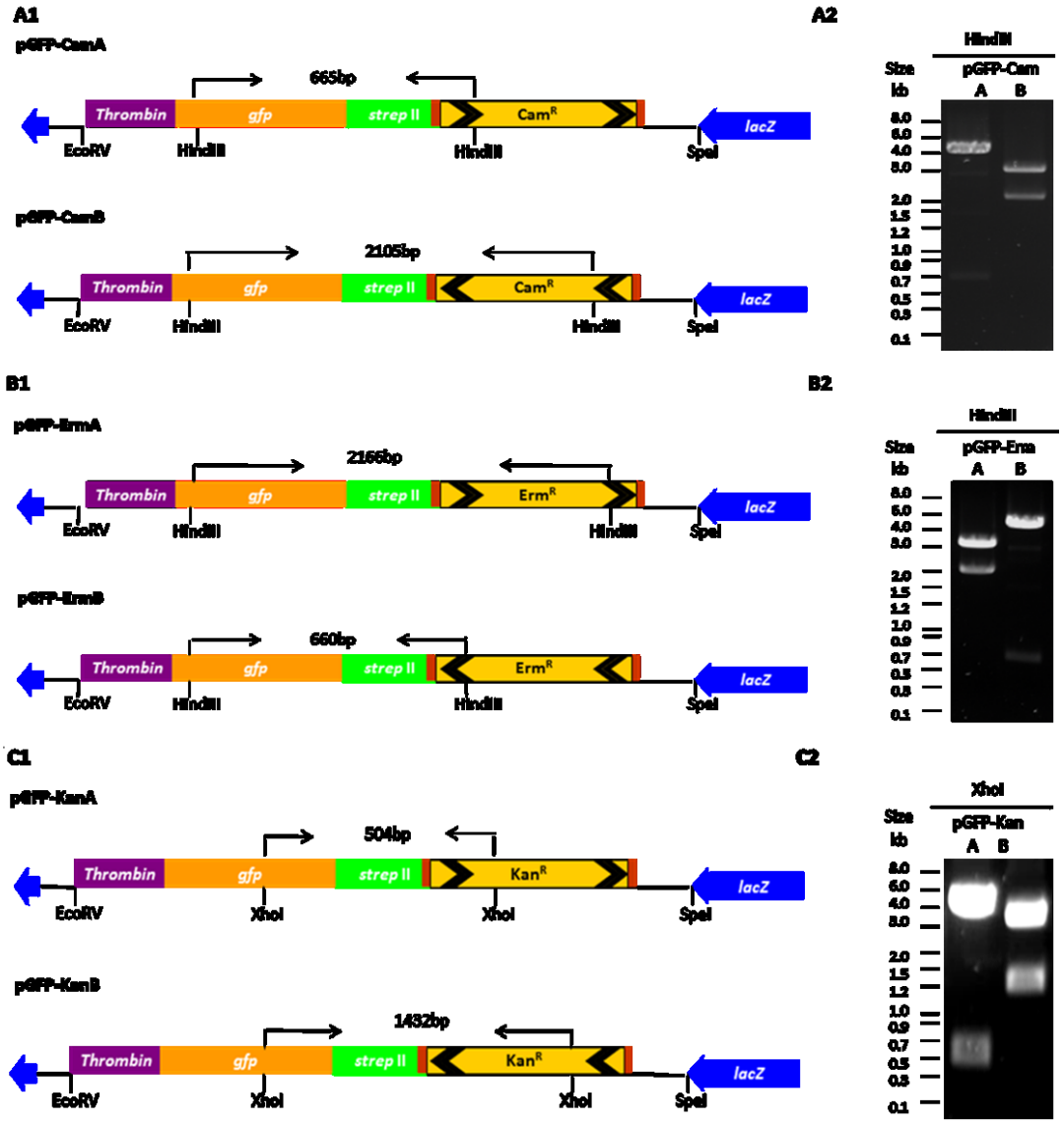

Figure 2.6: Construction of GFP tagging cassettes.
(A1, B1 and C1) show the layout of each GFP cassette, including the orientation of each antibiotic resistance cassette. The undrawn pGEM-T Easy vector backbone is ~3 kbp. (A2, B2 and C2) show the digest pattern on agarose gel. Cam^R: chloramphenicol resistance cassette; Erm^R: erythromycin resistance cassette; Kan^R: kanamycin resistance cassette.

2.7 Protein biochemistry techniques

2.7.1 Small-scale crude membrane preparation

Approximately 50 ml of cell culture (~75 µg of Chl in total) was harvested via centrifugation (centrifuge model J2-21; Beckman Coulter Limited, UK; JA-14 rotor; 2,450 g, 15 min, 4 °C). The supernatant was then carefully removed and the

remaining pellet was resuspended in 500 µl KPN buffer (40 mM K-phosphate, pH = 8.0, 100 mM NaCl), appropriate amount of EDTA-free protease inhibitor cocktail tablets (Roche, UK) was also supplemented to the KPN buffer prior to application. The resulting cell suspension was then transferred to a 2 ml centrifugation tube (Eppendorf, Germany) containing ~200 µl glass beads, the size of which was 212 to 300 µm (Sigma Aldrich, UK). The mixture was then pre-chilled on ice and then vortexed (Vortex-Genie 2, Scientific Industries, Inc. USA) under green light at the maximum speed for 1 minute. The mixture was then chilled on ice for 1 minute to reduce the heat generated in the vortexing step. Depending on the breakage efficiency, the cells were disrupted multiple times via the vortex-chill cycle, typically the breakage was performed 3 times per sample. After breakage, the supernatant was carefully transferred into a new 1.5 ml centrifuge tube and membrane fragments stuck in glass beads was rinsed with 800 µl KPN buffer containing protease inhibitor, and combined with the previously retrieved fraction. Unbroken cells in the lysate were span down in the microcentrifuge (Denville 2600, Denville Scientific Inc. USA) at 6,600 g for 1 min at 4 ^{o}C. The supernatant containing membrane fragments were carefully transferred to a new 1.5 ml centrifuge tube and further spun twice to remove as much unbroken cells as possible. Noteworthy, the colour of the supernatant should be dark-green and transparent at this stage. The supernatant was then span at 16,000 g for 40 min to harvest the membrane fraction. After the centrifugation, the blue supernatant containing soluble proteins was removed, and the membrane pellet was resuspended in 50 µl KPN buffer without protease inhibitor. The chlorophyll *a* concentration of the membrane sample was then measured and adjusted to desirable level, typically 0.4 µg µl^{-1}.

2.7.2 Protein purification techniques

2.7.2.1 Purification of FtsH-GST from *Synechocystis* sp. PCC6803

Approximately 10 litre of *Synechocystis* sp. PCC 6803 cell culture was initially

concentrated to ~2 litres using a tangential flow filtration system (Millipore Limited, UK) and then pelleted via centrifugation (centrifuge model J2-21; Beckman Coulter Limited, UK; JA-14 rotor; 9,600 g, 10 min, 4 °C). Then the pellet was washed with ~500 ml ice-cold KPN buffer (40 mM K-phosphate, pH = 8.0, 100 mM NaCl). Cells were pelleted again by centrifugation, and then resuspended with KPN buffer and a protease inhibitor cocktail tablet (Roche, UK) to a final volume of 50 ml. The cell suspension was then fractionated in a cell disruptor (Constant System Limited, UK) at 25 kPsi, 4 ^{o}C. After breakage, the suspension was centrifuged (centrifuge model Allegra 6R, Beckman Coulter Limited, UK; GH-3.8; 2,000 g, 15 min, 4 °C) to pellet unbroken cells. The supernatant was transferred into two type Ti45 ultracentrifugation tubes and centrifuged (ultracentrifuge model L-70; Beckman Coulter Limited, UK; Ti45 rotor; 100,000 g, 60 min, 4 °C). The pellet containing the thylakoid membrane was resuspended in 45 ml of Buffer A (50 mM HEPES, pH=7.2, 1.2 M Betaine, 10 % (v/v) Glycerol, 100 mM NaCl, 5 mM $MgCl_2$, 10 µM $ZnCl_2$). 5 ml of 10 % (w/v) n-dodecyl-β-maltoside (β-DM) was added to the thylakoid suspension to solubilise the membrane proteins. The Mixture was then kept on a rotating wheel in the dark for 30 min at 4 ^{o}C. Insoluble components were then pelleted by centrifugation (ultracentrifuge model L-70; Beckman Coulter Limited, UK; Ti70 rotor; 100,000 g, 30 min, 4 °C), and the soluble fraction was applied to 5 ml pre-equilibrated GST-Agarose resin. After 2 h incubation in the dark, on a rotating wheel at 4 °C, the resin was washed by ~200 ml of washing buffer (50 mM HEPES, pH=7.2, 5 % (v/v) Glycerol,100 mM NaCl, 5 mM $MgCl_2$, 10 µM $ZnCl_2$, 0.03 % (w/v) β-DM). Then the FtsH sample was either eluted with 10 ml of elution buffer (50 mM Tris/HCl, pH=8.0, 80 mM NaCl, 5 mM $MgCl_2$, 12.5 µM $ZnCl_2$, 0.005 % (w/v) β-DM, 1.4 mM 2-mercaptoethanol, 25 mM Reduced Glutathione), or a thrombin on column cleavage was performed by applying 5 ml cleavage buffer (50 mM Tris/HCl, pH=8.0, 80 mM NaCl, 5 mM $MgCl_2$, 12.5 µM $ZnCl_2$, 0.005 % (w/v) β-DM, 1.4 mM 2-mercaptoethanol, 50 unit thrombin). For on column cleavage, the resin was

incubated with cleavage buffer on a rotating wheel for 1.5 h at room temperature. Then the resin was pelleted by centrifugation (centrifuge model Allegra 6R, Beckman Coulter Limited, UK; GH-3.8; 2,000 g, 1 min, 4 °C). The supernatant contains GST-free FtsH sample, and the undigested samples were eluted with elution buffer.

2.7.2.2 Purification of recombinant protein from *E. coli*

The expression *E. coli* strain KRX (Promega) was firstly transformed with the targeting expression vector, then the transformants were grown overnight in advance. A 10 ml starting culture was prepared by inoculating a single colony from the transformation plate into 10 ml LB medium containing 100 μg ml^{-1} ampicillin, and then incubated at 37 ^{o}C overnight, 200 rpm. On the following day, the cell culture was then used to inoculate 1 L LB medium to a starting $OD600_{nm}$ of 0.1. The scaled up culture was then grown at 37 ^{o}C, 200 rpm until the $OD600_{nm}$ reach 0.4-0.5. The culture was then chilled to room temperature and induced with 0.1 % (w/v) L-rhamnose. The culture was then incubated at 18 ^{o}C overnight. On the following day, cells were harvested via centrifugation (JA-14 rotor; 4,000 g, 10 min, 4 °C) The resulting cell pellet was resuspended in 25 ml lysis buffer (50 mM Tris-HCl buffer pH = 7.9, 500 mM NaCl and 10 mM Imidazole) containing appropriate amount of EDTA-free protease inhibitor cOmplete (Roche) and disrupted via ultrasonication (Sonic Vibra-Cell VCX 130). The disruption was performed on ice bath with the cycle and strength setting of 5 sec on, 5 sec off, 75% amplitude. The insoluble fraction was then removed from the disrupted cell lysate via centrifugation (JA-14 rotor; 4,000 g, 40 min, 4 °C), and the resulting soluble fraction was further filtered with a 0.45 μm filter Minisart (Sartorius Stedim Biotech) and used for consequent purifications.

The consequent purification steps were conducted at 4 °C. The soluble fraction of cell lysate was applied to ~ 10 ml of Ni-NTA resin (Thermo Scientific), which was pre-equilibrated with lysis buffer. The mixture was then transferred to a rotating wheel

and incubated for 30 min. The supernatant was then removed and the resin was washed 3 times with 1 column volume of washing buffers (50 mM Tris-HCl pH=7.9 and 500 mM NaCl) containing a gradient of imidazole concentration (10 mM, 30 mM and 60 mM). After washing, the resin-bound protein was eluted with elution buffer (50 mM Tris-HCl pH=7.9, 500 mM NaCl and 500 mM imidazole).

2.7.3 Polyacrylamide gel electrophoresis (PAGE)

2.7.3.1 Sodium dodecyl sulphate gel electrophoresis (SDS-PAGE)

The SDS-PAGE gels were self-cast, 0.75 mm thick and run in the Bio-Rad Mini-PROTEAN III vertical gel system (Bio-Rad Laboratories Limited, UK). The separation gel was typically a 12.5 % (w/v) continuous polyacrylamide (PAA; from a 40 % acylamide/bisacrylamide = 37.5g l^{-1} stock solution), 6 M urea, 0.375 M Tris/HCl pH = 8.9, 0.01 % (v/v) N,N,N',N' tetramethylenediamine (TEMED); 0.1 % (w/v) ammonium persulphate (APS) SDS-PAGE gel. A 5 % (w/v) PAA (from a 40 % arylamide/bisacrylamide = 37.5/l stock solution) stacking gel containing 0.125 M Tris/HCl pH = 6.8, 0.01% (v/v) TEMED and 0.1% (w/v) APS was poured on top of the separation gel. Samples for SDS-PAGE analyses were mixed with 2x SDS sample buffer (2x concentrate: 125 mM Tris/HCl pH 6.8, 4 % (w/v) SDS, 20 % (v/v) glycerol, 0.1 % (w/v) bromophenol blue and 10% 2-mercaptoethanol added freshly before each use; final [1x]) and then incubated for 5 min at 95 ^{o}C to achieve quick solubilisation. Importantly, membrane proteins prepared from crude membrane preparation (see section 2.7.1) are not suitable for heat denaturation as extensive aggregation has been observed before. The alternative approach is to solubilise protein with SDS sample buffer at room temperature for 40 min. After solubilisation, insoluble materials were pelleted in a microcentrifuge at maximum speed for 10 min at room temperature. 10 µl samples were loaded in each well. The gels were run at room temperature with constant voltage of 125 V for 2-3 hours using a Bio-Rad PowerPac Basic (Bio-Rad Laboratories Limited, UK) in the Tris-glycine running buffer (25 mM Tris, 190 mM

glycine, 0.1 % (w/v) SDS, pH = 8.3).

2.7.3.2 Coomassie staining

The obtained gels were either stained with Coomassie (40 % (v/v) methanol, 10 % (v/v) acetic acid and 0.25 % (w/v) Coomassie-brilliant-blue-R-250) overnight a rocking shaker and destained with destain buffer (40 % (v/v) methanol, 10 % (v/v) acetic acid) for ~2 hours at room temperature to remove background strain; or used for immunoblotting (see 4.9.3)

2.7.3.3 Silver staining

After electrophoresis, the SDS-PAGE gel was incubated with fixation buffer (40 % (v/v) ethanol and 10 % (v/v) acetic acid) for 15 min, and then transferred into fresh fixation buffer for another 15 min. The gel was then washed with ddH_2O 3x 5 min, then transferred into sensitisation buffer (30 % (v/v) ethanol, 0.2 % (w/v) sodium thiosulfate and 6.8 % (w/v) sodium acetate) for 30 min. Then again, the gel was washed with ddH_2O 3x 5 min, prior to staining (0.25 % (w/v) silver nitrate) for 20 min. Excessive stains were washed away with ddH_2O 2x 1 min, and then the gel was incubated with development buffer (2.5 % (w/v) sodium carbonate and 0.04 % (v/v) formaldehyde (freshly added)). The gentle agitation was applied during the development period until the intensity of protein bands was satisfactory. Stop buffer (1.46 % (w/v) EDTA) was applied to mediated the reaction, and after 10 min incubation, the gel was washed with ddH_2O 3x 5 min.

2.7.4 Detection of the FtsH homologues, immunoblotting analysis

2.7.4.1 Design of FtsH-specific antibodies

Immunoblotting is a versatile tool to detect the presence/absence of the targeting antigen in the samples, and it was used in many experiments in this study to detect the protein level, to elucidate the association between FtsH homologues, to clarify the

location of FtsH complexes and so on. Hence the main focus of this study was to characterise the four FtsH homologues in *Synechocystis*, short-peptide antibodies specific to each homologue was needed. To ensure the specificity of each antibody, a short-peptide sequence, approximately 15-20 amino acid in length, from less-conserved regions and unique to each homologue was synthesised and used as the antigen to raise antibodies in rabbits (Table 2.6). In addition, another FtsH antibody (αFtsH global) that specific to a conserved sequence presents in all cyanobacterial FtsH homologues, and therefore detects all four homologues with equal sensitivity, was also raised to quantify the ratio of abundance among homologues.

There are three major domains present in FtsH: the transmembrane domain (TM), the AAA+ domain and the protease domain (PD), of which, only the AAA+ domain is highly conserved. Therefore, the sequence region for αFtsH global antibody was selected from the AAA+ domain according to the alignment. The PD domain is less conserved due to its functional variations (Lee et al. 2011), moreover, it is a soluble domain, which is an ideal location to search for soluble peptide sequences. The antigen sequences for FtsH1 and FtsH4 antibodies were selected from the PD region. Finally, although the TM is among the least conserved domain in FtsH, most of its sequences form hydrophobic helices spanning across lipid bilayer of membranes. The only soluble region in TM is the loop connecting the two helices, thus the sequences in the loop region of FtsH2 and FtsH3 were the targeting region for the respective antibodies.

Table 2.6: Design of the short-peptide FtsH antibodies.

Antibody	Peptide antigen	Targeting region
αFtsH (global)	**C-GGNDEREQTLNQLLTEMDG**	Conserved region in AAA+ domain
αFtsH1	**C-EGDRNFSGGDWGKRS**	Unique region in PD domain
αFtsH2	**RLRDSNIRLDSHPVRNNG**	Loop region between the two TM helices
αFtsH3	**SADRTQAQVPNPSGGPP**	Loop region between the two TM helices
αFtsH4	**C-NPRRMVSDDTAKEIDLEVK**	Unique region in PD domain

The sequence of each peptide antigen synthesised to raise antibodies was listed in the table, following by a brief description of the antibody targeting region.

Peptide antigens were then ordered and used to raise antibodies in rabbits (Seqlab sequence laboratories Limited, Germany). Blood sera containing antibodies were tested on membrane-protein extractions prepared from *Synechocystis* mutants to check specificity (data not shown). Satisfactory antibodies were consequently affinity-purified with the respective peptide-antigens to enhance specificity and sensitivity (Seqlab sequence laboratories Limited, Germany). According to the screening tests, αFtsH (global) and αFtsH4 were specific and highly sensitive to the targeting proteins, αFtsH2 and αFtsH3 were specific, however, less sensitive. αFtsH1 was specific, however, contaminated with αFtsH4 in the affinity purification process, and the remaining crude sera were not as sensitive as the purified version.

Overall, we have successfully obtained all antibodies highly specific to the targeting proteins, however, the sensitivity of αFtsH1, αFtsH2 and αFtsH3 was relatively poor.

2.7.4.2 Immunoblotting detection

1-D SDS-PAGE gels were used for immunoblotting analyses. Protein transfer was performed for at least 90 min in transfer buffer (3 mM Na_2CO_3, 10 mM $NaHCO_3$ and 20 % (v/v) methanol) onto nitrocellulose membrane (Trans Blot, Transfer medium nitrocellulose membrane, 0.2 μm; Bio-Rad Laboratories Limited, UK). The current

was set up constantly at 400mA. After the proteins were blotted, the nitrocellulose membrane was blocked for 1 hour with 1x PBS-T (150mM NaCl. 7.5 mM Na_2HPO_4, 2.5 mM NaH_2PO_4 and 0.1% (v/v) Tween 20) supplemented with 5 % (w/v) milk powder. The membrane was then briefly washed with 1x PBS-T and incubated overnight at 4 ^oC on a rocking shaker with a primary antibody of choice. On the next day the membrane was washed three times for 20 min with 1x PBS-T and subsequently incubated for 1 hour at room temperature with the appropriate secondary antibody (anti-rabbit IgG, horseradish peroxidase conjugate or anti-mouse IgG, horseradish peroxidase conjugate, 1:10,000 dilution in 1x PBS-T; Amersham Pharmacia, UK). Unbound secondary antibody was removed by washing the membrane three times for 10 min with 1x PBS-T and two times for 10 min with 1x PBS. The secondary antibody was detected by the enhanced chemiluminescence procedure. The membrane was incubated for 1 min in a 1:1 mixture of ECL reagent A (100 mM Tris/HCl pH = 8.3, 0.4 mM p-coumaric acid (90 mM stock solution in DMSO), 2.5 mM luminol (250 mM stock solution in DMSO)) and ECL reagent B (100 mM Tris/HCl pH = 8.3, 100 mM H_2O_2). The membrane was then enveloped into an A4 reinforced pocket and exposed to an X-Ray film (SuperRX, X-Ray film, 100 NIF, 18x24 cm; Fuji medical, UK) for 1 sec to 10 min. The film was developed according to the manufacturer's instructions.

2.7.5 Assay for nucleoside triphosphatase activity

The nucleoside triphosphatase activity was measured according to the liberation of phosphate from nucleoside triphosphates ATP, GTP, CTP and UTP (NTP). Appropriate amount of the testing protein was preloaded to the reaction buffer (50 mM Tris-Acetate, 5 mM magnesium chloride, 1.5 mM β-mercaptoethanol), and the mixture was heated to 55 °C (the optimal temperature for FtsH). Then, the reaction was initiated by adding 0.5 mM NTP, and was terminated by adding 6 % perchloric acid. Upon termination, malachite green solution (0.1 % (w/v) malachite green, 1.1 %

(w/v) ammonium molybdate, 1.5 % (w/v) Bismuth (III) citrate and 8.4 % (v/v) concentrated HCl) was added to the reaction mixture at 1:1 ratio. After 3 to 15 min of incubation, absorbance at 650 nm was measured. Four measurements were taken at 20, 40, 60 and 80 min. Serial diluted phosphate standards (0, 0.1, 0.4, 1.2, 3.7, 11.1, 33.3 and 100 μM of KH_2PO_4) were prepared and parallel treated for calibration.

2.7.6 Assay for proteolytic activity

The proteolytic activity of protease was examined using a fluorescence-based quantitative casein degradation assay (EnzChek Protease Assay Kits (Invitrogen)). Prior to the assay, the protease was firstly normalised to a concentration of 10 μg μl^{-1}, and then diluted to a concentration of 40 μg ml^{-1} with the reaction buffer supplied in the kit. To start the reaction, 100 μl of the reaction buffer containing protease was mixed with equal volume of the casein substrate according to the manufacturer's instruction menu. 1 μl of 100 mM ATP was added to the reaction mixture, and plate was immediately incubated at 55°C. Protease activity was determined by measuring the fluorescence with the filter excitation/emission = 485/530. Fluorescence reading was performed at 5 min, 30 min and 45 min.

2.7.7 Protein N-terminal sequencing

Purified protein samples (see section 2.7) were loaded on an SDS gel which was prepared one day in advance, and run with the Tris-glycine running buffer (see section 2.7.3.1), which is supplemented with 2mM-mercaptoacetic acid in addition to prevent N-terminal blockage. Consequently, separated proteins were transferred to PVDF membrane via blotting (see section 2.7.4.2), with a specific transfer buffer (10mM CAPS, 5mM DTT, 10 % Methanol, pH = 11). After blotting, the membrane was then stained (0.1 % Coomassie Blue R in 50 % MeOH, 1 % acetic acid) for 5min and destained in 50 % MeOH with several changes of 2-5min until the protein bands were clearly visible. The membrane was then air-dried and stored at 4 ^{o}C. To determine the

N-terminal sequence, Edman degradation was performed on the protein band of interest, and its sequence was analysed via ABI procise 494HT protein sequencer, this service was provided by PNAC facility (Cambridge).

2.7.8 Confocal fluorescence microscopy

The cells to be investigated were immobilised by drying a droplet of cell culture on the surface of a BG11 agar plate. A block of agar carrying cells was excised and covered with a microscopic coverslip, with the cells reside between agar and glass. Laser scanning confocal microscope (Leica TCS-S5) with a 63x immersion oil objective (NA 1.4) was used to examine the localisation of the GFP tagged fusion proteins. Samples were excited by 488nm argon laser (30% power) with confocal pinhole set to give resolution in the z-direction of 1μm. Fluorescent emission of GFP was selected with interference band pass filter at 502-512 nm. The fluorescence from the chlorophyll *a* was detected by long pass filter in range 670-720 nm. All images were recorded in 12-bit, with 512 x 512 pixels, scanned at 400 Hz and with line average of n = 2. The two images of fluorescence from GFP and chlorophyll a were then merged and smoothed for localisation analysis.

2.7.9 Single-particle analysis

Freshly isolated proteins samples were immediately applied to copper grids and negatively stained with 2 % (w/v) uranyl acetate. The prepared samples were then examined and analysed by Dr Jon Nield at Queen Mary University of London according to the following procedure. The grids carrying protein samples were examined using a Philips CM100 transmission electron microscope, operating at 80 kV and 350,850 magnification at room temperature. Micrographs were chosen for minimal astigmatism/drift and scanned using a Nikon LS9000 densitometer. 3400 particles was compiled using “boxer” of the EMAN software package (Ludtke et al., 2004). Further processing was performed using Imagic-5 (Image Science) at a

sampling frequency of 2.5 Å/pixel on the specimen scale. Reference-free alignment, multivariate statistical analysis, and iterative refinement resulted in two-dimensional class averages (Ruprecht and Nield, 2001). Eulerian angles were then assigned a priori by angular reconstitution (Van Heel, 1987) and iterative refinements implemented. The resolution of the final three-dimensional map, which comprised 263 class averages, merged from a broad range of relative orientation subpopulations representing 2964 particles, was estimated conservatively (0.5 correlation coefficient) by Fourier shell correlation (Van Heel and Schatz, 2005). Reprojections were taken from the final three-dimensional model and used to identify atypical views and further refine averages. Coordinate data sets were obtained from the Research Collaboratory Structural Bioinformatics Data Bank (www.rcsb.org) for 3KDS.pdb (structure of the cytosolic region of the Thermotoga maritima FtsH protease at 2.60 Å; Bieniossek et al., 2009) and 1GTA.pdb (structure of GST at 2.4 Å; McTigue et al., 1995). Structures were modeled into the final calculated three-dimensional map using PyMol (DeLano, 2008). Surfacerenderedviews are shown with a threshold of 2.5 s.

2.7.10 Protein identification via mass spectrometry analysis

Protein samples for mass spectrometry analysis were separated on SDS-PAGE and stained with silver. The candidate protein band was excised with a clean scalpel from the gel and transfer to a 1.5 ml centrifuge tube. Then the gel was destained in 15 mM potassium hexacyanoferrate (III) and 50 mM sodium thiosulfate for 8 min. Then the solution was removed and the colourless gel was stored at – 80 ^{o}C until departure. For sequence identity analysis, the collected protein samples were shipped to Prof. Michael Hippler, University of Münster, and analysed by co-workers using liquid chromatography-mass spectrometry according to the following procedure. Upon arrival, the protein gel band was digested with trypsin overnight. The tryptic peptides were then diluted in 10 µl of buffer A (0.1% (v/v) formic acid in 5% (v/v) acetonitrile, 95% (v/v) water) and centrifuged for 5 min at 12,000 × g. The peptide containing

supernatant fraction was then used for Liquid Chromatography-Mass Spectrometry analysis. The peptides were fractioned on an LC-Packings PepMap C_{18} column (75-µm [inner diameter] by 150 mm) with a 3-µm particle size and a 100-Å-pore diameter (NAN-75-15-03-PM) with the flow rate set at 250 nl/min. The column eluent was monitored at 214 and 280 nm with a rapid-scanning spectrophotometer equipped with a 3-nl flow cell (LC-Packings UZ-N10 160015). A LCQ Deca XP ion trap mass spectrometer (Thermofinnigan, USA) was used for MS/MS analysis. The tolerance for the selection of the MS-MS precursor ranged from 1.5 to 3.0 *m*/*z* (low to high *m*/*z*). The resulting data were then evaluated by comparing to the **Synechocystis** data base (cyanobase).

Chapter 3: FtsH complexes in Synechocystis, composition, localisation and structure

3.1 Probing the composition of FtsH proteases

FtsH proteases have been found to form large membrane-anchored complexes in both *E. coli* (see section 1.6.2) and in eukaryotic cells, where multiple FtsH-encoding genes are present. In the latter case, FtsH complexes might contain multiple types of FtsH isomers (see section 1.7). One of the major objectives of this work is to determine the composition of each type of FtsH complex found in the cyanobacterium *Synechocystis* 6803; hence a method for specifically isolating each of the target FtsH homologues was required. Affinity chromatography is a method commonly employed to isolate target proteins for *in vitro* characterisation; therefore, an affinity tag, glutathione-*S*-transferase (GST), was fused to the C-terminus of each FtsH homologue to enable isolation (see section 3.1.1). The resulting mutants were then selected for segregation and their genotypes were analysed (see section 3.1.2). Affinity tagging is a powerful tool to study protein architecture, however, it could potentially provide misleading information should the tag perturb the properties of the target protein. In fact, the C-terminal tagging applied in this work was based on the consideration that a N-terminal fusion of GST tag might disrupt membrane insertion of FtsH. Disruption of *ftsH* genes in *Synechocystis* leads to distinguishable growth defects, with the exception of *ftsH4* (see section 1.8), therefore, the phenotypes of the mutants generated in this work were assessed by growth assays (see section 3.1.3). Then the FtsH complexes were isolated from each mutant, the composition of which was probed with antibodies specific to each homologue (see section 3.1.4). Moreover, the N-termini of transmembrane proteins often carries a cleavable signalling peptide for membrane specific targeting, in this work, the N-terminal sequence of each FtsH homologue was analysed to examine the integrity of the mature proteins (see section 3.1.5).

3.1.1 Construction of *ftsH::gst* mutants

The *ftsH::gst* transformation vectors were constructed using the FtsH GST/GFP C-terminal tagging system constructed in this work (see section 2.6.11). Firstly, the *gst* tagging cassette was released from the pGST-ErmA vector via EcoRV and SpeI double digestion (see section 2.6.11.3), and then ligated into the EcoRV and XbaI sites of vector pGEMFtsHx (see section 2.6.11.2) to create the *ftsH::gst* transformation vectors, namely pFtsHxGSTery, where FtsHx is the particular *ftsH* homologue (Figure 3.1). The resulting plasmid vectors were then sequenced over the ligation junction to ensure no frame-shift had occurred during the cloning process.

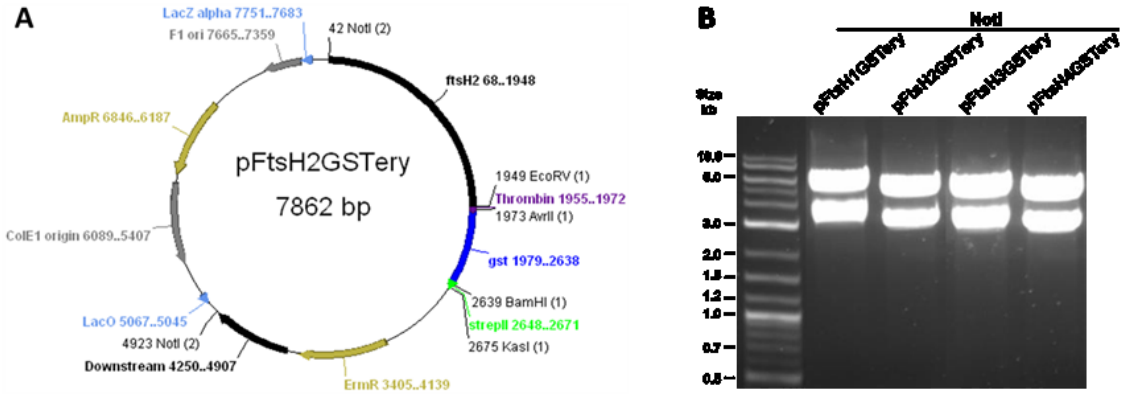

Figure 3.1: Construction of the pFtsHxGSTery transformation vectors.
(A) The plasmid map of pFtsH2GSTery vector. The size and location of NotI sites on the other three pFtsHxGSTery vectors are almost identical. (B) Restriction digests of each of the pFtsHxGFPcam vector using NdeI, where FtsHx represents the particular homologue.

Synechocystis strain WT-G was transformed with the pFtsHxGSTery vectors and the resulting mutants, namely SynFtsHxGSTery (where FtsHx represents the particular *ftsH* homologue), were selected for erythromycin resistance under low-light conditions, on BG11 plates supplemented with glucose, erythromycin and DCMU.

3.1.2 Genotyping of the SynFtsHxGSTery mutants

Synechocystis cells contain multiple genomes, therefore, it is important to check the genotype of the mutants to confirm that all copies of the untransformed WT genome

were fully eliminated. Genomic DNA from the mutant cells was extracted to check the segregation status of the mutant genome via Taq polymerase PCR using primer pair FtsHx-Seq3 and FtsHx-R (Table 2.5). The resulting PCR products were analysed on agarose gels, where the PCR products from the *ftsH::gst* constructs were bigger than their wild-type counterpart, due to the insertion of the *gst* and erythromycin-resistance cassette (Figure 3.2 C).

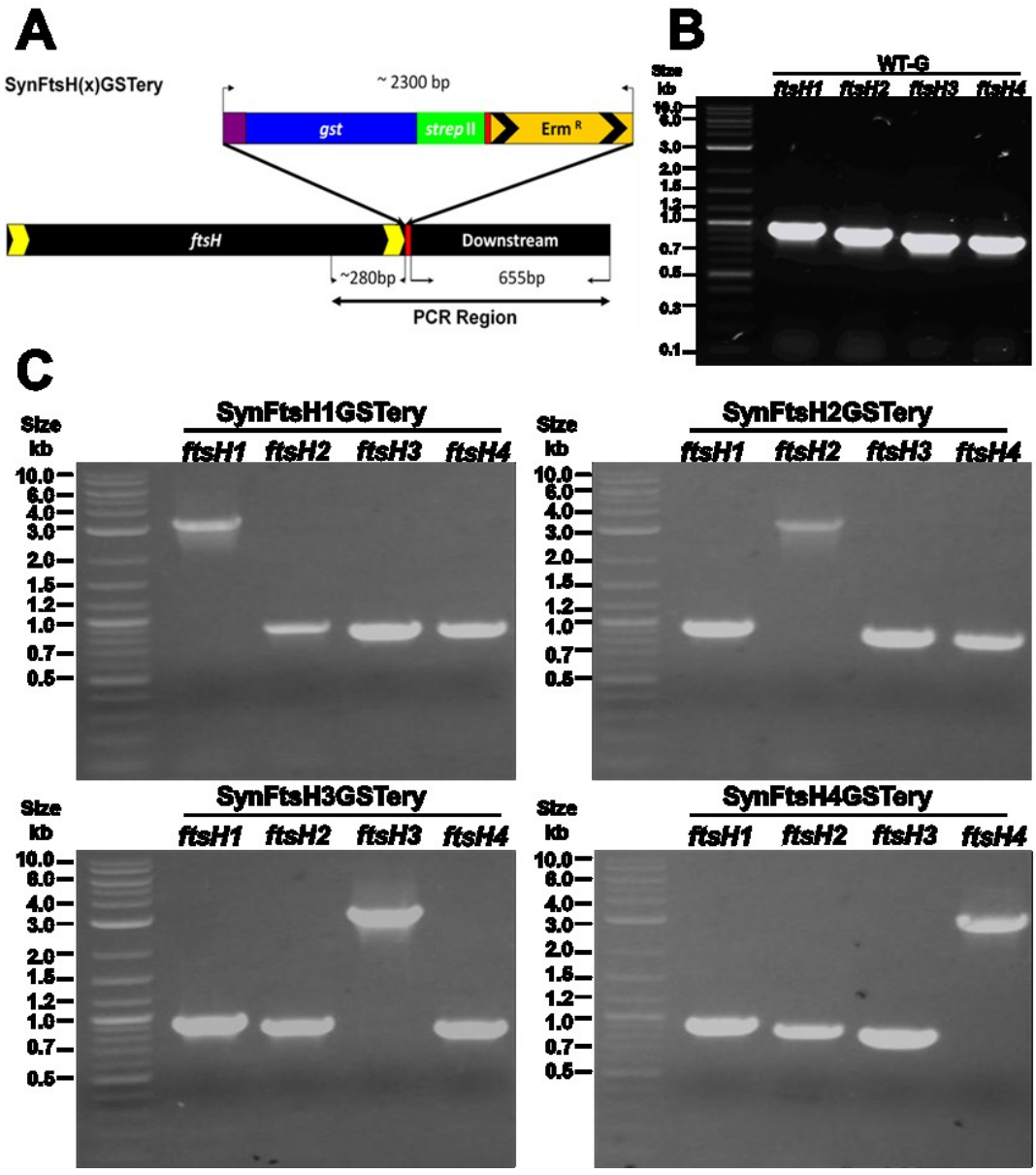

Figure 3.2: Genotyping of the SynFtsHxGSTery mutants.
(A) A schematic representation of the PCR amplification region. (B) PCR analysis of the wild-type *ftsH* 1-4. (C) PCR analysis of each SynFtsHxGSTery mutant.

The PCR results showed the absence of the wild-type band in each *ftsH::gst* lane, which confirmed full segregation of the mutant genome; moreover, the PCR bands of the remaining 3 *ftsH* homologues that were not manipulated were not shifted compared to the wild type, which proved that only the correct *ftsH* homologue was mutated in each mutant.

3.1.3 Phenotype analysis of SynFtsHxGSTery mutants

In order to test the physiological effect of the genetic modification in the mutants, a growth experiment was performed in which each mutant was streaked and tested on BG11 plates with and without glucose, under high and medium-light conditions (Table 2.2). Plates were incubated at 30 ^{o}C for approx. 4-7 days.

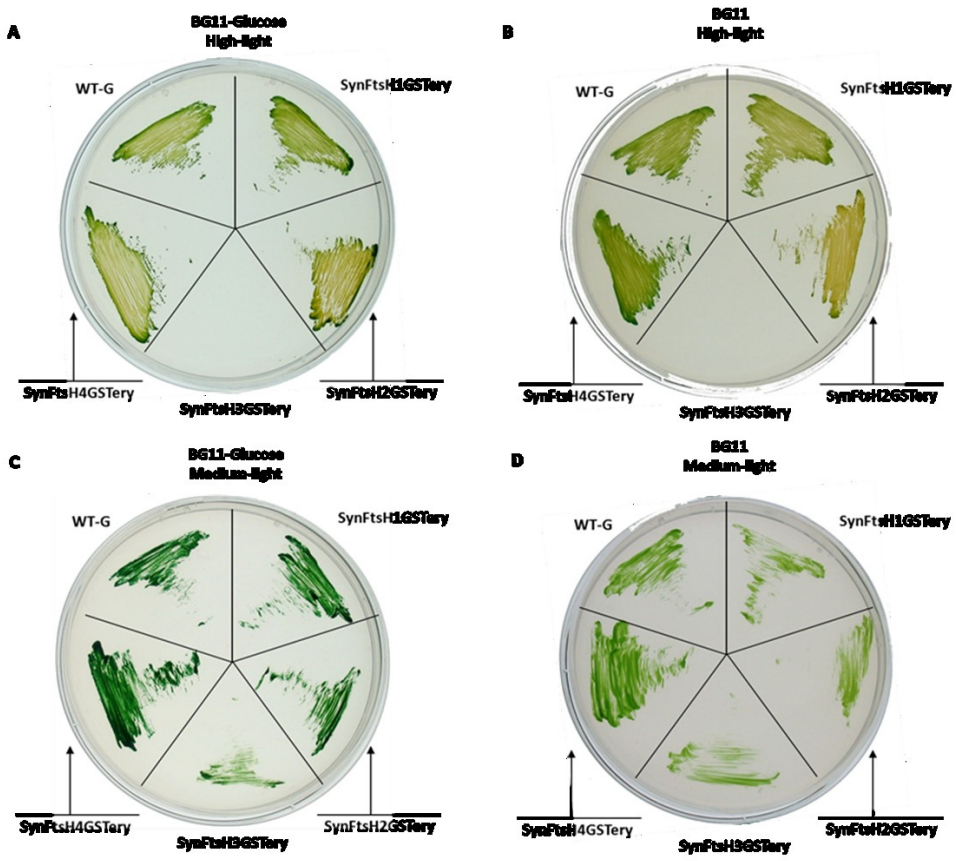

Figure 3.3: Growth experiment of SynFtsHxGSTery mutants.
WT-G: the wild-type strain; SynFtsHxGSTery: mutant stratins expressing FtsHx-GST fusion protein, where x represents the specific homologue. Cells were tested for growth under high (A and B) amd medium (C and D) light conditions on BG11 plates supplemented with 5 mM glucose (A and C) and plain BG11 (B and D).

All mutants grew well under low (data not shown) and medium light conditions, but under high light stress, SynFtsH3GSTery strain failed to grow. The results proved that the FtsH1-GST and FtsH2-GST fusion proteins retained the major functions compared to their wild-type counterpart. The SynFtsH3GSTery mutant was much more sensitive to high light stress than any other *gst* tagged mutants, suggesting its function might have been interfered with by the GST tag. On the other hand, cells cannot survive if *ftsH3* is disrupted (Mann et al. 2000); therefore, FtsH3-GST must have retained some degree of activity which rescued the mutant from lethality. The growth experiment could not provide clues about whether the function of FtsH4 was disrupted by the C-terminal GST tag as functional disruption of FtsH4 yields no distinguishable phenotype under these growth conditions (Mann et al. 2000).

3.1.4 Isolation of the GST-tagged FtsH complexes

To isolate the respective FtsH complexes, 1 L culture of each SynFtsHxGSTery mutant was prepared for this experiment. The cells were harvested when the optical density at 730 nm reached ~ 1.5, and cells broken for sequential purification steps. Purified FtsH-GST samples were then concentrated and analysed on 10 % SDS-PAGE gels, followed by immunoblotting with antibodies specific to GST, *E. coli* FtsH and each FtsH homologue (Figure 3.4).

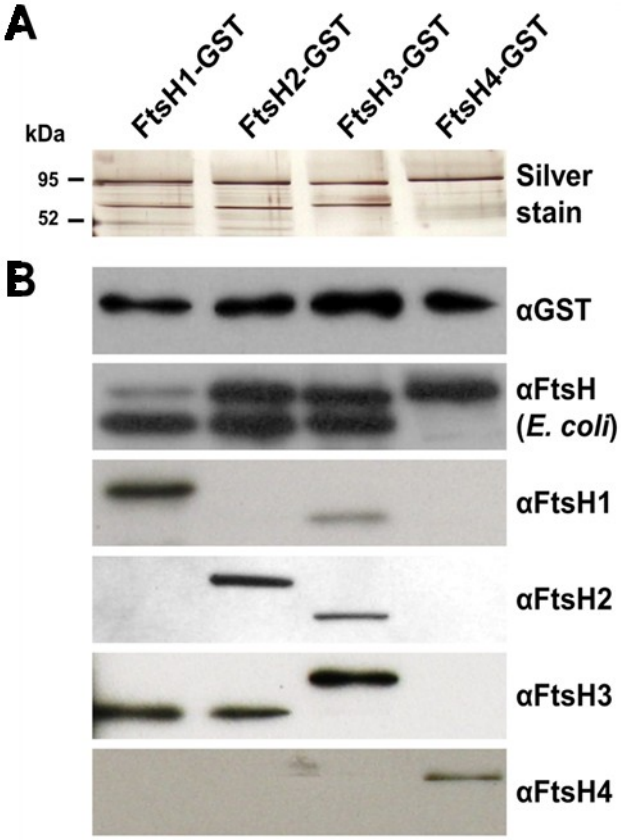

C

	αFtsH1	αFtsH2	αFtsH3	αFtsH4
FtsH1-GST	+		+	
FtsH2-GST		+	+	
FtsH3-GST	+	+	+	
FtsH4-GST				+

Figure 3.4: Affinity purification of GST-tagged FtsH complexes from each of the SynFtsHGSTery mutants.
(A) Purified FtsH-GST proteins were separated by SDS-PAGE and analysed by silver staining. (B) Immunoblot analysis using antibodies specific for GST, global FtsH and each FtsH homologue. (C) Table summarizing the interactions between the FtsH homologs.

Strikingly, two predominant bands were detected in the silver stained gel, with the exception of FtsH4-GST sample which only contained the upper band. The upper band, of ~ 100 kDa, matches the predicted size of FtsH-GST fusion protein, whereas, the lower band, of ~ 70 kDa, was similar to that of wild-type FtsH. The identity of the upper band was confirmed as the FtsH-GST fusion protein by immunobloting using

antibodies specific to GST and FtsH. Interestingly, the lower band was also detected an FtsH antibody raised against *E. coli* FtsH (αFtsH (*E. coli*)), indicating the presence of an additional FtsH subunit in the isolated complex. Further investigation using peptide antibodies specific to each FtsH homologue revealed that FtsH3 co-purified with FtsH1-GST and FtsH2-GST, and consistently, WT FtsH1 and FtsH2 were co-purified with FtsH3-GST. Therefore, our data suggested possible complex formation between FtsH1/FtsH3 and FtsH2/FtsH3. In contrast, FtsH4-GST seemed not to interact with other FtsH homologues.

3.1.5 N-terminal sequence analysis of purified FtsH proteases

The N-terminal transmembrane domain of FtsH is responsible for selective membrane integration and previous work on chloroplast thylakoid Type A and Type B FtsH proteases unveiled the presence of a potentially cleavable signalling peptide sequence at the N-terminal of the FtsH precursors, and that a similar cleavage site is also present in the peptide sequence of FtsH4 (Rodrigues et al. 2011). To clarify the proposed post-translational modification, the N-terminal sequence of each FtsH homologue was analysed. The N-terminal sequence of FtsH2-GST and the co-purified wild-type FtsH3 subunit isolated from a similar mutant (hereafter SynFtsH2GST) has already been determined (unpublished data from Dr M. Barker). Therefore, attempts were made to obtain N-terminal sequence data from the FtsH1-GST/FtsH3 and FtsH4-GST complexes isolated in this work.

To prepare samples for N-terminal protein sequencing, GST-tagged FtsH complexes from SynFtsH1GSTery and SynFtsH4GSTery were isolated via GST affinity chromatography (see section 2.7.2.1), and then separated on denaturing SDS-PAGE gels and blotted onto a PVDF membrane according to the specified procedure (see section 2.7.4). The blot was then stained accordingly (Figure 3.5) and sent to the Protein & Nucleic Acid Chemistry facility (PNAC, Cambridge) to be sequenced.

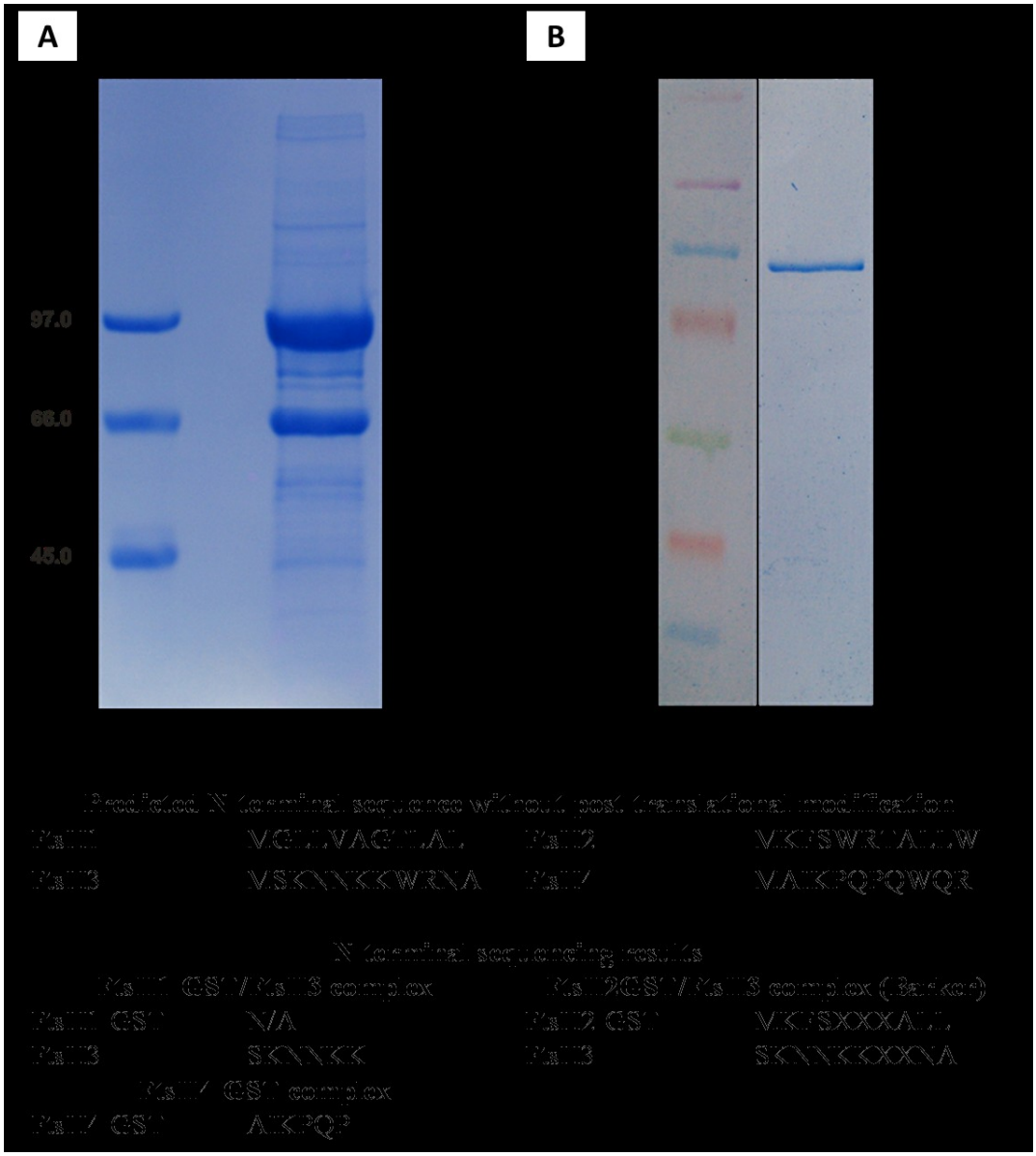

Figure 3.5: N-terminal sequence of mature FtsH proteases.
The stained blots of sequencing samples prepared from FtsH1-GST/FtsH3 (A) and FtsH4-GST (B) complexes. (C) Table of reference FtsH N-terminal sequence and sequencing results. The sequencing data of FtsH2-GST/FtsH3 complex are from unpublished preliminary work performed by Dr Myles Barker.

The first 6-10 residues of both FtsH3 and FtsH4 were successfully sequenced via Edman degradation (PNAC facility, Cambridge) although the identity of some of the residues was unclear. However, subunit FtsH1-GST failed to produce valid data, possibly due to N-terminal blockage. The available sequencing data confirmed that only the first methionine of FtsH3 and FtsH4 was missing in the mature protein and FtsH2 retained the full N-terminal sequence. Our data did not support the idea of a

post-translational removal of a signal peptide in the N-terminal region of *Synechocystis* FtsH. Moreover, the N-terminal sequences of FtsH3 co-purified with FtsH1-GST and FtsH2-GST were identical. Taking into account that FtsH1 and FtsH2 are separate complexes, the FtsH3 in both complexes seemed to be the same.

3.2 Probing the localisation of FtsH complexes

As membrane-anchored proteases, FtsH complexes are associated with proteolysis of membrane protein substrates. Therefore, probing the localisation of FtsH is an important step towards understanding the function of the proteases. Confocal fluorescence microscopy is one of the commonly used techniques to study the localisation of proteins *in situ*. In order to track the fluorescence signal of FtsH complexes, mutants expressing a C-terminal GFP-tagged FtsH homologue were analysed by fluorescence microscopy, in collaboration with Prof Conrad Mullineaux. In this section, the mutagenesis (see section 3.2.1), characterisation of mutants (see section 3.2.2-3.2.4) and localisation of each FtsH-GFP homologue (see section 3.2.5) are described. In addition to fluorescence microscopy, an independent approach to study the localisation of FtsH homologues in the wild-type strain by biochemical fractionation is also described (see section 3.2.6).

3.2.1 Construction of *ftsH::gfp* mutants

Benefitting from the GST/GFP C-terminal tagging system (see section 2.6.11), the *ftsH::gfp* transformation vectors were constructed by a simple one-step cloning. Firstly, the *gfp* tagging cassette was released from the pGFP-CamA vector via EcoRV and SpeI double digestion (see section 2.6.11.4), and then ligated into the EcoRV and XbaI sites of vector pGEMFtsHx (see section 2.6.11.2) to create the *ftsH::gfp* transformation vectors, namely pFtsHxGFPcam, where FtsHx is the particular *ftsH* homologue (Figure 3.6). The resulting plasmid vectors were then sequenced over the ligation junction to ensure no frame-shift occurred during the cloning process.

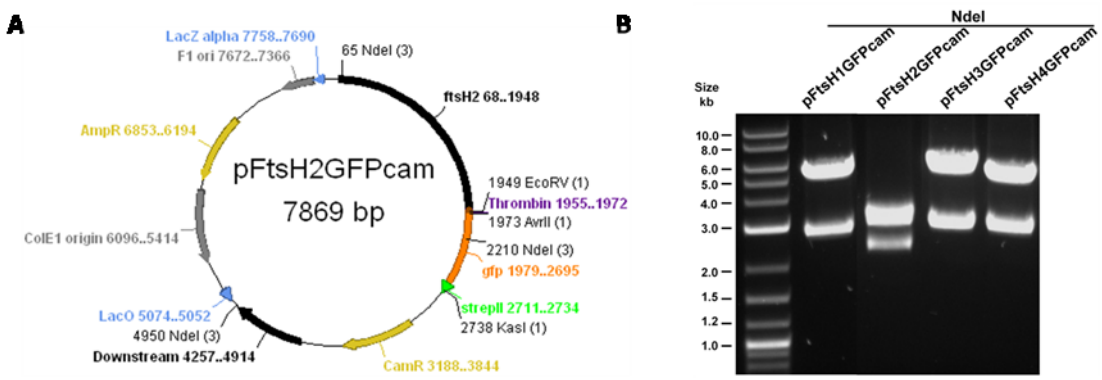

Figure 3.6: Construction of the pFtsHxGFPcam transformation vectors.
(A) The plasmid map of pFtsH2GFPcam vector. This vector contains an additional NdeI at the beginning of the ftsH2 ORF comparing to the other three vectors. (B) Restriction digests of each of the pFtsHxGFPcam vector using NdeI, where FtsHx represents the particular homologue.

Wild-type *Synechocystis* strain WT-G was transformed with the pFtsHxGFPcam vectors and the resulting mutants, namely SynFtsHxGFPcam (where FtsHx represents the particular ftsH homologue), were selected for chloramphenicol resistance under low-light, on BG11 plates supplemented with glucose, chloramphenicol and DCMU.

3.2.2 Genotyping of the SynFtsHxGFPcam mutants

Genomic DNA from the mutant cells was extracted to check the mutant genome segregation status via Taq polymerase PCR using primer pair FtsHx-Seq3 and FtsHx-R (Table 2.5). The resulting PCR products were analysed on agarose gels, where the PCR products from the *ftsH::gfp* constructs were separated from the wild-type due to the integration of the *gfp* sequence and chloramphenicol resistance cassette (Figure 3.7).

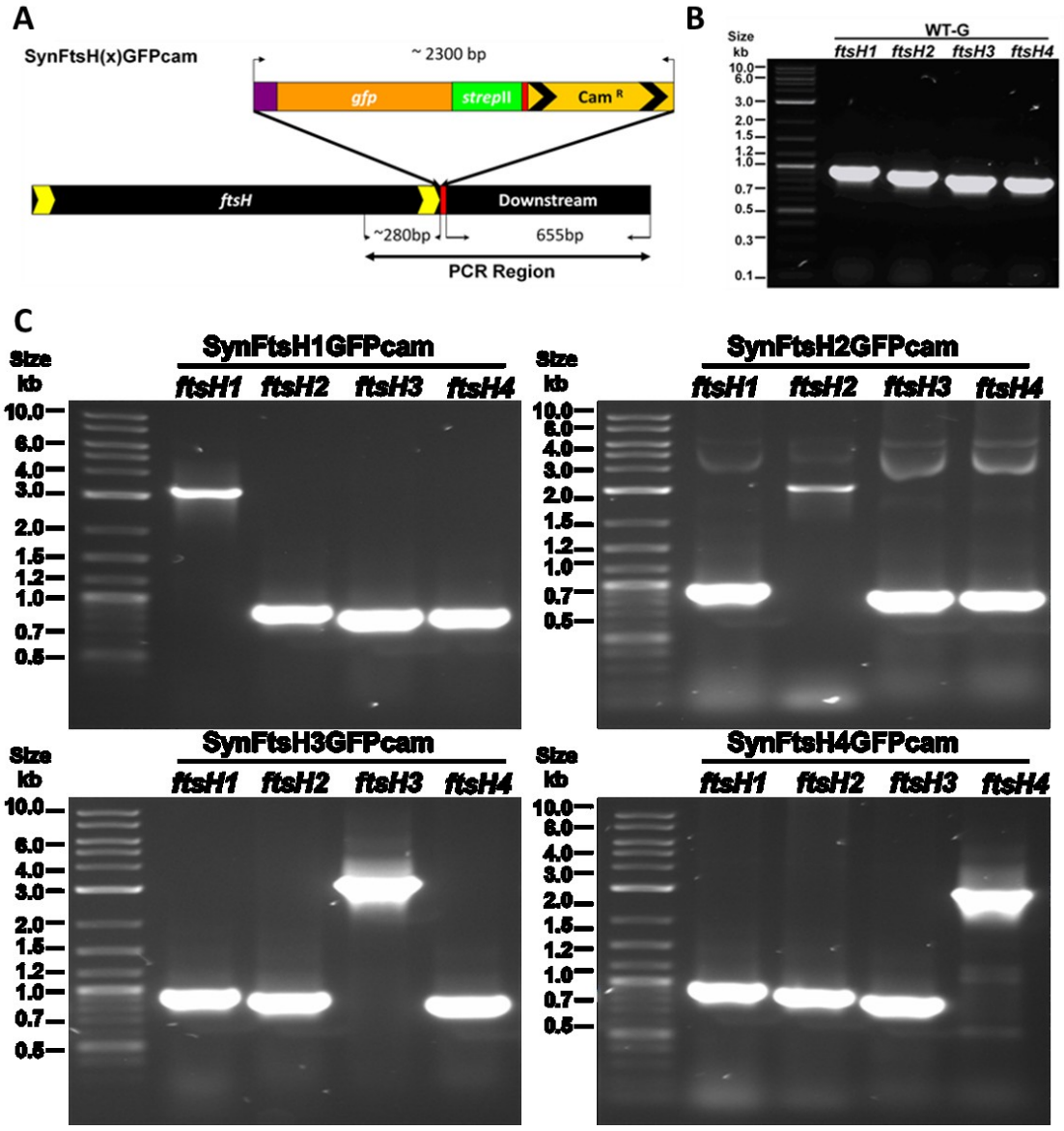

Figure 3.7: Genotyping of the SynFtsHxGFPcam mutants.
(A) A schematic representation of the PCR amplification region. (B) PCR analysis of the wild-type *ftsH* 1-4. (C) PCR analysis of each SynFtsHxGFPcam mutant.

The PCR results showed absence of the wild-type band in each *ftsH::gfp* lane, which provided evidence of full segregation of the mutant genotype. Moreover, the PCR bands of the remaining 3 *ftsH* homologues showed an identical migration profile to the wild-type, which proved that only the correct *ftsH* homologue was mutated in the mutants.

3.2.3 Immunochemical detection of the FtsH(x)-GFP recombinant proteins

Immunoblotting was used to examine the expression level and size of the FtsH-GFP recombinant proteins from the mutants. The protein samples used in analysis were either whole cell proteins through direct solubilisation of cell pellets with SDS sample buffer, or membrane proteins extracted from a crude membrane preparation. To prepare the protein samples for the assay, ~50 ml of each SynFtsH(x)GFPcam culture was harvested, and the crude membrane fraction was prepared. The membrane proteins were then separated on 8 % SDS-PAGE gels. After electrophoresis, the proteins were either stained with Coomassie Blue or transferred to a PVDF membrane for immunoblotting with specific antibodies.

An early experiment performed at the same time as fluorescence microscopy, using the whole cell extracts from the remaining cell cultures, showed that all four SynFtsHxGFPcam mutants expressed full-length FtsH-GFP fusion proteins. However, the expression level of FtsH1-GFP and FtsH3-GFP was much lower than the other two fusions (Figure 3.8 B). Furthermore, degradation products were detected from SynFtsH2GFPcam and SynFtsH4GFPcam samples. The size of the cleavage product was ~ 70 kDa, similar to that of the wild-type FtsH. However, the cleavage site was in the soluble fragment of FtsH, as the products contain the C-terminally fused GFP tag. Hence the cleavage product detected in this sample should be soluble. Whether degradation occurred during sample preparation is unclear. Similar degradation event cannot be ruled out from FtsH1-GFP and FtsH3-GFP, as the abundance of the resulting fragments might not be sufficient for antibody detection.

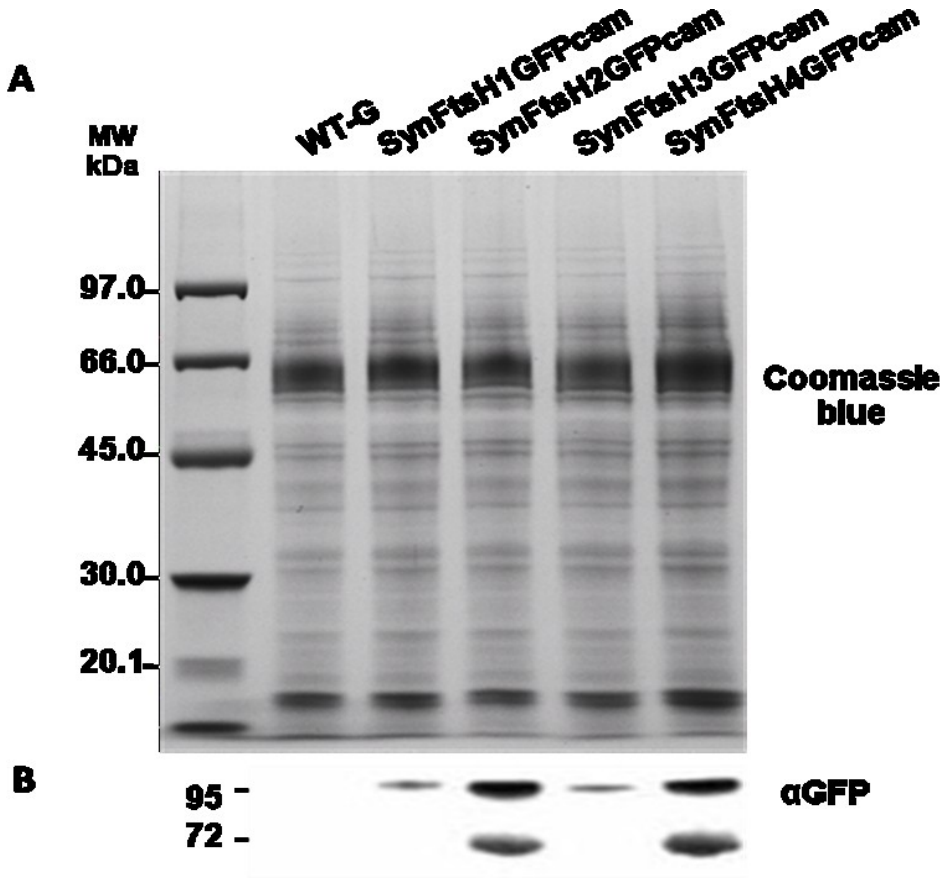

Figure 3.8: Immunoblotting analysis on *ftsH::gfp* mutants.
(A) Coomassie stained SDS-PAGE, *ftsH(s)::gfp* represents the membrane protein sample isolated from respective mutant. (B) Immunoblotting with GFP-specific antibody.

A second immunochemical analysis using membrane extracts isolated from a different batch of culture showed successful fusion of the GFP tag to the FtsH targets, with the exception of FtsH3 (Figure 3.9). Data from this experiment showed accumulation of truncated FtsH3-GFP, of slightly larger size than wild-type FtsH3, with no sign of GFP in the blot. These data are contradictory to the previous blot (Figure 3.8), which might reflect variations in the growth conditions and the presence of additional secondary mutations in the strain expressing FtsH3-GFP. The SynFtsH3GFPcam cultures from both batches were examined via confocal microscopy, signal quality from both were extremely poor. Other than FtsH3, the remaining GFP-fused FtsH derivatives seemed to be accumulating at the correct size, ~100 kDa, without detectable degradation in the membranes.

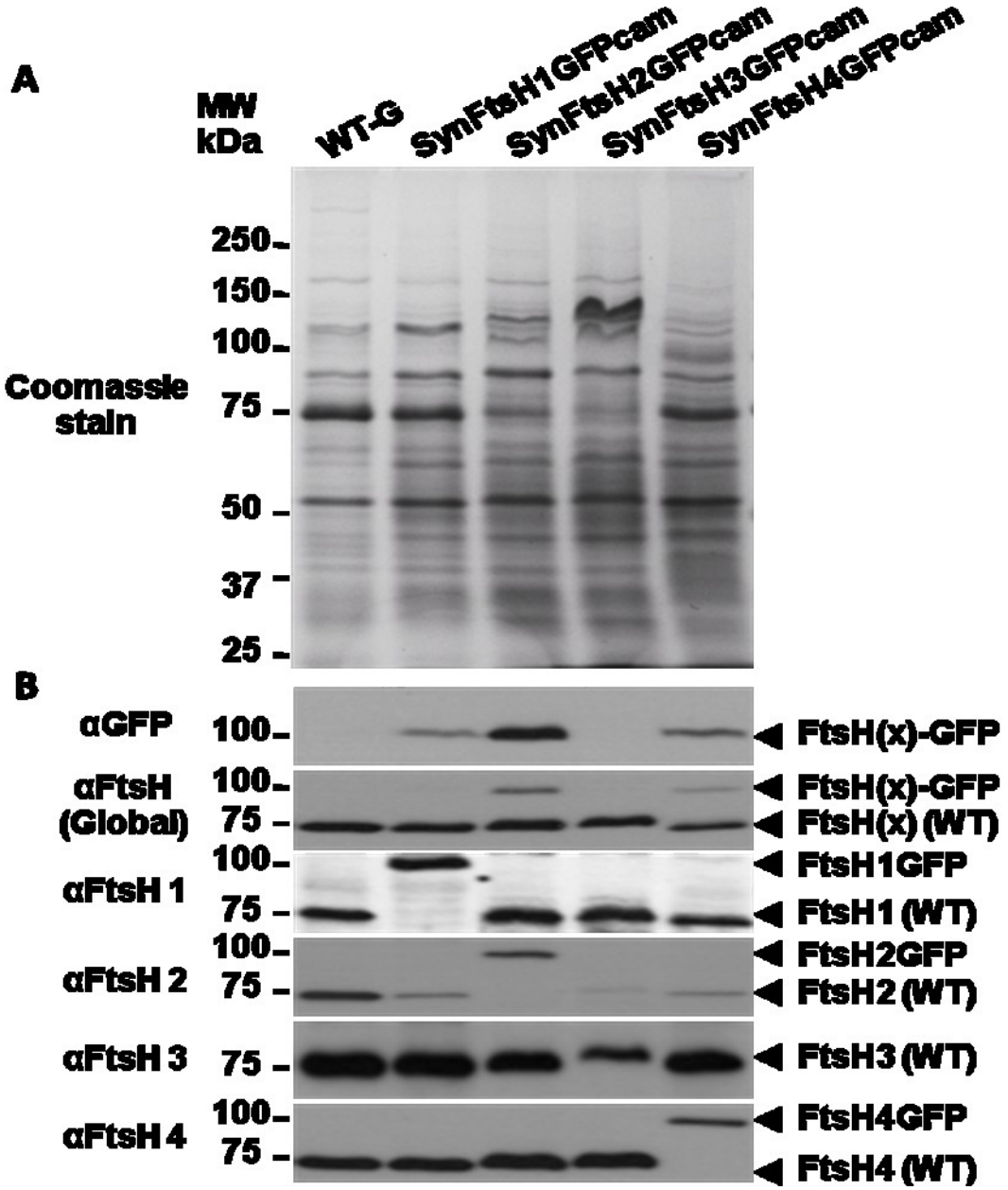

Figure 3.9: Immunochemical detection of FtsH(x)-GFP recombinant proteins.
(A) Coomassie stained gel of membrane proteins from SynFtsH(1-4)GFPcam mutants. (B) Immunoblotting of the protein samples with antibodies specific to GFP (αGFP), all FtsH (αFtsH Global) and each FtsH homologue (αFtsH 1-4). (This experiment was performed using cells recovered from cryo-stocks. Cells in this experiment were not examined by fluorescence microscopy)

Examination of the band intensities in Fig. 3.9 suggested that the FtsH1-GST protein was expressed at a comparable level to untagged FtsH1 in both wild type and in the other three FtsH-GFP mutants. On the other hand, the FtsH2 level in

SynFtsH1GFPcam was much reduced. The expression level of FtsH2-GFP was lower than FtsH2 in wild type. However, the expression level of the other three FtsH homologues in SynFtsH2GFPcam was fairly similar to the equivalent levels in wild-type, given the limitations of immunoblotting to estimate protein levels. The expression level of truncated FtsH3-GFP was about half of the wild-type level, surprisingly, the FtsH2 in this strain was barely detectable. The accumulation of FtsH1 and FtsH4 in SynFtsH3GFPcam was similar to that of the wild-type. Finally, the expression level of FtsH4-GFP was much lower than wild-type, and in addition, the level of FtsH2 was also dramatically reduced in this mutant. The level of FtsH1 in SynFtsH4GFPcam also appeared to be slightly reduced, and the presence of FtsH3 seemed to be at the normal level. In contrast to FtsH2, whose abundance was reduced dramatically by modification of other FtsH homologues, the level of FtsH4 was relatively insensitive.

Although immunoblotting as a semi-quantitative method is not an ideal way to clarify the accurate stoichiometry between FtsH homologues, it can provided hints as to the abundance of the target proteins. Among the four FtsH homologues subjected to C-terminal GFP tagging, the level of FtsH1 seemed to be the least affected one by its own tag, and was maintained to the wild-type level in the other three mutants. Given that the signal of FtsH1-GFP was the weakest using the anti-GFP antibody and FtsH1-GFP could not be detected by anti-FtsH (Global) antibody, this analysis would suggest that the abundance of FtsH1 is naturally low, much lower than FtsH2 and FtsH4.

3.2.4 Phenotype analysis of SynFtsHxGFPcam mutants

In order to test the physiological influence of the genetic modification in the mutants, a growth experiment under various light stresses was performed, where each mutant was streaked and tested on BG11 plates +/- glucose, under high, medium and low light conditions (Table 2.2). Plates were incubated at 30 ^{o}C for approx. 4-7 days.

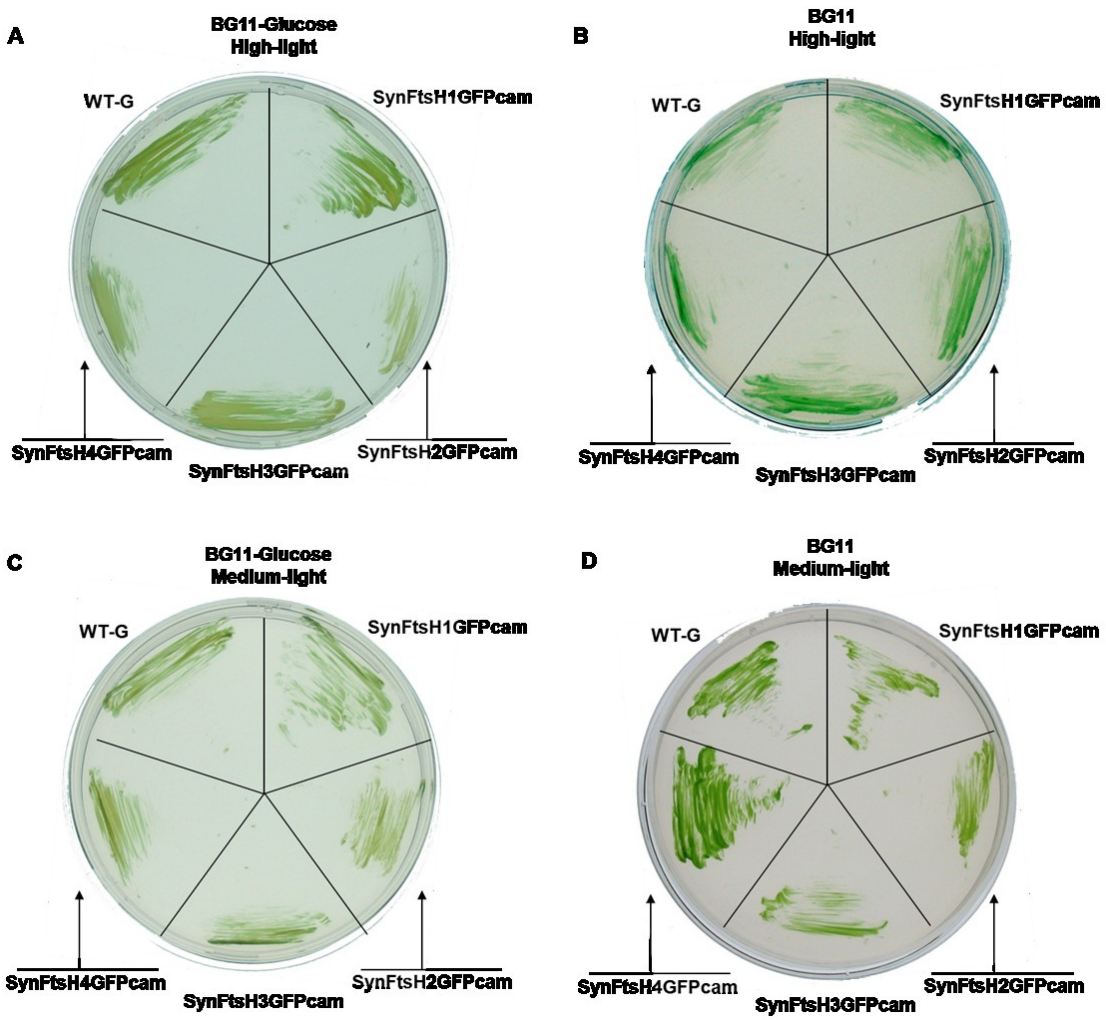

Figure 3.10: Growth experiment of SynFtsHxGFPcam mutants.
WT-G: the wild-type strain; SynFtsHxGFPcam: mutant stratins expressing FtsHx-GFP fusion protein, where x represents the specific homologue. Cells were tested for growth under high (A and B) amd medium (C and D) light conditions on BG11 plates supplemented with 5 mM glucose (A and C) and plain BG11 (B and D).

The growth experiment demonstrated that addition of a GFP tag to the C-terminus of FtsH did not impair the major function of FtsH1, FtsH2 and FtsH3.The function and growth impact of FtsH4 remain to be revealed, hence the influence of the C-terminal GFP fusion to FtsH4 is unclear. It is worth noting that the mutant expressing FtsH3-GFP fusion protein is more resistant to light stress than SynFtsH3GSTcam (see section 3.1.3), indicating a clear difference in the physiological impact of the two tags, even though they are of similar mass. This difference is very likely related to the fragmentation of FtsH3-GFP.

3.2.5 Localisation of FtsH complexes *in situ*

Confocal fluorescence microscopy is a powerful technique to visualise the localisation of proteins *in situ*. The basic principle of this method is to detect the fluorescence from the target proteins (in this case, the FtsH-GFP fusion proteins) and fluorescent signals from a marker, the localisation of which is already characterised (in cyanobacteria, chlorophyll fluorescence from the thylakoid membranes is conveniently used), then plot and analyse the correlation of the two signals.

SynFtsHxGFPcam mutants were grown in liquid BG11 medium for 4-7 days and then examined by fluorescence microscopy (see section 2.7.8) in collaboration with Prof. Conrad Mullineaux (Queen Mary University of London).

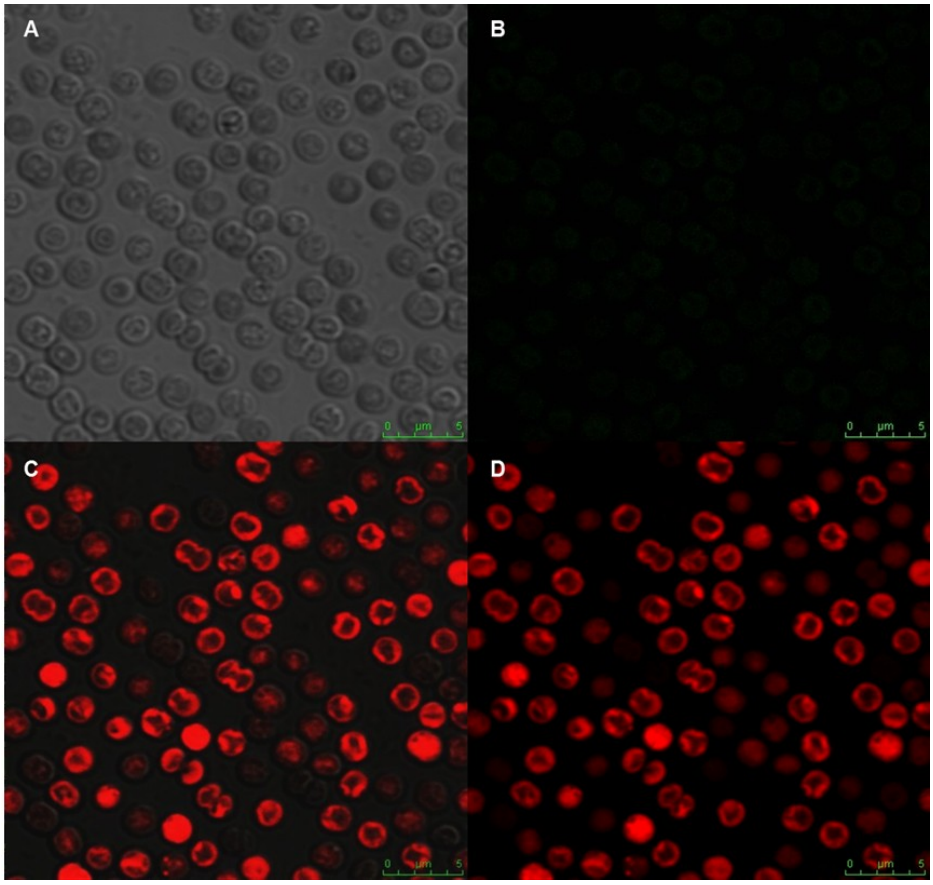

Figure 3.11: Wild type cells (WT-G) under fluorescence microscopy.
(A) Image under visible light. (B) GFP fluorescence emission at wavelengths 500-527 nm. (C) Chlorophyll *a* fluorescence emission at a wavelength of 665 nm. (D) Overlay image of B and C.

The WT-G cells were screened as the background control. Under the microscope, *Synechocystis* cells showed a "blood cell" appearance, as the fluorescence of chlorophyll marks the boundary of thylakoid membranes and the cytoplasmic membranes localised around the outer surface of the thylakoid membranes were not visible in the scanning channels. Although some green signals unrelated to GFP were detected during the imaging, the gain was adjusted so that the signal did not show in the final image (Figure 3.11 D). Further analysis of the SynFtsHxGFPcam mutants were carried out under the same condition, and GFP signals were detected in all four mutants, however, the accumulation level of FtsH2-GFP and FtsH4-GFP was much higher than that of FtsH1-GFP and FtsH3-GFP (Figure 3.12).

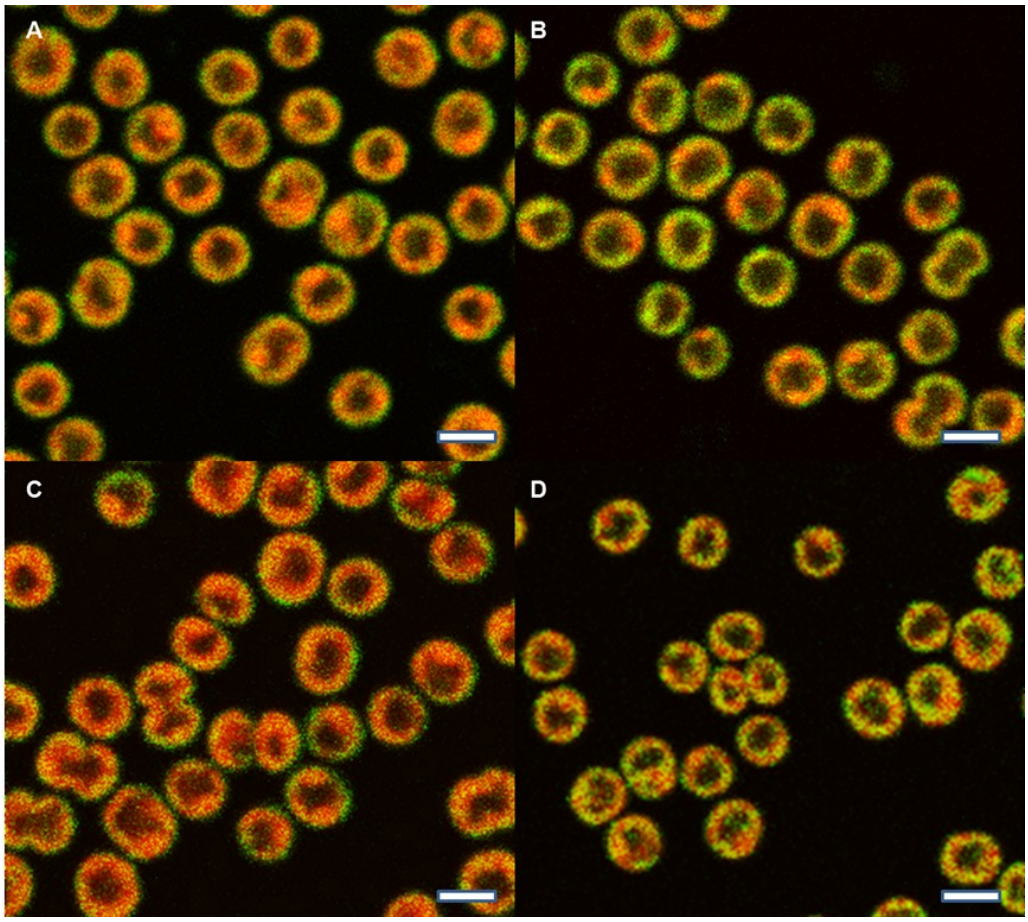

Figure 3.12: *ftsH::gfp* mutants under fluorescence microscopy.
Cells of SynFtsH1GFPcam (A); SynFtsH2GFPcam (B); SynFtsH3GFPcam (C) and SynFtsH4GFPcam (D) were imaged and presented in the figure. White scale bar = 2 µm. All images are the results of green (500-527 nm) and red (665 nm) channel overlay.

Signals from chlorophyll *a* outlined the location of thylakoid membranes *in situ*, which helps determine the localisation of the GFP-tagged FtsH homologues. FtsH2-GFP (Figure 3.12 B) and FtsH4-GFP (Figure 3.12 D) were expressed at high level, and clearly located in the thylakoid membrane. Although both proteins were abundant in the thylakoid membrane, the distribution pattern of FtsH2-GFP was relatively spread out (Figure 3.12 B). FtsH4-GFP fusion proteins, however, seemed to distribute more heterogeneously, the fluorescent signals clustered into bright spots, or straps on the thylakoid membrane, leaving empty area not covered (Figure 3.12 D). Accumulation of FtsH1-GFP (Figure 3.12 A) and FtsH3-GFP (Figure 3.12 C) was less, and seemed to be present mainly outside the thylakoid membrane, possibly in the cytoplasmic membrane.

3.2.6 Localisation of FtsH via immunoblotting analysis

Fluorescence microscopy is a powerful tool to visualise target proteins in real-time, however, extensive image processing is required when the expression level of the protein target is low. To further clarify the localisation of each FtsH homologue, a biochemical analysis was performed to investigate the presence of FtsH in thylakoid and cytoplasmic membranes. Two-phase partitioning procedure enables separation of proteins residing in the thylakoid and cytoplasmic membranes. Probing such preparations using FtsH-specific antibodies raised in this work (see section 2.7.4.1), will provide independent evidence on the location of each homologue. The separated thylakoid and cytoplasmic membrane samples were kindly provided by Dr Myles Barker.

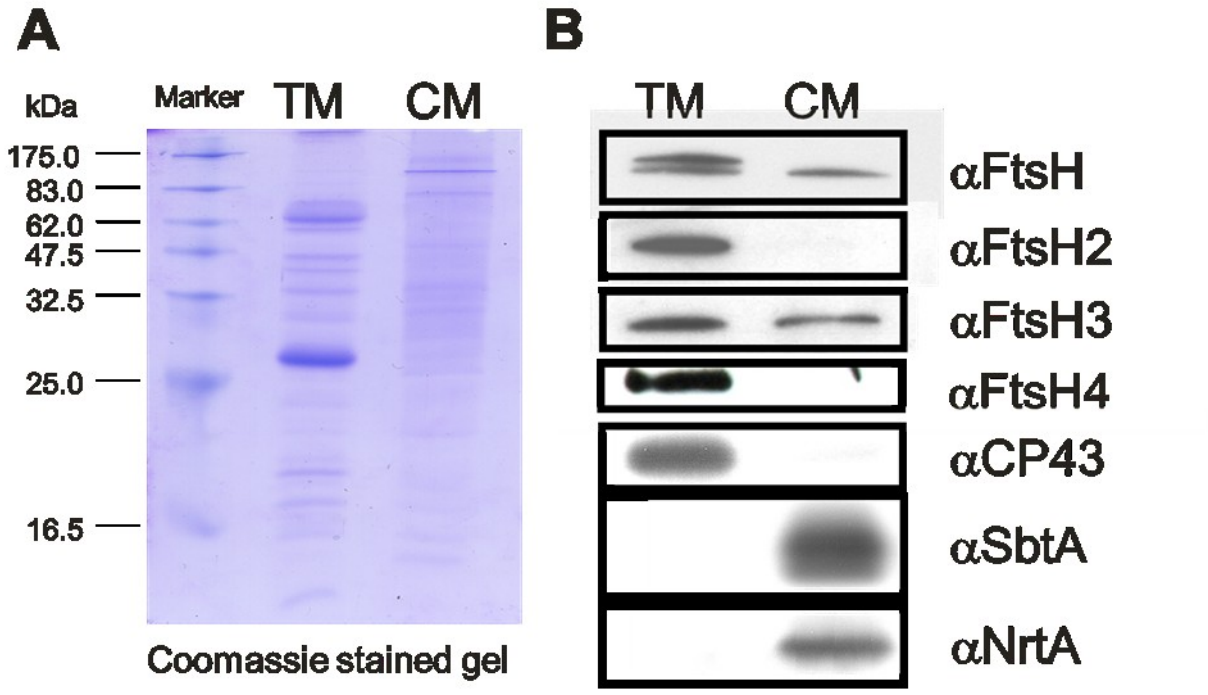

Figure 3.13: Localisation of FtsH via immunoblotting analysis.
(A) Coomassie stained gel of thylakoid (TM) and cytoplasmic membranes (CM). (B) Immunoblotting with a global FtsH antibody (αFtsH) and antibodies specific to FtsH2 (αFtsH2), 3(αFtsH3) and 4 (αFtsH4). Marker for TM (αCP43) and CM (αSbtA and αNrtA) (Zhang et al. 2004).

The separated membrane protein fractions were probed with control antibodies which are specific to thylakoid (CP43) or cytoplasmic (SbtA and NrtA) membrane proteins (Zhang et al. 2004). The clean signals from the control antibodies confirmed good separation of the two subpopulations of membrane proteins. Signals from immunoblotting suggested that FtsH2 and FtsH4 are exclusively present in the thylakoid membrane membrane, which is consistent with the data from fluorescence microscopy, and that FtsH3 is present in both thylakoid and cytoplasmic membranes. Unfortunately, time pressure and the lack of cytoplasmic and thylakoid membrane fractions prevented the location of FtsH1 subunit to be determined.

3.3 Structure of an FtsH2GST/FtsH3 complex

A *Synechocystis* mutant strain, namely SynFtsH2GST, made in a previous study by Dr M. Barker (Barker et al. 2006), was used to study the structure of the FtsH2 complex

in this work. Similar to the SynFtsH2GSTery mutant made in this study, SynFtsH2GST carries a GST-Strep II tag fused to the C-terminal of FtsH2, with the difference being that a tobacco etch virus (TEV) protease cleavage site was also included in the linker (see Appendix). The phenotype of the strain was characterised and found to be consistent with the data collected from SynFtsH2GSTery (see section 3.1.3 and 3.3.1). Isolated FtsH2GST/FtsH3 complexes were firstly analysed in terms of subunit composition (see section 3.3.2) and the structure then analysed by electron microscopy (see section 3.3.3).

3.3.1 Characterisation of the SynFtsH2GST mutant

The SynFtsH2GST mutant was characterised along with the WT-G control and an FtsH2 insertion mutant, SynFtsH2GENT (Boehm et al. 2012). Phenotype characterisation was performed to test the growth ability of SynFtsH2GST under light stress (Figure 3.14 A) and osmotic stress (Figure 3.14 C). In addition, the PSII activity (Figure 3.14 B) and expression level of each FtsH homologue (Figure 3.14 D) were also examined. Growth assays, isolation and protein analysis of the FtsH2-GST/FtsH3 complex was done by myself and Marko Boehm, electron microscopy was done by Dr Jon Nield and photoinhibition assays by Prof. Josef Komenda.

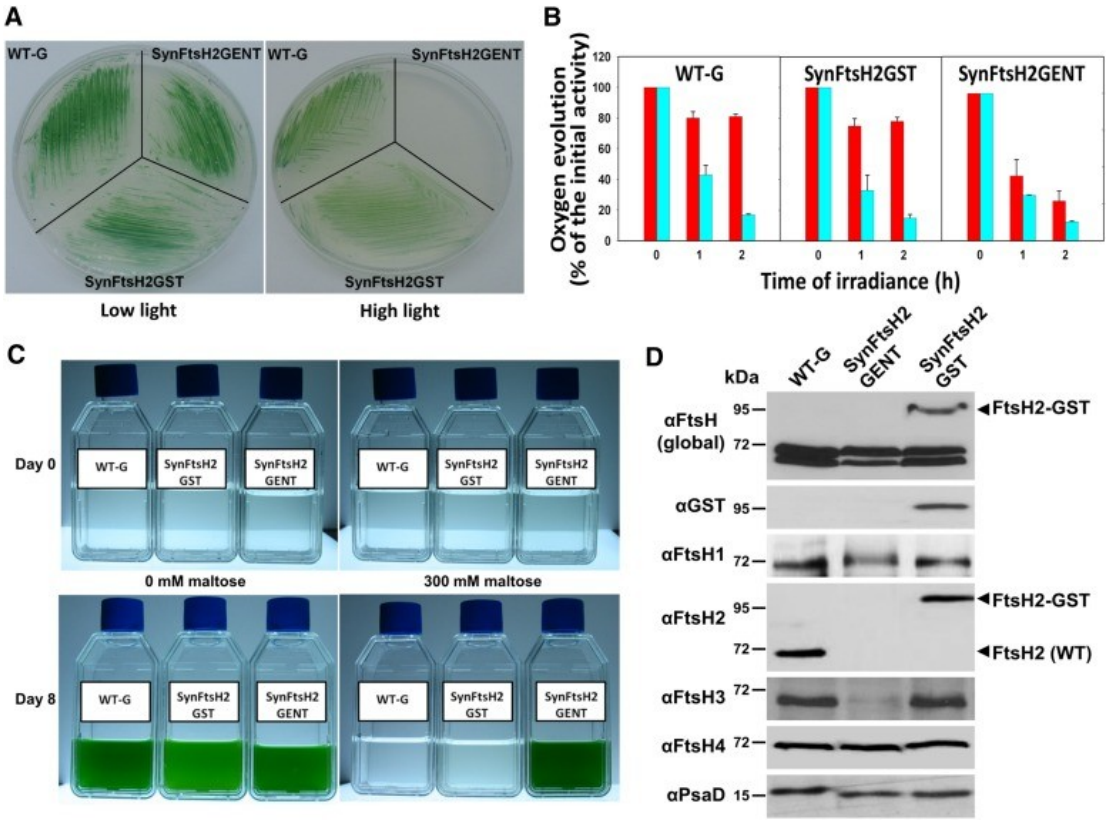

Figure 3.14: SynFtsH2GST expressing FtsH2-GST behaves like WT-G.
(A) Growth of WT-G, SynFtsHGENT (lacking FtsH2), and SynFtsH2GST on BG-11 plates under low (5 µE m^{-2} s^{-1}) and high light (100 µE m^{-2} s^{-1}). (B) PSII repair activity of WT-G, SynFtsH2GST, and SynFtsH2GENT assessed by measuring PSII oxygen-evolving activity in cells exposed to 300 µE m^{-2} s^{-1} white light at 29 °C with or without lincomycin (cyan and red columns, respectively), a protein synthesis inhibitor; initial rates of oxygen evolution were 731 ± 46, 802 ± 60, and 545 ± 43 µmol O_2 mg chlorophyll^{-1} h^{-1} for WT-G, SynFtsH2GST, and SynFtsH2GENT, respectively (means of two to three measurements for each of the two biological replicates ± se). (C) Growth of WT-G, SynFtsHGENT, and SynFtsH2GST in BG-11 in either the presence or absence of 300 mM maltose. (D) Immunoblotting analysis of the different strains using antibodies specific for all FtsH subunits (global FtsH), GST, and each of the FtsH subunits. PsaD was used a loading control. Protein samples were separated by SDS-PAGE using 8 % (w/v) polyacrylamide gels lacking urea.

The growth experiments showed that the phenotype of SynFtsHGST mutant was comparable to wild-type strain (Figure 3.14 A and C), implicating the FtsH-GST fusion protein retained PSII repair function (Nixon et al. 2005), and regulation to osmotic stress. The PSII repair analysis provided quantitative data showing that SynFtsH2GST was comparable to the wild-type. Immunoblotting data showed that the

FtsH2-GST fusion protein was expressed at similar level to that of wild-type and no cleavage of the fusion product was found. Besides, the expression levels of FtsH1, FtsH3 and FtsH4 were unaffected in the SynFtsH2GST mutant (Figure 3.14). In contrast loss of FtsH2 in the SynFtsH2GENT mutant led to a significant reduction in the level of FtsH3 (Figure 3.14).

3.3.2 Isolation of the FtsH2-GST/FtsH3 complexes

The GST-tagged FtsH2 was isolated from SynFtsHGST cells via glutathione-agarose resin and eluted with reduced glutathione. The obtained sample was then analysed by SDS-PAGE, followed by Coomassie Blue staining. Consistently, FtsH3 was co-purified as one of the two major bands in the eluate (Figure 3.15 A and C). Immunoblotting with antibodies specific to FtsH2, GST and Strep II tag (Figure 3.15 B and C) showed that the FtsH2-GST fusion protein migrated as a single band at ~ 100 kDa on the gel, no truncated product from the fusion protein was detected. Some minor bands were detected via silver staining, one of which was shown using specific antibodies to be prohibitin (Phb1) (Figure 3.15 B and C).

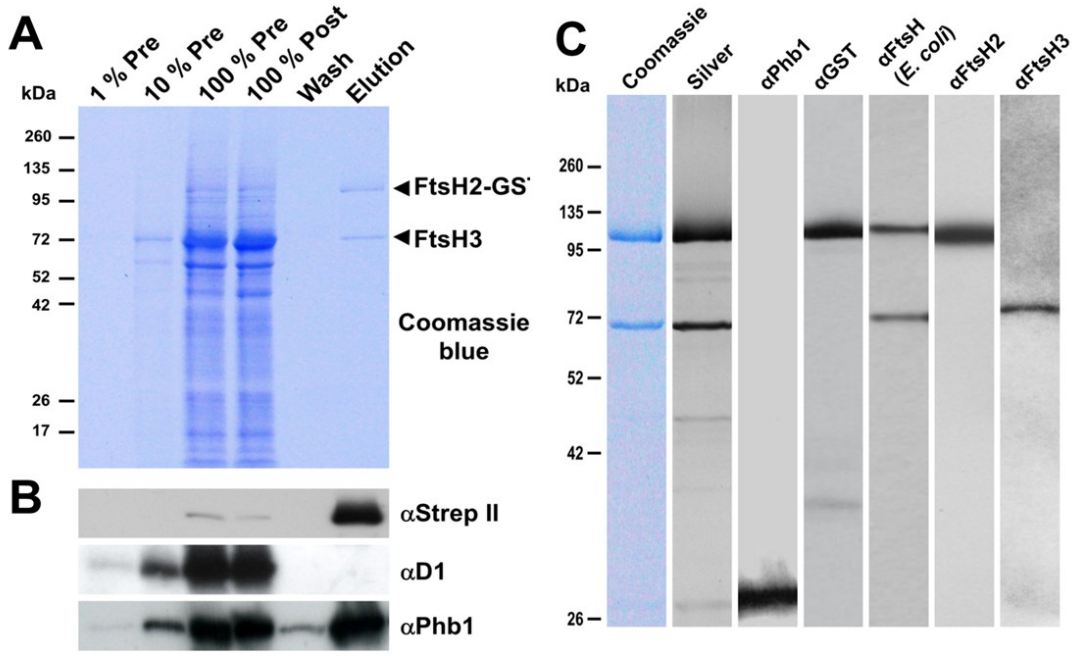

Figure 3.15: **Affinity purification of FtsH2-GST.**
(A) Detergent-solubilised thylakoid membranes from SynFtsH2GST before chromatography (Pre), the extract after binding to the glutathione resin (Post), the wash fraction just before elution (Wash) and the fraction eluted by glutathione (Elution) were separated by SDS-PAGE. The positions of the FtsH2-GST and FtsH3 proteins are indicated by arrowheads. (B) Analysis of column fractions by immunoblotting with antibodies specific for the Strep II tag (αStrep II), D1 (αD1) and Prohibitin (αPhb1). 100 % Pre corresponds to 1 µg Chl a. (C) Analysis of purified sample by Coomassie and silver staining and by immunoblotting with antibodies specific for Prohibitin (Phb1), GST, *E. coli* FtsH, FtsH2 and FtsH3.

3.3.3 EM structure of the FtsH2-GST/FtsH3 complex

The FtsH2-GST/FtsH3 complexes isolated via affinity chromatography were sent for single particle analysis using negative stain EM (collaboration with Dr J. Nield). The final structure was solved by analysing 263 classes comprising 2964 particles, and then fitted with the crystal structure of the cytosolic region of FtsH from *T. thermophilus* (Suno et al. 2006) and GST to localise the position of tags. The resulting 3-D structure unveiled a particle that has a diameter of ~ 120 Å, of which 3 GST tags were identified arranged in an alternating fashion. These data provided evidence that the isolated FtsH2-GST complex was composed of three FtsH2-GST subunits and three FtsH3 subunits alternately arranged in a hexameric complex (Figure 3.16).

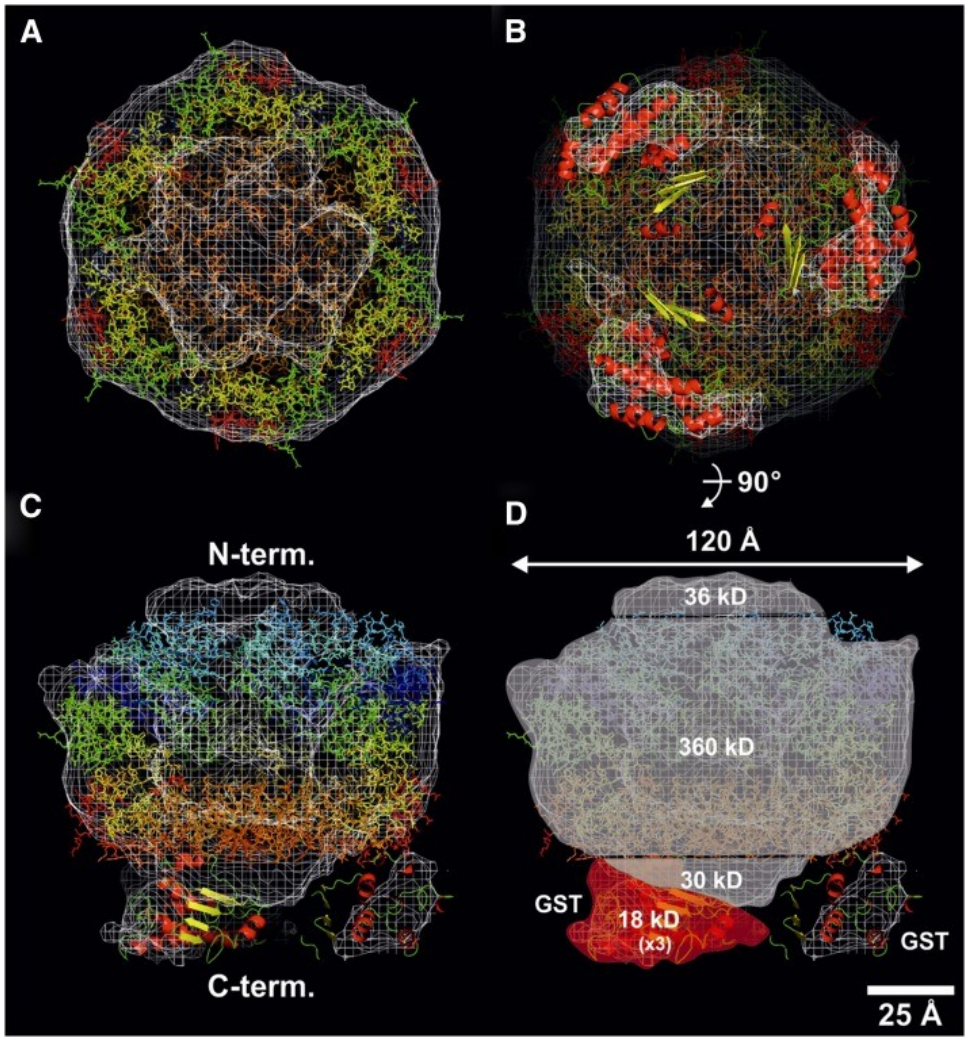

Figure 3.16: Three-Dimensional Modeling of the GST-Tagged FtsH2/FtsH3 complex.

An isomesh rendered molecular envelope, contoured with a threshold of 2.5 σ for the final calculated asymmetric three-dimensional map, is shown in white. The modeling in of the crystallography-derived hexameric soluble fragment of apoFtsH from T. maritima (3KDS.pdb) was done by visual inspection with atoms colored as a spectral rainbow from the N terminus (blue) to the C terminus (red). (A) A 5-nm-thick cross section viewed from the C-terminal PDs of 3KDS.pdb downwards, revealing its hexameric nature. (B) A 4-nm-thick cross section, viewed from the GST tags upwards, toward the C-terminal domains of the hexameric biological assembly of 3KDS.pdb. (C) A 5-nm-thick cross section, viewed from the side; the best fit for the six FtsH protomers is shown with the N-terminal AAA+ domain uppermost. (D) Four regions shown include an N-terminal cap, whose volume is calculated to be ~36 kD (assuming 0.844 Å3 per D at 2.5 σ), a central core of 360 kD, a C-terminal bottom of 30 kD, and three smaller outlying domains of 18 kD. In (B) to (D), these outlying domains, closest to the C-terminally orientated central core 3KDS.pdb file, are assigned to the GST tag (1GTA.pdb). Three such domains are observed, even though no threefold symmetry operators were applied during angular reconstitution. The maximum diameter of the complex was observed to be 120 Å. Bar = 25 Å.

3.4 Discussion

3.4.1 Composition of FtsH complexes in *Synechocystis*

Our data support the presence of FtsH1/FtsH3, FtsH2/FtsH3 and FtsH4 complexes in *Synechocystis* sp. PCC 6803. Phylogenetic analysis showed that both FtsH1 and FtsH2 are grouped with the Type B FtsH proteases from *A. thaliana* that interact with Type A isomers, and that FtsH3 is the only candidate sharing close phylogeny with Type A FtsH (Sakamoto et al. 2003). Therefore the hetero-complexes identified in *Synechocystis* might share close structural similarities with their counterparts in chloroplasts.

AFG3L2, one of the two *m*-AAA protease subunits in human is not only capable of forming hetero-complexes with paraplegin, but can also self-assemble into homo-complexes (Koppen et al. 2007). Therefore, besides the presence of FtsH1/FtsH3 and FtsH2/FtsH3 hetero-complexes, it remains possible that some FtsH1, FtsH2 and FtsH3 homo-complexes might accumulate under certain conditions. FtsH2 is so far the best studied FtsH homologue in *Synechocystis* and the EM structure of an FtsH2-GST/FtsH3 complex was determined in this work (see section 3.3.3). The structure was obtained by averaging nearly 3000 individual complexes, isolated via affinity purification of the FtsH2-GST subunits, and the resulting structure clearly showed three FtsH2 subunits arranged in an alternating fashion in each complex (see section 3.3.3). These data indicate that there is only one dominant species of FtsH2-GST/FtsH3 complex in the sample, with a strict alternating arrangement of subunits. If the arrangement of FtsH2-GST and FtsH3 subunits was random, the averaging procedure used in the image reconstitution would have led to a GST “ring” at the bottom of the complex, rather than three defined additional densities. These data also do not support the presence of FtsH2-GST homo-complexes, at least under the growth conditions used to grow the cyanobacterial strain. Currently, the structural data of the remaining FtsH complexes are not yet available, however, it seems unlikely that FtsH1 and FtsH3 form homo-complexes. Consistent with formation of an

FtsH2/FtsH3 heterocomplex, disruption of *ftsH2* resulted in the dramatic reduction in the amount of FtsH3 in the mutant cells lacking FtsH2 (Figure 3.14D). A more in-depth study revealed that the reduction of FtsH3 was due to enhanced degradation (Boehm et al. 2012), which leads to the conclusion that the presence of FtsH3 alone is unstable in the membranes and is prone to proteolytic degradation. Similarly, reduction of FtsH3 level using an inducible plasmid vector system also impaired accumulation of FtsH2 when the expression of FtsH3 was suppressed (Boehm et al. 2012), suggesting that losing either type of the subunits leads to extensive degradation of the other one. On that basis, FtsH1, which shares close similarities with FtsH2, is unlikely to accumulate without FtsH3.

3.4.2 Membrane targeting system

In vitro studies of the integration of thylakoid FtsH from *A. thaliana* have revealed that the insertion of FtsH5, a Type A FtsH subunit, is via the Sec pathway and NTP dependent, whereas the integration of FtsH2, a Type B protease, is via the Tat pathway and requiring a proton gradient across the membrane (Rodrigues et al. 2011). The striking difference is thought to be the result of variations in the N-terminal sequences of the Type A and Type B subfamilies. In particular, the N-terminus of Type B FtsH exclusively features a twin arginine motif just before the first transmembrane helix, which is a sign of Tat-directed signal peptide. Moreover, both Type A and Type B FtsH contain an A-X-A motif (where X is any amino acid), the cleavage site for the thylakoidal processing peptidase (TPP), immediately after the first transmembrane helix, suggesting that the mature proteins will have the first transmembrane region removed, leaving only one transmembrane anchor and a lumenal-facing small domain (Rodrigues et al. 2011). However the N-terminal sequence of chloroplast FtsH subunits present in the final FtsH complex has not yet been determined, which leaves open the possibility that the observed cleavage of imported FtsH subunits was non-physiological. We examined the N-terminal sequence of the four FtsH homologues in *Synechocystis* (see section 3.1.5) by N-terminal sequencing. Our data

suggested that the N-terminus of FtsH2 remains intact, and only the first formylmethionine of FtsH3 and FtsH4 is removed in the mature FtsH proteases *in vivo*.

It is surprising that FtsH4, which also features the twin arginine motif and an A-P-A cleavage site around the first transmembrane domain, similar to that of Type B FtsH in *A. thaliana*, retained almost its full N-terminal sequence. However, removal of the signal peptide is not obligatory for Tat-dependent thylakoid transport (Molik et al. 2001). Cleavage of the TAT signal peptide requires charged or polar residuals flanking the A-X-A cleavage site, possibly to enhance the lumenal exposure to TPP or release the protein from the Tat translocon (Frielingsdorf and Klosgen 2007). Further bioinformatic analysis on the N-terminal region of FtsH4 suggested that in contrast to chloroplastic FtsH, the predicted peptidase cleavage site in FtsH4 is located in the first transmembrane helix, which might be embedded in the lipid bilayer and not accessible to TPP. Nevertheless, the presence of the twin arginine motif in FtsH4 implies that insertion of FtsH4 is likely to be via the Tat pathway, which integrates fully folded FtsH4 but without removing the signal peptide.

FtsH3 might be the only FtsH homologue localised in both thylakoid and cytoplasmic membranes (see section 3.2.6). The N-terminal sequence analysis of FtsH3 in FtsH1-GST/FtsH3 complexes showed no difference to that in FtsH2-GST/FtsH3 complexes, indicating that specific N-terminal cleavage of FtsH3 does not control the integration of FtsH3 into either of the complexes. Considering that FtsH3 is the only Type A-like FtsH homologue in *Synechocystis* (Sakamoto et al. 2003), the Sec pathway is most likely to be responsible for the integration of FtsH3. Unlike the Tat pathway, which transports both folded and unfolded substrates, Sec pathway transports unfolded proteins through a SecYE channel into the membrane which is unable to transport folded domains (Henry et al. 1997). Studies on chimeric Type A

and Type B chloroplast-targeted FtsH proteins that have swapped signal peptides showed that the Sec pathway is unable to insert Type B FtsH, suggesting the domains of the fusion protein were folded in the stroma prior to membrane integration, whereas the folding process of Type A FtsH occur after integration (Rodrigues et al. 2011).

Out of the three FtsH homologues that have been N-terminally sequenced, FtsH2 is the only one to have an intact sequence. Although related to the Type B FtsH subunits in chloroplasts, no twin arginine motif was found in the TM domain, therefore, the integration of FtsH2 is unlikely to be Tat dependent. The TM domain of FtsH homologues in *Synechocystis* is the least conserved region over the whole sequence, hence the possibility of a Sec dependent membrane integration mechanism cannot be ruled out for FtsH2. On the other hand, the N-terminal sequence of FtsH2 only contains 4 residues before the first transmembrane helix. Therefore, FtsH2 might simply spontaneously insert into the thylakoid membrane without using Sec or Tat translocons, similar to that of PsbW (Kim et al. 1998).

No data were obtained from N-terminal analysis of FtsH1, possibly due to N-terminal blockage during gel electrophoresis. However, it is still noteworthy that the N-terminal sequence of FtsH1 is much longer than any other homologues. There are 19 residues before the start of the first alpha-helix and 116 residues between the two transmembrane helices, which makes it the largest TM domain among the four. Although further analysis is required to unambiguously clarify the localisation of FtsH1, the current data suggest that FtsH1 is exclusively present in or close to the cytoplasmic membrane. The long N-terminal sequence might contain specific membrane targeting signals, however, it is unlikely to utilise Tat pathway as the twin arginine motif is missing.

3.4.3 Localisation of FtsH proteases in *Synechocystis*

The localisation of all four FtsH homologues in *Synechocystis* was investigated via both fluorescence microscopy (see section 3.2.5) and immunoblotting (see section 3.2.6). Benefiting from the high abundance of FtsH2 and FtsH4, it was clear that the two homologues are present on the thylakoid membranes, and further immunoblotting assays also showed that FtsH2 and FtsH4 are exclusively present in the thylakoid membrane fraction. The localisation of FtsH1 and FtsH3 was less obvious by fluorescence microscopy, this is due to the lower expression level of FtsH1 (see section 3.2.3) and low expression and instability of the FtsH3-GFP fusion (see Figure 3.9). Nevertheless, the images from fluorescence microscopy showed weak signals from the cytoplasmic membrane area. The immunoblotting assay further confirmed that FtsH3 is present in both thylakoid and cytoplasmic membranes; unfortunately, blotting data could not be obtained for FtsH1. In parallel work, strains of *Synechococcus elongatus* PCC 7942 and *Synechocystis* PCC 6803 expressing C-terminal GFP-tagged FtsH derivatives also yielded similar fluorescence data to that shown here (unpublished data from Prof. C. Mullineaux group). Therefore, collectively all the data indicate that the FtsH complexes occupy distinct regions of the cyanobacterial cell: FtsH2 and FtsH4 complexes are found in the thylakoid membranes, FtsH3 is localised to both thylakoid and cytoplasmic membranes and, given the available data, FtsH1 is located in or close to the cytoplasmic membrane.

The abundance of FtsH3-GFP fusion protein in SynFtsH3GFPcam mutants was relatively low compared to amount of FtsH3 in WT-G (Figure 3.8). However, FtsH3 from WT-G, which is slightly smaller than the other three homologues, ran as a lower band on appropriate SDS-PAGE gels, is relatively abundant (Figure 3.13 B and Figure 3.14 D). Hence the fusion of a GFP tag might have disturbed the stability of FtsH3 and enhanced degradation (Boehm et al. 2012). FtsH3 was found to interact with both FtsH1 and FtsH2 (Figure 3.4). However, FtsH3 predominantly interacts with FtsH2 in

WT-G as FtsH3 only accumulated to 10 % of the wild-type level in an FtsH2 defective mutant (Boehm et al. 2012). This is also in line with a comparison of the immunodetectable levels of FtsH1 and FtsH2 in Figure 3.9B. The low level of GFP signal detected in SynFtsH3GSTcam was mostly spread towards the cytoplasmic membrane region and little was found in the thylakoid membrane where FtsH2/FtsH3 complexes will be located (Figure 3.12 B and C). One possible explanation is that the non-fluorescent cleaved FtsH3-GFP protein is mainly present in the FtsH2/FtsH3 complexes in the thylakoid membrane, and that the residual FtsH3-GFP interacts more strongly with FtsH1 than FtsH3 and so is preferentially located with FtsH1 in the cytoplasmic membrane.

3.4.4 Structure of hetero-oligomeric FtsH complexes

Although crystal structures for the cytosolic domains of bacterial FtsH proteases have been determined, there is much less structural information on the intact FtsH complex. Indeed the widely assumed hexameric structure for FtsH is dependent on the analysis of soluble fragments not the intact complex. Our work on the structure of the native FtsH2-GST/FtsH3 complex from *Synechocystis* therefore provides important new information on the structure of an intact hetero-oligomeric FtsH complex. Importantly our structural model suggests that the intact complex is indeed hexameric. Additionally, the subunit arrangement within the hetero-complex, elucidated by localising the additional GST density on the FtsH2 subunits, showed a clear alternating arrangement of FtsH2-GST and FtsH3 protomers. Given the co-purification of FtsH1 and FtsH3 and the close phylogenetic relationship between FtsH1 and FtsH2, it seems likely that the subunits within the FtsH1/FtsH3 complex might also alternate.

During the course of this thesis, a cryo-EM structure of the Yta10/Yta12 complex, a mitochondrial FtsH complex from yeast, was determined at ~ 12 Å resolution (Lee et al. 2011). The structure of the Yta10/12 complex also exhibited a hexameric structure

of similar size to the model present here. Although the EM data was of insufficient resolution to differentiate between the Yta10 and Yta12 subunits, a computational analysis on the subunit arrangement of Yta10/Yta12 complexes also suggested alternating protomers (Lee et al. 2011). Interestingly, a ~ 13 Å gap was identified between the trans-membrane domain and the substrate binding site in the soluble fragment of FtsH, which is equivalent to the length of a polypeptide chain consisting of ~ 20 residues (Lee et al. 2011). This finding is consistent with previous work showing that the length of the N-terminal tail of D1 is crucial for FtsH-mediated degradation and that FtsH-mediated degradation of D1 is likely to be initiated at the N-terminus (Komenda et al. 2007b).

Chapter 4: Functional characterisation of FtsH *proteases in vivo* and *in vitro*

4.1 Functional analysis of FtsH-deficient mutants

Early mutagenesis experiments revealed that the *ftsH1* and *ftsH3* genes of *Synechocystis* 6803 are required for cell viability whereas *ftsH2* and *ftsH4* are non-essential (Mann et al. 2000). More recent studies have confirmed that FtsH2 is involved in removal of photodamaged D1 protein (Silva et al. 2003; Komenda et al. 2006b) and osmoregulation (Stirnberg et al. 2007). On the other hand, the function of FtsH4 is not yet known as disruption of this gene did not yield a distinctive phenotype under the conditions tested (Mann et al. 2000). It has been shown that in the chloroplasts of *A. thaliana*, PSII repair is maintained by multiple types of FtsH complexes composed of different isomers of Type A and Type B proteases (Yu et al. 2005). Among the four homologues in *A. thaliana*, FtsH1 and FtsH8 appear to function as minor isomers, disruption of which results in no obvious phenotype (Sakamoto et al. 2003). These results therefore raised the speculation that FtsH4 in *Synechocystis* might have functional overlap with other FtsH complexes. To explore the potential function of FtsH4, a double mutant deficient in both FtsH2 and FtsH4 was made (see section 4.1.2-4.1.3) and characterised in this work (see section 4.1.4-4.1.5). In addition, a bioinformatic analysis was performed to identify suitable residues for mutagenesis (see section 4.1.1 and section 4.2).

4.1.1 Defining the functional domains of each cyanobacterial FtsH.

Bioinformatic analysis is a great tool to identify conserved amino-acid residues and motifs between homologous proteins. Benefiting from the previous experimental data, especially the crystal structures of the cytosolic domains of several bacterial FtsHs, a few conserved motifs in FtsH have been defined (Suno et al. 2006). After aligning FtsH homologues from both *Synechocystis* 6803 and *T. elongatus* with that of *T.*

thermophilus, we were able to locate the conserved alanine (A144, designation according to the sequence of FtsH from *T. thermophilus* and hereafter) and glycine (G399) at each end of the AAA+ domain (Figure 4.1). The transmembrane and protease domains are less conserved due to the diverse physiological functions; therefore, the actual boundary of these two domains might vary among individuals. The conserved motifs that define the FtsH protease family were aligned (Figure 4.1, blue boxes), including the classic Walker A, Walker B and second region of homology (SRH) motifs responsible for nucleotide hydrolysis, and the zinc ion-binding motif (ZnBD) that enables metalloproteolytic activity. Notably, the FtsH family also features a conserved @XG (@ represents hydrophobic residue, X represents any residue) sequence in the AAA+ domain, in this case Phe-Val-Gly. According to the crystal structures of the *T. maritima* and *T. thermophilus* FtsH hexameric complexes, this motif appears aligned around the entrance of the central pore, and is believed to be responsible for initial substrate binding and translocation through the pore to the protease catalytic site (Bieniossek et al. 2006). Moreover, unlike other known zincins, the third ligand to the zinc ion in FtsH is an aspartic acid, instead of glutamic acid, in the protease domain (Suno et al. 2006).

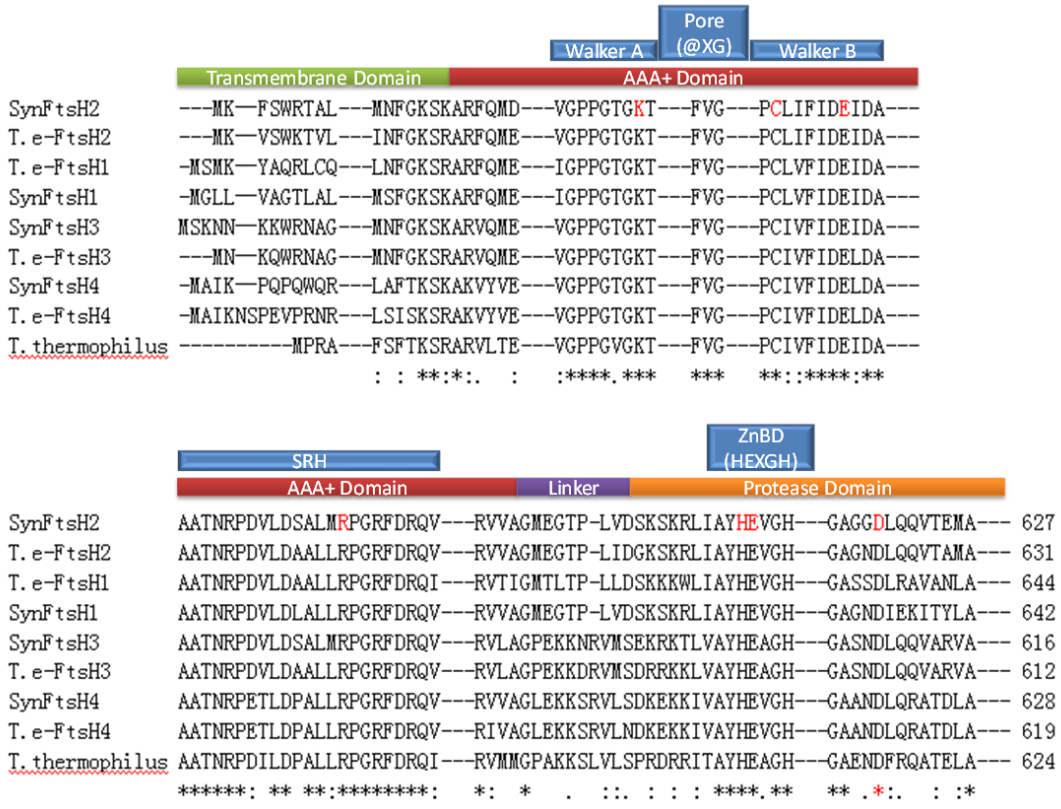

Figure 4.1: Alignment of the cyanobacterial FtsH homologues.
Sequences of FtsH homologues in cyanobacteria *Synechocystis* sp. PCC 6803 (SynFtsH1-4) and *T. elongatus* (T.e-FtsH1-4) were aligned against that of *T. thermophilus*. The motifs that define the FtsH protease family are labelled in blue boxes, and residues that will be subject to site-directed mutagenesis in this work are marked in red. Please note that only selected portions of FtsH are shown.

4.1.2 Construction of deletion strains

Knockout mutants are useful tools to study the function of target genes, and moreover, they can be used as recipient strains for functional complementation studies (Koppen et al. 2007; Lee et al. 2011; Zhang et al. 2010). It has already been shown that FtsH1 and FtsH3 are essential to cell viability (Mann et al. 2000), therefore, *ftsH2*, *ftsH4* and an *ftsH2/4* double null mutant were generated in this study.

Although a few FtsH2 and FtsH4 insertion-disruption mutants have been made and characterised in previous work (Boehm et al. 2012; Mann et al. 2000), alternative mutants were required in this work as the *ftsH* knockout mutants were also to be used

as recipient strains for site-directed mutagenesis (see section 4.2). The locations for site-directed mutagenesis were identified in sequence alignments (Figure 4.1). To help improve the efficiency of incorporation of mutations into the genome via homologous recombination, part of the *ftsH* open reading frame (ORF) containing the sites of interest was replaced with an antibiotic-resistance cassette (Figure 4.2).

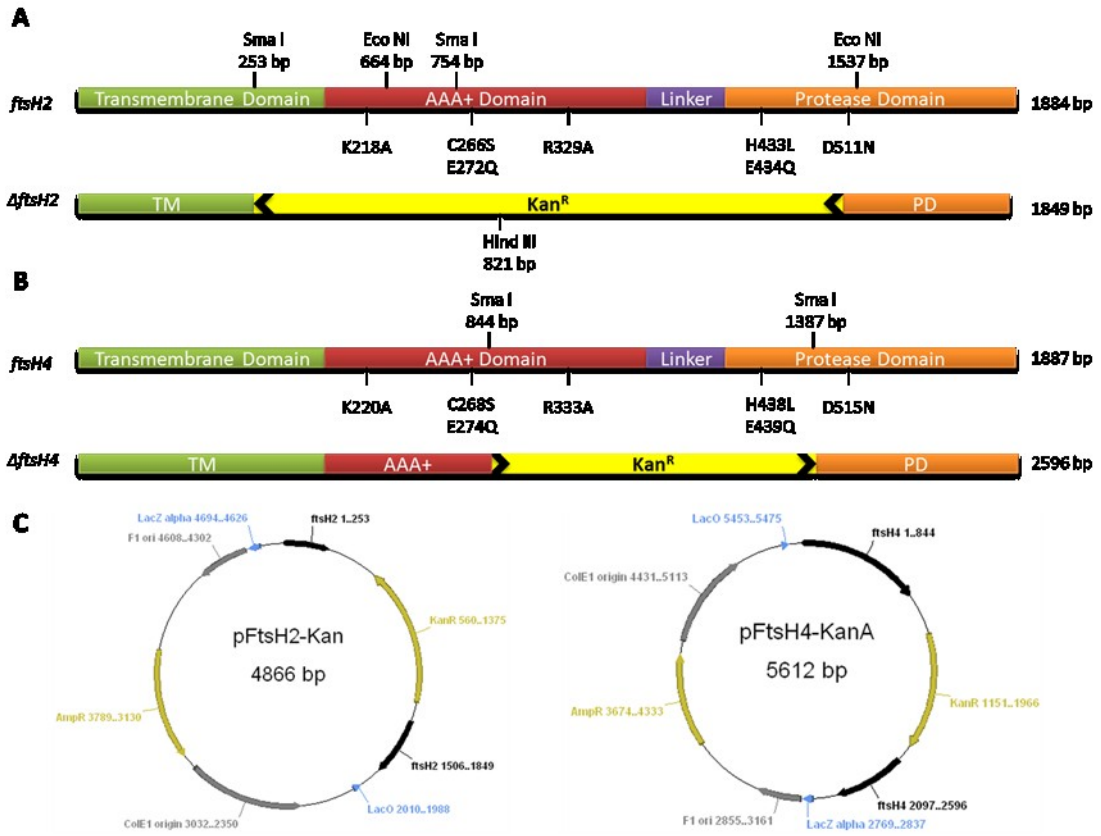

Figure 4.2: Construction of the FtsH2 and FtsH4 knockout vectors.
Schematic representations of the knockout construct design of FtsH2 (A) and FtsH4 (B), and the plasmid maps of the two knockout vectors (C). The wild-type DNA sequence of *ftsH2* between the first SmaI and the last EcoNI sites was replaced with a kanamycin-resistance cassette (A), whereas only the region between the two SmaI sites of *ftsH4* was replaced with a kanamycin-resistance cassette (B). The locations of the sequences encoding candidate residues to be mutated are indicated. The size of the wild-type and knockout constructs are labelled on the right (A and B).

To create the *ftsH2* deletion construct, the entire *ftsH2* ORF was amplified from wild-type genomic DNA of *Synechocystis*, using primer set FtsH2-F and FtsH2-R1 (Table 2.5). The resulting PCR product was then cloned into pGEM-T Easy vector to

create pFtsH2WT. To replace the region that encodes the candidate residues listed in Table 4.2, the parental vector pFtsH2WT was digested with SmaI and EcoNI, and the resulting fragments were then separated on an agarose gel. The large fragment carrying the 5' and 3' ends of *ftsH2* was gel purified and blunt-ended using Klenow fragment, and then ligated with a kanamycin-resistance cassette to create the final transformation vector pFtsH2-Kan (Figure 4.2 C).

Similar to the construction of the *ftsH2* knockout vector, the full sequence of wild-type *ftsH4* was amplified using primer set FtsH4-F and FtsH4-R1 (Table 2.5), and then cloned into pGEM-T Easy to create pFtsH4WT. Unlike the *ftsH2* construct, which possesses suitable restriction sites to enable the region encoding all 7 candidate residues to be removed via endonuclease digestion, the *ftsH4* ORF did not contain desirable restriction sites. Therefore, only a small fragment between the two SmaI sites was removed from pFtsHWT via digestion. A kanamycin-resistance cassette was then ligated with the backbone fragment of pFtsHWT purified from agarose gel, to create pFtsH4-KanA (Figure 4.2 C).

4.1.3 Genotyping of the *ftsH2* and *ftsH4* deletion mutants

Synechocystis WT-G cells were transformed with pFtsH2-Kan and pFtsH4-KanA vectors and selected on BG11 plates supplemented with glucose, kanamycin and DCMU. In addition to wild-type cells, an *ftsH2* insertion mutant namely *Δ0228-Cam* (Komenda et al. 2006a) was also used as a recipient strain for the pFtsH4-KanA vector to create a double *ftsH2/ftsH4* null mutant. The double mutant was selected for resistance to both chloramphenicol and kanamycin. All three mutants were grown under low-light conditions and restreaked weekly until segregation was complete as judged by PCR.

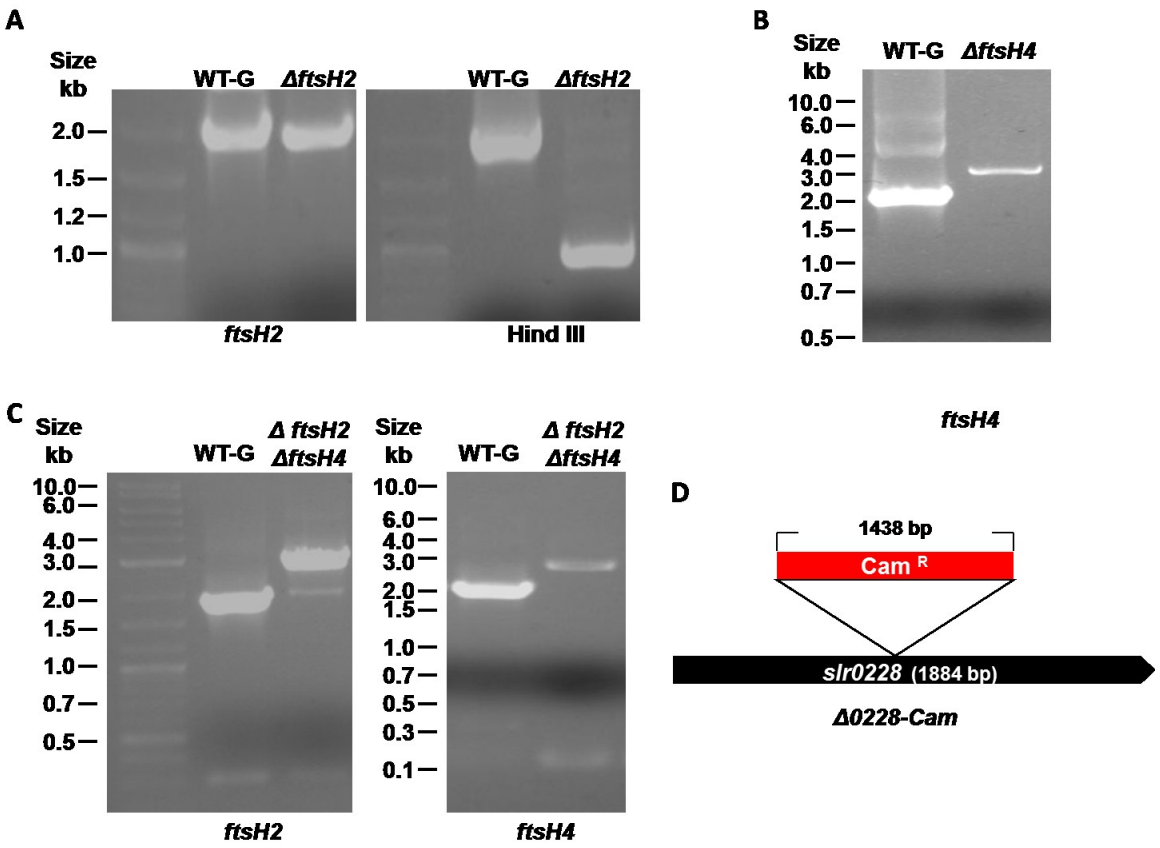

Figure 4.3: Genotyping of the *ftsH2* and *ftsH4* deletion mutants.
Mutated *ftsH* genes were amplified via PCR and analysed on agarose gels to show segregation of the mutant genotype (A, B and C). The PCR fragments amplified from *ftsH2* cells were further digested with HindIII (A, right panel) to confirm integration of the kanamycin resistance cassette. (D) A schematic representation of the disruption construction of *ftsH2* in *Δ0228-Cam*.

The genomic DNA of the newly constructed mutants, namely *ΔftsH2*, *ΔftsH4* and *ΔftsH2ΔftsH4*, was extracted via phenol-chloroform extraction and the mutated ORFs were amplified with primer pair FtsH2-F/FtsH2-R1 and/or FtsH4-F/FtsH4-R1, respectively (Figure 4.3 A B and C). The *ftsH4* construct is ~700 bp longer than the wild-type; the *ftsH2* knockout construct, however, is almost the same size as the wild-type. Therefore a diagnostic restriction digest with HindIII, which exclusively cuts the kanamycin-resistance cassette (Figure 4.3 A), was performed (Figure 4.3 A, right panel). According to the PCR and digestion results, all three mutants, *ΔftsH2*, *ΔftsH4* and *ΔftsH2ΔftsH4* were either fully segregated or virtually fully segregated. The extra higher molecular mass bands observed in the WT samples might reflect the

production of larger DNA fragments due to non-optimised PCR conditions.

4.1.4 Immunochemical detection of FtsH2 and FtsH4 in the deletion mutants

In addition to the genotype analysis, immunochemical detection of FtsH2 and FtsH4 was performed to provide direct and independent evidence to the knockout status of the target proteins.

To prepare the protein samples for the assay, ~50 ml of *ΔftsH2*, *ΔftsH4* and *ΔftsH2ΔftsH4* cultures was harvested, and the crude membrane fraction was prepared (see section 2.7.1). The membrane proteins were then separated on 8 % SDS-PAGE gels (see section 2.7.3.2). After electrophoresis, the proteins were either stained with Coomassie Blue or transferred to a PVDF membrane for immunoblotting with specific antibodies.

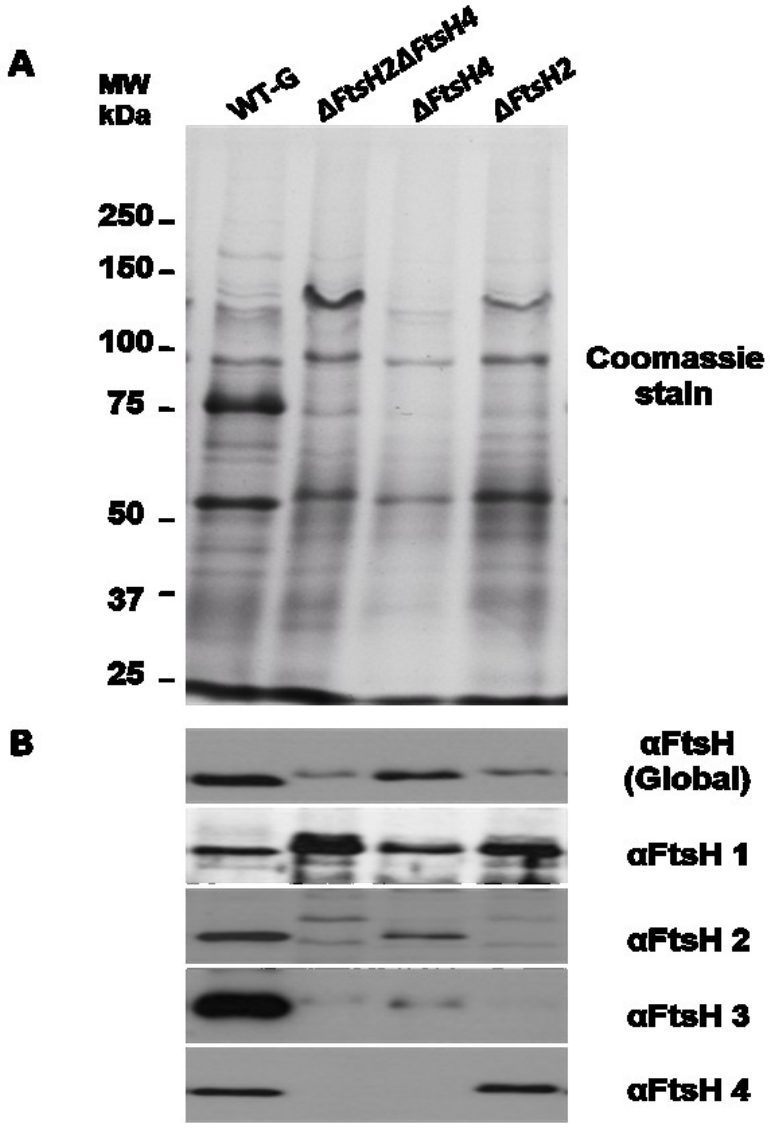

Figure 4.4: Immunochemical detection of FtsH2 and FtsH4.
(A) Coomassie stained gel of membrane protein extractions. (B) Immunoblotting of the protein samples with antibodies specific to all FtsH (αFtsH Global) and each FtsH homologue (αFtsH 1-4). Some weaker non-specific signals were detected with the FtsH2 antibody.

The immunoblotting data showed lack of detectable FtsH2 and/or FtsH4 in the three deletion mutants. Interestingly, two additional faint protein bands were detected by anti-FtsH2 antibody exclusively in *ΔftsH2* and *ΔftsH2ΔftsH4* samples, the sizes of which are either bigger or smaller than the theoretical size of FtsH2. The identities of these bands are unclear, possibly non-specific detection of proteins that accumulate on the membrane when the function of FtsH2 is disrupted. Notably, the accumulation of

FtsH3 was dramatically reduced in the mutants lacking FtsH2 (Figure 4.4 B), which is consistent with previous work on another FtsH2 deficient mutant (Boehm et al. 2012). Because protein loading was not controlled in the experiment shown in Figure 4.4, care has to be taken drawing conclusions on relative abundance between mutants and WT-G.

4.1.5 Phenotype analysis of the deletion strains

Growth of the *Synechocystis ΔftsH2*, *ΔftsH4* and Δ*ftsH2ΔftsH4* mutants was tested on BG11 plates or BG11 plates supplemented with 5 mM glucose under low, medium and high-light conditions.

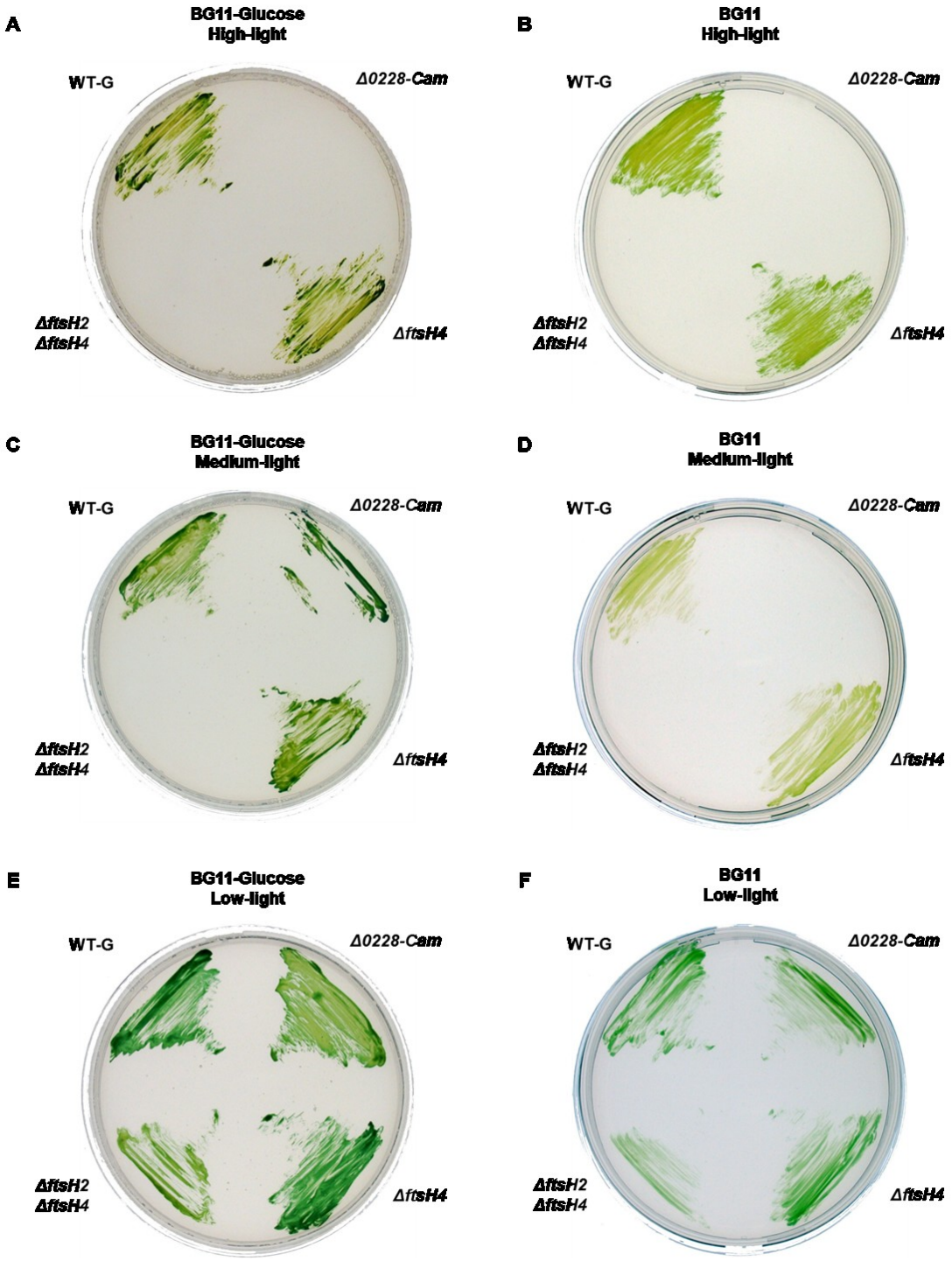

Figure 4.5: Growth experiment of *ftsH* knock out mutants.
Each plate carries 4 strains: WT-G: wild-type strain, *ΔftsH2-Cam*: FtsH2 null mutant, *ΔftsH4*: FtsH4 null mutant and the *ΔftsH2ΔftsH4*: FtsH2/FtsH4 double deletion mutant. Cells were tested for growth under high (A and B), medium (C and D) and low (E and F) light conditions on BG11 plates supplemented with 5 mM glucose (A, C and E) and plain BG11 plates (B, D and F).

Similar to the *ftsH* insertion-disruption mutant characterised by Mann et al. (2000),

the *ftsH4* null mutant displayed a WT-like phenotype (Figure 4.5 A) and the *ftsH2* null mutant was more susceptible to light stress (Silva et al. 2003) (Figure 4.5 A). Interestingly, the double mutant was even more sensitive to light stress comparing to the *ftsH2* single mutant (Figure 4.5 C), indicating FtsH4 could play a minor role in counteracting photoinhibition.

4.2 Construction of FtsH site-directed mutants

Previous studies on chloroplast, mitochondrial and bacterial FtsH proteases have identified conserved residues that have a great impact on the correct function of the protease complex (Arlt et al. 1996; Karata et al. 1999; Suno et al. 2006; Zhang et al. 2010). In this work, we took advantage of the available data to target seven *Synechocystis* residues in the AAA+ and PD domains for mutagenesis (Table 4.1 and Table 4.2), with the aim to generate protease inactive complexes to allow identification of potential substrates in pull-down assays. Six of the characterised residues were chosen to test for effects on protease activity or ATP-ase activity (Table 4.1). The conserved residues at Walker A and Walker B motifs are essential for correct docking of ATP into the binding pocket of the AAA+ domain, whereas, the conserved "arginine finger" on the second region of homology (SRH) has been proposed to be essential to the hydrolysis of ATP (Suno et al., 2006). The remaining three residues located at the protease domain are the three ligands that coordinate the zinc ion at the proteaolytic site, some of which have been shown to be essential to the proteolytic activity (Karata et al., 1999; Zhang et al., 2010). In addition, a conserved cysteine residue found in the Walker B motif, and found in all cyanobacterial FtsH homologues, was mutated to serine to test for a potential role in redox-control of the enzyme (Mata-Cabana et al., 2007). Notably, the cysteine is unique to five of the eight cyanobacterial FtsH proteases covered in this study, only SynFtsH1, TheFtsH1 and TheFtsH4 have a second cysteine downstream of the HEXGH motif. Moreover, this cysteine is not universally conserved across the entire FtsH family; according to the phylogenetic analysis, most mitochondrial FtsH orthologues have a serine or alanine

instead.

Table 4.1: List of candidate residues targeted for site-directed mutagenesis and the supporting references.

Site-directed mutagenesis						
Reference	This work	Zhang 2010	Karata 1999	Koppen 2007	Suno 2006	Notes
Organism	SynFtsH2 *Synechocystis*	*A. thaliana*	*E. coli*	*S. cerevisiae*	*T. thermophilus*	
Walker A motif	K218-A	G267-D	K201-N			ATP binding
Walker B motif	E272-Q	P320-L D326-N	E255-Q			ATP binding
SRH	R329-A		N301-A D307-A R312-A R315-A		N302 R313	ATP binding Arginine Finger
Pore (@XG)			G302-S		F229	Initial substrate binding site
GAD motif			G433-R			Essential motif for proteolytic activity
ZnBD motif	H433-L E434-Q	H488-L	E418-Q H421-Y	E614-Q		Primary and secondary Zn^{2+} coordinates
Zn ligand	D511-N				D493	3rd Zn^{2+} coordinate
Others	C266-S				G399-L A310C-L527C	Redox control (Walker B) Enhance Crystal ATP-Protease domain Crosslinking S-S bond

FtsH2 of *Synechocystis* (SynFtsH2) was used as an example of alignment in this table, along with FtsH residues previous characterised in other organisms. Seven conserved residues essential to the function of each motif/domain were selected in this study (residues listed under SynFtsH2) and their counter parts in other organisms were also highlighted in red.

4.2.1 Construction of site-directed mutagenesis transformation vectors

In this study, only FtsH2, FtsH3 and FtsH4 from *Synechocystis* were targeted for site-directed mutagenesis (Table 4.2). This was due to the time limitation, and because the thylakoid FtsH proteases are more closely associated with photosynthesis, which is the focus of this research.

Table 4.2: List of the site-directed mutants chosen for construction in this work.

	FtsH2	FtsH3	FtsH4
Walker A	K218A	K207A	K220A
Walker B	E272Q	E261Q	E274Q
SRH	R329A	R318A	R333A
ZnBD (HEXGH)	H433L	H423L	H438L
	E434Q	E424Q	E439Q
ZnBD	D511N	D504N	D515N
Trx control	C266S	C255S	C268S

The construction of the site-directed mutagenesis vectors was similar to that of the pFtsH(x)GSTery vectors, with the following changes: pGEMFtsH(x) plasmid vectors were used as the DNA template, instead of the wild-type genomic DNA, in the first overlap extension PCR with primer pairs FtsH(x)-F/FtsH(x)(R)-R and FtsH(x)(R)-F/FtsH(x)-R, where FtsH(x) represents the particular homologue and (R) represents the particular mutation. The PCR products from the first PCR reactions were gel extracted and used as the DNA templates in the second overlap extension PCR reaction with primer pairs FtsH(x)-F/FtsH(x)-R. The resulting PCR fragments were gel extracted and ligated into pGEM-T Easy vector after addition of an A overhang at the 3' ends, to yield the intermediate vectors pGEMFtsH(x)(R). The sequence of the resulting vectors was then checked to ensure only the correct mutation was present in the vectors.

To enable affinity purification of the mutated FtsH proteases, the *gst* tagging cassette from pGST-CamA was used to fuse a *gst::strepII* tag and a chloramphenicol-resistance cassette to the 3' end of *ftsH* via the EcoRV and XbaI sites. The resulting transformation vectors, namely pFtsH(x)(R)GSTcam, were then sequenced over the ligation junctions to ensure no frame-shift occurred during the cloning process.

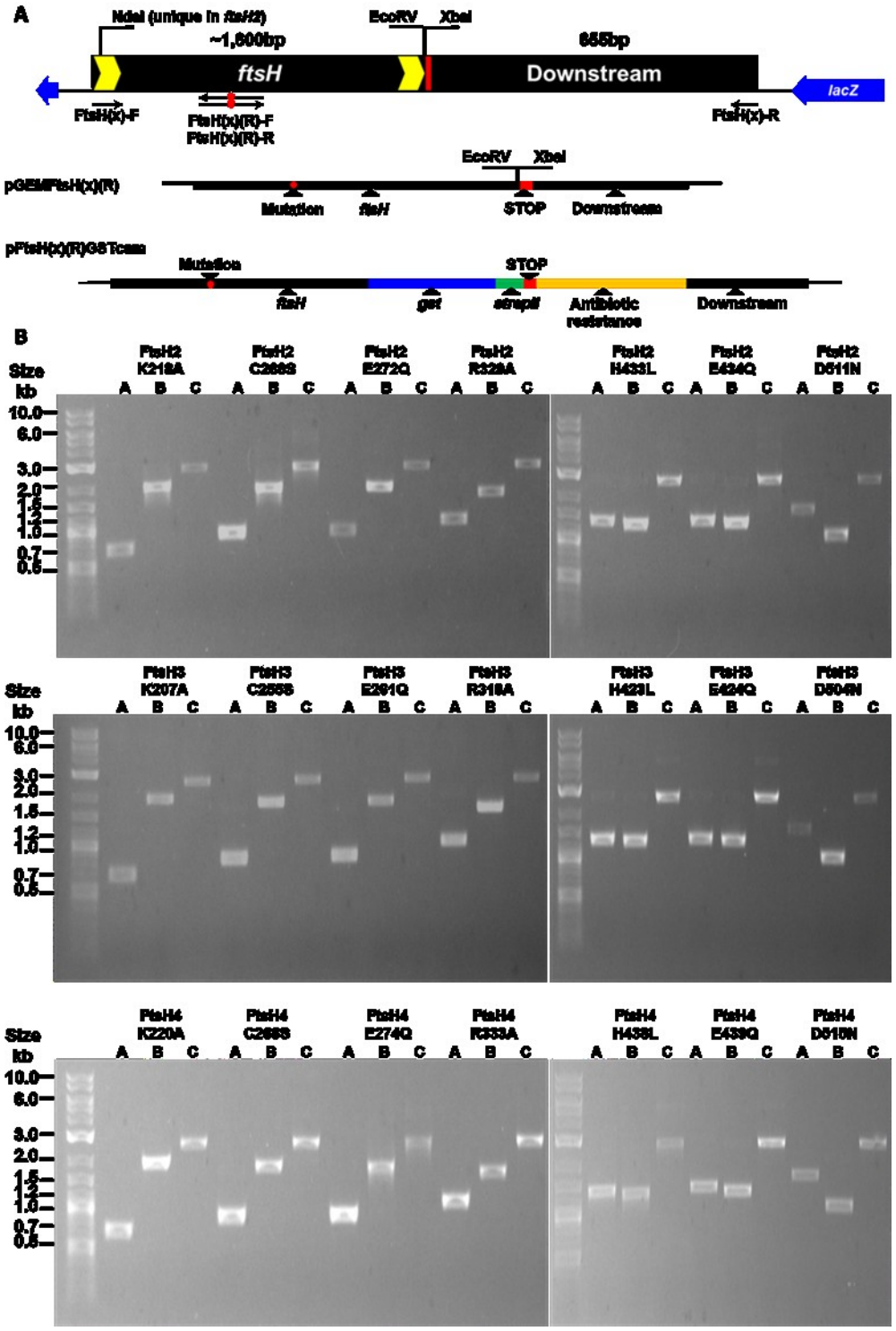

Figure 4.6: Construction of the FtsH mutagenesis vectors.

(A) A schematic representation of the construction of the pGEMFtsH(x)(R) and pFtsH(x)(R)GSTcam vectors. FtsH(x) represents the particular FtsH homologue and (R) represents the particular mutation. (B) Purified PCR fragments from the overlap extension PCR reactions. Lane A is the fragment amplified with primer pair FtsH(x)-F/FtsH(x)(R)-R, lane B is resulting fragment of FtsH(x)(R)-F/FtsH(x)-R and lane C is the PCR product of FtsH(x)-F/FtsH(x)-R, using fragments from lane A and B as DNA templates.

4.2.2 Generation of tag-free protease inactive mutants of FtsH2

A previous study on the *var2* mutant of *A. thaliana* has shown that chloroplast FtsH2 carrying point-mutations in the zinc-ion binding motif, but not motifs in the AAA+ domain, was able to rescue leaf variegation caused by *var2* disruption (Zhang et al. 2010). This observation provided evidence in support of a hetero-oligomeric structure for the FtsH complex. To test whether a similar effect holds for the cyanobacterial system, pGEMFtsH2(R) vectors lacking the antibiotic-resistance cassette were used to transform *ΔftsH2* directly and the mutants were selected on BG11 plates under high-light illumination. The resulting mutants, namely SynFtsH2(R), are free of the *gst::strepII* tagging cassette. Interestingly, out of the 7 missense mutations targeted, 4 mutants SynFtsH2H433L, E434Q, D511N and C266S successfully restored growth at high light intensities (Figure 4.7), whereas SynFtsH2K218A, E272Q and R329A failed to grow. The genotypes of the resulting PS+ mutants were confirmed by PCR and the resulting fragments sequenced to confirm that the correct mutations had been incorporated into the genome (data not shown).

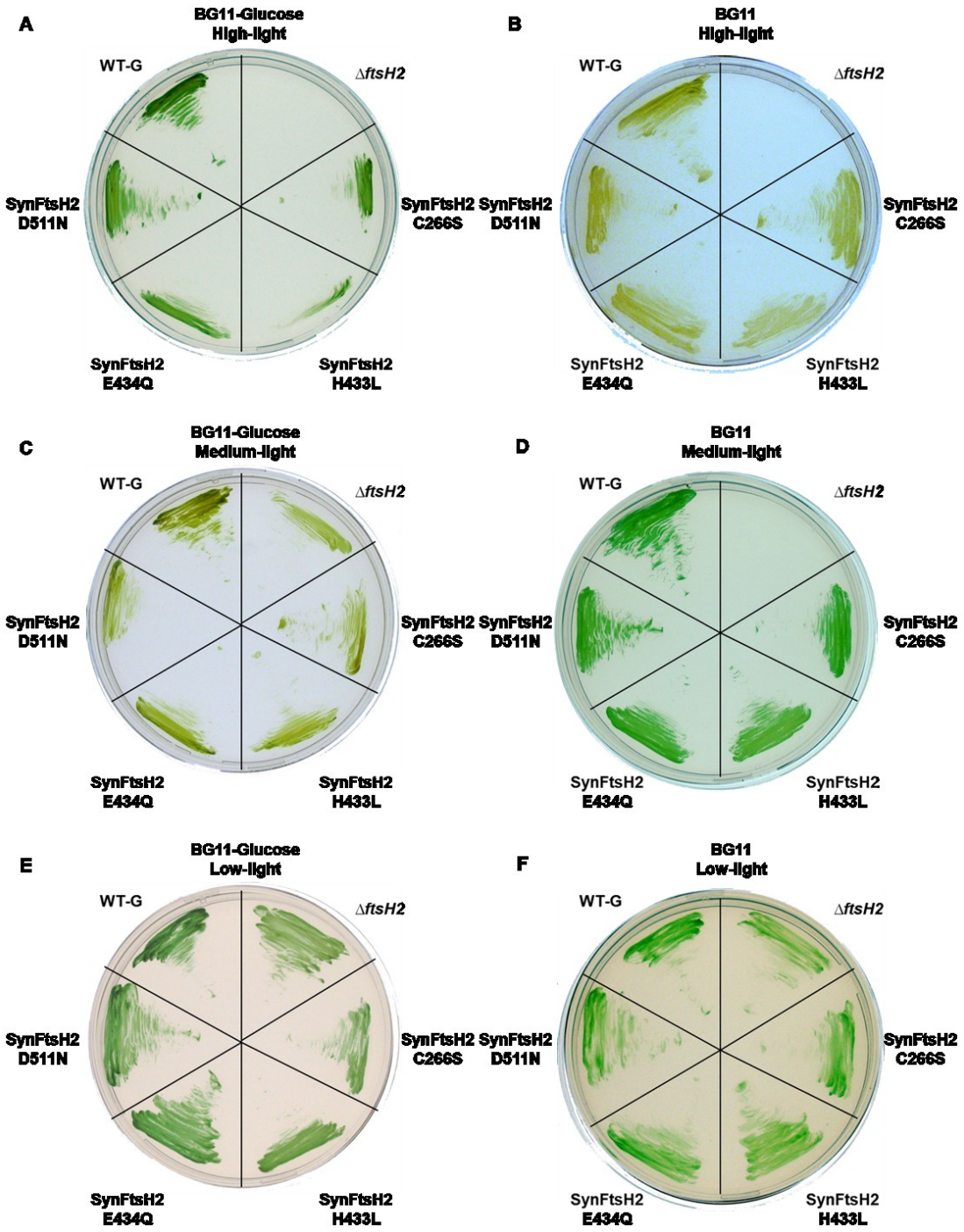

Figure 4.7: Growth experiment of FtsH2 mutants.
Each plate carries 6 strains: WT-G: wild-type strain, *ΔftsH2*: FtsH2 null mutant and the mutants expressing FtsH2 that carrying point-mutations at C266 (SynFtsH2C266S), H433 (SynFtsH2H433L), E434 (SynFtsH2E434Q) and D511 (SynFtsH2D511N). Cells were tested for growth under high (A and B), medium (C and D) and low (E and F) light conditions on BG11 plates supplemented with 5 mM glucose (A, C and E) and plain BG11 plates (B, D and F).

The restoration of photoautotrophic growth under high-light conditions strongly

suggests that the conserved protease activity of FtsH2 is not essential to the activity of the complex, which is consistent with the observation in plants and the results in Chapter 3 showing that FtsH2 forms a hetero-oligomeric complex with FtsH3. Moreover, the conserved cysteine in the AAA+ domain of FtsH2 seemed to be relatively unimportant to the function of the AAA+ domain, as judged by the ability of the mutant to survive the high-light stress.

4.2.3 Generation of GST-tagged FtsH mutants

Three recipient strains, WT-G, *ΔftsH2* and *ΔftsH4*, were used to generate the FtsH-inactive mutants. Vectors pFtsH2(R)GSTcam were used to transform *ΔftsH2*, which has ~1,200bp of the *ftsH2* ORF replaced with a kanamycin-resistance cassette (see section 4.1.2), the resulting mutants were named SynFtsH2(R)GSTcam. Vectors pFtsH4(R)GSTcam were used to transform *ΔftsH4*, which has ~550bp of the *ftsH4* ORF replaced with a kanamycin-resistance cassette (see section 4.1) and the resulting mutants were named SynFtsH4(R)GSTcam. The pFtsH3(R)GSTcam vectors were used to transform WT-G, to create SynFtsH3(R)GSTcam. The mutants were selected for chloramphenicol resistance under low-light conditions on BG11 plates supplemented with glucose, chloramphenicol and DCMU.

Table 4.3: List of mutants obtained.

	FtsH2	**N/A**	**CM**	**FtsH3**	**CM**	**FtsH4**	**CM**
Walker A	K218A			K207A	√	K220A	
Walker B	E272Q		√	E261Q		E274Q	√
SRH	R329A			R318A	√	R333A	√
ZnBD	H433L	√	√	H423L	√	H438L	
(HEXGH)	E434Q	√		E424Q		E439Q	√
ZnBD	D511N	√	√	D504N	√	D515N	√
Trx control	C266S	√		C255S	√	C268S	√

Ticked box on the right of each mutation represents colonies being maintained, red tick represents the genotype of the mutant is checked to be correct. In the first line of boxes, N/A: mutant without selectable marker, CM: mutants confer chloramphenicol resistance.

Among the 21 constructs made in this project, the screening of FtsH4 protease-inactive mutants was one of the top priorities as FtsH4 does not form hetero-complexes (see section 3.1.4), hence the inactivation of FtsH4 complexes is not subject to the residual activity from the other type of subunit. Four mutants carrying designated mutations at C268, E274, R333 and E439 have been generated so far with the DNA sequence of the resulting mutants confirmed via sequencing. Further protein analysis using immunoblotting with anti-FtsH4 antibody showed the FtsH4-GST fusion protein was intact, however, the expression level of the fusion protein was much lower than that of wild-type, which is consistent with the previous observations on SynFtsH4GFPcam strain, indicating the C-terminal tag affects the accumulation of the protease (Figure 4.8).

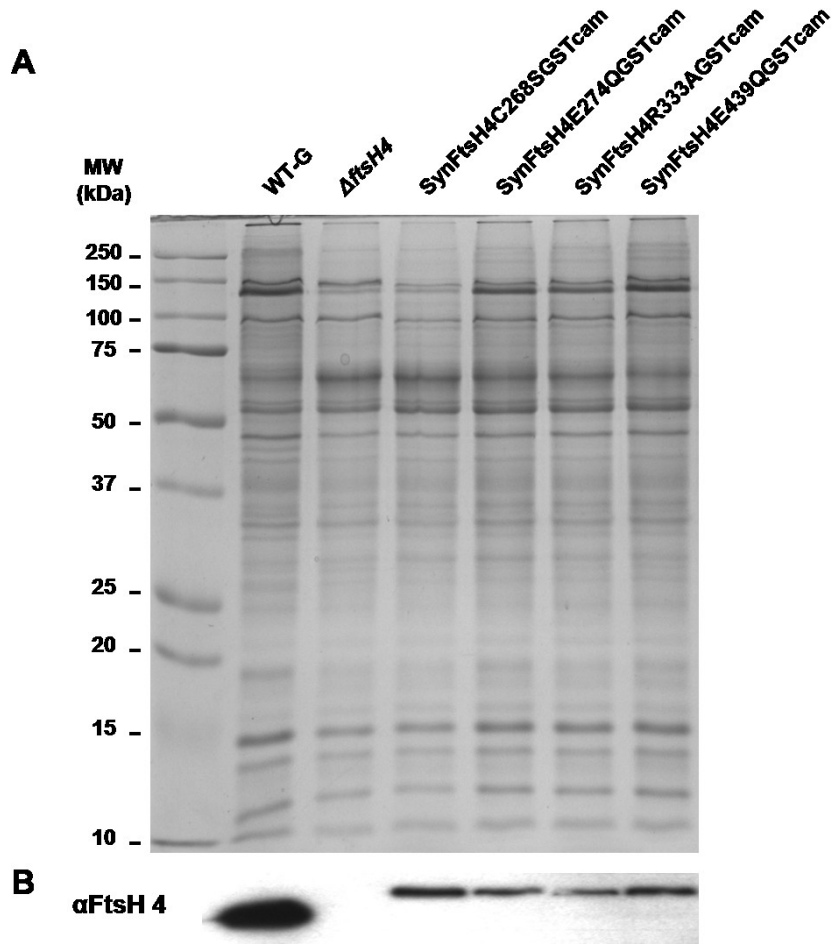

Figure 4.8: Immunochemical detection of FtsH4(R)-GST recombinant proteins.
(A) Coomassie stained gel of membrane proteins from SynFtsH4(R)GSTcam mutants. (B) Immunoblotting of the protein samples with antibodies specific to FtsH4.

4.3 Physiological influence of the C-terminal GST tag on FtsH protease activity

As described in Chapter 3 (see section 3.2.4), the addition of a C-terminal GFP tag to FtsH1, FtsH2 and FtsH4 did not alter the sensitivity of the mutants to light stress. In contrast, addition of a GST tag to the C-terminus of FtsH3 led to increased susceptibility to photoinhibition (see section 3.1.3). Immunoblotting analysis further provided hints that the increased sensitivity might be attributed to the presence of the C-terminal GST tag, whereas the FtsH3-GFP strain was not affected possibly due to the cleavage of the GFP tag from the C-terminus (see section 3.2.3). As multiple types of FtsH complex were identified in this work (see section 3.1.4), it is possible that the functions of complexes with different composition might show functional overlap (see section 5.1.1). To further examine the physiological influence of the C-terminal GST tag of each FtsH homologue with reduced functional interference from other types of FtsH complexes, the double deletion mutant*ΔftsH2ΔftsH4* was used as the recipient strain instead of WT-G cells to construct double and triple mutants expressing FtsH-GST derivative proteases.

4.3.1 Construction and phenotype analysis of the mutants

pFtsHxGSTery vectors (see section 3.1.1) was used to transform the FtsH2/4 null mutant *ΔftsH2ΔftsH4*, yielding a triple mutant SynFtsH1GSTΔ24, and two double mutants SynFtsH2GSTΔ4 and SynFtsH4GSTΔ2. The transformation was carried out following the same procedure as described earlier (see section 3.1.1). Growth of the resulting mutants was then compared to the wild-type and the parental strain *ΔftsH2ΔftsH4* under various light intensities.

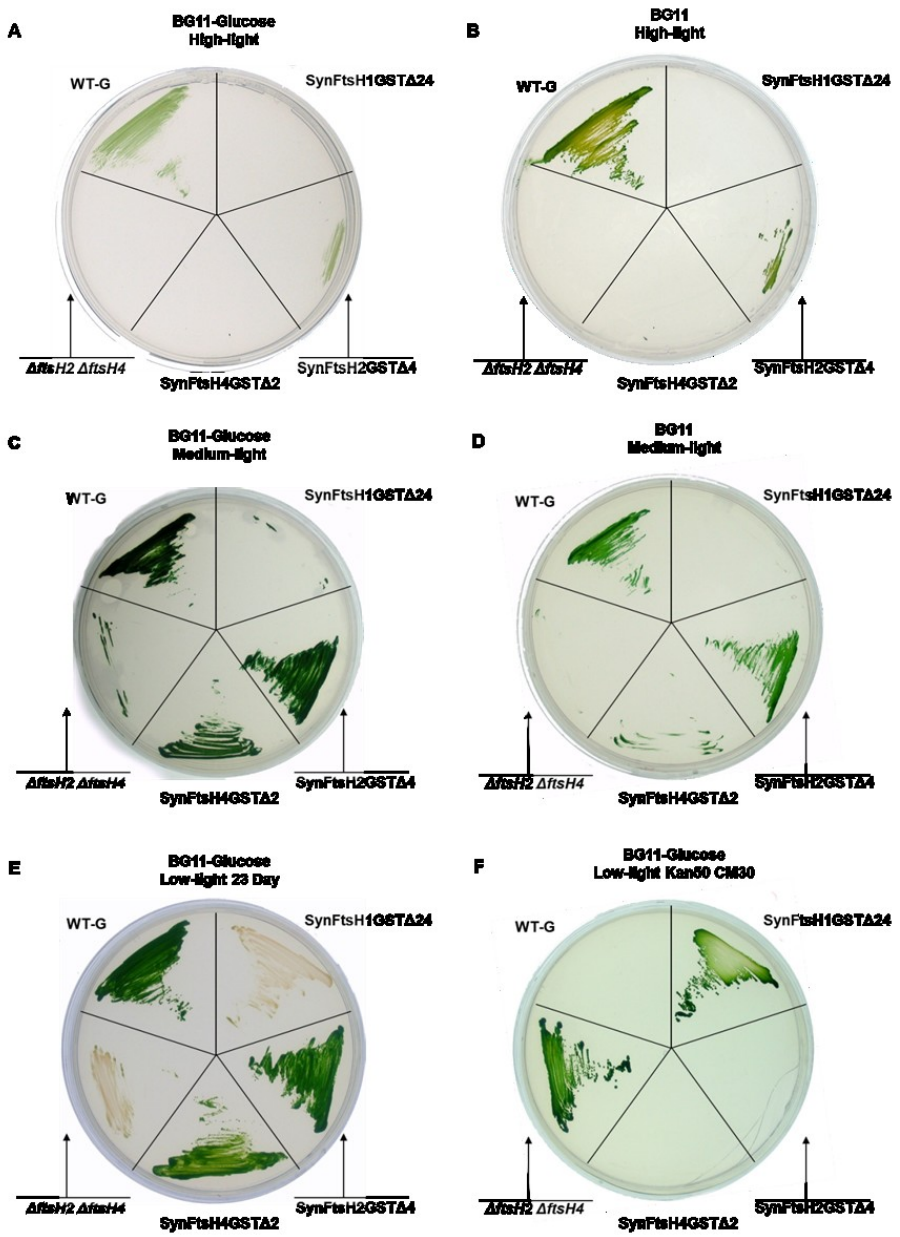

Figure 4.9: Growth experiment of SynFtsH1GSTΔ24, SynFtsH2GSTΔ4 and SynFtsH4GSTΔ2 mutants.

WT-G: the wild-type strain; *ΔftsH2ΔftsH4*: FtsH2/FtsH4 double deletion mutant. SynFtsH1GSTΔ24: *ftsH1::gst* with *ftsH2/4* null genotype; SynFtsH2GSTΔ4: *ftsH2::gst* with *ftsH4* null genotype and SynFtsH4GSTΔ2: *ftsH4::gst* with *ftsH2:Cam* null genotype. Cells were tested for growth under high (A and B) amd medium (C and D) light conditions on BG11 plates supplemented with 5 mM glucose (A and C) and plain BG11 (B and D). (E) Extended growth period over 23 days under low-light condition. (F) Conformation of segregation of the mutant from the recipient genome. Upon full segregation, the chloramphenicol resistance cassette used to disrupt FtsH2 in *ΔftsH2ΔftsH4* was replaced with *ftsH2::gst* fusion construct in SynFtsH2GST Δ4; respectively, the kanamycin resistance cassette was replaced with *ftsH4::gst* in SynFtsH4GSTΔ2. Hence fully segregated SynFtsH2GST Δ4 and SynFtsH4GSTΔ2 are sensitive to kanamycin/chloramphenicol double selection.

The growth experiment showed that restoration of FtsH2 with the FtsH2-GST fusion construct recovered the growth ability under high-light, although the growth seemed to be poorer than that of wild-type, possibly due to the reduced expression level of FtsH2 (immunoblotting data, not shown). The FtsH1 was successfully tagged with GST in the *ftsH2/ftsH4* double knockout genome (data not shown) and the resulting triple mutant SynFtsH1GSTΔ24 exhibited a similar phenotype under light stress to the *ΔftsH2ΔftsH4* recipient strain, providing no evidence over the potential influence of the GST tag to FtsH1. Strikingly, no colonies were obtained following transformation of *ΔftsH2ΔftsH4* cells with pFtsH3GSTery vector. Further attempt to knockout *ftsH2* in SynFtsH3GSTery strain was also unsuccessful (data not shown).

4.3.2 Isolation of FtsH4 complexes from SynFtsH4GSTΔ2

Among the four homologues, FtsH3 has been found to interact with both FtsH1 and FtsH2 (see section 3.1.4), hence it is interesting to explore the possibility of a potential interaction between FtsH3 and FtsH4 when FtsH2 is not available in the thylakoid membrane. Therefore, FtsH4-GST was purified from SynFtsH4GSTΔ2 cells and analysed by SDS-PAGE, followed by immunoblotting with anti-FtsH (global) and anti-FtsH4 antibodies (see section 2.7.4.1).

Proteins of the concentrated elution faction only separated into a single strong band at ~ 100 kDa on the gel (Figure 4.10 A). The identity of the band was further confirmed to be FtsH4 by antibodies (Figure 4.10 B). Faint protein bands were also visible on the Coomassie Blue-stained gel, and they seemed to be degradation products of FtsH4-GST. Therefore, our data do not support the presence of FtsH3/FtsH4-GST complex. Furthermore, the anti-FtsH (*E. coli*) antibody showed degradation products of FtsH in the pre-column binding sample, the majority of the immunodetectable FtsH seemed to be cleaved into ~ 40-kDa products. This observation might reflect the enhanced turnover of FtsH3 when FtsH2 is disrupted. The *E. coli* FtsH antibody only recognises FtsH4 relatively weakly; hence FtsH4-GST is only detected in the final

purified fraction.

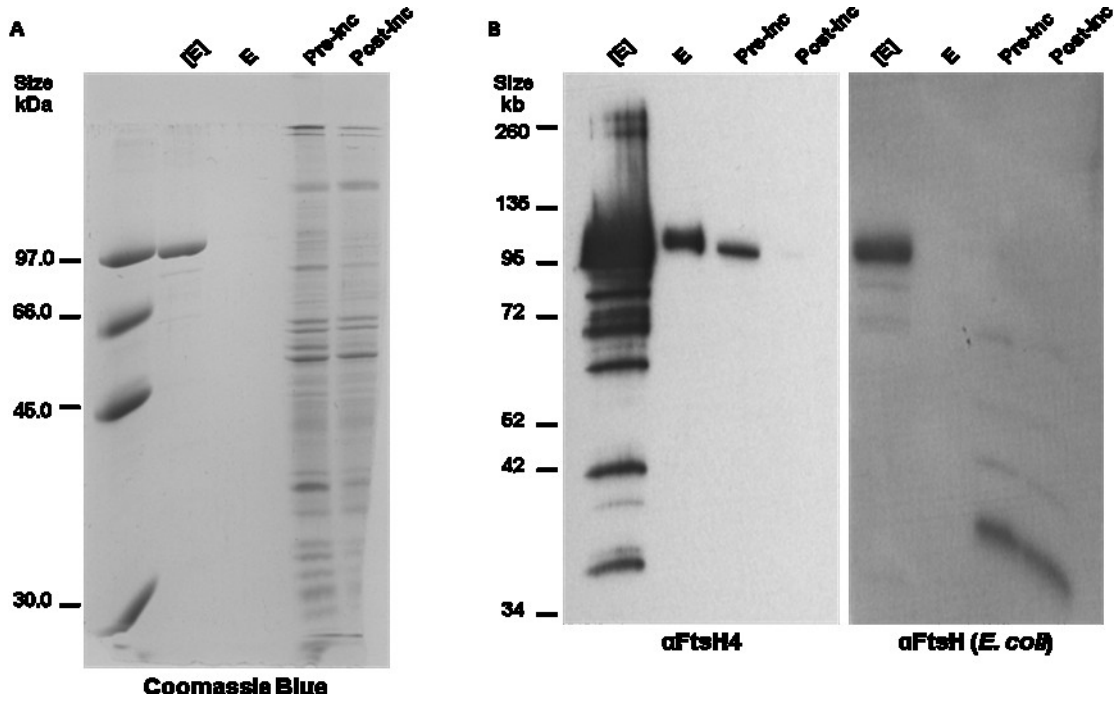

Figure 4.10: Isolation of FtsH4 complexes from SynFtsH4GSTΔ2.
(A) Detergent-solubilised thylakoid membranes from SynFtsH2GST before chromatography (Pre-inc), the extract after binding to the glutathione resin (Post-inc), and the fraction eluted by glutathione E and the final concentrated elution fraction [E] were separated by SDS-PAGE and stained in Coomassie blue. (B) Analysis of the column fractions by immunoblotting with antibodies specific for FtsH4 and *E. coli* FtsH.

4.4 *In vitro* characterisation of FtsH homologues

Despite the many studies on cyanobacterial FtsH, there has been no rigorous biochemical analysis of enzyme activity. To explore the NTP hydrolysis and proteolytic activity of the FtsH proteases, *in vitro* assays (see section 2.7.5 and 2.7.6) were used to examine the activity of FtsH proteases. Unfortunately, indigenous FtsH complexes purified from SynFtsH(x)GSTery mutants failed to show significant activity in the assays (data not shown). This was possibly due to the fact that the reaction condition was not optimal and the membrane anchored complexes was not stable in the detergent micelles.

The bottleneck to the optimisation of the *in vitro* assays was the insufficient supply of

the *Synechocystis* FtsH samples, due to its low abundance in the cells. To overcome this problem, an *E. coli* over-expression system was developed to produce large quantities of recombinant FtsH protease. Although the transmembrane domain of FtsH was speculated to be beneficial to the oligomerisation of FtsH complexes (Kihara et al. 1998), it was not essential to the function and complex formation of some bacterial FtsH (Suno et al. 2006). Therefore, to further reduce the challenges in protein purification and *in vitro* assays, only the soluble cytosolic region of each FtsH homologue, namely Δ(tm)FtsH, was expressed.

Although vectors expressing *Synechocystis* FtsH homologues were constructed (data not shown), the work described in this study was more focused on the expression of *T. elongatus* FtsH proteases. The focus on *T. elongatus* was mainly because of the potential to conduct structural studies. To initiate the study, only FtsH2, FtsH3 and FtsH4 from *T. elongatus* were expressed and tested in this project (Table 4.3). Proteins from *T. elongatus* are more robust and thermostable, which make them highly suitable for structural and biochemical studies. Due to time pressure, FtsH1 was not included in this work because it seemed least likely to be involved in PSII repair, based on its location within the cell (Figure 3.12 A).

4.4.1 Defining the FtsH homologues from Thermosynechococcus elongatus

As the model organism for physiological study of proteins involved in photosynthesis, the four FtsH homologues in *Synechocystis* sp. PCC6803, *ftsH1* (slr1390), *ftsH2* (slr0228), *ftsH3* (slr1604) and *ftsH4* (sll1463), have been defined in previous studies (Mann et al. 2000; Sokolenko et al. 2002). In contrast, although four FtsH homologues, tll1832, tll0734, tll0131 and tlr0528 have been annotated in the *Thermosynechococcus elongatus* genome, none of the four ORFs has been properly defined. To clarify the evolutionary relationship between the FtsH homologues found in *T. elongatus* with their orthologues in *Synechocystis* sp. PCC 6803, the phylogeny

of the candidate genes were mapped using Promlk (Figure 4.11). According to the phylogenetic tree, the genes encoding each FtsH homologue in the *T. elongatus* genome can be annotated as the following: *ftsH1* (tll1832), *ftsH2* (tll0734), *ftsH3* (tll0131) and *ftsH4* (tlr0528).

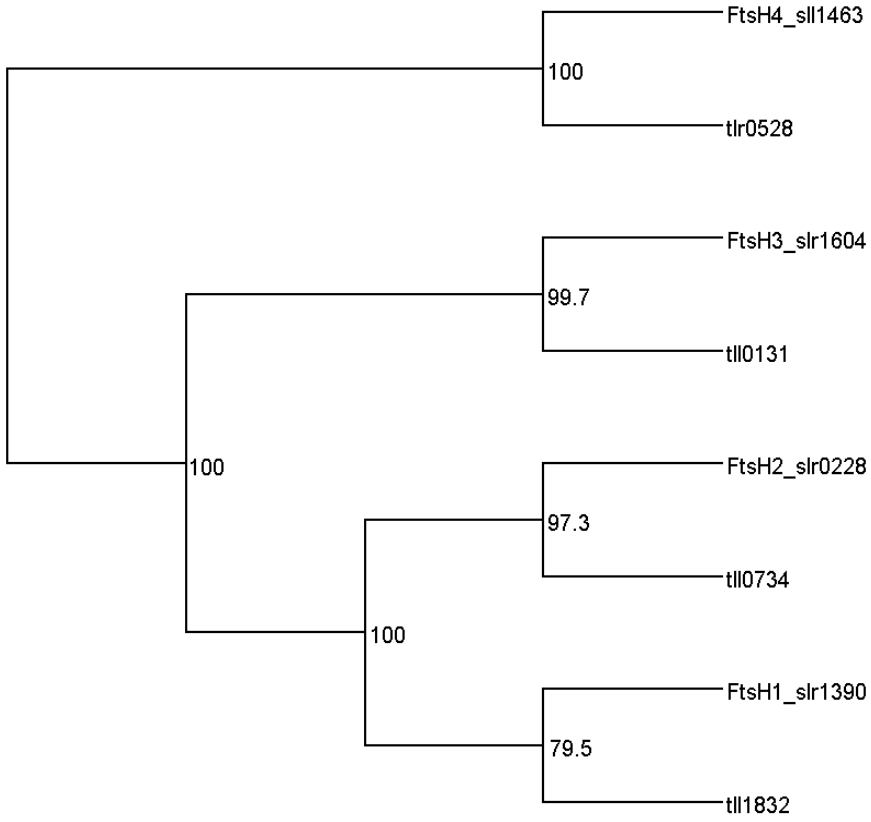

Figure 4.11: Phylogeny of FtsH orthologs between *Synechocystis* sp. PCC 6803 and *T. elongatus*.
Phylogenetic analysis by maxium likelihood of the FtsH genes in *Synechocystis* and *T. elongatus* genome was performed using Montpellier server, branch support was calculated using bootstrap mehod. FtsH homologues from *Synechocystis* were labelled FtsHx, where x is the specific number of the homologue. The FtsH homologues from *T. elongatus* were labelled according to the designations from the database (Cyanobase, see section 2.1).

4.4.2 Construction of the expression vectors and transformation of the *E. coli* expression strain

The cytosolic region of each FtsH homologue was identified after a protein sequence alignment with Δ(tm)FtsH from *T. thermophilus*. To enable future investigation into the potential formation of an FtsH2/FtsH3 complex, a StrepII tag was fused to the

C-terminus of the FtsH2 sequence (Figure 4.12 A). As a result, the formation of an FtsH2strep/FtsH3 complex could be potentially tested by co-purification of FtsH3 following Strep-Tactin affinity chromatography.

Table 4.4: Fragments of FtsH chosen for expression in *E. coli*

Name	Source gene	Expressed region (AA)	Vector
Δ(tm)FtsH2strep	*tll0734*	144-631	pRSET2strep
Δ(tm)FtsH3	*tll0131*	127-612	pRSET3
Δ(tm)FtsH4	*tlr0528*	155-619	pRSET4

The expression vector used in this work is a pRSETA (Life technologies limited, UK) derivative, in which the sequence encoding the T7 gene 10 leader (a transcript stabilising sequence), Xpress™ Epitope (peptide tag) and enterokinase cleavage site was replaced with that of the thrombin cleavage site (Figure 4.12B).

The target *ftsH* genes were PCR amplified using primer set TheFtsH(x)-F and TheFtsH(x)-R, where TheFtsHx represents the particular FtsH homologue from *T. elongatus*. The resulting PCR fragments were then gel purified and digested with BamHI and XhoI. The digested PCR fragments were then purified and ligated into the pRSET vector via BamHI and XhoI sites (Figure 4.12 B). The resulting FtsH expression vectors namely pRSET2strep, pRSET3 and pRSET4 were then validated by sequencing with a T7 primer.

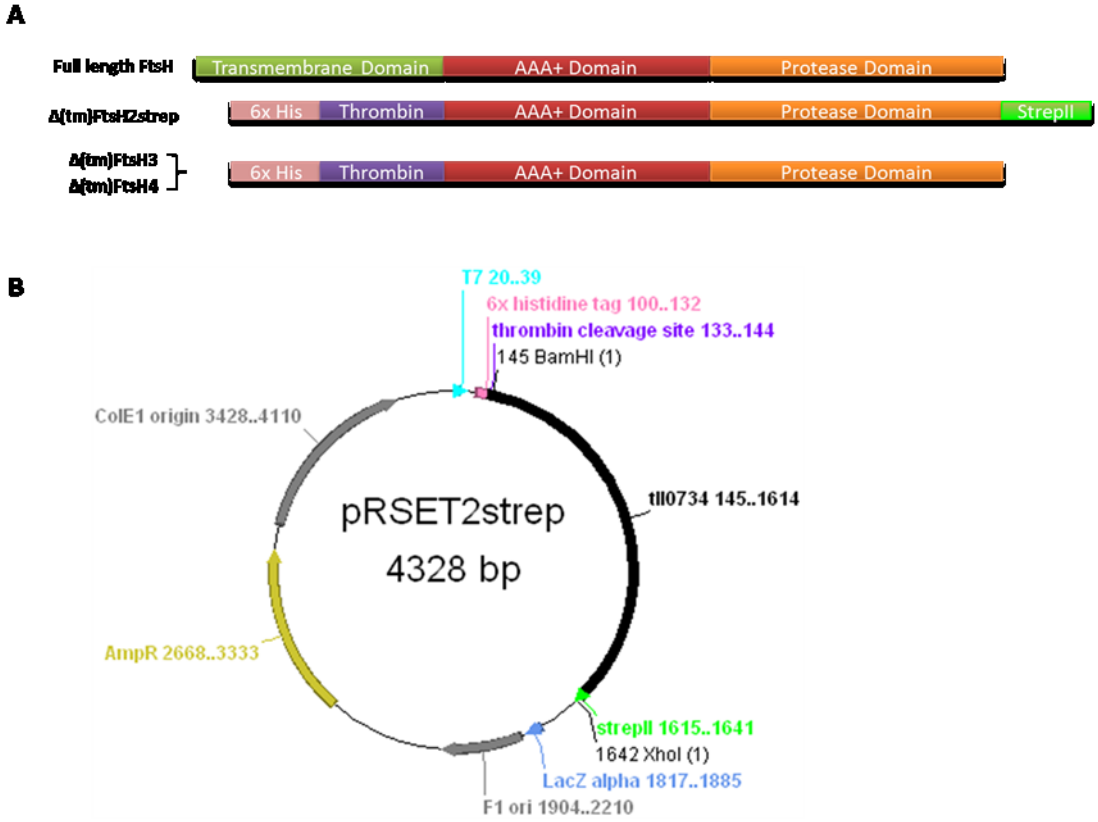

Figure 4.12: Construction of the cytosolic-FtsH expression vectors.
(A) A schematic representation of the cytosolic FtsH proteases expressed from the vectors. (B) A plasmid map of the expression vector producing Δ(tm)FtsH2strep. The vectors for FtsH3 and FtsH4 do not have the *strepII* tag at the 3' end of the *ftsH* sequence.

4.4.3 Expression and purification FtsH2, 3 and 4 fragments from *E. coli*

E. coli expression strain KRX (Promega, UK) was transformed with the FtsH expression vectors. The recombinant FtsH proteins were induced with L-rhamnose according to the induction protocol (see section 2.7.2.2). After overnight incubation at 18 ^{o}C, cells were harvested and the recombinant proteins were purified via nickel affinity chromatography (see section 2.7.2.2). Samples from each fraction during the purification procedure were collected and analysed on 10 % SDS-PAGE gels (Figure 4.13).

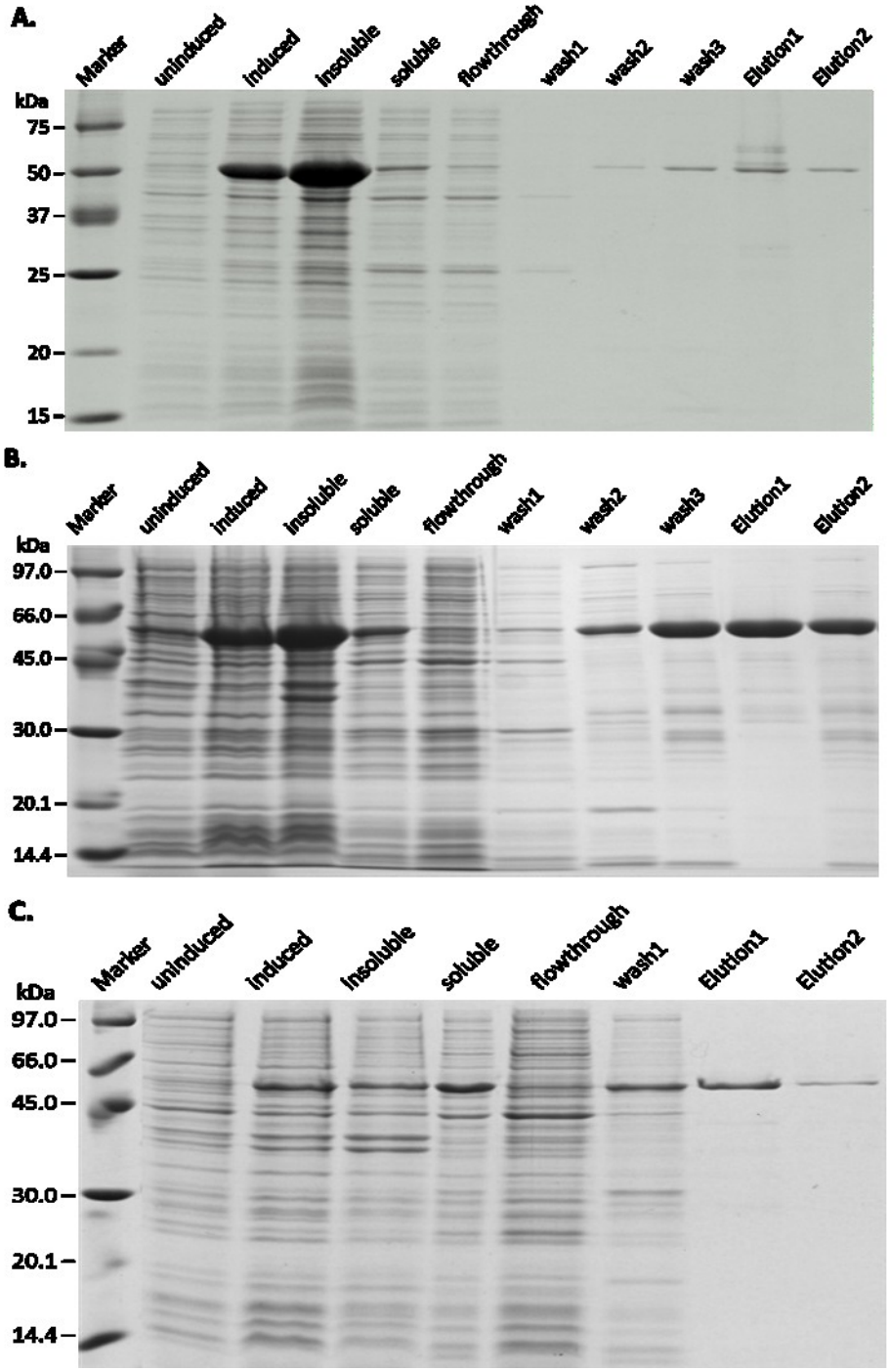

Figure 4.13: Over-expression and purification of Δ(tm)FtsH4, Δ(tm)FtsH2strep and Δ(tm)FtsH3.

Δ(tm)FtsH4 (A), Δ(tm)FtsH2strep (B) and Δ(tm)FtsH3 (C) samples from each step of the purification procedure were collected and analysed on 10 % SDS-PAGE. The "uninduced" and "induced" lanes were loaded with whole cell samples collected before/after induction and cell disruption, respectively, and "soluble" "insoluble" were samples from soluble/insoluble fractions after cell disruption.

The fractionation profile showed that although all three FtsH constructs were

successfully expressed, a large amount of the recombinant protein was found in the insoluble fraction, which might due to the formation of inclusion bodies under sub-optimal induction condition. Nevertheless, the elution profile of Δ(tm)FtsH2strep, Δ(tm)FtsH3 and Δ(tm)FtsH4 showed that the three recombinant FtsH proteases were successfully induced and purified (Figure 4.13). The purified recombinant proteins in the elution lane were relatively pure and matched the theoretical masses of 52.27 kDa for Δ(tm)FtsH4, 55.93 kDa for Δ(tm)FtsH2strep and 55 kDa for Δ(tm)FtsH3. The eluates were subsequently concentrated and tested for NTPase and protease activities.

4.4.4 NTPase activity of Δ(tm)FtsH4, Δ(tm)FtsH2strep and Δ(tm)FtsH3

FtsH proteases have been reported to utilise diverse nucleoside-5'-triphosphate for proteolytic activities (Bruckner et al. 2003). To further investigate the nucleotide specificity of the AAA+ domain in our FtsH constructs, four nucleotides ATP, GTP, CTP and UTP were tested. Data from the NTP hydrolysis assay showed that the activity of Δ(tm)FtsH4 was in general much higher than the other two proteases and capable of hydrolysing both ATP and CTP. The hydrolysis rate of CTP by Δ(tm)FtsH2 was also comparatively high, in fact CTP seemed to be the most favourable nucleotide among the four (Figure 4.14 A). A negative control using His-tagged Psb28, a known PSII assembly factor, purified from the same expression strain according to the same procedure gave an ATPase activity of approximately 20% of the ATP only control (data not shown).

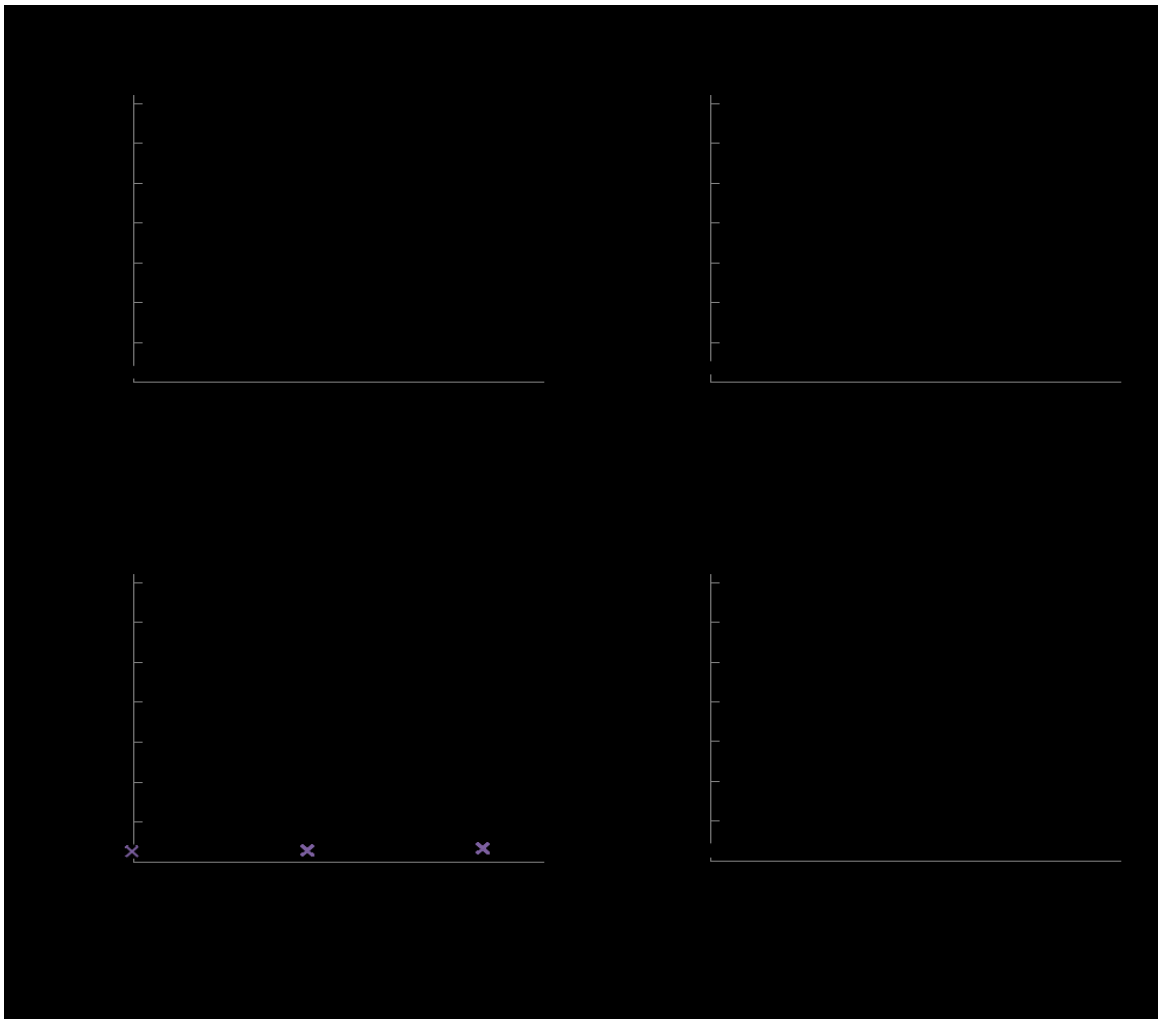

Figure 4.14: Preliminary test on the nucleotide specificity of Δ(tm)FtsH2, 3 and 4. The specificity of the AAA+ domain of each FtsH homologue to ATP, GTP, CTP and UTP was tested by measuring the phosphate libration rate from hydrolysis. For each reaction, measurements were taken at time 0, 30 and 60 min. an NTP only sample, without addition of FtsH protease was also analysed along with other samples as the negative control.

4.4.5 Proteolytic activity of Δ(tm)FtsH2, Δ(tm)FtsH3 and Δ(tm)FtsH4

Preliminary examination of the proteolytic activity of the over-expressed FtsH recombinant proteins was carried out using an EnzChek Protease Assay Kit (Invitrogen). In the hope of detecting activities from FtsH2/FtsH3 hetero-complexes, the two proteins were also mixed at 1:1 ratio and tested in the assay (Figure 4.15). Unsurprisingly, Δ(tm)FtsH4 was the only sample that showed a clear activity in the test. The fluorescence readings from Δ(tm)FtsH2 and Δ(tm)FtsH3, and the combined

sample were slightly higher than that of His-tagged Psb28, hence minor activity from these samples still cannot be excluded. Moreover, previous studies showed the activity of FtsH from *E. coli* is highly dependent on oligomerisation (Kihara et al 1998). In this experiment, the combined Δ(tm)FtsH2 and Δ(tm)FtsH3 sample did not show improved activity, possibly because inducing oligomerisation of FtsH might not be straightforward.

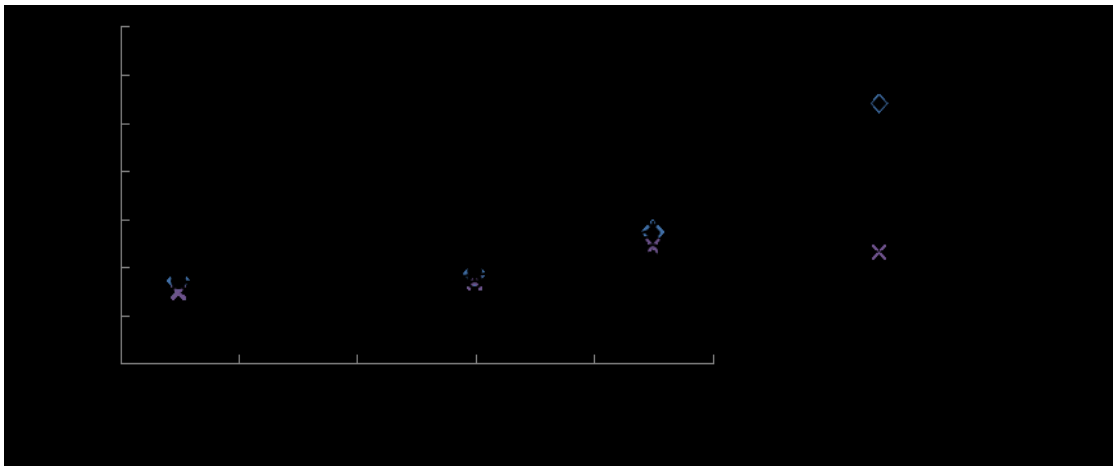

Figure 4.15: A fluorescence-based quantitative protease assay trial.
The proteolytic activity of each FtsH homologue was assessed according to the degradation rate of the casein substrate. In addition to Δ(tm)FtsH2, Δ(tm)FtsH3 and Δ(tm)FtsH4, recombinant Psb28 expressed and purified using the same expression system was also included in this experiment as negative control of contamination of *E. coli* proteases. To explore the potential oligomerisation of active FtsH2/FtsH3 complex in vitro, a sample containing equal amount of Δ(tm)FtsH2, Δ(tm)FtsH3 was also prepared and analysed.

4.5 Discussion

4.5.1 The dispensability of subunits within FtsH hetero-complex

Previous work has shown that the FtsH hetero-complexes residing in the thylakoid membrane of *A. thaliana* are still capable of participating in the PSII repair process when the protease activity, but not the AAA+ domain, of the Type B subunit is inactivated (Zhang et al. 2010). To test whether the FtsH2/FtsH3 hetero-complex in cyanobacteria also exhibited a similar characteristic, similar mutations were generated in the Type B-like homologue FtsH2, and the resulting mutants were selected for

growth under high-light conditions. Among the 7 designed mutations, only 4 mutants were able to grow after transformation, including the three mutations at the zinc ion-binding residues and the cysteine that proposed to play a role in thioredoxin control. None of the three mutations designed to disrupt ATP hydrolysis were able to restore photoautotrophic growth at high light. These mutants have subsequently been isolated by introducing a GST tagging cassette and selecting with antibiotics (data not shown). Therefore, the current data suggest that the proteolytic activity of FtsH2 in the FtsH2/FtsH3 complex is not essential for D1 degradation function. Presumably the proteolytic activity still present in the FtsH3 subunit confers sufficient activity to the FtsH2/FtsH3 complex to allow growth at high light. In contrast, the AAA+ domain of FtsH2 appears to play a much more important role for the function of the complex.

It is still unclear whether inactivating the protease domain of FtsH3 but not FtsH2 would impair D1 degradation. It is conceivable that FtsH3 plays a more important proteolytic role in the degradation of substrates in the hetero-complex, at least the degradation of D1. It cannot be ruled out that the function of FtsH2, and perhaps the other type B-like homologue, FtsH1, might mainly be to act as a molecular scaffold to stabilise FtsH3 and to assist the ATP-dependent proteolytic activities. Similar complexes that consist of inactivated FtsH subunits are naturally present in the chloroplast envelope of *A. thaliana*, where FtsH12 forms complexes with FtsHi, an FtsH sub-family that lacks the zinc ion binding motif. The partially inactive FtsH12/FtsHi complexes are essential for embryogenesis in plants (Wagner et al. 2012). Conceivably, formation of some FtsH hetero-complexes might have evolved for better substrate specificity, at the expense of maximal proteolytic activity.

4.5.2 Effect of C-terminal GST tag on FtsH function

C-terminal GST/ GFP tags have been fused to each of the four FtsH homologues in the WT-G *Synechocystis* strain and the growth of the resulting mutants was then

assessed under a range of illumination intensities. Firstly, we showed that the addition of the C-terminal GST or GFP tag did not cause lethality, hence the tag did not abolish the function of FtsH1 or FtsH3 completely. On the other hand, mutant SynFtsH3GSTery, which expresses the FtsH3-GST fusion protein, exhibited increased sensitivity to light and was unable to grow under strong illumination (Figure 3.3). The degree of the sensitivity was similar to that of the FtsH2 null mutant (Figure 4.5). Since the FtsH2/FtsH3 hetero-complexes are responsible for maintenance of PSII activity under light stress (Boehm et al. 2012), it is conceivable that the PSII repair function of the FtsH2/3 complexes was impaired by addition of the GST tag at the C-terminus of FtsH3. Further attempts to construct an FtsH2 null mutant that expressed GST-tagged FtsH3 derivative failed to yield colonies after transformation. Three approaches were tried: either introducing *ftsH3::gst* construct into *ΔftsH2* and *ΔftsH2ΔftsH4*, then disrupting *ftsH2* in SynFtsH3GSTery; all proved unsuccessful (see section 4.3.1). Therefore, it seems the genotype is lethal to cell viability. Disruption of *ftsH2* destabilises and prohibits the accumulation of FtsH3 in the thylakoid membranes (Boehm et al. 2012), hence the lethality of the *ΔftsH2/ftsH3::gst* genotype should be attributed to the functionally impaired FtsH1/FtsH3 complexes, or effects on the expression of FtsH3.

In contrast, the GST tag fused to the C-termini of FtsH1 and FtsH2 seemed not to affect drastically the growth phenotype of the resulting mutants. The phenotype of SynFtsH1GSTΔ24, presumably only expressing FtsH1GST/FtsH3 complexes, was comparable to that of the recipient *ΔftsH2ΔftsH4* strain. Together, the presence of a GST or GFP tag at the C-terminal of the Type B-like FtsH subunits seemed to not affect the major function of the complexes. Considering the diverse cellular activities that FtsH proteases play, the possibility that some minor functions of the FtsH hetero-complexes might be interrupted by the C-terminal tag on Type B-like subunits cannot be rule out at this stage.

FtsH4 is the only FtsH subunit in *Synechocystis* that did not show any detectable interaction with other homologues, and also the only one that did not show distinguishable phenotype upon disruption. Hence it remains unclear whether the GST and GFP tagged FtsH4 fusion proteins are functional *in vivo* or not. The immunoblotting data have consistently showed drastic reduction of the FtsH4 level in the mutant strains compared to wild-type (Figure 3.9 and 4.8), which might be a sign of functional disruption of the complexes causing enhanced instability in the membrane. Alternatively, the effect might simply reflect effects on transcript abundance due to the destabilising effect of the antibiotic-resistance cassette on the 3' region of the transcript.

4.5.3 Types of FtsH complex in the thylakoid membranes

FtsH proteases play an important house-keeping role in maintaining the quality of membrane proteins. Proteins embedded in the thylakoid membranes are maintained by three FtsH homologues, FtsH2, FtsH3 and FtsH4 (see section 3.2.5 and 3.2.6). Preliminary studies showed FtsH2 and FtsH3 form hetero-complexes that play a dominant role in D1 degradation. However, mutants lacking FtsH2 were also viable for photoautotrophic growth under low-light conditions. Taken into account that D1 is a short-lived membrane protein which undergoes irreversible damage even under low-light conditions, it is likely that additional proteolytic systems capable of D1 removal exist. The FtsH2/FtsH4 double deletion mutant generated in this work displayed increased sensitivity to light stress compare to the FtsH2 single deletion mutant (see section 4.1.5), which raised speculation that FtsH4 homo-complexes might also contribute to PSII repair, albeit, only play a minor role or an indirect one.

In human mitochondria, FtsH can form both homo and hetero-complexes (Koppen et al. 2007), which raises the possibility that potentially FtsH4 could form a hetero-complex with FtsH3 in the absence of FtsH2. To test this theory, the

composition of FtsH4 complexes from SynFtsH4GSTΔ2 was examined, as the potential interaction between FtsH3 and FtsH4 should be enhanced when the major competitor FtsH2 is missing in this strain. The results showed no evidence for co-purification of other types of FtsH with FtsH4. Therefore, the current data still favour functional overlap between FtsH4 and FtsH2/FtsH3 complexes or a indirect role for FtsH4 to aid D1 degradation. Furthermore, the FtsH2/FtsH4 double deletion mutant is still capable of photoautotrophic growth. The underlying maintenance mechanisms are still to be elucidated. In addition a notable phenotype observed with the double mutant was enhanced senescence under low light (Figure 4.9).

4.5.3 Nucleotides hydrolysis and proteolytic activity of Δ(tm)FtsH4, Δ(tm)FtsH2 and Δ(tm)FtsH3

The cytosolic domains of FtsH2, FtsH3 and FtsH4 were cloned and expressed in *E. coli*, with the aim to provide activity data for cyanobacterial FtsH proteases. The activity of FtsH includes hydrolysis of nucleotides in the AAA+ domain and processing of protein substrates through the Zn^{2+}-binding motif. According to one current model, which were established on the basis of the crystal structure of FtsH from *T. thermophilus* (Suno et al. 2006) and supported by *in vivo* assays (Zhang et al. 2010), the hydrolysis of a nucleotide in the AAA+ domain requires synergetic movement between neighbouring protomers in the hexameric complex. However, an individual subunit can also hydrolyse NTP in an inefficient manner. Our results showed NTPase activities from all three FtsH proteases, of which, FtsH4 displayed a much higher activity than the other two. The striking difference might reflect the potential presence of some complex formation in the FtsH4 sample. However, it is noteworthy that the rate of nucleotide hydrolysis was extremely low, even that of FtsH4 comparing to other bacterial FtsH presented in the literature (Suno et al. 2006). Studies on *E. coli* FtsH have shown that the AAA+ domain of FtsH is rather unspecific to substrates, in particular, CTP was also a favourable nucleotide in *in vitro* assays (Bruckner et al. 2003). Our data is largely in line with this conclusion, as

the hydrolysis rate of CTP was even higher than that of ATP. Only FtsH4 was able to degrade the casein substrates in the protease assay. The other FtsH proteases, including a sample with FtsH2 and FtsH3 combined did not yield any activity, possibly because heterocomplex formation was unsuccessful. The trans-membrane domain of *E. coli* FtsH is important for complex formation, however, cytosolic domains of FtsH from *T. thermophilus* can form hetero-complexes without the trans-membrane region. Therefore, the necessity of N-terminal truncation for oligomerisation is dependent on the characteristic of each complex and so we cannot exclude the possibility that only full-length FtsH2 and FtsH3 from cyanobacteria can form a complex. The ability to isolate soluble fragments of FtsH from *T. elongatus* demonstrated here paves the way for more detailed structural studies on cyanobacterial FtsH.

Chapter 5: Probing physiological function and regulatory mechanisms of FtsH in *Synechocystis*

5.1 Identification of potential substrates and auxiliary proteins

Very little is known about the substrate specificity of the FtsH complexes in *Synechocystis* 6803 and the proteins with which they interact. FtsH in *E. coli* has been found to form supercomplexes with members of the Band 7 superfamily and to bind to YccA (reviewed by Ito and Akiyama 2005). Therefore, we explored the potential substrates and auxiliary proteins of FtsH in *Synechocystis* by analysing the identity of proteins that co-purified with each FtsH-GST derivative (see section 5.1.1). A range of proteins was identified in each FtsH sample, among which, both prohibitin and a cyanobacterial homologue of YccA were detected in the FtsH2 and FtsH3 samples. Interestingly, a homologue of the *Arabidopsis* ethylene-dependent gravitropism-deficient and yellow-green-like 2 protein (EGY2), encoded by *sll0862*, was also co-purified with FtsH2 and FtsH3. EGY2 is one of the few metalloproteases involved in intramembrane proteolysis in *A. thaliana* and contributes to fatty acid biosynthesis (Chen et al. 2012). Preliminary work to characterise the function of the *Synechocystis* EGY2 and YccA homologues was also performed in this study (see section 5.1.2). In addition, I have investigated whether Psb29 might also play a role in controlling the expression level of FtsH proteases in *Synechocystis* as previous work in *Arabidopsis* has made such a link.

5.1.1 Potential substrates/auxiliary proteins co-purified with FtsH proteases

To elucidate the potential binding partners and substrates of FtsH complexes, proteins co-purified with each FtsH-GST construct were analysed via peptide mass fingerprinting (PMF); this work was carried out in collaboration with Prof. Michael Hippler, University of Münster.

To prepare samples for mass spectrometry sequencing, GST-tagged FtsH complexes from SynFtsH1GSTery, SynFtsH3GSTery, SynFtsH4GSTery (see section 3.1) and SynFtsH2GST (see section 3.3) were isolated via GST affinity chromatography, then separated on SDS-PAGE gel, followed by silver staining. Major protein bands from each protein sample were cut out and sent for identification. A number of proteins were identified in the PMF data (see Appendix for full list); noteworthy, the abundance of a few co-purifying proteins was relatively high in the FtsH2 sample suggesting a rather specific interaction with FtsH2GST/FtsH3 complexes (Figure 5.1).

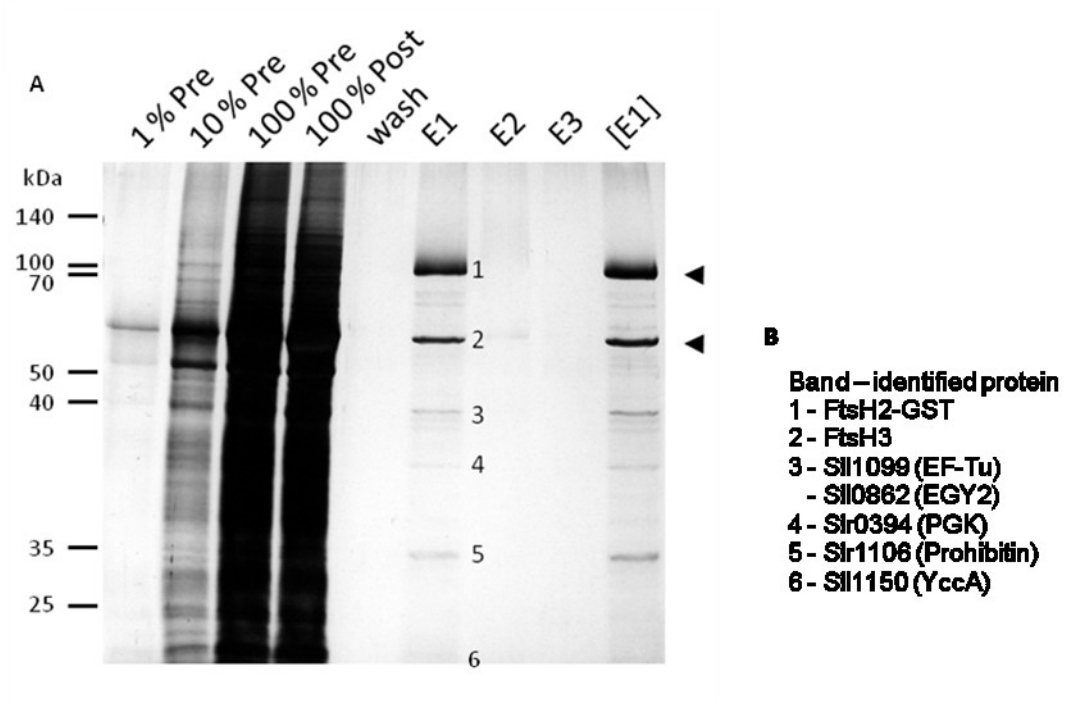

Figure 5.1: Proteins co-purified with FtsH2GST/FtsH3 complex.
(A) Detergent-solubilised thylakoid membranes from SynFtsH2GST before chromatography (Pre), the extract after binding to the glutathione resin (Post), the wash fraction just before elution (Wash), and the fractions eluted by glutathione (E1-E3) and concentrated E1 fraction [E1] were separated by SDS-PAGE. The positions of the FtsH2-GST and FtsH3 proteins are indicated by arrowheads. (B) List of proteins the major proteins present in the elution sample.

Six major protein bands were analysed from the FtsH2-GST sample. As expected the FtsH3 isomer was identified in the FtsH2-GST complex. In addition, elongation factor

(EF-Tu) and phosphoglycerate kinase (PGK), both soluble components, were identified. These results indicated that the FtsH2-GST/FtsH3 complex might play a role in regulation of translation and glycolysis. Prohibitin or Band 7 homologues have been shown to form complexes with bacterial and mitochondrial FtsH (Steglich et al. 1999; Van Aken et al. 2007), possibly to help stabilise the complex (Janska et al. 2013). A prohibitin homologue (Slr1106) was also found in the sample, hence a similar regulatory interaction between FtsH and prohibitin might also be present in the cyanobacterial system. A homologue of YccA, which is known to be a substrate and also an auxiliary binding partner of FtsH in *E. coli* (Kihara et al. 1998), was also identified in the eluate. Recent work has suggested that YccA might down-regulate the activity of FtsH in *E. coli* (van Stelten et al. 2009). Surprisingly, the homologue of *Arabidopsis* EGY2, encoded by *sll0862*, was also co-purified with FtsH2, and its interaction with FtsH3-GST was also confirmed (see Appendix). EGY2 belongs to the Site-2 protease (S2P) family and is one of the few intra-membrane proteases localised in the chloroplast thylakoid membrane. It also features a Zn^{2+}-binding motif in the peptidase domain and is capable of degrading casein substrate in an ATP hydrolysis-independent manner (Chen et al. 2012). An interesting point is that the proteolytic site of Sll0862 is likely to be within the membrane, whereas its FtsH counterpart is in the cytoplasm. This raises the interesting possibility that Sll0862 might co-operate with FtsH complexes to help remove recalcitrant substrates from the membrane.

5.1.2 Probing the function of Sll0862 and Sll1150

5.1.2.1 Construction of *sll0862* null mutants

The entire ORF of *sll0862* was removed from the genome and replaced by an antibiotic-resistance cassette. To achieve the goal, a deletion vector was constructed in two steps. First, two flanking sequences, 445 bp upstream and 555 bp downstream of the *sll0862* ORF were joined together via overlap extension PCR using primer set

Sll0862 (containing four primers 1F, 2R, 3F and 4R). The resulting DNA fragment, which lacks the entire *sll0862* ORF was then ligated with the recipient vector backbone pGEM-T easy to produce the parental vector pGEMSll0862 (Figure 5.2 A). In the second step, a selectable marker conferring resistance to chloramphenicol was inserted into pGEMSll0862 at an EcoRV site, and depending on the insert orientation, the resulting vectors were named pSll0862camA or B (Figure 5.2 A and B).

The transformation vectors were then used to transform the WT-G strain of *Synechocystis* and the resulting mutants were selected on BG11 plates supplemented with glucose, chloramphenicol and DCMU. After restreaking three times from a single colony, the mutants were subjected to DNA analysis to check the segregation status, using the primer set Sll0862-1F and 4R (Table 2.5). The size of the chloramphenicol-resistance cassette is similar to that of *sll0862*, hence DNA restriction digestion was performed using the PCR fragments (Figure 5.2 C). Cells from two individual colonies of each type of transformant were analysed, and all four mutants were confirmed to be correct (Figure 5.2 D).

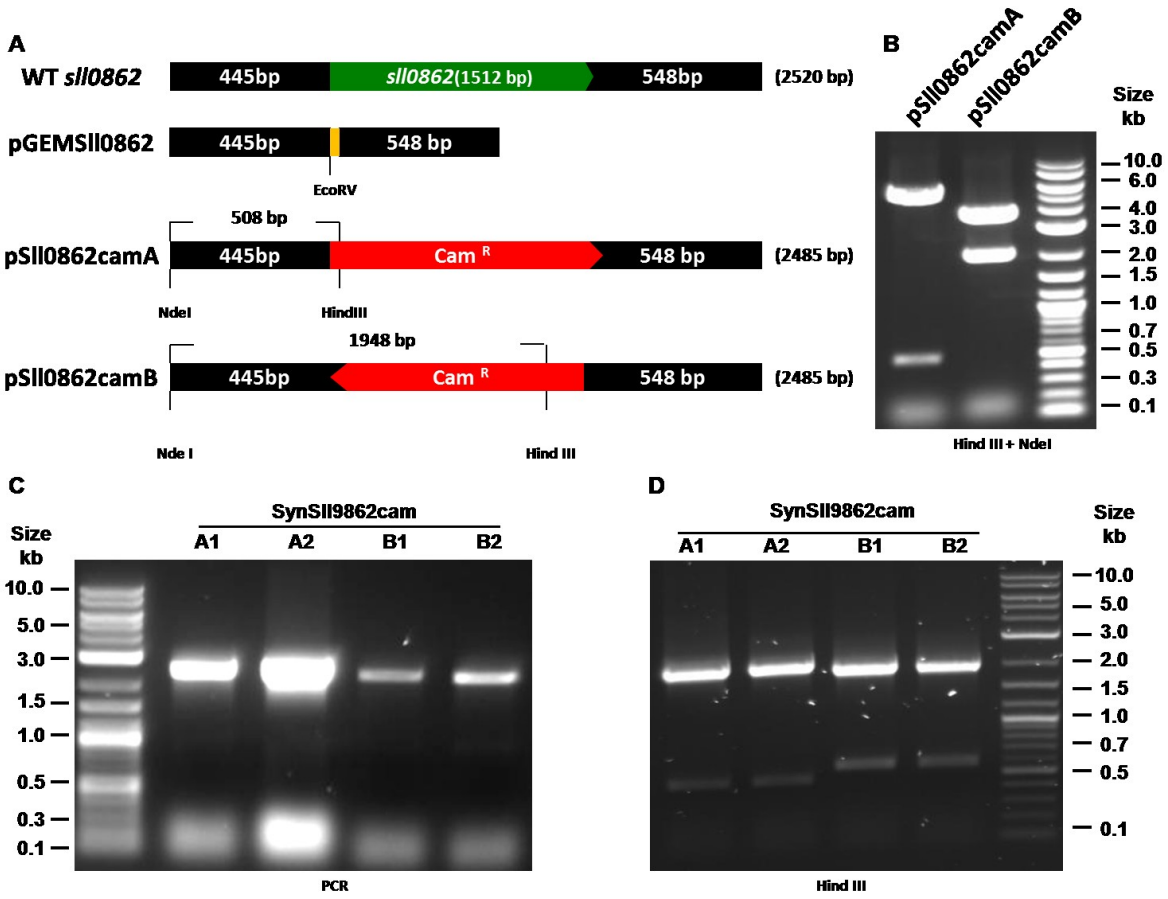

Figure 5.2: Construction of Sll0862 defective mutants.
(A) A schematic representation of the disruption design. (B) The digestion pattern of the two transformation vectors. (C) Genotyping via PCR analysis, the primers used were Sll0862-1F and 4R. (D) Restriction digestion of the PCR fragments. A1 and A2 are two colonies picked from a plate of cells transformed with pSll0862camA, whereas B1 and B2 were transformed by pSll0862camB.

5.1.2.2 Construction of *sll1150* null mutant

A similar procedure was applied to knock-out *sll1150*. A 445-bp upstream DNA fragment and a 555-bp downstream fragment were joined together via overlap extension PCR using primer set Sll1150 (containing four primers 1F, 2R, 3F and 4R). The resulting DNA fragments, which also had the entire sll1150 ORF replaced by an EcoRV site, was then cloned into pGEM-T easy to form parental vector pGEMSll1150. Then the chloramphenicol-resistance cassette was inserted into pGEMSll1150 (Figure 5.3 A). Only one transformation vector, named pSll1150cam (Figure 5.3 A), was obtained at this stage, in which the transcription direction of the

chloramphenicol-resistance gene is in the same direction as *sll1150* ORF.

Synechocystis WT-G was transformed with pSll1150cam and selected under dim light on BG11 plates supplemented with glucose, chloramphenicol and DCMU. After restreaking three times, the genotype of the resulting mutants were checked for segregation and the resulting mutant was named SynSll1150cam (Figure 5.3 B).

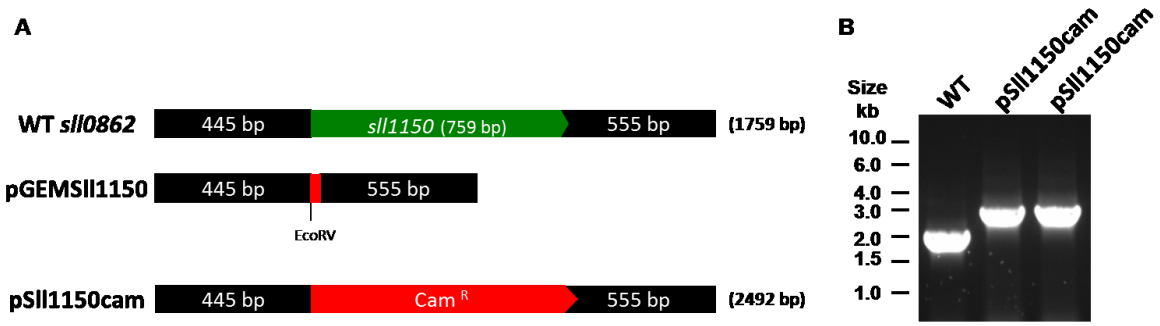

Figure 5.3: Construction of Sll1150 defective mutants.
(A) A schematic representation of the disruption design. (B) Genotyping via PCR analysis, the primers used were Sll1150-1F and 4R. Two individual colonies were screened in genotyping.

5.1.2.3 Phenotype analysis of *sll0862* and *sll1150* null mutants

To test whether Sll0862 and Sll1150 might be critical for PSII repair and photoprotection, growth assays were performed under high, medium and low light conditions, to compare the growth of the three mutants lacking Sll0862 and Sll1150 with the FtsH2 defective mutant, *ΔftsH2*.

All three mutants were able to grow photoautotrophically under the high-light condition and did not show a distinguishable phenotype compare to the wild-type control in terms of growth rate and pigmentation. In contrast, the FtsH2 defective mutant *ΔftsH2* was consistently unable to cope with the high-light environment, and even photoautotrophic growth under medium light was affected (Figure 5.4 and see section 4.1.5). Moreover, the growth rate of *ΔftsH2* also seemed to be slower.

In summary, the growth assays showed that growth of mutants lacking Sll0862 and Sll1150 at high irradiances was not drastically affected, hence the function of FtsH2 was not drastically impaired by the respective mutations. Nevertheless, these data are insufficiently sophisticated to exclude a possible role of Sll0862 and Sll1150 in FtsH function. The physiological functions of Sll0862 and Sll1150 also remain unclear as the mutants exhibited wild-type-like phenotype under the tested conditions.

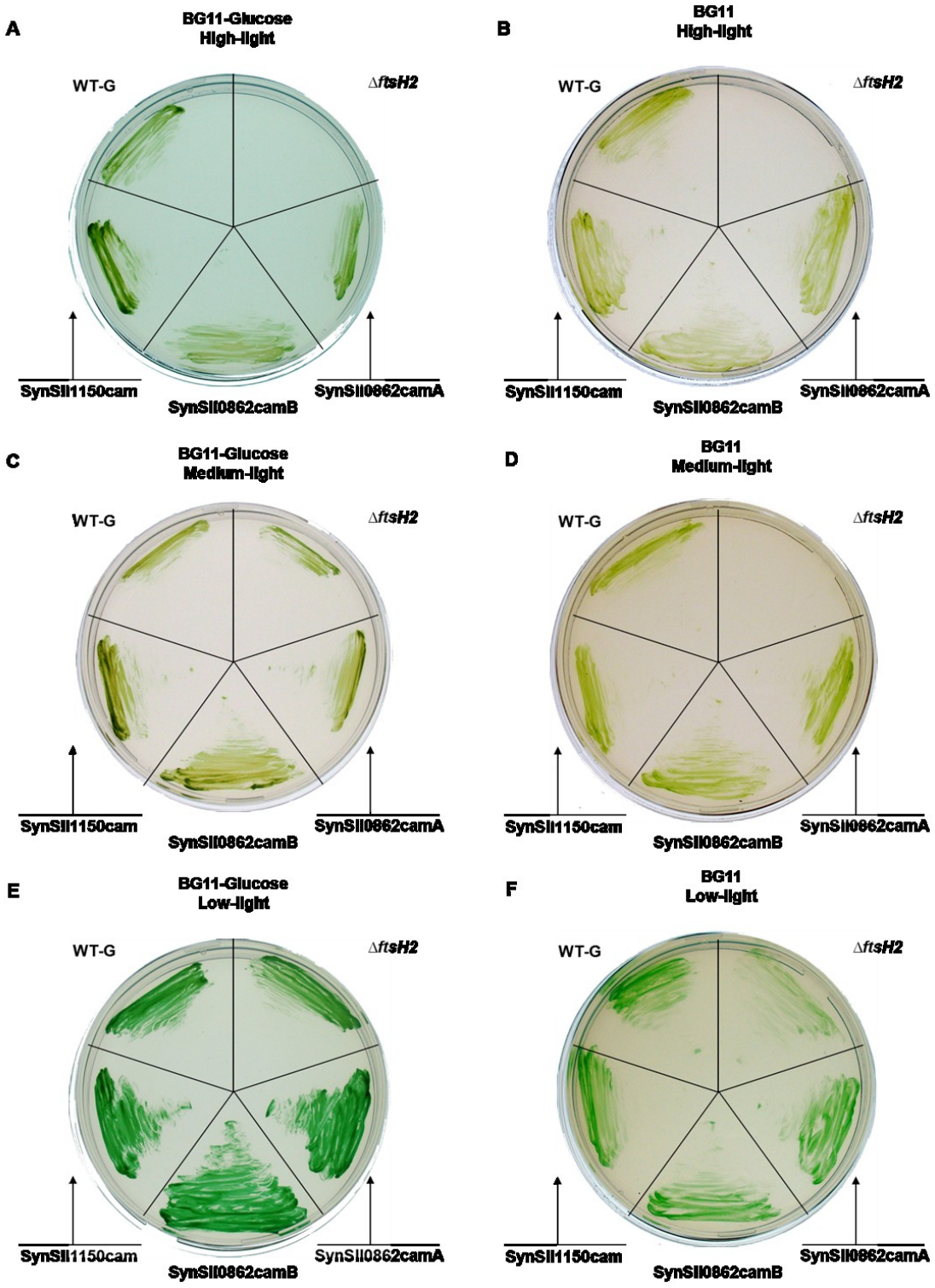

Figure 5.4: Growth experiment of Sll0862 and Sll1150 defective mutants.
Each plate carries 5 strains: WT-G: wild-type strain, *ΔftsH2*: FtsH2 null mutant and the disruption mutants SynSll0862camA/B and SynSll1150cam strains. Cells were tested for growth under high (A and B), medium (C and D) and low (E and F) light conditions on BG11 plates supplemented with 5 mM glucose (A, C and E) and plain BG11 plates (B, D and F).

5.2 Role of Psb29 in accumulation of the FtsH2/3 complex

The formation of PSII requires a range of accessory proteins to assist the assembly of intermediate complexes and cofactors (see section 1.4.1). Psb29 has been identified as a component that interacts with PSII complexes in *Synechocystis* (Kashino et al. 2002) , and further analysis in higher plants has suggested that Psb29 is involved in the formation of PSII-supercomplexes in chloroplasts and the PSII repair cycle (Shi et al. 2012). Studies on the Psb29 null mutant of *A. thaliana* (also known as *thf1*) have demonstrated that the thylakoid FtsH level is decreased in the absence of Psb29 (Zhang et al. 2009), however, the precise mechanism remains unclear. The initial work on cyanobacterial Psb29 showed that disruption of *psb29* leads to increased light sensitivity (Keren et al. 2005), which raises the obvious possibility that the expression level of FtsH proteases in cyanobacteria might also be regulated via Psb29. Therefore, Psb29 null mutants were constructed and characterised to test this hypothesis.

5.2.1 Construction of the Psb29 defective mutants

The *psb29* (*sll1414*) disruption vectors were achieved in two steps: first, overlap-extension PCR was used to construct a parental vector, pGEMPsb29, that contains 445 bp of upstream and 555 bp of downstream flanking sequences but which lacks the entire Psb29 ORF (Table 2.5). In the second step, a selectable marker conferring resistance to chloramphenicol was inserted into pGEMPsb29 at a unique EcoRV restriction site, and depending on the insertion orientation, the resulting vectors were named pPsb29camA or B (Figure 5.5 A).

The transformation vectors were then used to transform the WT-G strain of *Synechocystis*, and the resulting mutants were selected on BG11 plates supplemented with glucose, chloramphenicol and DCMU. After restreaking three times, the mutants were subjected to DNA analysis to check the segregation status. The resulting PCR fragments from both mutants using primers amplifying the entire flanking sequences showed complete segregation of the mutants (Figure 5.5 B).

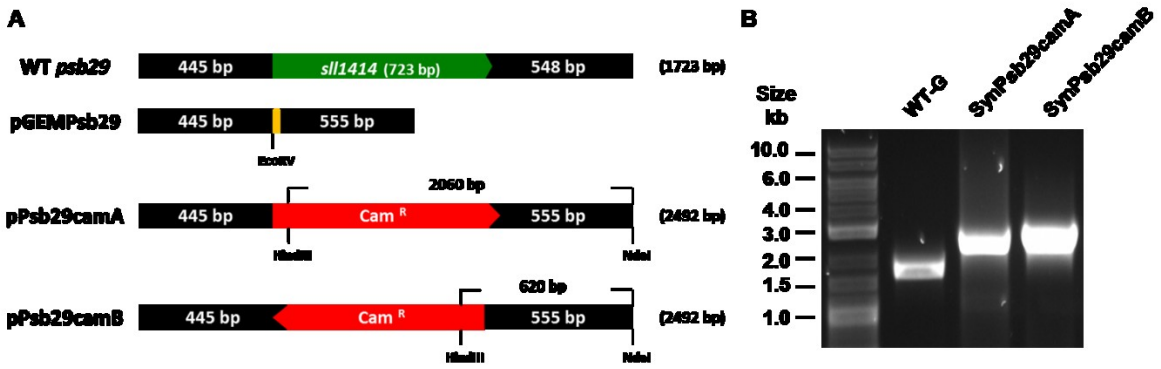

Figure 5.5: Construction and characterisation of Psb29 defective mutants.
(A) schematic representation of the vector construct used to disrupt *psb29* and (B) PCR analysis to confirm complete segregation of the mutants.

5.2.2 Probing the FtsH level in Psb29 defective mutants

Benefiting from the FtsH specific antibodies generated in this thesis (see section 2.7.4.1), the accumulation level of each FtsH homologue in the Psb29 defective mutants was investigated. The WT-G strain and SynPsb29CamA and B were cultivated in 50 ml of liquid BG11 medium, with and without the supplementation of glucose for ~ 1 week until stationary phase was reached. The cells were then harvested and lysed for protein analysis. The membrane proteins were separated on SDS-PAGE gels and blotted for immunodetection with antibodies specific for each FtsH protease.

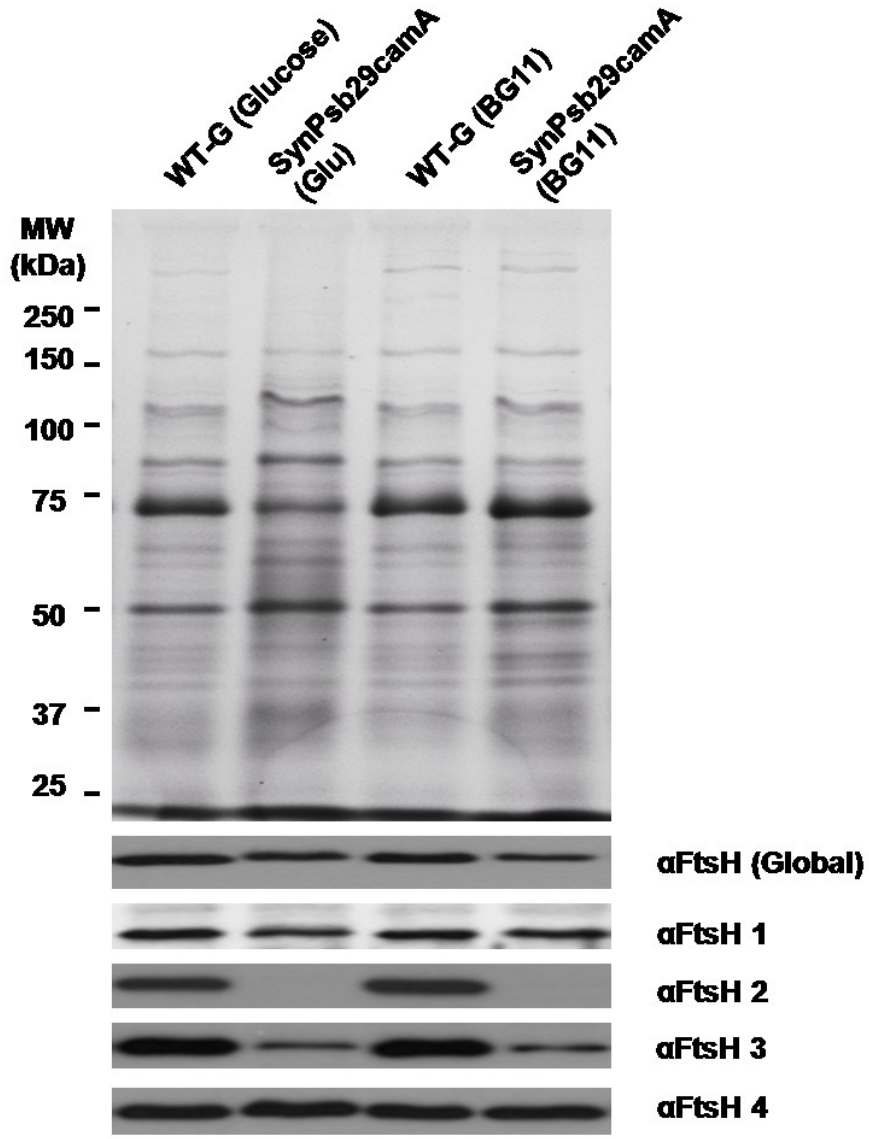

Figure 5.6: Probing the FtsH level in a *psb29* null mutant.
Proteins solubilised from the membrane fraction were separated by SDS-PAGE and then immunoblotted using antibodies specific to FtsH homologues.

The data from SDS-PAGE indicated that the protein expression profile of the *psb29* null mutant varied with supplementation of glucose, with for example the intensity of the band at ~75 kDa dramatically reduced, suggesting that Psb29 might play a role in regulation of glucose metabolism. The immunoblotting experiment revealed a dramatic change in the FtsH2 and FtsH3 levels in the *psb29* mutant, FtsH2 was undetectable, whereas, only a small amount of FtsH3 remained in the mutant (Figure 5.6). The levels of FtsH1 and FtsH4 were comparable to that of WT-G. Therefore, our

data suggest that in cyanobacteria, the accumulation of FtsH2 and FtsH3 is dependent on Psb29. The other *psb29* knockout mutant SynPsb29camB was also examined via immunochemical detection, and comparable results were obtained (data not shown).

5.2.3 Phenotype analysis of the Psb29 defective mutant

Growth of Psb29 defective mutants of *Synechocystis* 6803 has been previously reported to be more sensitive to strong illumination (Keren et al. 2005). To confirm this finding, a growth experiment was performed to compare the light sensitivity between SynPsb29camA and the FtsH2 null mutant *ΔftsH2*.

The data from the growth experiment showed that disruption of *psb29* led to increased light sensitivity (Figure 5.7 B). However, the phenotype of the *psb29* mutant was not as severe as the FtsH2 defective mutant as SynPsb29camA grew, although more poorly than WT-G, under high-light with glucose and moderate-light without glucose (Figure 5.7 A and D). A plausible explanation is that there might be trace amounts of FtsH2 present in the *psb29* null mutant which evaded detection by the FtsH2 antibody. Alternatively, expression of FtsH2 might be aberrant in the *psb29* mutant under low light levels or in flask-grown liquid cultures but could be overcome to some degree at increased irradiance levels in the presence of glucose.

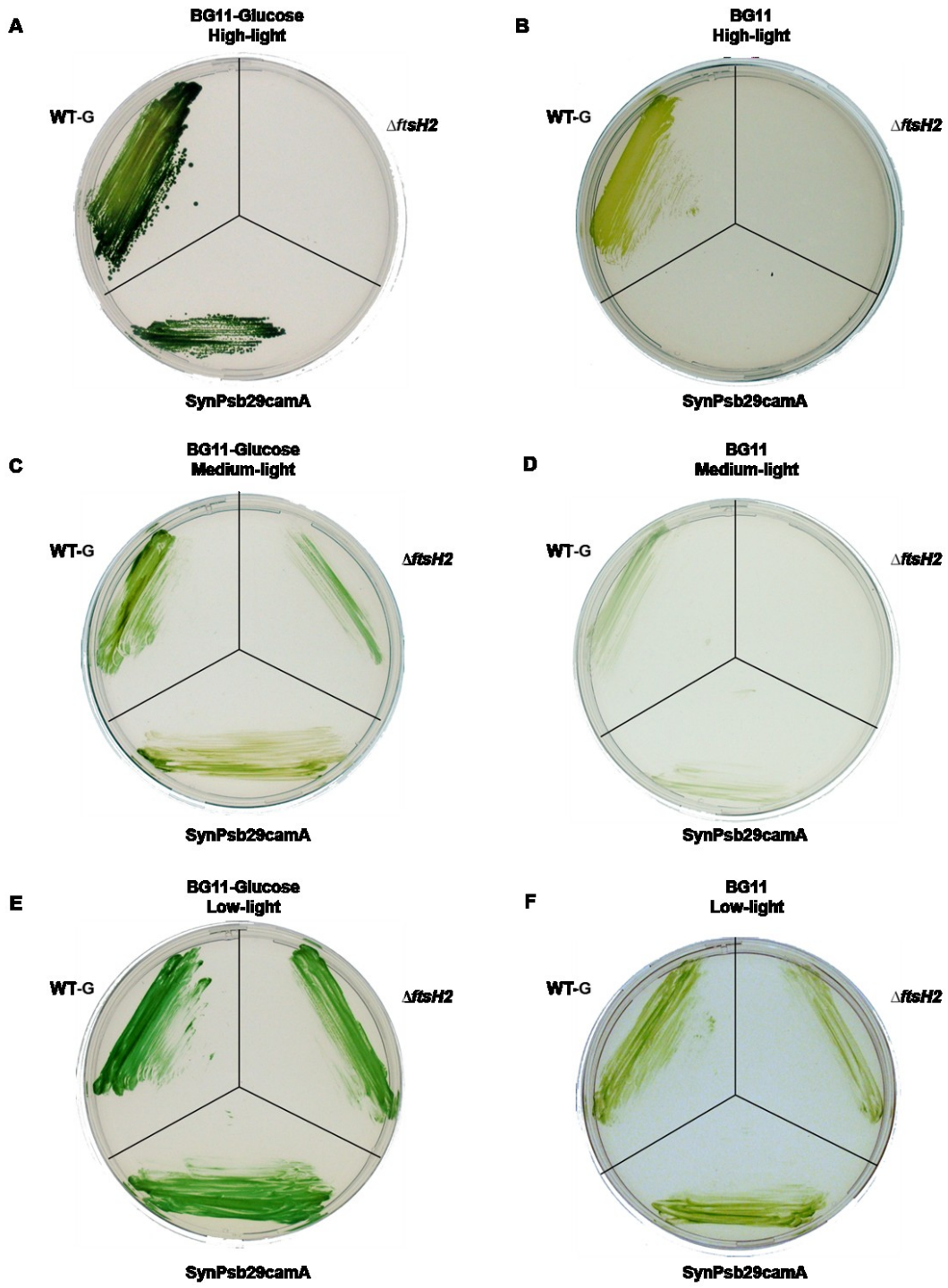

Figure 5.7: Growth experiment of Psb29 defective mutant.

Each plate carries 3 strains: WT-G: wild-type strain, *ΔftsH2*: FtsH2 null mutant and SynPsb29camA: Psb29 null mutant. Cells were tested for growth under high (A and B), medium (C and D) and low (E and F) light conditions on BG11 plates supplemented with 5 mM glucose (A, C and E) and plain BG11 plates (B, D and F). Note: Plate (A) was grown under high light for 4 days, and then transferred to low light to grow a further 1 week as SynPsb29camA grew very poorly under constant hight light condition.

5.3 Discussion

5.3.1 Identification of co-purifying proteins

In vivo studies using FtsH2 deficient mutants have demonstrated a serious growth defect under a range of abiotic stress conditions including high light and heat stress (Nixon et al. 2010), hence FtsH2 is considered to be a general housekeeping protease that plays a quality control duty in cyanobacteria (Nixon et al. 2010). On the other hand, little is known about the functions of the other three FtsH homologues in *Synechocystis*, due to the challenges generating null mutants (FtsH1 and FtsH3) and a lack of a distinguishable phenotype (FtsH4). Analysis of co-purifying proteins in various GST-tagged FtsH preparations is one way that candidate substrates or interacting proteins can be identified for further investigation. Both soluble and membrane proteins with diverse cellular functions have been found to apparently interact with FtsH proteases (see section 5.1.1 and Appendix), suggesting that all four FtsH proteases are involved in various cellular activities in *Synechocystis*. We propose that the identified proteins that co-purify with FtsH complexes might be: (1) subunits of the complex (2) auxiliary modules that form supercomplexes with FtsH or (3) substrates of FtsH proteases. On the other hand, due to the high sensitivity, contaminants inside samples are often detected by PMF and resulting in false reading. For instance, trace amount of FtsH4 was identified in FtsH1-GST sample by PMF (see Appendix), which is contradictory to the immunoblotting (see section 3.1.4) and fluorescence microscopy data (see section 3.2.5). Further investigation showed the size of the protein band where FtsH4 was detected was just ~ 20 kDa (data not shown), therefore, it is likely to be contamination due to the high abundance of FtsH4 in vivo (Figure 3.12). To minimise the influence from contamination, control experiments with wild-type cells should be included in the future.

Members of the Band 7 protein family are known to form supercomplexes with FtsH in both *E. coli* and mitochondria (Back et al. 2002; Kihara et al. 1996). Since FtsH alone retains proteolytic activity *in vitro* (Suno et al. 2006), the Band 7 proteins are

considered to be auxiliary proteins thought to play a regulatory role in FtsH activity (Janska et al. 2013). Given this, it is highly significant that members of the Band 7 protein family of *Synechocystis* were also detected in three out of the four FtsH samples (see section 5.1.1 and Appendix). The trace amount of Band 7 proteins in the *Synechocystis* samples might reflect instability during purification or the presence of only small amounts of supercomplex. Such low amounts help explain why larger supercomplexes were not detected by electron microscopy. Prohibitin1 (Slr1106), a Band 7 protein of unknown function (Boehm et al. 2009), was co-purified with FtsH4 in addition to previously identified interaction with FtsH2/FtsH3 complex (see section 3.3.2). Interestingly, Prohibitin 5 (Sll1021), another member of Band 7 family, was detected exclusively in the FtsH4 sample. However, due to the lack of phenotype from the FtsH4 defective mutant, it is difficult to probe the physiological function of this interaction. Neither of the two prohibitins was detected in the FtsH1 sample, hence it is not clear whether FtsH1/FtsH3 complexes interact with Band 7 proteins. Prohibitin1 is a membrane protein localised on both thylakoid and cytoplasmic membranes (Boehm et al. 2009), therefore, a potential interaction with FtsH1/FtsH3 complex remains plausible.

YccA is a small integral membrane protein, containing 7 transmembrane helices (Kihara et al. 1998). Interestingly, YccA can interact with FtsH both as a substrate (Ito and Akiyama 2005) or an inhibitor (van Stelten et al. 2009). *In vivo* studies have showed that accumulation of YccA is regulated by FtsH-mediated degradation in *E. coli* (Kihara et al. 1998), and that the abundance or stability of YccA suppresses the activity of FtsH (van Stelten et al. 2009). Again it is highly significant that the *Synechocystis* homologue of YccA (Sll1150) was also detected in the FtsH preparations. To gain insight into the function of the YccA homologue in *Synechocystis*, a mutant (SynSll1150cam) having the entire DNA coding region removed, was constructed in this work. Preliminary characterisation via growth assay

showed no distinguishable phenotype comparing to the wild-type strain (see section 5.1.2.3). Hence the function of YccA in *Synechocystis* remains unclear. Nevertheless, the growth assay showed that the function of the FtsH2/FtsH3 complexes was not compromised by the lack of YccA. However, this is to be expected if Sll1150 acts as a negative regulator.

YccA is a bacterial homologue of Bax Inhibitor-1 (BI-1), a protein conserved in both mammalian and plants cells (Huckelhoven 2004). In mammalian cells, BI-1 plays a regulatory role in Bax-mediated programmed cell death (Grzmil et al. 2003; Villalva et al. 2002). Strikingly, despite having no Bax-mediated pathway in plants, the BI-1 homologues in *Arabidopsis* are not only conserved, but are also capable of complementing the function of their mammalian counterparts (Huckelhoven 2004). Therefore, it is conceivable that BI-1 might execute its function via regulation of FtsH, which is also conserved in both mammalian and plants system.

A number of proteins that are part of photosynthetic complexes were also identified exclusively in the FtsH2 and/or FtsH3 samples (see appendix for full list), including the phycobilisome rod linker (Sll1580), the phycocyanin alpha subunit (Sll1578) and the gamma chain of ATP synthase (Sll1327). These data indicate the FtsH2/FtsH3 complex might play a general role in maintaining the photosynthetic machinery, however, the D1 protein, which is in the centre of FtsH-mediated PSII repair cycle (Nixon et al. 2005), has so far not been detected in any of the samples. Characterisation of mutants lacking FtsH2 has shown that D1 degradation is impaired at an early stage (Silva et al. 2003); however, evidence of direct contact between the two proteins is still lacking. A possible explanation is that FtsH-mediated D1 degradation is a rapid process, so that the abundance of D1 trapped in FtsH complexes is low. Alternatively, D1 could be released from the FtsH complexes during purification. Recent work on FtsH in *E. coli* has identified new substrates via mutating

the Zn^{2+}-binding motif, hence fast processing substrates were "trapped" in the protease inactive FtsH derivative (Westphal et al. 2012). A similar approach could be applied to explore the D1-FtsH interaction using the mutants described in Chapter 4.

The function of FtsH4 is unclear due to lack of distinctive phenotype in the protease defective mutants. The PMF data showed FtsH4 interacts with several proteins which were also detected in other FtsH samples (see Appendix). Therefore, the functional redundancy across FtsH homologues is likely to compensate the loss of FtsH4. However, a few proteins carrying distinctive physiological functions were exclusively detected in the FtsH4 sample, including the homologue of *Arabidopsis* KaiC (Slr0758) involved in regulation of circadian clock, the precursor of phosphate-binding periplasmic protein (Sll0680) that might play a role in cell adhesion (Zaborina et al. 2008), a homologue of the FkbM family of methyltransferases (Sll1530), which is involved in the synthesis of FK506 associated with immunosuppression (Chen et al. 2013). These preliminary data therefore open up interesting new avenues to explore the role of FtsH4.

Although FtsH2/FtsH3 complexes appear to play a major role in D1 degradation, it remains feasible that additional proteases might associate with FtsH complexes *in vivo* to help aid processive proteolysis of transmembrane proteins. That is why it is so exciting to identify a second protease, a homologue of *Arabidopsis* EGY2 (Sll0862), interacting with the FtsH2/FtsH3 complex (see section 5.1.1). EGY2 is an ATP-independent, Zn^{2+}-binding metalloprotease thought to cleave proteins within transmembrane regions (Chen et al. 2012). Using the FtsH complex as an anchor would generate a general "membrane protein degradation centre" capable of removing recalcitrant membrane substrates. To test for a role for sll0862 in photoprotection, two sll0862 null mutants were constructed and photoautotrophic growth was assessed under strong illumination. However, both mutants showed no distinguishable defect

compared to the wild-type, in contrast to the FtsH2 defective mutant (see section 5.1.2.3). Therefore, these data do not indicate a critical role for Sll0862 in photoprotection, which would suggest that FtsH2/FtsH3 complexes are capable of maintaining the PSII repair cycle in the absence of Sll0862. Given that there is a homologue of Sll0862 encoded in the *Synechocystis* genome (annotated as Slr0643) it still remains possible that loss of Sll0862 might be compensated for by this protein. This can be tested by analysis of a double mutant.

5.3.2 A role for Psb29 in controlling levels of the FtsH2/3 complex

Psb29 is universally conserved in cyanobacteria, green algae and all vascular plants for which genome data are available (Keren et al. 2005). Psb29 was initially identified as a novel PSII-associated protein in His-tagged PSII preparations isolated from *Synechocystis* (Kashino et al. 2002). Subsequent characterisation revealed that the *Synechocystis* Psb29 defective mutant exhibited slow-growth and increased light sensitivity.

Psb29 is the homologue of THYLAKOID FORMATION 1 (THF1) in *A. thaliana* (Wang et al. 2004), which is ubiquitously expressed in all organs of *A. thaliana*, and dual targeted to the membrane envelop and the stroma (Huang et al. 2006). THF1 plays diverse cellular roles including a G-protein-coupled signalling pathway that regulates sugar transport and FtsH accumulation in chloroplasts (Huang et al. 2006; Zhang et al. 2009). The data presented in this chapter suggest that the level of the FtsH2/FtsH3 complex is also dependent on Psb29 in *Synechocystis*. In addition the protein expression profile is abnormal in *psb29* null mutants grown in the presence of glucose (Figure 5.5), suggesting that Psb29 might also be somehow involved in glucose sensing. The link between Psb29 and FtsH is still unclear. The decrease in FtsH accumulation in the *psb29/thf1* null mutant of *Arabidopsis* is not due to effects on transcript levels (Zhang et al. 2009), but rather seems to be post-transcriptional.

Given that unassembled FtsH2 and FtsH3 are rather sensitive to degradation (Boehm et al. 2012; Sakamoto 2003), it seems plausible that Psb29 might play a direct role in the assembly of the FtsH2/FtsH3 complex. Notably, the accumulation level of FtsH1 and FtsH4 was comparable to that of wild-type (Figure 5.5), which would suggest that Psb29 is not involved in, or not important for, the assembly of FtsH4 complexes and FtsH1/3 complexes.

Disruption of *thf1* in *Arabidopsis* leads to a dramatic reduction in the level of FtsH heterocomplexes in the thylakoid membrane. Interestingly, the accumulation of the FtsH subunits in the membrane depends on the type of FtsH subunit with the abundance of Type A subunits reduced to ~ 20 % of the wild-type level whereas the Type B subunit was only reduced to 60 %. It is possible that Psb29 might act as a molecular scaffold assisting the correct folding of Type A subunits, or coordinating the assembly of the FtsH2/3 complex. Given the similarities in the phenotypes of the cyanobacterial and *Arabidopsis* mutants with regard to effects on FtsH complexes, it seems that this role for Psb29 has been conserved through evolution. Localisation data for Psb29 in *Synechocystis* are still lacking, but on the basis of the interaction between Psb29 and His-tagged PSII, and also the fact that the FtsH2/FtsH3 complex resides in the thylakoid, it is likely that Psb29 does indeed attach to the thylakoid membrane.

Chapter 6: Conclusions and future work

This work has investigated the FtsH family proteases in the cyanobacterium *Synechocystis* sp. PCC 6803, and has provided further insights into the structure, function and regulation of these proteases. FtsH proteases are universally preserved in eubacteria, mitochondria and chloroplasts (Ito and Akiyama 2005). Most bacteria only express one type of FtsH and, in the case of *E. coli*, it is essential to cell viability (Ogura et al. 1999). In contrast four FtsH homologues have been identified in *Synechocystis*, of which, FtsH1 and FtsH3 are essential (Mann et al. 2000), FtsH2 plays important role in maintaining photosynthesis (Nixon et al. 2005), and the function of FtsH4 is unknown. Little was known at the outset of this thesis about the structure and function of these FtsH proteases, in particular, the interaction between the different homologues. The experimental data presented in this work has provided new insights into the composition, localisation and structure of FtsH proteases (see Chapter 3; see section 6.1), functional mechanisms (see Chapter 4; see section 6.2) and the substrates and regulation of FtsH proteases (see Chapter 5; see section 6.3). Some data obtained in this work, including the composition analysis of FtsH complexes and the EM structure of the FtsH2GST/FtsH3 hetero-hexameric complex both in Chapter 3 were published in Boehm et al., 2012. In this final chapter, the most important results from previous chapters will be briefly summarised, followed by an outlook on potential future work (see section 6.4).

6.1 FtsH complexes in *Synechocystis*, composition, localisation and structure

FtsH proteases are integral membrane proteases that have been implicated to form large complexes *in vivo* (Ito and Akiyama 2005). In the case of yeast mitochondria, both homo- and heterocomplexes are found in the inner membrane. Genetic and biochemical studies have also provided early indications that the FtsH complexes

found in *Arabidopsis* chloroplasts are also homo-oligomeric and hetero-oligomeric (Sakamoto 2003; Zaltsman et al. 2005); the latter composed of two types of FtsH subunit: type A and type B. However, no FtsH complex has been isolated from chloroplasts and characterised so there is a lack of direct evidence. In addition, FtsH can form large supercomplexes with members of the Band 7 (or SPFH) family of proteins. Whether such a situation exists in plant chloroplasts or cyanobacteria is unclear (Janska et al. 2013). Although FtsH is widely considered to be a hexamer, this is based on the crystal structures for the cytosolic domains of bacterial FtsH over-expressed in *E. coli*. Although this would appear a reasonable assumption, the structure of the native FtsH complex is still lacking, hence vital details concerning the size, shape and subunit positioning within the complex, particular important in the case of hetero-complexes of FtsH, remain important questions to answer.

In this work, mutagenesis was performed to fuse a C-terminal GST tag to each of the four FtsH homologues found in the cyanobacterium *Synechocystis* sp. PCC 6803. The resulting mutants showed wild-type-like phenotype, with the exception of the mutant encoding FtsH3-GST, which showed an increased light sensitivity (see Figure 3.3). Nevertheless, the ability to segregate the mutation plus the phenotype analysis suggested that fusion of a C-terminal tag did not inactivate activity of the FtsH proteases (see section 3.1.3). Subsequently, each FtsH homologue was isolated via affinity purification and subjected to biochemical and structural analysis. The immunoblotting analysis revealed co-purification of FtsH1/FtsH3 and FtsH2/FtsH3, suggesting the presence of hetero-complexes, although formation of a small proportion of homocomplexes cannot be excluded, whereas no other FtsH homologue was detected in the FtsH4 sample (Figure 3.4). Structural analysis of an FtsH-GST/FtsH3 complex revealed the presence of a hexameric particle that has a diameter of ~ 120 Å, with FtsH2-GST and FtsH3 subunits arranged in an alternating fashion (Figure 3.16). This work has been published (Boehm et al. 2012).

As a membrane protease, correct localisation is vital to gain access to membrane bound substrates. In addition to the cytoplasmic membrane, cyanobacteria contain a unique thylakoid system in which the photosynthetic machinery resides (Vermaas 2001). In chloroplasts, different FtsH homologues have been found either in the thylakoid membranes (Zaltsman et al. 2005) or in the chloroplast envelope membranes (Ferro et al. 2010), which raised speculation that the localisation of FtsH complexes in *Synechocystis* might also be membrane specific. Localisation data were collected using two independent approaches: first, fluorescence microscopy showed that GFP-tagged FtsH2 and FtsH4 were mainly detected in the thylakoid membrane system, whereas weak signals of FtsH1 and FtsH3 were detected in or close to the cytoplasmic membranes. Second, immunoblotting of protein fractions comprising cytoplasmic and thylakoid membranes of wild-type *Synechocystis* using FtsH-specific antibodies confirmed that FtsH2 and FtsH4 were present in the thylakoid membrane fraction, whereas, signals of FtsH3 were detected in both the cytoplasmic and thylakoid membrane fractions (Figure 3.13). The localisation of FtsH1was not elucidated in biochemical analysis due to time limitations. Further work is required to assess whether the FtsH complexes are found in defined regions of the membrane system, such as biogenesis centres where the photosystems are thought to be assembled or repair centres where PSII may be repaired following photodamage (Komenda et al. 2012).

The compositional and structural analysis, in tandem with data from localisation studies, therefore suggests that the four FtsH homologues could form two heterocomplexes (FtsH1/FtsH3 and FtsH2/FtsH3) and an FtsH4 homocomplex. FtsH2/FtsH3 complex along with FtsH4 appear to be located in the thylakoid membranes, whereas, the FtsH1/FtsH3 complex is likely to reside in or close to the cytoplasmic membrane. N-terminal sequencing data did not support the hypothesis that the first predicted transmembrane helix of FtsH acts a cleavable signal peptide as

suggested for chloroplast FtsH from import experiments (Rodrigues et al. 2011). Hence my current view is that FtsH proteases in *Synechocystis* contain both transmembrane helices. It should be noted that this conclusion does not rule out a targeting function for the first transmembrane helix and does not extend to FtsH1 for which no N-terminal sequence data were obtained.

6.2 Functional characterisation of FtsH proteases *in vivo* and *in vitro*

The function of FtsH is vital and diverse and in *E. coli* substrates of FtsH-mediated degradation cover a range of soluble and membrane proteins (Ito and Akiyama 2005). Similarly, in *Synechocystis*, FtsH2 plays a general housekeeping role in maintaining the quality of membrane proteins (Nixon et al. 2005). Preliminary work on *Synechocystis* FtsH showed the essentiality of FtsH1 and FtsH3 and dispensability of FtsH2 and FtsH4 (Mann et al. 2000). Among the four homologues, the function of FtsH4 is totally unknown as no distinguishable phenotype was observed in the FtsH4 null mutant (Mann et al. 2000). Our localisation data clearly showed that both FtsH2 and FtsH4 are present in the thylakoid membranes, although a location in different regions cannot be totally excluded, (see section 3.12), which raised the speculation that the function of FtsH4 might be overshadowed by the FtsH2/FtsH3 complex due to functional redundancies. Hence an FtsH2/FtsH4 double knockout mutant was constructed and compared with FtsH2 single deletion strain under increased illumination intensity (see Figure 4.5). Growth of the double mutant showed a higher sensitivity to light stress comparing to the FtsH2 single mutant, indicating FtsH4 also contributes to photoprotection. However, the underlying mechanism is still unclear.

In chloroplasts, FtsH isomers are believed to mainly form heterocomplexes (Sakamoto 2003). Despite having no structural data, an interesting observation is that inactivation of only one type of subunits on the AAA+ domain via amino acid substitution rendered the entire protease non-functional, whereas, inactivation of the

Zn^{2+}–binding motif only had minor effect on the proteolytic function of the FtsH complex (Zhang et al. 2010). A similar effect also seems to hold for the *Synechocystis* FtsH2/FtsH3 complex. Indeed, FtsH2 mutants containing mutations which lead to loss of protease activity in homologous FtsH subunits were still capable of growing under high-light conditions (see Figure 4.7). Along with the protease defective mutants, the C266S mutant also survived light stress. C266 is a conserved residue localised in the AAA+ domain, which has been speculated to play a role in regulatory control of the FtsH complex (Mata-Cabana et al. 2007). However, the function of FtsH2 seemed to be unaffected in this preliminary test.

Despite *in vivo* studies showing that FtsH is at the centre of D1 degradation in the PSII repair cycle (Nixon et al. 2005), evidence of direct interaction between FtsH and D1 protein is still lacking. Inactivation of the Zn^{2+} binding motif has been shown to "trap" fast degrading substrates in the proteolytic chamber (Westphal et al. 2012). Hence construction of the protease defective FtsH might increase the chance of detecting such interaction. Unfortunately, the protease domain of FtsH2/FtsH3 complex functions redundantly as with their counterparts in *Arabidopsis* (Zhang et al. 2010), which possess greater challenge to achieve complete inactivation of the protease domain. On the other hand, since FtsH4 functions alone, inactivation of the protease domain is much simpler. In this work, four FtsH4 mutants carrying point mutations were made (see Figure 4.8) and ready for future characterisation.

The C-terminal GST tag fused to each FtsH homologue did not compromise the major function of FtsH, however, mutant expressing FtsH3-GST fusion protein exhibited increased sensitivity to light stress (see Figure 3.3). To gain further insight into the influence of the GST tag on the physiological function of FtsH, the *ftsH2/ftsH4* double deletion strain, which was used as recipient strain to minimise the functional overlap from other FtsH homologues, was transformed with the four GST tagging

vectors. In contrast to the other three mutants, cells transformed with pFtsH3GSTery construct failed to grow. A reverse approach was also attempted, by disrupting *ftsH2* from SynFtsH3GSTery strain, and again, no colonies were obtained (data not shown). Hence GST tag at the C-terminus of FtsH3 did lead to functional disturbance, however, the fusion protein still retained limited activity as judged from transformation of WT-G. Interestingly, and in contrast to FtsH3, the GST-tagged FtsH1 seemed not to affect cell viability; the phenotype of the triple mutant was indistinguishable to the recipient strain (see Figure 4.9).

FtsH4 is the only homologue not found interacting with other FtsH homologues. We explored the possibility that competition from FtsH2 might prevent the interaction between FtsH3 and FtsH4, which are both found in the thylakoid membrane. Hence a protein preparation of FtsH4 was performed to isolate FtsH4-GST fusion protein from SynFtsH4GSTΔ2, the double mutant lacking FtsH2. The isolated protein sample, again, containing only one major band (see Figure 4.10), hence the interaction between FtsH homologues is rather specific.

FtsH is a member of AAA+ superfamily, and contains three functional domains: a transmembrane domain, an AAA+ domain and a Zn^{2+} binding protease domain (Sauer and Baker 2011); hence FtsH possesses both ATPase and protease activity. There is however very limited characterisation of native FtsH activity from either cyanobacteria or chloroplasts mainly due to low abundance and insolubility. To bypass this limitation, an *E. coli* heterologous expression system was used to over-express the cytosolic region of FtsH2, FtsH3 and FtsH4. Noteworthy, to maximise the chance of getting stable proteins, the coding sequence of the recombinants proteins were cloned from a thermophilic cyanobacterial strain, *T. elongatus* (see Table 4.3). The resulting recombinant proteins lacking the transmembrane domain were purified from the soluble fraction (see Figure 4.13) and

then tested for NTPase and protease activity. Among the three homologues investigated, FtsH4 exhibited the highest NTP hydrolysis activity (see Figure 4.14), and was the only one possessing proteolytic activity *in vitro* using casein as a substrate (see Figure 4.15). Both FtsH2 and FtsH3 exhibited comparatively low activity in the NTP hydrolysis assay, however, the activity of FtsH2 was dramatically increased when incubating with CTP (see Figure 4.14). In fact, among the four nucleotides, CTP seemed to be the preferred substrate to all three FtsH proteases, followed by ATP, GTP and UTP. Early functional characterisation of *E. coli* FtsH suggested complex formation is key to efficient ATP hydrolysis and proteolytic activities (Akiyama and Ito 2000), therefore, it is conceivable that hexameric-oligomers might be present in the FtsH4 sample and contribute to the higher activities. The availability of these soluble fragments of cyanobacterial FtsH in high yield opens up the possibility of conducting crystallisation trials to enable more detailed structural information to be obtained.

6.3 Probing physiological function and regulatory mechanisms of FtsH in *Synechocystis*

Proteins that co-purify with FtsH are potential substrates of the complex, possibly trapped in the complex (Westphal et al. 2012). Further work is required to confirm that they are truly substrates such as by comparing turnover of the protein *in vivo* in WT and mutant. In agreement with the general housekeeping role that FtsH play, both soluble and membrane proteins with diverse cellular functions have been found interacting with FtsH proteases (see Appendix). Thus, the composition of the candidate substrates varies between homologues, indicating that each homologue carries out specific duties. In the case of the FtsH2/FtsH3 complex, a few subunits of photosynthetic complexes were detected in FtsH2 and/or FtsH3 samples, hence providing direct evidence that FtsH2/FtsH3 complex is involved in maintenance of photosynthetic pathway. Previous *in vivo* characterisation was unable to elucidate the function of FtsH4 due to the lack of distinguishable phenotype of the defective mutant

(Mann et al. 2000). Interestingly proteins involved in the circadian cycle, and ion uptake were detected. Hence FtsH4 might play a role in these pathways and be located in regions of the thylakoid membrane close to the periplasm, such as the PratA-defined membranes (Schottkowski et al. 2009).

The function of FtsH in other systems is thought to be regulated via interaction with auxiliary proteins, such as members of the Band 7 family of proteins and possibly YccA homologues. Although Prohibitin 1, a member of the Band 7 family, was consistently detected in FtsH2-GST/FtsH3 protein samples (see section 3.3.2, 5.1.1 and Appendix), a regulatory function of Prohibitin 1 in FtsH activity in *Synechocystis* has not been observed so far (Boehm et al. 2009). Therefore, the regulation of FtsH complexes remains unclear. Two more candidates that might regulate or work with FtsH complexes were tested in this work. These included the homologues of *E. coli* YccA (Sll1150) and *Arabidopsis* EGY2 (Sll0862). YccA is a substrate and inhibitor of *E. coli* FtsH (Ito and Akiyama 2005; van Stelten et al. 2009), whose abundance and stability influence the FtsH activity. In our preliminary study, a sll1150 null mutant was constructed and tested for photoautotrophic growth. The resulting mutant exhibited wild-type-like phenotype; hence did not yield functional insights into the FtsH complex. EGY2 is an membrane-bound Zn^{2+}-binding protease involved in cleaving transmembrane regions of membrane proteins. A working hypothesis for the interaction between FtsH and Sll0862 was that by anchoring on the FtsH2/FtsH3, the two proteases can form a repair centre to degrade a wider range of substrates, possibly through a synergetic process. Defective mutants of Sll0862 were made and checked for photoautotrophic growth, however, the mutants exhibited a wild-type-like phenotype (Figure 5.3). Hence the involvement of Sll1150 and Sll0862 in FtsH-mediated PSII repair remains unclear. It therefore remains possible that Sll0862 is actually a substrate of FtsH rather than a co-protease. More work is therefore required to monitor D1 degradation in the absence of Sll0862, to see if D1 turnover is

slower for instance, and to test for possible overlap of function with a close homologue of Sll0862 also found in *Synechocystis*. This can be done through construction of a double mutant.

Psb29 has previously been identified as an auxiliary factor of PSII (Kashino et al. 2002). A mutant of *Arabidopsis* lacking a functional homologue of Psb29, also termed Thf1, shows striking leaf variegation similar to that of FtsH defective mutants (Zhang et al. 2009). In this work, *psb29* null mutants were constructed and tested for growth. Growth of the *psb29* null mutant was sensitive to light stress, but the effect was less severe than that of *ftsH2* null mutants (see Figure 5.6). Analysis of FtsH protein levels in the psb29 mutant revealed a remarkable reduction in both FtsH2 and FtsH3 but not FtsH1 and FtsH4 (see Figure 5.5). Our working model is that the phenotype of the *psb29* mutant is related to perturbed accumulation of specifically the FtsH2/FtsH3 heterocomplex. The underlying mechanism remains unclear but we assume that it has been conserved through evolution. Based on the data obtained with the *thf1* mutant, the effect appears to be post-transcriptional, possibly at the level of assembly of the FtsH complex.

6.4 Future work

Significant progress has been made in this work in understanding the structure and function of the FtsH proteases in *Synechocystis* 6803. Among the three FtsH complexes identified in this work, only the structure of the FtsH2/FtsH3 complex has been studied to any great depth. The size and subunit organisation of FtsH1/FtsH3 complex might be similar to that of the determined FtsH2/FtsH3 complex, however, little is known about FtsH4 as the evidence of homocomplex formation is lacking. Subsequent work, such as by electron microscopy, could address the size and composition of the remaining complexes.

I have provided evidence that the protease domain of FtsH2 is not required for a functional FtsH2/FtsH3 complex, which is consistent to the observation in *Arabidopsis* (Zhang et al. 2010). On the other hand, a number of mutants carrying mutations in the AAA+ domain and having drastic effects on function have been constructed but have yet to be analysed. The equivalent mutations in *Arabidopsis* FtsH2 (VAR2) led to inactivation of the whole complex. Moreover, to clarify the potential thioredoxin control of FtsH complexes, a mutant carrying C266S mutation was made. The mutant displayed wild-type-like phenotype in the preliminary growth experiment. Growth experiments under different environmental conditions might identify a growth defect.

Growth experiments showed that affinity-tagging of FtsH1 and FtsH2 does not compromise the function of the proteases. However, the C-terminal GST tag showed partial functional interference of FtsH3, whereas the influence of GST tagging on FtsH4 remains unclear. Further investigations would be beneficial to clarify the differential interference of GST tagging between Type A-like (FtsH3) and Type B-like (FtsH1 and FtsH2) subunits.

Substrate analysis unveiled the potential functions of FtsH4, which suggested directions for future experiments. A series of mutants expressing inactive FtsH derivatives have been made, some of which were designed to “trap” substrates, hence capable of capturing fast degrading degradants (Westphal et al. 2012). Future work is required to analysis the composition of co-purified proteins, in a hope to identify previously unknown substrates, and also possibly D1.

The auxiliary proteins that form supercomplexes with FtsH are potentially involved in regulation the activity of the FtsH complexes. Two potential candidates, homologues of YccA and EGY2 were examined in preliminary studies, but no evidence of

regulation has so far been observed. Further investigations might be beneficial towards understanding the interaction between these proteins and FtsH. It is worth noting that in *E. coli*, the N-terminus of YccA seems to be essential to FtsH-mediated degradation, and truncated YccA lacking the N-terminal region, which is not degradable, could stably interact with FtsH and inhibit its activity (Saikawa et al. 2004; van Stelten et al. 2009). Therefore, future studies on mutants expressing truncated Sll1150 are suggested.

The accumulation of FtsH2/FtsH3 complex is mediated by Psb29, however, the underlying regulatory mechanism is so far unclear. The crystal structure of Psb29 from *T. elongatus* has recently been solved (Nixon and Murray, unpublished), and has revealed it to be a "pin" shape. On the basis of the structure of Psb29, a potential working hypothesis to be tested is that Psb29 might act as a molecular scaffold to stabilise unassembled FtsH3 or FtsH2 isomers on the thylakoid membrane as unassembled FtsH subunits have been shown to be unstable and rapidly degraded (Boehm et al. 2012).

Finally, vectors expressing the cytosolic domain of FtsH2, FtsH3 and FtsH4 from *T. elongatus*, were constructed in this work and the resulting recombinant proteins displayed low level of NTPase activity. In contrast to FtsH2 and FtsH3, the recombinant FtsH4 exhibited higher activity in NTP hydrolysis, and is the only one that displayed proteolytic activity. The *in vitro* data raised the speculation that the increased activity from FtsH4 might be a result of homo-oligomerisation Therefore, future work might include examining the size of FtsH4, also *in vitro* oligomerisation of FtsH2 and FtsH3. Attempts to crystallise the over-expressed FtsH proteins could be made to yield the necessary atomic resolution structural data to help elucidate the molecular mechanism of cyanobacterial FtsH proteases.

References

Adam Z, Clarke AK (2002) Cutting edge of chloroplast proteolysis. Trends Plant Sci 7: 451-456

Akiyama Y (1999) Self-processing of FtsH and its implication for the cleavage specificity of this protease. Biochemistry 38: 11693-11699

Allakhverdiev SI, Murata N (2004) Environmental stress inhibits the synthesis *de novo* of proteins involved in the photodamage-repair cycle of Photosystem II in *Synechocystis* sp. PCC 6803. Biochim Biophys Acta 1657: 23-32

Allen JF (2003) Botany. State transitions--a question of balance. Science 299: 1530-1532

Allen JF, Forsberg J (2001) Molecular recognition in thylakoid structure and function. Trends Plant Sci 6: 317-326

Allred DR, Staehelin LA (1986) Spatial organization of the cytochrome b_6-f complex within chloroplast thylakoid membranes. Biochim Biophys Acta 849: 94-103

Amarnath K, Zaks J, Park SD, Niyogi KK, Fleming GR (2012) Fluorescence lifetime snapshots reveal two rapidly reversible mechanisms of photoprotection in live cells of *Chlamydomonas reinhardtii*. Proc Natl Acad Sci U S A 109: 8405-8410

Anderson JM (1986) Photoregulation of the composition, function, and structure of thylakoid membranes. Annual Review of Plant Physiology 37: 93-136

Andersson B, Anderson JM (1980) Lateral heterogeneity in the distribution of chlorophyll-protein complexes of the thylakoid membranes of spinach chloroplasts. Biochim Biophys Acta 593: 427-440

Antal TK, Lo W, Armstrong WH, Tyystjarvi E (2009) Illumination with ultraviolet or visible light induces chemical changes in the water-soluble manganese complex, [Mn(4)O(6)(bpea)(4)]Br(4). Photochem Photobiol 85: 663-668

Arlt H, Tauer R, Feldmann H, Neupert W, Langer T (1996) The YTA10-12 complex, an AAA protease with chaperone-like activity in the inner membrane of mitochondria. Cell 85: 875-885

Arnold I, Langer T (2002) Membrane protein degradation by AAA proteases in mitochondria. Biochim Biophys Acta 1592: 89-96

Arnon DI (1971) The light reactions of photosynthesis. Proc Natl Acad Sci U S A 68: 2883-2892

Aro EM, McCaffery S, Anderson JM (1993a) Photoinhibition and D1 Protein Degradation in Peas Acclimated to Different Growth Irradiances. Plant Physiol 103: 835-843

Aro EM, Virgin I, Andersson B (1993b) Photoinhibition of Photosystem II. Inactivation, protein damage and turnover. Biochim Biophys Acta 1143: 113-134

Asada K (1999) THE WATER-WATER CYCLE IN CHLOROPLASTS: Scavenging of Active Oxygens and Dissipation of Excess Photons. Annu Rev Plant Physiol Plant Mol Biol 50: 601-639

Asada K (2000) The water-water cycle as alternative photon and electron sinks. Philos Trans R Soc Lond B Biol Sci 355: 1419-1431

Atorino L, Silvestri L, Koppen M, Cassina L, Ballabio A, Marconi R, Langer T, Casari G (2003) Loss of m-AAA protease in mitochondria causes complex I deficiency and increased sensitivity to oxidative stress in hereditary spastic paraplegia. J Cell Biol 163: 777-787

Badger MR, von Caemmerer S, Ruuska S, Nakano H (2000) Electron flow to oxygen in higher plants and algae: rates and control of direct photoreduction (Mehler reaction) and rubisco oxygenase. Philos Trans R Soc Lond B Biol Sci 355: 1433-1446

Bailey S, Thompson E, Nixon PJ, Horton P, Mullineaux CW, Robinson C, Mann NH (2002) A critical role for the Var2 FtsH homologue of *Arabidopsis thaliana* in the photosystem II repair cycle *in vivo*. J Biol Chem 277: 2006-2011

Bailleul B, Rogato A, de Martino A, Coesel S, Cardol P, Bowler C, Falciatore A, Finazzi G (2010) An atypical member of the light-harvesting complex stress-related protein family modulates diatom responses to light. Proc Natl Acad Sci U S A 107: 18214-18219

Banks RD, Blake CC, Evans PR, Haser R, Rice DW, Hardy GW, Merrett M, Phillips AW (1979) Sequence, structure and activity of phosphoglycerate kinase: a possible hinge-bending enzyme. Nature 279: 773-777

Barber J (2007) Biological solar energy. Philos Transact A Math Phys Eng Sci 365: 1007-1023

Barber J, Andersson B (1992) Too much of a good thing: light can be bad for photosynthesis. Trends Biochem Sci 17: 61-66

Barber J, Nield J, Morris EP, Zheleva D, Hankamer B (1997) The structure, function and dynamics of photosystem two. Physiol Plant 100: 817-827

Barber J, Tran PD (2013) From natural to artificial photosynthesis. Journal of the Royal Society, Interface / the Royal Society 10: 20120984

Barker M, de Vries R, Nield J, Komenda J, Nixon PJ (2006) The Deg proteases protect *Synechocystis* sp. PCC 6803 during heat and light stresses but are not essential for removal of damaged D1 protein during the photosystem two repair cycle. J Biol Chem 281: 30347-30355

Barker M, Boehm M, Nixon PJ, Nield J (2008) Structural analysis of an FtsH2/FtsH3 complex isolated from Synechocystis sp. PCC 6803. In Photosynthesis. Energy from the Sun, J.F. Allen, E. Gannt, J. Golbeck, and B. Osmond, eds (Dordrecht, The Netherlands: Springer), pp. 738–740.

Bellafiore S, Barneche F, Peltier G, Rochaix JD (2005) State transitions and light adaptation require chloroplast thylakoid protein kinase STN7. Nature 433: 892-895

Betterle N, Ballottari M, Zorzan S, de Bianchi S, Cazzaniga S, Dall'osto L, Morosinotto T, Bassi R (2009) Light-induced dissociation of an antenna hetero-oligomer is needed for non-photochemical quenching induction. J Biol Chem 284: 15255-15266

Bieniossek C, Niederhauser B, Baumann UM (2009) The crystal structure of apo-FtsH reveals domain movements necessary for substrate unfolding and translocation. Proc Natl Acad Sci U S A 106: 21579-21584

Bieniossek C, Schalch T, Bumann M, Meister M, Meier R, Baumann U (2006) The molecular architecture of the metalloprotease FtsH. Proc Natl Acad Sci U S A 103: 3066-3071

Boehm M, Nield J, Zhang P, Aro EM, Komenda J, Nixon PJ (2009) Structural and mutational analysis of band 7 proteins in the cyanobacterium *Synechocystis* sp. strain PCC 6803. J Bacteriol 191: 6425-6435

Boehm M, Romero E, Reisinger V, Yu J, Komenda J, Eichacker LA, Dekker JP, Nixon PJ (2011) Investigating the early stages of photosystem II assembly in *Synechocystis* sp. PCC 6803: isolation of CP47 and CP43 complexes. J Biol Chem 286: 14812-14819

Boehm M, Yu J, Krynicka V, Barker M, Tichy M, Komenda J, Nixon PJ, Nield J (2012) Subunit organization of a *Synechocystis* hetero-oligomeric thylakoid FtsH complex involved in photosystem II repair. Plant Cell 24: 3669-3683

Bonardi V, Pesaresi P, Becker T, Schleiff E, Wagner R, Pfannschmidt T, Jahns P, Leister D (2005) Photosystem II core phosphorylation and photosynthetic acclimation require two different protein kinases. Nature 437: 1179-1182

Bonente G, Ballottari M, Truong TB, Morosinotto T, Ahn TK, Fleming GR, Niyogi KK, Bassi R (2011) Analysis of LhcSR3, a protein essential for feedback de-excitation in the green alga *Chlamydomonas reinhardtii.* PLoS Biol 9: e1000577

Bonente G, Howes BD, Caffarri S, Smulevich G, Bassi R (2008) Interactions between the photosystem II subunit PsbS and xanthophylls studied *in vivo* and *in vitro*. J Biol Chem 283: 8434-8445

Brimblecombe P, Davies TD (1982) The Earth's Atmosphere. In Cambridge Encylopaedia of Earth Sciences (Ed. D. Smith). Cambridge University Press.

Bruckner RC, Gunyuzlu PL, Stein RL (2003) Coupled kinetics of ATP and peptide hydrolysis by *Escherichia coli* FtsH protease. Biochemistry 42: 10843-10852

Bugos RC, Yamamoto HY (1996) Molecular cloning of violaxanthin de-epoxidase from romaine lettuce and expression in *Escherichia coli*. Proc Natl Acad Sci U S A 93: 6320-6325

Campbell D, Eriksson MJ, Oquist G, Gustafsson P, Clarke AK (1998) The cyanobacterium *Synechococcus* resists UV-B by exchanging photosystem II reaction-center D1 proteins. Proc Natl Acad Sci U S A 95: 364-369

Campbell D, Öquist G (1996) Predicting light acclimation in cyanobacteria from non-photochemical quenching of photosystem II fluorescence, which reflects state transitions in these organisms. Plant Physiol 111: 1293-1298

Cardona T, Sedoud A, Cox N, Rutherford AW (2012) Charge separation in photosystem II: a comparative and evolutionary overview. Biochim Biophys Acta 1817: 26-43

Cassman KG (1999) Ecological intensification of cereal production systems: yield potential, soil quality, and precision agriculture. Proc Natl Acad Sci U S A 96: 5952-5959

Chen D, Zhang L, Pang B, Chen J, Xu Z, Abe I, Liu W (2013) FK506 maturation involves a cytochrome P450 protein-catalyzed four-electron C-9 oxidation in parallel with a C-31 O-methylation. J Bacteriol 195: 1931-1939

Chen G, Law K, Ho P, Zhang X, Li N (2012) EGY2, a chloroplast membrane metalloprotease, plays a role in hypocotyl elongation in *Arabidopsis*. Mol Biol Rep 39: 2147-2155

Chen GX, Kazimir J, Cheniae GM (1992) Photoinhibition of hydroxylamine-extracted photosystem II membranes: studies of the mechanism. Biochemistry 31: 11072-11083

Chen H, Zhang D, Guo J, Wu H, Jin M, Lu Q, Lu C, Zhang L (2006) A Psb27 homologue in *Arabidopsis thaliana* is required for efficient repair of photodamaged photosystem II. Plant Mol Biol 61: 567-575

Cheregi O, Sicora C, Kos PB, Barker M, Nixon PJ, Vass I (2007) The role of the FtsH and Deg proteases in the repair of UV-B radiation-damaged Photosystem II in the cyanobacterium *Synechocystis* PCC 6803. Biochim Biophys Acta 1767: 820-828

Clarke AK, Campbell D, Gustafsson P, Öquist G (1995) Dynamic responses of photosystem II and phycobilisomes to changing light in the cyanobacterium *Synechococcus* sp. PCC 7942. Planta 197: 553-562

Clarke AK, Soitamo A, Gustafsson P, Oquist G (1993) Rapid interchange between two distinct forms of cyanobacterial photosystem II reaction-center protein D1 in response to photoinhibition. Proc Natl Acad Sci U S A 90: 9973-9977

Clarke JE, Johnson GN (2001) *In vivo* temperature dependence of cyclic and pseudocyclic electron transport in barley. Planta 212: 808-816

Dal Corso G, Pesaresi P, Masiero S, Aseeva E, Schunemann D, Finazzi G, Joliot P, Barbato R, Leister D (2008) A complex containing PGRL1 and PGR5 is involved in the switch between linear and cyclic electron flow in *Arabidopsis*. Cell 132: 273-285

Danielsson R, Suorsa M, Paakkarinen V, Albertsson PA, Styring S, Aro EM, Mamedov F (2006) Dimeric and monomeric organization of photosystem II. Distribution of five distinct complexes in the different domains of the thylakoid membrane. J Biol Chem 281: 14241-14249

de Winter F, Swenson RB (2006) Dawn of the solar era: A wake-up call. Solar Today 2: 15-9

Dekker JP, Boekema EJ (2005) Supramolecular organization of thylakoid membrane proteins in green plants. Biochim Biophys Acta 1706: 12-39

DeLano WL (2008) The PyMOL Molecular Graphics System. (Palo Alto, CA: DeLano Scientific)

Demmig-Adams B, Adams III WW (1996) The role of xanthophyll cycle carotenoids in the protection of photosynthesis. Trends Plant Sci 1: 21-26

Di Mascio P, Devasagayam TP, Kaiser S, Sies H (1990) Carotenoids, tocopherols and thiols as biological singlet molecular oxygen quenchers. BiochemSoc Trans 18: 1054-1056

Dobakova M, Sobotka R, Tichy M, Komenda J (2009) Psb28 protein is involved in the biogenesis of the photosystem II inner antenna CP47 (PsbB) in the cyanobacterium *Synechocystis* sp. PCC 6803. Plant Physiol 149: 1076-1086

Eichacker LA, Helfrich M, Rudiger W, Muller B (1996) Stabilization of chlorophyll a-binding apoproteins P700, CP47, CP43, D2, and D1 by chlorophyll a or Zn-pheophytin a. J Biol Chem 271: 32174-32179

Ejima K, Kawaharada T, Inoue S, Kojima K, Nishiyama Y (2012) A change in the sensitivity of elongation factor G to oxidation protects photosystem II from photoinhibition in *Synechocystis* sp. PCC 6803. FEBS Lett 586: 778-783

Elrad D, Niyogi KK, Grossman AR (2002) A major light-harvesting polypeptide of photosystem II functions in thermal dissipation. Plant Cell 14: 1801-1816

Erzberger JP, Berger JM (2006) Evolutionary relationships and structural mechanisms of AAA+ proteins. Annu Rev Biophys Biomol Struct 35: 93-114

Escoubas JM, Lomas M, LaRoche J, Falkowski PG (1995) Light intensity regulation of *cab* gene transcription is signaled by the redox state of the plastoquinone pool. Proc Natl Acad Sci U S A 92: 10237-10241

Ferrante P, Ballottari M, Bonente G, Giuliano G, Bassi R (2012) LHCBM1 and LHCBM2/7 polypeptides, components of major LHCII complex, have distinct functional roles in photosynthetic antenna system of *Chlamydomonas reinhardtii*. J

Biol Chem 287: 16276-16288

Ferreira KN, Iverson TM, Maghlaoui K, Barber J, Iwata S (2004) Architecture of the photosynthetic oxygen-evolving center. Science 303: 1831-1838

Ferro M, Brugiere S, Salvi D, Seigneurin-Berny D, Court M, Moyet L, Ramus C, Miras S, Mellal M, Le Gall S, Kieffer-Jaquinod S, Bruley C, Garin J, Joyard J, Masselon C, Rolland N (2010) AT_CHLORO, a comprehensive chloroplast proteome database with subplastidial localization and curated information on envelope proteins. MCP 9: 1063-1084

Frielingsdorf S, Klosgen RB (2007) Prerequisites for terminal processing of thylakoidal Tat substrates. J Biol Chem 282: 24455-24462

Gal A, Zer H, Ohad I (1997) Redox-controlled thylakoid protein phosphorylation. News and views. Physiol Plant 100: 869-885

Garcia-Lorenzo M, Sjodin A, Jansson S, Funk C (2006) Protease gene families in Populus and *Arabidopsis*. BMC Plant Biol 6: 30

Golden SS, Brusslan J, Haselkorn R (1986) Expression of a family of *psbA* genes encoding a photosystem II polypeptide in the cyanobacterium *Anacystis nidulans* R2. EMBO J 5: 2789-2798

Gombos Z, Wada H, Murata N (1994) The recovery of photosynthesis from low-temperature photoinhibition is accelerated by the unsaturation of membrane lipids: a mechanism of chilling tolerance. Proc Natl Acad Sci U S A 91: 8787-8791

Goral TK, Johnson MP, Brain AP, Kirchhoff H, Ruban AV, Mullineaux CW (2010) Visualizing the mobility and distribution of chlorophyll proteins in higher plant thylakoid membranes: effects of photoinhibition and protein phosphorylation. Plant J 62: 948-959

Goral TK, Johnson MP, Duffy CD, Brain AP, Ruban AV, Mullineaux CW (2012) Light-harvesting antenna composition controls the macrostructure and dynamics of thylakoid membranes in *Arabidopsis*. Plant J 69: 289-301

Gottesman S (2003) Proteolysis in bacterial regulatory circuits. Annu Rev Cell Dev Biol 19: 565-587

Gould SB, Waller RF, McFadden GI (2008) Plastid evolution. Annu Rev Plant Biol 59: 491-517

Graef M, Seewald G, Langer T (2007) Substrate recognition by AAA+ ATPases: distinct substrate binding modes in ATP-dependent protease Yme1 of the mitochondrial intermembrane space. Mol Cell Biol 27: 2476-2485

Grossman AR, Bhaya D, Apt KE, Kehoe DM (1995) Light-harvesting complexes in oxygenic photosynthesis: diversity, control, and evolution. Annu Rev Genet 29: 231-288

Grossman AR, Schaefer MR, Chiang GG, Collier JL (1993) The phycobilisome, a light-harvesting complex responsive to environmental conditions. Microbiol Rev 57: 725-749

Grzmil M, Thelen P, Hemmerlein B, Schweyer S, Voigt S, Mury D, Burfeind P (2003) Bax inhibitor-1 is overexpressed in prostate cancer and its specific down-regulation by RNA interference leads to cell death in human prostate carcinoma cells. Am J Pathol 163: 543-552

Guindon S, Dufayard JF, Lefort V, Anisimova M, Hordijk W, Gascuel O (2010) New Algorithms and Methods to Estimate Maximum-Likelihood Phylogenies: Assessing the Performance of PhyML 3.0. Systematic Biology, 59(3):307-21

Gwizdala M, Wilson A, Kirilovsky D (2011) *In vitro* reconstitution of the cyanobacterial photoprotective mechanism mediated by the Orange Carotenoid Protein in *Synechocystis* PCC 6803. Plant Cell 23: 2631-2643

Hakala M, Rantamaki S, Puputti EM, Tyystjarvi T, Tyystjarvi E (2006) Photoinhibition of manganese enzymes: insights into the mechanism of photosystem II photoinhibition. J Exp Bot 57: 1809-1816

Hakala M, Tuominen I, Keranen M, Tyystjarvi T, Tyystjarvi E (2005) Evidence for the role of the oxygen-evolving manganese complex in photoinhibition of Photosystem II. Biochim Biophys Acta 1706: 68-80

Hakala-Yatkin M, Sarvikas P, Paturi P, Mantysaari M, Mattila H, Tyystjarvi T, Nedbal L, Tyystjarvi E (2011) Magnetic field protects plants against high light by slowing down production of singlet oxygen. Physiol Plant 142: 26-34

Hankamer B, Morris E, Nield J, Carne A, Barber J (2001) Subunit positioning and transmembrane helix organisation in the core dimer of photosystem II. FEBS Lett 504: 142-151

Harries JE, Brindley HE, Sagoo PJ, Bantges RJ (2001) Increases in greenhouse forcing inferred from the outgoing longwave radiation spectra of the Earth in 1970 and 1997. Nature 410: 355-357

Haussuhl K, Andersson B, Adamska I (2001) A chloroplast DegP2 protease performs the primary cleavage of the photodamaged D1 protein in plant photosystem II. EMBO J 20: 713-722

Havaux M, Eymery F, Porfirova S, Rey P, Dormann P (2005) Vitamin E protects against photoinhibition and photooxidative stress in *Arabidopsis thaliana*. Plant Cell 17: 3451-3469

Henry R, Carrigan M, McCaffrey M, Ma X, Cline K (1997) Targeting determinants and proposed evolutionary basis for the Sec and the Delta pH protein transport systems in chloroplast thylakoid membranes. J Cell Biol 136: 823-832

Herman C, Thevenet D, D'Ari R, Bouloc P (1995) Degradation of sigma 32, the heat shock regulator in *Escherichia coli*, is governed by HflB. Proc Natl Acad Sci U S A 92: 3516-3520

Herman C, Thevenet D, D'Ari R, Bouloc P (1997) The HflB protease of *Escherichia coli* degrades its inhibitor lambda cIII. J Bacteriol 179: 358-363

Hihara Y, Ikeuchi M (1997) Mutation in a novel gene required for photomixotrophic growth leads to enhanced photoautotrophic growth of *Synechocystis* sp. PCC 6803. Photosynth Res 53: 243-252

Hill TM, Kennett JP, Valentine DL, Yang Z, Reddy CM, Nelson RK, Behl RJ, Robert C, Beaufort L (2006) Climatically driven emissions of hydrocarbons from marine sediments during deglaciation. Proc Natl Acad Sci U S A 103: 13570-13574

Horton P, Ruban AV (1992) Regulation of Photosystem II. Photosynth Res 34: 375-385

Horton RM, Ho SN, Pullen JK, Hunt HD, Cai Z, Pease LR (1993) Gene splicing by overlap extension. Methods Enzymol 217: 270-279

Huang J, Taylor JP, Chen JG, Uhrig JF, Schnell DJ, Nakagawa T, Korth KL, Jones AM (2006) The plastid protein THYLAKOID FORMATION1 and the plasma membrane G-protein GPA1 interact in a novel sugar-signaling mechanism in *Arabidopsis*. Plant Cell 18: 1226-1238

Huang J, Taylor JP, Chen JG, Uhrig JF, Schnell DJ, Nakagawa T, Korth KL, Jones AM (2006) The plastid protein THYLAKOID FORMATION1 and the plasma membrane G-protein GPA1 interact in a novel sugar-signaling mechanism in *Arabidopsis*. Plant Cell 18: 1226-1238

Huckelhoven R (2004) BAX Inhibitor-1, an ancient cell death suppressor in animals and plants with prokaryotic relatives. Apoptosis 9: 299-307

Huesgen PF, Schuhmann H, Adamska I (2006) Photodamaged D1 protein is degraded in *Arabidopsis* mutants lacking the Deg2 protease. FEBS Lett 580: 6929-6932

Ito K, Akiyama Y (2005) Cellular functions, mechanism of action, and regulation of FtsH protease. Annu Rev Microbiol 59: 211-231

Ivleva NB, Shestakov SV, Pakrasi HB (2000) The carboxyl-terminal extension of the precursor D1 protein of photosystem II is required for optimal photosynthetic performance of the cyanobacterium *Synechocystis* sp. PCC 6803. Plant Physiol 124: 1403-1412

Iwai M, Katoh H, Katayama M, Ikeuchi M (2004) Improved genetic transformation of the thermophilic cyanobacterium, *Thermosynechococcus elongatus* BP-1. Plant Cell Physiol 45: 171-175

Janska H, Kwasniak M, Szczepanowska J (2013) Protein quality control in organelles - AAA/FtsH story. Biochim Biophys Acta 1833: 381-387

Johnson MP, Ruban AV (2011) Restoration of rapidly reversible photoprotective energy dissipation in the absence of PsbS protein by enhanced DeltapH. J Biol Chem 286: 19973-19981

Kamata T, Hiramoto H, Morita N, Shen JR, Mann NH, Yamamoto Y (2005) Quality control of Photosystem II: an FtsH protease plays an essential role in the turnover of the reaction center D1 protein in *Synechocystis* PCC 6803 under heat stress as well as light stress conditions. Photochem Photobiol Sci 4: 983-990

Kanemori M, Nishihara K, Yanagi H, Yura T (1997) Synergistic roles of HslVU and other ATP-dependent proteases in controlling *in vivo* turnover of sigma32 and abnormal proteins in *Escherichia coli*. J Bacteriol 179: 7219-7225

Kanervo E, Suorsa M, Aro EM (2005) Functional flexibility and acclimation of the thylakoid membrane. Photochem Photobiol Sci 4: 1072-1080

Karamoko M, Cline S, Redding K, Ruiz N, Hamel PP (2011) Lumen Thiol Oxidoreductase1, a disulfide bond-forming catalyst, is required for the assembly of photosystem II in *Arabidopsis*. Plant Cell 23: 4462-4475

Karata K, Inagawa T, Wilkinson AJ, Tatsuta T, Ogura T (1999) Dissecting the role of a conserved motif (the second region of homology) in the AAA family of ATPases. Site-directed mutagenesis of the ATP-dependent protease FtsH. J Biol Chem 274: 26225-26232

Kashino Y, Lauber WM, Carroll JA, Wang Q, Whitmarsh J, Satoh K, Pakrasi HB (2002) Proteomic analysis of a highly active photosystem II preparation from the cyanobacterium *Synechocystis* sp. PCC 6803 reveals the presence of novel polypeptides. Biochemistry 41: 8004-8012

Keren N, Liberton M, Pakrasi HB (2005a) Photochemical competence of assembled photosystem II core complex in cyanobacterial plasma membrane. J Biol Chem 280: 6548-6553

Keren N, Ohkawa H, Welsh EA, Liberton M, Pakrasi HB (2005b) Psb29, a conserved 22-kD protein, functions in the biogenesis of Photosystem II complexes in *Synechocystis* and *Arabidopsis*. Plant Cell 17: 2768-2781

Kerfeld CA, Sawaya MR, Brahmandam V, Cascio D, Ho KK, Trevithick-Sutton CC, Krogmann DW, Yeates TO (2003) The crystal structure of a cyanobacterial water-soluble carotenoid binding protein. Structure 11: 55-65

Kerr RA (2005) Earth science. The story of O_2. Science 308: 1730-1732

Kettunen R, Pursiheimo S, Rintamäki E, Van Wijk KJ, Aro EM (1997) Transcriptional and translational adjustments of *psbA* gene expression in mature chloroplasts during photoinhibition and subsequent repair of photosystem II. Eur J Biochem 247: 441-448

Kihara A, Akiyama Y, Ito K (1998) Different pathways for protein degradation by the FtsH/HflKC membrane-embedded protease complex: an implication from the

interference by a mutant form of a new substrate protein, YccA. J Mol Biol 279: 175-188

Kim SJ, Robinson C, Mant A (1998) Sec/SRP-independent insertion of two thylakoid membrane proteins bearing cleavable signal peptides. FEBS Lett 424: 105-108

Klimov VV, Shafiev MA, Allakhverdiev SI (1990) Photoinactivation of the reactivation capacity of photosystem II in pea subchloroplast particles after a complete removal of manganese. 23: 59-65

Klinkert B, Ossenbuhl F, Sikorski M, Berry S, Eichacker L, Nickelsen J (2004) PratA, a periplasmic tetratricopeptide repeat protein involved in biogenesis of photosystem II in *Synechocystis* sp. PCC 6803. J Biol Chem 279: 44639-44644

Knox JP, Dodge AD (1985) Singlet oxygen and plants. Phytochemistry 24: 889-896

Kok B, Forbush B, McGloin M (1970) Cooperation of charges in photosynthetic O_2 evolution-I. A linear four step mechanism. Photochem Photobiol 11: 457-475

Komenda J, Barker M, Kuvikova S, de Vries R, Mullineaux CW, Tichy M, Nixon PJ (2006a) The FtsH protease slr0228 is important for quality control of photosystem II in the thylakoid membrane of *Synechocystis* sp. PCC 6803. J Biol Chem 281: 1145-1151

Komenda J, Hassan HA, Diner BA, Debus RJ, Barber J, Nixon PJ (2000) Degradation of the Photosystem II D1 and D2 proteins in different strains of the cyanobacterium *Synechocytis* PCC 6803 varying with respect to the type and level of *psbA* transcript. Plant Mol Biol 42: 635-645

Komenda J, Knoppova J, Kopecna J, Sobotka R, Halada P, Yu J, Nickelsen J, Boehm M, Nixon PJ (2012a) The Psb27 assembly factor binds to the CP43 complex of photosystem II in the cyanobacterium *Synechocystis* sp. PCC 6803. Plant Physiol 158: 476-486

Komenda J, Kuvikova S, Granvogl B, Eichacker LA, Diner BA, Nixon PJ (2007a) Cleavage after residue Ala352 in the C-terminal extension is an early step in the maturation of the D1 subunit of Photosystem II in *Synechocystis* PCC 6803. Biochim Biophys Acta 1767: 829-837

Komenda J, Nickelsen J, Tichy M, Prasil O, Eichacker LA, Nixon PJ (2008) The cyanobacterial homologue of HCF136/YCF48 is a component of an early photosystem II assembly complex and is important for both the efficient assembly and

repair of photosystem II in *Synechocystis* sp. PCC 6803. J Biol Chem 283: 22390-22399

Komenda J, Reisinger V, Muller BC, Dobakova M, Granvogl B, Eichacker LA (2004) Accumulation of the D2 protein is a key regulatory step for assembly of the photosystem II reaction center complex in *Synechocystis* PCC 6803. J Biol Chem 279: 48620-48629

Komenda J, Sobotka R, Nixon PJ (2012b) Assembling and maintaining the Photosystem II complex in chloroplasts and cyanobacteria. Curr Opin Plant Biol 15: 245-251

Komenda J, Tichy M, Prasil O, Knoppova J, Kuvikova S, de Vries R, Nixon PJ (2007b) The exposed N-terminal tail of the D1 subunit is required for rapid D1 degradation during photosystem II repair in *Synechocystis* sp PCC 6803. Plant Cell 19: 2839-2854

Koppen M, Metodiev MD, Casari G, Rugarli EI, Langer T (2007) Variable and tissue-specific subunit composition of mitochondrial m-AAA protease complexes linked to hereditary spastic paraplegia. Mol Cell Biol 27: 758-767

Kruger TP, Ilioaia C, Johnson MP, Ruban AV, Papagiannakis E, Horton P, van Grondelle R (2012) Controlled disorder in plant light-harvesting complex II explains its photoprotective role. Biophys J 102: 2669-2676

Kuvikova S, Tichy M, Komenda J (2005) A role of the C-terminal extension of the photosystem II D1 protein in sensitivity of the cyanobacterium *Synechocystis* PCC 6803 to photoinhibition. Photochem Photobiol Sci 4: 1044-1048

Langklotz S, Baumann U, Narberhaus F (2012) Structure and function of the bacterial AAA protease FtsH. Biochim Biophys Acta 1823: 40-48

Lee H-Y, Hong Y-N, Chow WS (2001) Photoinactivation of photosystem II complexes and photoprotection by non-functional neighbors in *Capsicum annuum* L. leaves. Planta 212: 332-342

Lee S, Augustin S, Tatsuta T, Gerdes F, Langer T, Tsai FT (2011) Electron cryomicroscopy structure of a membrane-anchored mitochondrial AAA protease. J Biol Chem 286: 4404-4411

Leffers GG, Jr., Gottesman S (1998) Lambda Xis degradation *in vivo* by Lon and FtsH. J Bacteriol 180: 1573-1577

Li XP, Bjorkman O, Shih C, Grossman AR, Rosenquist M, Jansson S, Niyogi KK (2000) A pigment-binding protein essential for regulation of photosynthetic light harvesting. Nature 403: 391-395

Lindahl M, Spetea C, Hundal T, Oppenheim AB, Adam Z, Andersson B (2000) The thylakoid FtsH protease plays a role in the light-induced turnover of the photosystem II D1 protein. Plant Cell 12: 419-431

Lindahl M, Yang D-H, Andersson B (1995) Regulatory proteolysis of the major light-harvesting chlorophyll a/b protein of Photosystem II by a light-induced membrane-associated enzymic system. Eur J Biochem 231: 503-509

Liu Z, Yan H, Wang K, Kuang T, Zhang J, Gui L, An X, Chang W (2004) Crystal structure of spinach major light-harvesting complex at 2.72 A resolution. Nature 428: 287-292

Long SP, Humphries S, Falkowski PG (1994) Photoinhibition of photosynthesis in nature. Annu Rev Plant Physiol Plant Mol Biol 45: 633-662

Ludtke SJ, Chen DH, Song JL, Chuang DT, Chiu, W (2004) Seeing GroEL at 6 A resolution by single particle electron cryomicroscopy. Structure 12: 1129–1136

Mann NH, Novac N, Mullineaux CW, Newman J, Bailey S, Robinson C (2000) Involvement of an FtsH homologue in the assembly of functional photosystem I in the cyanobacterium *Synechocystis* sp. PCC 6803. FEBS Lett 479: 72-77

Mata-Cabana A, Florencio FJ, Lindahl M (2007) Membrane proteins from the cyanobacterium *Synechocystis* sp. PCC 6803 interacting with thioredoxin. Proteomics 7: 3953-3963

Matsubara S, Chow WS (2004) Populations of photoinactivated photosystem II reaction centers characterized by chlorophyll a fluorescence lifetime *in vivo*. Proc Natl Acad Sci U S A 101: 18234-18239

Mattoo AK, Hoffman-Falk H, Marder JB, Edelman M (1984) Regulation of protein metabolism: Coupling of photosynthetic electron transport to *in vivo* degradation of the rapidly metabolized 32-kilodalton protein of the chloroplast membranes. Proc Natl Acad Sci U S A 81: 1380-1384

McTigue MA, Williams DR, Tainer JA (1995) Crystal structures of a schistosomal drug and vaccine target: glutathione Stransferase from Schistosoma japonica and its complex with the leading antischistosomal drug praziquantel. J. Mol. Biol. 246:

21–27.

Melis A (1999) Photosystem-II damage and repair cycle in chloroplasts: what modulates the rate of photodamage ? Trends Plant Sci 4: 130-135

Michoux F, Takasaka K, Boehm M, Komenda J, Nixon PJ, Murray JW (2012) Crystal structure of the Psb27 assembly factor at 1.6 Å: implications for binding to Photosystem II. Photosynth Res 110: 169-175

Miyagawa Y, Tamoi M, Shigeoka S (2000) Evaluation of the defense system in chloroplasts to photooxidative stress caused by paraquat using transgenic tobacco plants expressing catalase from Escherichia coli. Plant Cell Physiol 41: 311-320

Miyake C, Shinzaki Y, Miyata M, Tomizawa K (2004) Enhancement of cyclic electron flow around PSI at high light and its contribution to the induction of non-photochemical quenching of chl fluorescence in intact leaves of tobacco plants. Plant Cell Physiol 45: 1426-1433

Molik S, Karnauchov I, Weidlich C, Herrmann RG, Klosgen RB (2001) The Rieske Fe/S protein of the cytochrome b_6/f complex in chloroplasts: missing link in the evolution of protein transport pathways in chloroplasts? J Biol Chem 276: 42761-42766

Moon BY, Higashi S, Gombos Z, Murata N (1995) Unsaturation of the membrane lipids of chloroplasts stabilizes the photosynthetic machinery against low-temperature photoinhibition in transgenic tobacco plants. Proc Natl Acad Sci U S A 92: 6219-6223

Muller P, Li XP, Niyogi KK (2001) Non-photochemical quenching. A response to excess light energy. Plant Physiol 125: 1558-1566

Mullineaux C (1999) The thylakoid membranes of cyanobacteria: structure, dynamics and function. Functional Plant Biol. 26: 671-677

Mullineaux CW, Emlyn-Jones D (2005) State transitions: an example of acclimation to low-light stress. J Exp Bot 56: 389-393

Munekage Y, Hashimoto M, Miyake C, Tomizawa K, Endo T, Tasaka M, Shikanai T (2004) Cyclic electron flow around photosystem I is essential for photosynthesis. Nature 429: 579-582

Murata N, Allakhverdiev SI, Nishiyama Y (2012) The mechanism of photoinhibition *in vivo*: re-evaluation of the roles of catalase, alpha-tocopherol, non-photochemical quenching, and electron transport. Biochim Biophys Acta 1817: 1127-1133

Murata N, Sugahara K (1969) Control of excitation transfer in photosynthesis. 3. Light-induced decrease of chlorophyll a fluorescence related to photophosphorylation system in spinach chloroplasts. Biochim Biophys Acta 189: 182-192

Neely WC, Martin JM, Barker SA (1988) Products and relative reaction rates of the oxidation of tocopherols with singlet molecular oxygen. Photochem Photobiol 48: 423-428

Neuwald AF, Aravind L, Spouge JL, Koonin EV (1999) AAA+: A class of chaperone-like ATPases associated with the assembly, operation, and disassembly of protein complexes. Genome Res 9: 27-43

Nickelsen J, Rengstl B (2013) Photosystem II assembly: from cyanobacteria to plants. Annu Rev Plant Biol 64: 609-635

Nishiyama Y, Allakhverdiev SI, Yamamoto H, Hayashi H, Murata N (2004) Singlet oxygen inhibits the repair of photosystem II by suppressing the translation elongation of the D1 protein in *Synechocystis* sp. PCC 6803. Biochemistry 43: 11321-11330

Nishiyama Y, Yamamoto H, Allakhverdiev SI, Inaba M, Yokota A, Murata N (2001) Oxidative stress inhibits the repair of photodamage to the photosynthetic machinery. EMBO J 20: 5587-5594

Nixon PJ, Barker M, Boehm M, de Vries R, Komenda J (2005) FtsH-mediated repair of the photosystem II complex in response to light stress. J Exp Bot 56: 357-363

Nixon PJ, Michoux F, Yu J, Boehm M, Komenda J (2010a) Recent advances in understanding the assembly and repair of photosystem II. Annal Bot 106: 1-16

Niyogi KK (1999) Photoprotection revisited: Genetic and molecular approaches. Annu Rev Plant Physiol Plant Mol Biol 50: 333-359

Niyogi KK, Truong TB (2013) Evolution of flexible non-photochemical quenching mechanisms that regulate light harvesting in oxygenic photosynthesis. Curr Opin Plant Biol doi: 10.1016/j.pbi.2013.03.011.

Nolden M, Ehses S, Koppen M, Bernacchia A, Rugarli EI, Langer T (2005) The m-AAA protease defective in hereditary spastic paraplegia controls ribosome assembly in mitochondria. Cell 123: 277-289

Nouwen N, Piwowarek M, Berrelkamp G, Driessen AJ (2005) The large first periplasmic loop of SecD and SecF plays an important role in SecDF functioning. J Bacteriol 187: 5857-5860

Nowaczyk MM, Hebeler R, Schlodder E, Meyer HE, Warscheid B, Rogner M (2006) Psb27, a cyanobacterial lipoprotein, is involved in the repair cycle of photosystem II. Plant Cell 18: 3121-3131

Ogura T, Inoue K, Tatsuta T, Suzaki T, Karata K, Young K, Su LH, Fierke CA, Jackman JE, Raetz CR, Coleman J, Tomoyasu T, Matsuzawa H (1999) Balanced biosynthesis of major membrane components through regulated degradation of the committed enzyme of lipid A biosynthesis by the AAA protease FtsH (HflB) in *Escherichia coli*. Mol Microbiol 31: 833-844

Ohad I, Keren N, Zer H, Gong H, Mor TS, Gal A, Tal S, Domovich Y (1994) Light-induced degradation of the PSII reaction centre D1 protein *in vivo*: an integrative approach. In: Baker NR, Bowyer JR, eds. Photoinhibition of photosynthesis. Oxford: Bios Scientific Publishers: 161-177

Ohad I, Kyle DJ, Arntzen CJ (1984) Membrane protein damage and repair: removal and replacement of inactivated 32-kilodalton polypeptides in chloroplast membranes. J Cell Biol 99: 481-485

Ohnishi N, Allakhverdiev SI, Takahashi S, Higashi S, Watanabe M, Nishiyama Y, Murata N (2005) Two-step mechanism of photodamage to Photosystem II: Step 1 occurs at the oxygen-evolving complex and step 2 occurs at the photochemical reaction center. Biochemistry 44: 8494-8499

Okamoto S, Ikeuchi M, Ohmori M (1999) Experimental analysis of recently transposed insertion sequences in the cyanobacterium *Synechocystis* sp. PCC 6803. DNA Res 6: 265-273

Onai K, Morishita M, Kaneko T, Tabata S, Ishiura M (2004) Natural transformation of the thermophilic cyanobacterium *Thermosynechococcus elongatus* BP-1: a simple and efficient method for gene transfer. Mol Genet Genomics 271: 50-59

Ossenbühl F, Gohre V, Meurer J, Krieger-Liszkay A, Rochaix JD, Eichacker LA (2004) Efficient assembly of photosystem II in *Chlamydomonas reinhardtii* requires Alb3.1p, a homolog of *Arabidopsis* ALBINO3. Plant Cell 16: 1790-1800

Ossenbuhl F, Inaba-Sulpice M, Meurer J, Soll J, Eichacker LA (2006) The *Synechocystis* sp PCC 6803 oxa1 homolog is essential for membrane integration of reaction center precursor protein pD1. Plant Cell 18: 2236-2246

Peers G, Truong TB, Ostendorf E, Busch A, Elrad D, Grossman AR, Hippler M, Niyogi KK (2009) An ancient light-harvesting protein is critical for the regulation of algal photosynthesis. Nature 462: 518-521

Prasil O, Adir N, Ohad I (1992) Dynamics of PSII: mechanism of photoinhibition and recovery processes. In: Barber J, ed. The photosystems: structure, function and molecular biology. Amsterdam: Elsevier Science Publishers: 295-298

Pribil M, Pesaresi P, Hertle A, Barbato R, Leister D (2010) Role of plastid protein phosphatase TAP38 in LHCII dephosphorylation and thylakoid electron flow. PLoS Biol 8: e1000288

Prommeenate P, Lennon AM, Markert C, Hippler M, Nixon PJ (2004) Subunit composition of NDH-1 complexes of *Synechocystis* sp. PCC 6803: identification of two new *ndh* gene products with nuclear-encoded homologues in the chloroplast Ndh complex. J Biol Chem 279: 28165-28173

Rengstl B, Oster U, Stengel A, Nickelsen J (2011) An intermediate membrane subfraction in cyanobacteria is involved in an assembly network for Photosystem II biogenesis. J Biol Chem 286: 21944-21951

Reuter W, Muller C (1993) New trends in photobiology : Adaptation of the photosynthetic apparatus of cyanobacteria to light and co2. J Photochem Photobiol 21: 3-27

Rivalta I, Brudvig GW, Batista VS (2012) Oxomanganese complexes for natural and artificial photosynthesis. Curr Opin Chem Biol 16: 11-18

Rochaix JD (2007) Role of thylakoid protein kinases in photosynthetic acclimation. FEBS Lett 581: 2768-2775

Rodrigues RA, Silva-Filho MC, Cline K (2011) FtsH2 and FtsH5: two homologous subunits use different integration mechanisms leading to the same thylakoid multimeric complex. Plant J 65: 600-609

Roose JL, Pakrasi HB (2004) Evidence that D1 processing is required for manganese binding and extrinsic protein assembly into photosystem II. J Biol Chem 279: 45417-45422

Roose JL, Pakrasi HB (2008) The Psb27 protein facilitates manganese cluster assembly in photosystem II. J Biol Chem 283: 4044-4050

Ruban AV, Johnson MP, Duffy CD (2012) The photoprotective molecular switch in the photosystem II antenna. Biochim Biophys Acta 1817: 167-181

Ruban AV, Young AJ, Horton P (1993) Induction of Nonphotochemical energy dissipation and absorbance changes in leaves (Evidence for changes in the state of the light-harvesting system of Photosystem II *in vivo*). Plant Physiol 102: 741-750

Ruprecht J, Nield, J (2001) Determining the structure of biological macromolecules by transmission electron microscopy, single particle analysis and 3D reconstruction. Prog. Biophys. Mol. Biol. 75: 121–164.

Saikawa N, Akiyama Y, Ito K (2004) FtsH exists as an exceptionally large complex containing HflKC in the plasma membrane of *Escherichia coli*. J Struct Biol 146: 123-129

Sakamoto W (2003) Leaf-variegated mutations and their responsible genes in *Arabidopsis thaliana*. Genes Gen Syst 78: 1-9

Sakamoto W, Zaltsman A, Adam Z, Takahashi Y (2003) Coordinated regulation and complex formation of yellow variegated1 and yellow variegated2, chloroplastic FtsH metalloproteases involved in the repair cycle of photosystem II in *Arabidopsis* thylakoid membranes. Plant Cell 15: 2843-2855

Sarvikas P, Hakala M, Patsikka E, Tyystjarvi T, Tyystjarvi E (2006) Action spectrum of photoinhibition in leaves of wild type and npq1-2 and npq4-1 mutants of *Arabidopsis thaliana*. Plant Cell Physiol 47: 391-400

Sarvikas P, Tyystjarvi T, Tyystjarvi E (2010) Kinetics of prolonged photoinhibition revisited: photoinhibited Photosystem II centres do not protect the active ones against loss of oxygen evolution. Photosynth Res 103: 7-17

Sauer RT, Baker TA (2011) AAA+ proteases: ATP-fueled machines of protein destruction. Annu Rev Biochem 80: 587-612

Schirmer EC, Glover JR, Singer MA, Lindquist S (1996) HSP100/Clp proteins: a common mechanism explains diverse functions. Trends Biochem Sci 21: 289-296

Scholz O, Thiel A, Hillen W, Niederweis M (2000) Quantitative analysis of gene expression with an improved green fluorescent protein. Eur J Biochem 267: 1565-1570

Schottkowski M, Gkalympoudis S, Tzekova N, Stelljes C, Schunemann D, Ankele E, Nickelsen J (2009) Interaction of the periplasmic PratA factor and the PsbA (D1) protein during biogenesis of photosystem II in *Synechocystis* sp. PCC 6803. J Biol Chem 284: 1813-1819

Schottkowski M, Ratke J, Oster U, Nowaczyk M, Nickelsen J (2009b) Pitt, a novel tetratricopeptide repeat protein involved in light-dependent chlorophyll biosynthesis and thylakoid membrane biogenesis in *Synechocystis* sp. PCC 6803. Mol Plant 2: 1289-1297

Shapiguzov A, Ingelsson B, Samol I, Andres C, Kessler F, Rochaix JD, Vener AV, Goldschmidt-Clermont M (2010) The PPH1 phosphatase is specifically involved in LHCII dephosphorylation and state transitions in *Arabidopsis*. Proc Natl Acad Sci U S A 107: 4782-4787

Sherman DM, Troyan TA, Sherman LA (1994) Localization of membrane proteins in the cyanobacterium *Synechococcus* sp. PCC 7942. Plant Physiol 106: 251-262

Shi LX, Hall M, Funk C, Schroder WP (2012) Photosystem II, a growing complex: updates on newly discovered components and low molecular mass proteins. Biochim Biophys Acta 1817: 13-25

Shikanai T, Munekage Y, Kimura K (2002) Regulation of proton-to-electron stoichiometry in photosynthetic electron transport: physiological function in photoprotection. J Plant Res 115: 3-10

Shikanai T, Takeda T, Yamauchi H, Sano S, Tomizawa KI, Yokota A, Shigeoka S (1998) Inhibition of ascorbate peroxidase under oxidative stress in tobacco having bacterial catalase in chloroplasts. FEBS Lett 428: 47-51

Shinopoulos KE, Brudvig GW (2012) Cytochrome b-559 and cyclic electron transfer within photosystem II. Biochim Biophys Acta 1817: 66-75

Shinopoulos KE, Yu J, Nixon PJ, Brudvig GW (2013) Using site-directed mutagenesis to probe the role of the D2 carotenoid in the secondary electron-transfer pathway of photosystem II. Photosynth Res (in press)

Shotland Y, Shifrin A, Ziv T, Teff D, Koby S, Kobiler O, Oppenheim AB (2000) Proteolysis of bacteriophage lambda CII by Escherichia coli FtsH (HflB). J Bacteriol 182: 3111-3116

Silva P, Thompson E, Bailey S, Kruse O, Mullineaux CW, Robinson C, Mann NH, Nixon PJ (2003) FtsH is involved in the early stages of repair of photosystem II in *Synechocystis* sp PCC 6803. Plant Cell 15: 2152-2164

Sippola K, Aro EM (2000) Expression of *psbA* genes is regulated at multiple levels in the cyanobacterium *Synechococcus* sp. PCC 7942. Photochem Photobiol 71: 706-714

Sokolenko A, Pojidaeva E, Zinchenko V, Panichkin V, Glaser VM, Herrmann RG, Shestakov SV (2002) The gene complement for proteolysis in the cyanobacterium *Synechocystis* sp. PCC 6803 and *Arabidopsis thaliana* chloroplasts. Curr Genet 41: 291-310

Spetea C, Hundal T, Lohmann F, Andersson B (1999) GTP bound to chloroplast thylakoid membranes is required for light-induced, multienzyme degradation of the photosystem II D1 protein. Proc Natl Acad Sci U S A 96: 6547-6552

Stanier RY, Kunisawa R, Mandel M, Cohen-Bazire G (1971) Purification and properties of unicellular blue-green algae (order Chroococcales). Bacteriol Rev 35: 171-205

Steglich G, Neupert W, Langer T (1999) Prohibitins regulate membrane protein degradation by the m-AAA protease in mitochondria. Mol Cell Biol 19: 3435-3442

Stengel A, Gugel IL, Hilger D, Rengstl B, Jung H, Nickelsen J (2012) Initial steps of photosystem II *de novo* assembly and preloading with manganese take place in biogenesis centers in *Synechocystis*. Plant Cell 24: 660-675

Stewart DH, Brudvig GW (1998) Cytochrome b559 of photosystem II. Biochim Biophys Acta 1367: 63-87

Stirnberg M, Fulda S, Huckauf J, Hagemann M, Kramer R, Marin K (2007) A membrane-bound FtsH protease is involved in osmoregulation in *Synechocystis* sp. PCC 6803: the compatible solute synthesizing enzyme GgpS is one of the targets for proteolysis. Mol Microbiol 63: 86-102

Styring S, Virgin I, Ehrenberg A, Andersson B (1990) Strong light photoinhibition of electron-transport in Photosystem II - Impairment of the function of the 1st quinone acceptor, Qa. Biochim Biophys Acta 1015: 269-278

Suno R, Niwa H, Tsuchiya D, Zhang X, Yoshida M, Morikawa K (2006) Structure of the whole cytosolic region of ATP-dependent protease FtsH. Mol Cell 22: 575-585

Symes MD, Lutterman DA, Teets TS, Anderson BL, Breen JJ, Nocera DG (2013) Photo-active cobalt cubane model of an oxygen-evolving catalyst. ChemSusChem 6: 65-69

Takahashi S, Milward SE, Fan DY, Chow WS, Badger MR (2009) How does cyclic electron flow alleviate photoinhibition in *Arabidopsis*? Plant Physiol 149: 1560-1567

Takeda T, Yokota A, Shigeoka S (1995) Resistance of photosynthesis to hydrogen peroxide in algae. Plant Cell Physiol 36: 1089-1095

Tamoi M, Murakami A, Takeda T, Shigeoka S (1998) Acquisition of a new type of fructose-1,6-bisphosphatase with resistance to hydrogen peroxide in cyanobacteria: molecular characterization of the enzyme from *Synechocystis* PCC 6803. Biochim Biophys Acta 1383: 232-244

Tikkanen M, Nurmi M, Kangasjarvi S, Aro EM (2008) Core protein phosphorylation facilitates the repair of photodamaged photosystem II at high light. Biochim Biophys Acta 1777: 1432-1437

Tikkanen M, Piippo M, Suorsa M, Sirpio S, Mulo P, Vainonen J, Vener AV, Allahverdiyeva Y, Aro EM (2006) State transitions revisited-a buffering system for dynamic low light acclimation of *Arabidopsis*. Plant Mol Biol 62: 779-793

Tilman D, Cassman KG, Matson PA, Naylor R, Polasky S (2002) Agricultural sustainability and intensive production practices. Nature 418: 671-677

Tomoyasu T, Gamer J, Bukau B, Kanemori M, Mori H, Rutman AJ, Oppenheim AB, Yura T, Yamanaka K, Niki H, et al. (1995) *Escherichia coli* FtsH is a membrane-bound, ATP-dependent protease which degrades the heat-shock transcription factor sigma 32. EMBO J 14: 2551-2560

Tsukazaki T, Mori H, Echizen Y, Ishitani R, Fukai S, Tanaka T, Perederina A, Vassylyev DG, Kohno T, Maturana AD, Ito K, Nureki O (2011) Structure and function of a membrane component SecDF that enhances protein export. Nature 474: 235-238

Umena Y, Kawakami K, Shen J-R, Kamiya N (2011) Crystal structure of oxygen-evolving photosystem II at a resolution of 1.9Å. Nature 473: 55-60

Van Aken O, Pecenkova T, van de Cotte B, De Rycke R, Eeckhout D, Fromm H, De Jaeger G, Witters E, Beemster GT, Inze D, Van Breusegem F (2007) Mitochondrial type-I prohibitins of *Arabidopsis thaliana* are required for supporting proficient meristem development. Plant J 52: 850-864

Van Heel M (1987) Angular reconstitution: a posteriori assignment of projection directions for 3D reconstruction. Ultramicroscopy 21: 111–123

Van Heel M, Schatz M (2005) Fourier shell correlation threshold criteria. J. Struct. Biol. 151: 250–262

van Stelten J, Silva F, Belin D, Silhavy TJ (2009) Effects of antibiotics and a proto-oncogene homolog on destruction of protein translocator SecY. Science 325: 753-756

Vass I, Styring S, Hundal T, Koivuniemi A, Aro EM, Andersson B (1992) Reversible and irreversible intermediates during photoinhibition of Photosystem II. Stable reduced Qa species promote chlorophyll triplet formation. Proc Natl Acad Sci USA 89: 1408-1412

Vasudevan D, Fu A, Luan S, Swaminathan K (2012) Crystal structure of *Arabidopsis* cyclophilin38 reveals a previously uncharacterized immunophilin fold and a possible autoinhibitory mechanism. Plant Cell 24: 2666-2674

Wada H, Gombos Z, Murata N (1994) Contribution of membrane lipids to the ability of the photosynthetic machinery to tolerate temperature stress. Proc Natl Acad Sci U S A 91: 4273-4277

Wagner R, Aigner H, Funk C (2012) FtsH proteases located in the plant chloroplast. Physiol Plant 145: 203-214

Wang Q, Sullivan RW, Kight A, Henry RL, Huang J, Jones AM, Korth KL (2004) Deletion of the chloroplast-localized Thylakoid formation1 gene product in *Arabidopsis* leads to deficient thylakoid formation and variegated leaves. Plant Physiol 136: 3594-3604

Wei Z, Cady CW, Brudvig GW, Hou HJ (2011) Photodamage of a Mn(III/IV)-oxo mixed-valence compound and photosystem II: evidence that a high-valent manganese

species is responsible for UV-induced photodamage of the oxygen-evolving complex in photosystem II. J Photochem Photobiol 104: 118-125

Westphal K, Langklotz S, Thomanek N, Narberhaus F (2012) A trapping approach reveals novel substrates and physiological functions of the essential protease FtsH in *Escherichia coli*. J Biol Chem 287: 42962-42971

Williams JGK (1988) Construction of specific mutations in photosystem II photosynthetic reaction center by genetic engineering methods in *Synechocystis* 6803. In: Lester Packer ANG (ed) Methods in Enzymology: Cyanobacteria. Academic Press, pp 766-778

Wingler A, Lea PJ, Quick WP, Leegood RC (2000) Photorespiration: metabolic pathways and their role in stress protection. Philos Trans R Soc Lond B Biol Sci 355: 1517-1529

Yamamoto T, Burke J, Autz G, Jagendorf AT (1981) Bound ribosomes of pea chloroplast thylakoid membranes: Location and release *in vitro* by high Salt, puromycin, and RNase. Plant Physiol 67: 940-949

Yang Y, Ramelot TA, Cort JR, Wang D, Ciccosanti C, Hamilton K, Nair R, Rost B, Acton TB, Xiao R, Everett JK, Montelione GT, Kennedy MA (2011) Solution NMR structure of photosystem II reaction center protein Psb28 from *Synechocystis* sp. Strain PCC 6803. Proteins 79: 340-344

Yu F, Park S, Rodermel SR (2005) Functional redundancy of AtFtsH metalloproteases in thylakoid membrane complexes. Plant Physiol 138: 1957-1966

Zaborina O, Holbrook C, Chen Y, Long J, Zaborin A, Morozova I, Fernandez H, Wang Y, Turner JR, Alverdy JC (2008) Structure-function aspects of PstS in multi-drug-resistant *Pseudomonas aeruginosa*. PLoS pathogens 4: e43

Zaltsman A, Ori N, Adam Z (2005) Two types of FtsH protease subunits are required for chloroplast biogenesis and Photosystem II repair in *Arabidopsis*. Plant Cell 17: 2782-2790

Zhang D, Kato Y, Zhang L, Fujimoto M, Tsutsumi N, Sodmergen, Sakamoto W (2010) The FtsH protease heterocomplex in *Arabidopsis*: dispensability of type-B protease activity for proper chloroplast development. Plant Cell 22: 3710-3725

Zhang L, Wei Q, Wu W, Cheng Y, Hu G, Hu F, Sun Y, Zhu Y, Sakamoto W, Huang J (2009) Activation of the heterotrimeric G protein alpha-subunit GPA1 suppresses the

ftsH-mediated inhibition of chloroplast development in *Arabidopsis*. Plant J 58: 1041-1053

Zhang P, Sicora CI, Vorontsova N, Allahverdiyeva Y, Battchikova N, Nixon PJ, Aro EM (2007) FtsH protease is required for induction of inorganic carbon acquisition complexes in *Synechocystis* sp. PCC 6803. Mol Microbiol 65: 728-740

Zhang PP, Battchikova N, Jansen T, Appel J, Ogawa T, Aro EM. (2004) Expression and functional roles of the two distinct NDH-1 complexes and the carbon acquisition complex NdhD3/NdhF3/CupA/Sll1735 in Synechocystis sp PCC 6803. Plant Cell 16: 3326–3340

Zolla L, Rinalducci S (2002) Involvement of active oxygen species in degradation of light-harvesting proteins under light stresses. Biochemistry 41: 14391-14402

Zouni A, Witt HT, Kern J, Fromme P, Krauss N, Saenger W, Orth P (2001) Crystal structure of photosystem II from *Synechococcus elongatus* at 3.8 Å resolution. Nature 409: 739-743

Zurawski G, Bohnert HJ, Whitfeld PR, Bottomley W (1982) Nucleotide sequence of the gene for the M(r) 32,000 thylakoid membrane protein from *Spinacia oleracea* and *Nicotiana debneyi* predicts a totally conserved primary translation product of M(r) 38,950. Proc Natl Acad Sci USA 79: 7699-7703

Appendix

Mass spectrometry data

Table S1: Full list of proteins identified in the FtsH sample from PMF

ORF	FtsH1 GST	*FtsH2 GST	FtsH3 GST	FtsH4 GST	Note
sll0067	√	√	√	√	glutathione S-transferase
sll1150	√	√	√	√	hypothetical protein (YccA)
sll1106	√		√	√	hypothetical protein (conserved membrane protein with unknown function)
slr0236	√		√	√	similar to glutathione S-transferase
sll1577		√	√		phycocyanin beta subunit
slr1106		√	√	√	Prohibitin (Phb1)
sll1099	√	√	√		elongation factor Tu
sll0862		√	√		hypothetical protein (membrane-associated, Zn metalloprotease, M55 peptidase family)
slr0774			√	√	protein-export membrane protein SecD
Above is the list of co-purified proteins detected in more than one type of FtsH-GST					
slr1390	√	√			FtsH1
slr0228		√	√		FtsH2
slr1604	√	√	√		FtsH3
sll1463	√			√	FtsH4
Above is the list of co-purified FtsH					

sll1580		√			phycobilisome rod linker polypeptide
slr0394		√			phosphoglycerate kinase
Above is the list of co-purified proteins detected exclusively in FtsH2-GST					
sll1578			√		phycocyanin alpha subunit
slr0244			√		hypothetical protein (USP: universal stress protein)
sll1450			√		nitrate/nitrite transport system substrate-binding protein
sll1327			√		ATP synthase gamma chain
sll1196			√		phosphofructokinase
slr1299			√		UDP-glucose dehydrogenase
sll1536			√		molybdopterin biosynthesis MoeB protein
Above is the list of co-purified proteins detected exclusively in FtsH3-GST					
slr0758				√	circadian clock protein KaiC homolog
sll0680				√	phosphate-binding periplasmic protein precursor (PBP)
sll0689				√	Na+/H+ antiporter
sll1530				√	unknown protein (FkbM family methyltransferase)
sll1021				√	hypothetical protein (Band 7 protein, Phb5)
Above is the list of co-purified proteins detected exclusively in FtsH4-GST					

Genotype and cloning procedure of SynFtsH2GST

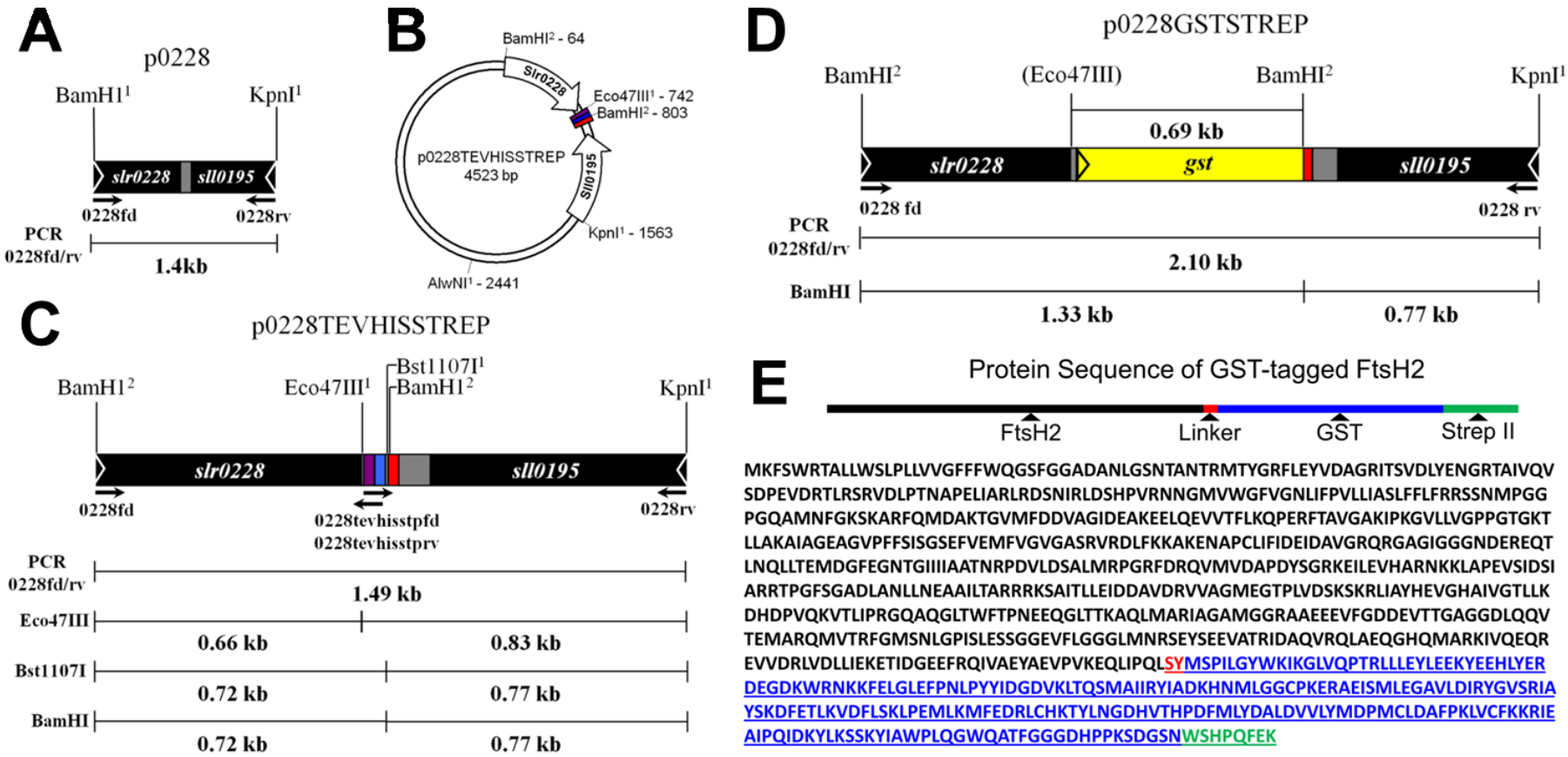

Figure S1: Plasmids used to construct SynFtsH2GST. Schematic representations of the inserts found in the (A) p0228, (C) p0228TEVHISSTREP and (D) p0228GSTSTREP plasmids and (B) a vector map of the p0228TEVHISSTREP plasmid. A detailed description of how the individual plasmids were constructed can be found in the Materials and Methods section. (A-D) Black and yellow boxes indicate genes, grey boxes indicate non-coding sequence and triangular arrows depict the direction of transcription of the labeled genes. The purple box indicates the TEV protease site, the blue box the His9 and the red box the Strep tag-II encoding sequences. Restriction sites used for cloning steps or construct identification are labeled including the number of sites in superscript type. Restriction sites in brackets indicate that the respective site has been destroyed. Primers used for gene amplification, construct confirmation and sequencing are marked. Gene sizes, PCR products and restriction fragments are labeled in kb and annotated with the fragment name or restriction enzyme used to digest the fragment. (E) Predicted primary structure of the FtsH2-GST fusion protein including sequence of the linker.

Confocal flurescence microscopy images of each *ftsH::gfp* mutant

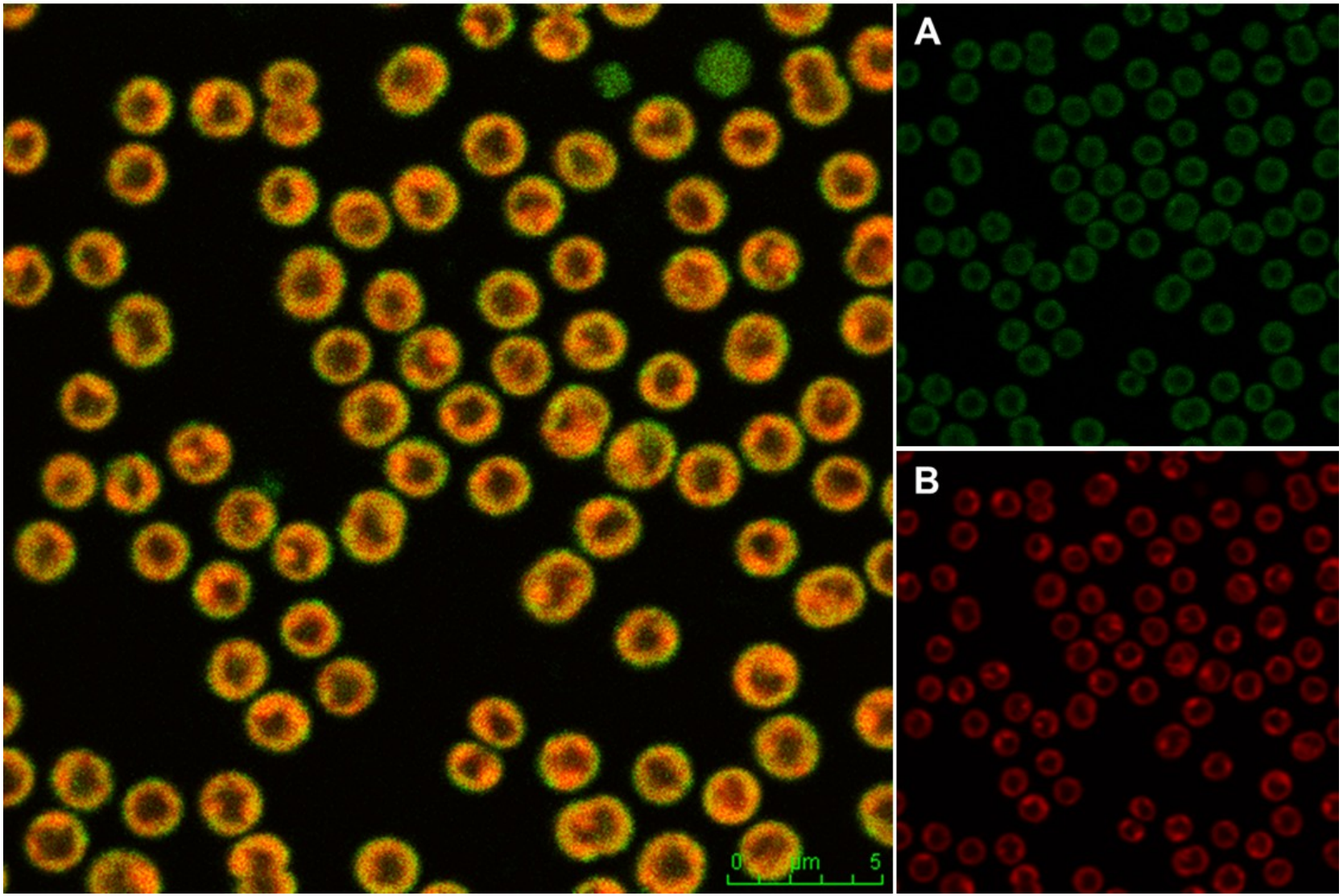

Figure S2: SynFtsH1GFPcam under confocal fluorescence microscopy.

(A) Image of GFP fluorescence emission scanned at wavelengths 500-527 nm. (B) Image of Chlorophyll *a* fluorescence emission at a wavelength of 665 nm. The overlay image of A and B are enlarged and presented on the left, scale bar 0-5 µm

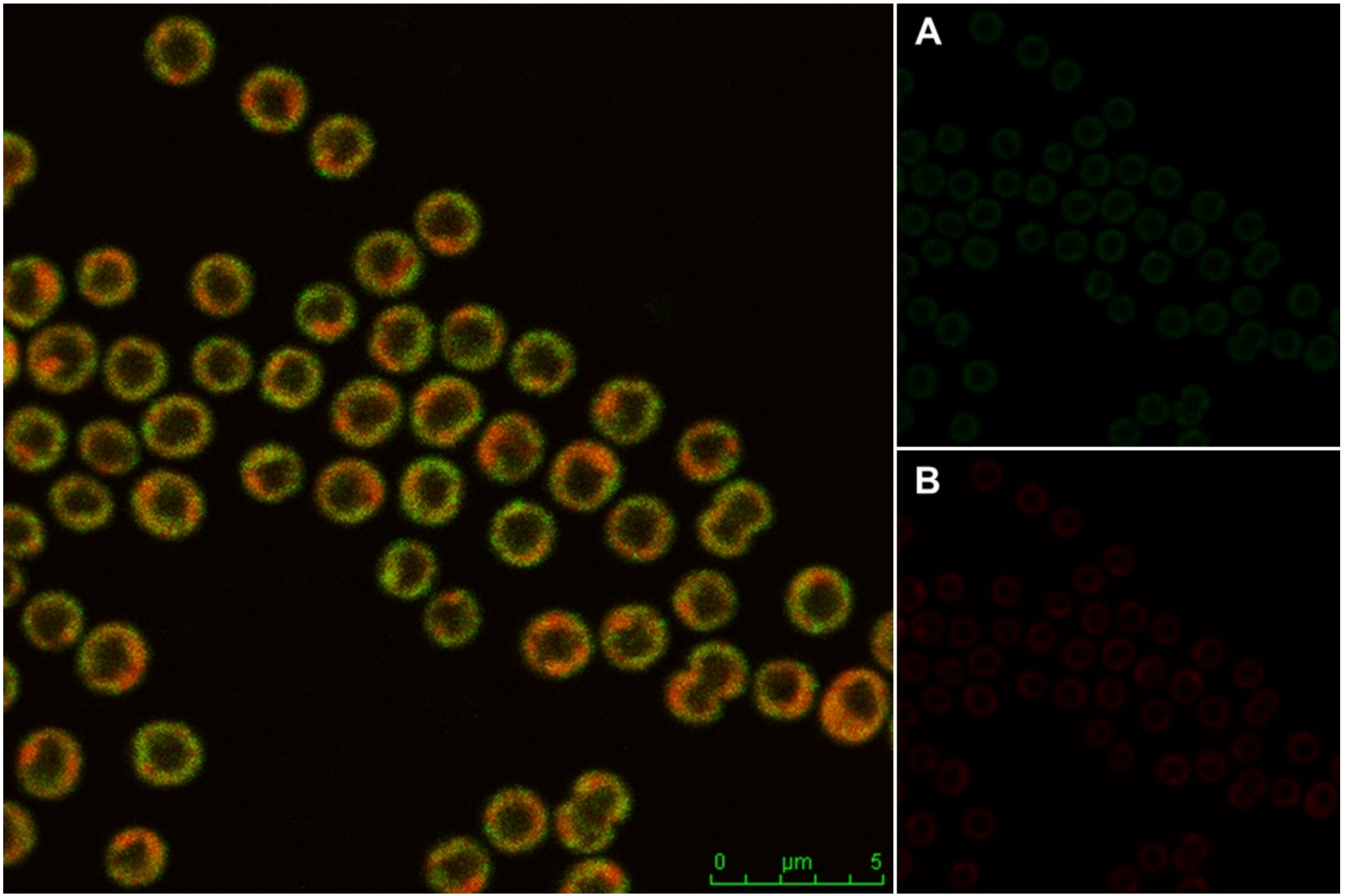

Figure S3: SynFtsH2GFPcam under confocal fluorescence microscopy.

(A) Image of GFP fluorescence emission scanned at wavelengths 500-527 nm. (B) Image of Chlorophyll *a* fluorescence emission at a wavelength of 665 nm. The overlay image of A and B are enlarged and presented on the left, scale bar 0-5 µm.

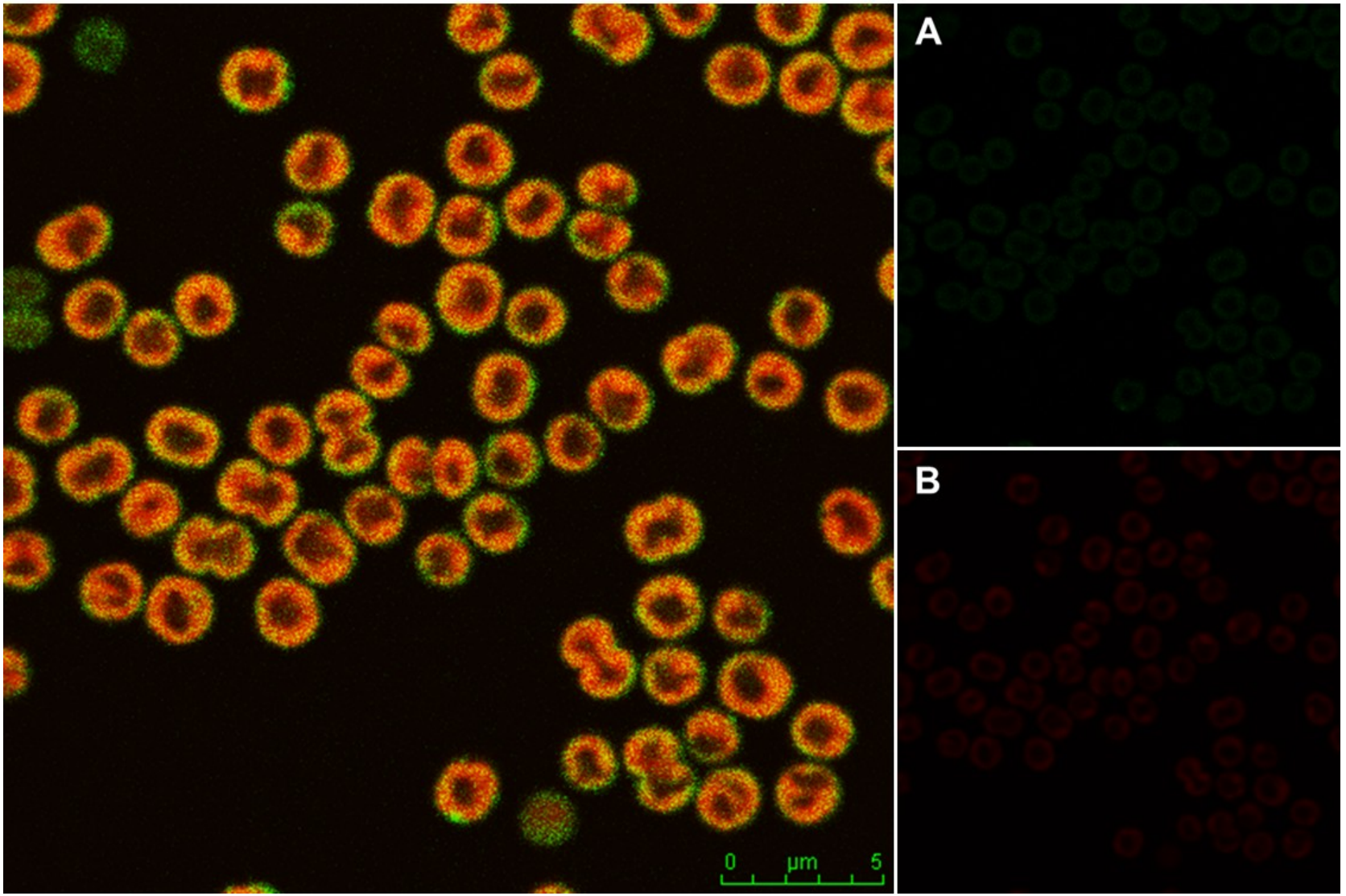

Figure S4: SynFtsH3GFPcam under confocal fluorescence microscopy.

(A) Image of GFP fluorescence emission scanned at wavelengths 500-527 nm. (B) Image of Chlorophyll *a* fluorescence emission at a wavelength of 665 nm. The overlay image of A and B are enlarged and presented on the left, scale bar 0-5 µm.

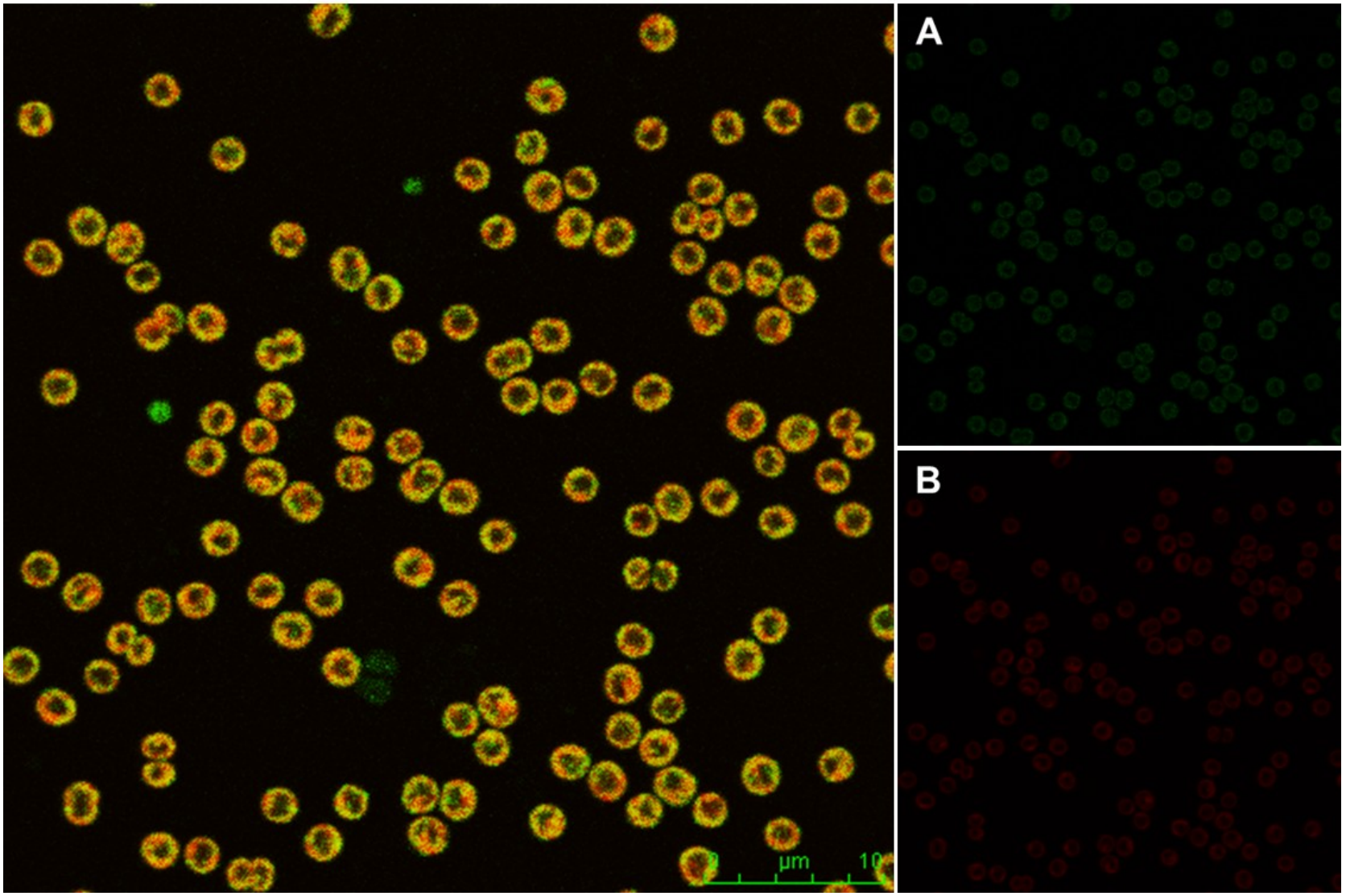

Figure S5: SynFtsH4GFPcam under confocal fluorescence microscopy.
(A) Image of GFP fluorescence emission scanned at wavelengths 500-527 nm. (B) Image of Chlorophyll *a* fluorescence emission at a wavelength of 665 nm. The overlay image of A and B are enlarged and presented on the left, scale bar 0-10 µm.